

**THE DESIGN AND DEVELOPMENT OF A MOBILE COLONOSCOPY
ROBOT**

by

Joseph Christopher Norton

Submitted in accordance with the requirements for the degree of
Doctor of Philosophy

The University of Leeds

Institute of Functional Surfaces
School of Mechanical Engineering

January 2017

The candidate confirms that the work submitted is his/her own, except where work which has formed part of jointly-authored publications has been included. The contribution of the candidate and the other authors to this work has been explicitly indicated below. The candidate confirms that appropriate credit has been given within the thesis where reference has been made to the work of others.

The work included in the papers below is partly used in Chapters 1 – 6:

“RollerBall: a mobile robot for intraluminal locomotion” – IEEE BioRob, 2016 proceedings

Authors: J. Norton, A. Hood, A. Neville, D. Jayne, P. Culmer, A. Alazmani and J. Boyle

I was responsible for the technical work carried-out, the co-authors were responsible for reviewing the paper.

This copy has been supplied on the understanding that it is copyright material and that no quotation from the thesis may be published without proper acknowledgement.

© 2017 The University of Leeds and Joseph Christopher Norton

Acknowledgements

I would first like to thank my four, incredibly talented supervisors – Anne Neville, Pete Culmer, Jordan Boyle and Ali Alazmani – for their support over a challenging three years. Anne, thank you for your wisdom. Pete, your inspirational enthusiasm and approachable attitude have made this PhD so much more enjoyable. Jordan, thank you for your friendship and for always being available for a “quick” one hour brainstorm. Ali, your professionalism and work ethic have inspired me, thank you for believing in me and pushing me to aim higher.

I would also like to thank the rest of the CoDIR team; past, present and from both the University of Leeds and University of Dundee. It has been a pleasure working with you on this project. Thank you to Graham Brown for putting up with what must have been hundreds of discussions on 3D printing and reasons for failed builds.

Thank you to my family and friends for gathering around me and keeping me going in the difficult times. I am truly blessed to have you all.

I would like to thank my beloved wife for supporting what I do and encouraging me to pursue my dreams. Thank you for putting up with the late nights and bad moods, and for always trying to put my needs before yours. I could not have done this without your sacrificial love.

Thank you, God, for always being faithful and good.

Truly my soul finds rest in God;
my salvation comes from him.
Truly he is my rock and my salvation;
he is my fortress, I will never be shaken.

...

One thing God has spoken,
two things I have heard:
“Power belongs to you, God,
and with you, Lord, is unfailing love.”

Psalm 62

Abstract

The conventional colonoscopy is a common procedure used to access the colon. Despite it being considered the Gold Standard procedure for colorectal cancer diagnosis and treatment, it has a number of major drawbacks, including high patient discomfort, infrequent but serious complications and high skill required to perform the procedure. There are a number of potential alternatives to the conventional colonoscopy, from augmenting the colonoscope to using Computed Tomography Colonography (CTC) - a completely non-invasive method. However, a truly effective, all-round alternative has yet to be found.

This thesis explores the design and development of a novel solution: a fully mobile colonoscopy robot called "RollerBall". Unlike current passive diagnostic capsules, such as PillCam, this device uses wheels at the end of adjustable arms to provide locomotion through the colon, while providing a stable platform for the use of diagnostic and therapeutic tools. The work begins by reviewing relevant literature to better understand the problem and potential solutions. RollerBall is then introduced and its design described in detail. A robust prototype was then successfully fabricated using a 3D printing technique and its performance assessed in a series of benchtop experiments. These showed that the mechanisms functioned as intended and encouraged the further development of the concept. Next, the fundamental requirement of gaining traction on the colon was shown to be possible using hexagonal shaped, macro-scale tread patterns. A friction coefficient ranging between 0.29 and 0.55 was achieved with little trauma to the tissue substrate. The electronics hardware and control were then developed and evaluated in a series of tests in silicone tubes. An open-loop strategy was first used to establish the control algorithm to map the user inputs to motor outputs (wheel speeds). These tests showed the efficacy of the locomotion technique and the control algorithm used, but they highlighted the need for autonomy. To address this, feedback was included to automate the adjusting of the arm angle and amount of force applied by the device; a forward facing camera was also used to automate the orientation control by tracking a user-defined target. Force and orientation control were then combined to show that semi-autonomous control was possible and as a result it was concluded that clinical use may be feasible in future developments.

Table of Contents

ACKNOWLEDGEMENTS	III
ABSTRACT	IV
TABLE OF CONTENTS	V
LIST OF FIGURES	VIII
LIST OF TABLES	XII
CHAPTER 1 INTRODUCTION	1
1.1. Background.....	1
1.2. The CoDIR project.....	2
1.3. PhD aim and contribution	3
1.4. Thesis structure.....	4
CHAPTER 2 LITERATURE REVIEW	6
2.1. The colon	6
2.2. Colonic inspection and intervention	8
2.3. Current procedures.....	8
2.3.1. Virtual colonoscopy.....	8
2.3.2. Conventional colonoscopy.....	10
2.3.3. Alternative colon distension: Hydro-colonoscopy	15
2.3.4. Augmenting the colonoscope	16
2.3.5. Robot-assisted colonoscopy.....	17
2.4. A mobile colonoscopy robot.....	21
2.4.1. Device requirements and environmental challenges	22
2.5. Locomotion techniques	24
2.5.1. Swimming forms of locomotion	24
2.5.2. Contact-based forms of locomotion.....	31
2.6. Conclusions from literature.....	42
CHAPTER 3 MECHANICAL DESIGN, FABRICATION AND CHARACTERISATION	44
3.1. Specifications of a mobile colonoscopy robot	44
3.2. RollerBall: a mobile, wheeled robot.....	45
3.2.1. Concept overview.....	45
3.3. RollerBall V4	48
3.3.1. Electronics module	49
3.3.2. Stability considerations	50
3.3.3. Arm design	52
3.3.4. Preliminary encapsulation considerations.....	52
3.3.5. Fabrication and assembly	53
3.4. Detailed design.....	53
3.4.1. Wheel mechanism	54
3.4.2. Expansion mechanism.....	56
3.4.3. Electronics housing and cable routing	58
3.5. Prototype fabrication and assembly	60
3.5.1. Fabrication	60
3.5.2. Assembly.....	60
3.6. Benchtop characterisation	64

3.6.1.	Theoretical performance.....	64
3.6.2.	Actual (Benchtop) performance.....	66
3.6.3.	Results and discussion	68
3.7.	Summary.....	69
CHAPTER 4 GAINING TRACTION IN THE COLON.....		71
4.1.	Introduction	71
4.2.	The colonic mucosa.....	74
4.2.1.	Tissue properties.....	74
4.2.2.	Surface features.....	75
4.2.3.	Mucus layer	75
4.2.4.	Summary of properties	76
4.3.	Frictional regime	77
4.4.	Looking to nature.....	78
4.4.1.	Considering hydrodynamics.....	80
4.5.	Tread patterns for biological use.....	82
4.5.1.	Micro-treads	82
4.5.2.	Macro-treads	83
4.6.	Literature summary and discussion.....	84
4.7.	Experimental work.....	87
4.7.1.	Tread design and fabrication.....	88
4.7.2.	Test apparatus	92
4.7.3.	Tissue preparation.....	94
4.7.4.	Traction test protocol.....	95
4.7.5.	Data analysis.....	96
4.8.	Results and discussion.....	97
4.8.1.	Effect of Colon and colon region used.....	98
4.8.2.	Effect of tread geometry	99
4.8.3.	Effect of scale and aspect ratio.....	100
4.8.4.	Effect of Normal load	100
4.8.5.	Limitations	100
4.9.	Trauma assessment.....	102
4.9.1.	Method	102
4.9.2.	Results and discussion	104
4.10.	Traction and trauma conclusions.....	105
4.10.1.	An optimum tread for the colon?	106
CHAPTER 5 SYSTEM INTEGRATION AND OPEN-LOOP CONTROL.....		107
5.1.	Introduction	107
5.1.1.	System requirements.....	107
5.1.2.	System development strategy	109
5.2.	Hardware.....	109
5.3.	Open-loop control strategy	111
5.3.1.	System architecture.....	112
5.4.	Expansion control.....	114
5.5.	Orientation and position control.....	115
5.5.1.	Motor speed control.....	117
5.5.2.	Summary	122
5.6.	Test environment.....	123
5.7.	Open-loop system evaluation.....	126

5.7.1.	Method.....	126
5.7.2.	Results.....	128
5.7.3.	Discussion.....	130
5.7.4.	Conclusions	131
CHAPTER 6 CLOSED-LOOP CONTROL.....		133
6.1.	Closed-loop control system.....	133
6.2.	Expansion control.....	133
6.2.1.	Instrumentation.....	134
6.2.2.	Characterisation.....	135
6.2.3.	Calibration and validation	140
6.2.4.	Material creep compensation – feasibility trials	141
6.2.5.	Summary – Force sensing.....	142
6.2.6.	Expansion control strategy.....	143
6.3.	Orientation control.....	149
6.3.1.	Conceptual control strategy.....	149
6.3.2.	Preliminary development.....	152
6.4.	Closed-loop system evaluation.....	160
6.4.1.	Test environments.....	161
6.4.2.	Method.....	163
6.4.3.	Results and discussion	165
6.5.	Summary – Closed-loop control.....	177
CHAPTER 7 DISCUSSION AND CONCLUSIONS.....		179
7.1.	Discussion	179
7.2.	Conclusions.....	184
CHAPTER 8 FUTURE WORK.....		187
8.1.	Miniaturisation and fabrication	187
8.2.	Encapsulation and design refinements.....	188
8.3.	Optimising functional surfaces for high traction and low trauma against soft tissues.....	188
8.4.	Electronics and control.....	189
8.5.	Test environment.....	190
REFERENCES.....		191
APPENDIX A: DC MOTOR AND GEARBOX DATA SHEETS.....		199
APPENDIX B: 3D PRINTER RESIN (LS600) DATA SHEET		201
APPENDIX C: CALCULATIONS FOR THE TISSUE TENSION DURING TRACTION TESTS		202
APPENDIX D: AN ALTERNATIVE, SOFT ROBOTIC LOCOMOTION CONCEPT		202
D.1.	Soft robotics.....	202
D.1.2.	Variable compliance.....	205
D.1.3.	Soft actuators	208
D.1.4.	Summary.....	208
D.2.	Soft colonoscopy robot - Conceptual design	209
D.2.1.	Sweeping action.....	210
D.2.2.	Paddling action.....	212

List of Figures

Figure 1.1 - A conventional colonoscope. [7]	1
Figure 2.1 - A diagram of the large intestine (colon), showing its various segments and a cross-section of the multi-layered tissue. [18]	7
Figure 2.2 - Colonoscope within the colon, including detail of the colonoscope tip. [28] ...	11
Figure 2.3 - Simplified diagram showing colonoscope insertion. [30]	13
Figure 2.4 - Diagram showing the unwanted stretching of the colon due to lack of control of the colonoscope. [31]	13
Figure 2.5 - Pillcam, a common passive capsule used to investigate the GI tract (ca. 11 x 32 mm). [60]	19
Figure 2.6 - Illustration of an active capsule platform showing key requirements [61].....	20
Figure 2.7 - A capsule controlled using an external magnet field [62]	20
Figure 2.8 - A device powered by four conventional propellers. [64]	25
Figure 2.9 - An exploded view of a ring propeller. [65]	25
Figure 2.10 - Example of a device that uses rotating helixes. [67]	26
Figure 2.11 - An example of a device that uses a pressurized jet. [63]	27
Figure 2.12 - A device that uses on-board centrifugal pumps. [69]	27
Figure 2.13 - The generating of vortex rings. [71]	28
Figure 2.14 – Example #1 of a simple finned device using IPMC actuators. [73]	29
Figure 2.15 - Example #2 of a simple finned device using SMA actuation. [74].....	29
Figure 2.16 - Rajiform swimming using a flexible fin. [75]	30
Figure 2.17 - Example #3 of a simple finned device. [76]	30
Figure 2.18 - Impact-driven capsule device. [77]	32
Figure 2.19 - Elongated toroid form of locomotion. a. The locomotion technique. b. An example of such a device. [78]	33
Figure 2.20 - Various wheeled / tracked devices. a. – c. Tracked devices. [79], [80], [81] d. Pipe inspection, wheeled device. [82] e. Device using Whegs. [83].....	35
Figure 2.21 - Screw thread-based locomotion. a. The locomotion technique. b. An example of a device. [84]	36
Figure 2.22 - Amphibious, snake-like device. [85]	37
Figure 2.23 - Example 1 of an inchworm device. [87]	38
Figure 2.24 - Example 2 of an inchworm device. [88]	38
Figure 2.25 - Example 3 of an inchworm device, showing a novel method of controlling friction. [89]	39
Figure 2.26 - Example 1 of a legged device. [91]	40
Figure 2.27 - Example 2 of a legged device. [92]	40
Figure 2.28 - Example of a device using a "moving anchor." [93]	41
Figure 3.1 - An illustration of the core RollerBall concept.....	46
Figure 3.2 - The various iterations of RollerBall, from the start of the CoDIR project - V1 - to the concept adopted at the start of this PhD - V3.....	47
Figure 3.3 - An illustration of how spherical wheels offer a more functional, less traumatic solution in the intestine.....	47
Figure 3.4 - Renders showing the advancement of the RollerBall concept from V3 to V4 made during this PhD.	49
Figure 3.5 – Considering RollerBall’s stability.....	50

Figure 3.6 – Integrating a passive spring element.....	51
Figure 3.7 – Renders showing the design progression of the arm (wheel mechanism).	52
Figure 3.8 – A cross-sectional view of RollerBall V4 showing the three main components.	53
Figure 3.9 – The wheel mechanism of the robot.....	54
Figure 3.10 – A screenshot of the simple FEA carried out on the arm.....	56
Figure 3.11 – The expansion mechanism of the robot.....	57
Figure 3.12 – The electronics module.	58
Figure 3.13 – A cross-sectional view showing the route of the tether core.....	59
Figure 3.14 – The tether attachment comprising of an end cap and strain reliever.....	59
Figure 3.15 – A sequence of photos taken during the assembly of the three arms.	61
Figure 3.16 – A sequence of photos taken during the assembly of the chassis and rest of the prototype.....	63
Figure 3.17 – The relationship between the Arm force (F_A) and the resulting Normal force (F_N).	65
Figure 3.18 – A close-up view of the test rig used to measure the maximum tractive effort of the wheel mechanism.	67
Figure 3.19 – A close-up view of the test rig used to measure the maximum expansion speed of the arm.....	67
Figure 4.1 – An illustration of <i>some</i> of the many factors contributing to the overall traction achieved by a wheel on colonic tissue.....	73
Figure 4.2 – The stress-strain curves of two colon specimens (large bowel) under transversal and axial tensile loading. [109]	75
Figure 4.3 – The hierarchy of features on a tree frog toe pad, modified from [130].....	79
Figure 4.4 – A sequence of images showing out-flow of fluid from a patterned surface. ...	81
Figure 4.5 – An illustration of how tissue deforms into perpendicular (to shear) tread features.....	86
Figure 4.6 – The geometric patterns assessed in this experimental work and their given names.	89
Figure 4.7 – The 3D printed tread patterns.....	91
Figure 4.8 – A microscopic view of the “smooth” surface of the control.	91
Figure 4.9 – The traction rig and key components.....	93
Figure 4.10 – A tissue sample clamped in a pre-tensioned state.....	95
Figure 4.11 – A typical traction profile from one repetition.	97
Figure 4.12 – A boxplot showing the traction coefficients from the <i>static condition</i>	98
Figure 4.13 – A boxplot showing the traction coefficients from the dynamic condition.	98
Figure 4.14 – An illustration showing one of the prepared tissue samples pre-histology.	102
Figure 4.15 – Visible grooves or ‘dents’ seen post-test (Parallel tread, 50 g load).	104
Figure 5.1 – The majority of the components that make up the RollerBall platform.	110
Figure 5.2 – A schematic of the core RollerBall system communication architecture.....	111
Figure 5.3 – The RollerBall system architecture showing the distribution of the peripheral devices, the main programs and flow of data.....	112
Figure 5.4 – A modified render showing the location and naming of the four DC motors (M1 – 4) and camera (CAM). It also shows the coordinate frame used.....	113
Figure 5.5 – An illustration of the Xbox controller showing the inputs used.....	114
Figure 5.6 – A flow chart of the open-loop expansion control.....	115

Figure 5.7 – An isometric, free body diagram of RollerBall in a lumen	116
Figure 5.8 – A 2D (x-y plane) view from the rear of RollerBall showing the even spacing of the three wheels/motors (M1 – 3).	116
Figure 5.9 – The right joystick is used to set the desired <i>Target</i> (T) which is defined in the x-y plane.	118
Figure 5.10 – A schematic summarising how the user inputs are mapped onto the motor outputs which move the robot.....	119
Figure 5.11 – A schematic showing how the relative motor speeds are assigned using the angle of the Target.....	120
Figure 5.12 – An overview of the <i>Position and Orientation control</i> program.	122
Figure 5.13 – A schematic showing the geometry and dimensions of the two main tubes used to evaluate RollerBall.	125
Figure 5.14 – The silicone tube with multiple corners, suspended by thin nylon line from an aluminium frame.	126
Figure 5.15 – The idle/starting position of RollerBall in the changing diameter tube.	127
Figure 5.16 – The idle/starting position of RollerBall in the tube with multiple corners... ..	127
Figure 5.17 – A sequence of images from one repetition in the changing diameter tube tests.	128
Figure 5.18 – A sequence of images from one repetition in the tube with multiple corners.	129
Figure 5.19 – An image of RollerBall stuck in a corner.	130
Figure 6.1 – A schematic of the force sensing system.....	134
Figure 6.2 – A plot showing the first 2.5 seconds of the collected strain data.	136
Figure 6.3 – An annotated plot showing a strain response from a long duration step input.	138
Figure 6.4 – A flowchart showing the various stages used to compensate for the material creep.	141
Figure 6.5 – An example output from the material creep compensation program.....	142
Figure 6.6 – A simplified overview of the closed-loop force control programs.	145
Figure 6.7 – The silicone tube and support frame used to secure RollerBall during closed-loop force control tests.	146
Figure 6.8 – A plot showing the undesirable continuous oscillation present when the Proportional (P) constant was too high.....	147
Figure 6.9 – Two plots showing the force response from a series of set point changes by the user.	148
Figure 6.10 – The actual GUI, modified to represent the hypothetical functionality.	150
Figure 6.11 – A flowchart showing an overview of the hypothetical orientation control.	150
Figure 6.12 – An example of the image processing steps likely required.	151
Figure 6.13 – An overview of the preliminary closed-loop orientation control program. .	153
Figure 6.14 – A diagram showing the coordinate conversion.	154
Figure 6.15 – A schematic showing an overview of the closed-loop orientation control strategy/program.	154
Figure 6.16 – An overview of the system architecture, showing just the items associated with Orientation control.....	155

Figure 6.17 – An overview of the system architecture, showing just the items associated with Orientation control.....	157
Figure 6.18 – An overview of the control program used for the LED array.	158
Figure 6.19 – The results from one repetition of tuning the automated orientation control.	159
Figure 6.20 – Three of the silicone tubes used to test the closed-loop control of RollerBall.	162
Figure 6.21 – A sequence of images from the manual tests which included camera feedback.	165
Figure 6.22 – A screenshot of the GUI during one test.	166
Figure 6.23 – Plots showing the maximum arm force and Global speed (user input) from one repetition in the tube with changing diameter.	167
Figure 6.24 – Plots showing the maximum arm force and Global speed (user input) from one repetition in the tube with multiple corners.....	168
Figure 6.25 – Plots showing the maximum arm force and Global speed (user input) from one repetition in the tube with changing diameter – under both manual and auto force control.....	169
Figure 6.26 – Plots showing the maximum arm force and Global speed (user input) from one repetition in the tube with changing (global and local) diameter – under both manual and auto force control.....	170
Figure 6.27 – Plots showing the maximum arm force and Global speed (user input) from one repetition in the tube with multiple corners – under both manual and auto force control.....	171
Figure 6.28 – A plot showing the high variability between force outputs from all three arms during one test.....	173
Figure 6.29 – A comparison of the x-y plots of the tracked Target, from all repetitions, under Manual and Auto orientation control.	174
Figure 6.30 – A comparison of the error plots of the tracked Target, from one repetition, under Manual and Auto orientation control.	175
Figure 6.31 – A comparison of the x-y plots of the tracked Target, from one repetition, under Manual and Auto orientation control – during forward movement.	176
Figure 6.32 – A comparison of the error plots of the tracked Target, from one repetition, under Manual and Auto orientation control – during forward movement.	177
Figure 8.1 – An image showing an approximately 30 % smaller model of RollerBall, next to the existing prototype. The grid is comprised of 1 cm squares.....	187
Figure A.D.1 – A range of elastic moduli of several common materials. [144]	203
Figure A.D.2 – Example #1 of a soft robot (GoQBot). [147]	204
Figure A.D.3 – Example 2 of a soft, multi-gait robot. [148].....	204
Figure A.D.4 – An example of a hybrid robotic device that uses both soft and rigid materials. [154].....	209
Figure A.D.5 – The basic muscle layout of an octopus tentacle. N – central nervous fibres, T – transverse muscles, L – longitudinal muscles and O – Oblique muscles. [155].....	209
Figure A.D.6 – A robotic octopus tentacle. L – longitudinal actuators, T – transverse actuators, W – central wires and S – support structure. [155]	210
Figure A.D.7 – Concept using sweeping locomotion. a) Side view. b) Front view.....	211

Figure A.D.8 – Diagram showing locomotion inefficiency in small diameter colon.....	212
Figure A.D.9 – Schematic showing basic paddle action.....	213

List of Tables

Table 2.1 - The advantages and disadvantages of Virtual colonoscopy (CTC):	9
Table 2.2 - Colonoscopy indications [13]:.....	10
Table 2.3 - The advantages and disadvantages of Hydro-colonoscopy:.....	16
Table 2.4 - Examples of automated / robotic colonoscopes:	18
Table 2.5 - General requirements for a mobile robotic platform for hydro-colonoscopy. ..	22
Table 2.6 - General requirements for a mobile robotic platform for hydro-colonoscopy (Continued).	23
Table 3.1 – A list of the major specifications of a mobile colonoscopy robot.....	44
Table 3.2 - A summary of the major changes made to RollerBall and the work carried-out to progress it to a working prototype.	48
Table 3.3 - The theoretical and actual performance of the wheel and expansion mechanisms.	68
Table 4.1 - A comparison of the small and large intestine.	76
Table 4.2 - A matrix showing the total number of repetitions carried out in the traction tests.	96
Table 4.3 - A summary of the features used to rank the tread trauma.	103
Table 4.4 - Tread trauma results showing the degree of trauma seen and the load it first occurred at.....	105
Table 5.1 – The major (ideal) control attributes.....	108
Table 5.2 – The major requirements of the electronic (control) Hardware.....	108
Table 5.3 – Cornering success rate.	129
Table 6.1 – The average strain outputs for all Strain gauges and multiple loads.....	138
Table 6.2 – The average model coefficients from different masses (SG2).....	139
Table 6.3 – The calibration constants for all strain gauges.	140
Table 6.4 – Force sensing validation.....	140
Table 6.5 – The main results from the Manual tests with camera feedback.	166
Table 6.6 – The results from the Manual and Auto force control tests.	172
Table 6.7 – The results from the manual and automated orientation control tests.....	175
Table 6.8 – The results from the manual and automated orientation control tests.....	177
Table 7.1 – A summary of how the RollerBall prototype met the desired specifications..	185
Table A.D.1 – Some methods of achieving variable compliance.....	206

Chapter 1

Introduction

1.1. Background

The colon, or large bowel, is part of the gastro-intestinal tract, positioned between the small intestine and rectum. The thin, sensitive tissue and tortuous shape make this region of the body extremely challenging to access. This is a significant issue as there are a number of common diseases that affect the colon: rates of inflammatory bowel disease (mainly ulcerative colitis and Crohn's disease) and colorectal cancer are high in the Western world and are rapidly increasing in developing countries – costing Europe alone billions of Euros [1, 2]. Colorectal cancer is the world's 3rd leading cause of cancer related death [3] and as with all forms of cancer, the stage at which it is diagnosed greatly impacts patient survival [4, 5]. If detected at any early stage, treatment is relatively simple, cheap and highly effective. Since the patient will typically have no symptoms and no reason to suspect that anything is wrong at this point, the only way to ensure early detection is through a reliable mass-screening program. This should be applied to a subset of the healthy population based on risk factors, of which age is the most significant. A number of screening methods exist including fecal occult blood testing, virtual colonoscopy, sigmoidoscopy and conventional colonoscopy (which is generally considered to be the most common and effective [6]).

A colonoscopy, typically performed under sedation, involves the use of a colonoscope (Figure 1.1; a long, flexible endoscope) to visually inspect the entire inner surface of the colon over a period of about 30 minutes.



Figure 1.1 - A conventional colonoscope. [7]

Despite their frequent use and powerful diagnostic and therapeutic capabilities, colonoscopies are a decidedly imperfect solution. The colonoscope is a largely passive device (only the tip can be actively steered) while the colon is long (up to 1.8m), loosely anchored and has a highly complex shape with multiple acute bends [8]. The force necessary to advance the colonoscope can only be applied from outside the patient, so when the tip encounters resistance (e.g. when trying to navigate a corner) a compressive force is applied to the flexible shaft, causing it to buckle outwards and even looping back on itself. This can stretch the connective tissue that anchors the colon to the abdominal wall and cause severe discomfort. Indeed, more than 10% of attempted colonoscopies are aborted due to excessive looping and patient discomfort [9]. Unsurprisingly, it can be difficult to convince asymptomatic people to undergo a painful procedure purely for screening purposes, and compliance rates – even among those in elevated risk categories – were found to be below 60% [10].

In order to increase success rates and patient compliance with routine colonoscopies, the procedure should be made as easy, reliable and as comfortable as possible. This in turn will require new procedure that avoids the shortcomings of the conventional colonoscopy, including the high forces placed on the colonoscope and the resulting looping. Intuitively, these phenomena could be eradicated by pulling the instrument from the tip rather than pushing it from the back and the overall size of the device, and its mobility, improved. Motivated by this logical hypothesis, an increasing number of research groups have been working to develop mobile, self-propelled endoscopy robots over the past 20 years. This is a challenging task and so, despite several attempts, a successful, commercial mobile robot has yet to be developed.

1.2. The CoDIR project

CoDIR (Colonic Disease Investigation by Robot hydro-colonoscopy) is an EU funded project¹ that aims to produce a novel robotic alternative to colonoscopy. It is a collaborative effort by The University of Leeds and The University of Dundee.

The overall aim of the project is to produce a mobile robotic platform to investigate the colon and carry-out tasks such as taking biopsies – ultimately overcoming the drawbacks of conventional colonoscopy. The complete system (the device, the console and all the associated hardware and software) will be developed. The key features of this alternative approach are to:

¹ European Research Council – Reference: CoDIR (268519)

- Use warm water to distend the colon (hydro-colonoscopy), instead of carbon dioxide. Preliminary trials have shown that this could reduce patient discomfort and globally distend the colon. The denser liquid medium could also assist the locomotion of the robotic device.
- Minimize trauma by using a miniature robotic device that applies small forces to the colonic tissue. This could allow it to be used in weakened colons (such as those with inflammatory bowel disease) and could further reduce patient discomfort.
- Improve mobility within the colon by having full control over the device's position and orientation (ie. an on-board locomotion mechanism), increasing diagnostic and therapeutic efficacy.

If successful, this system would have a global impact. The potential to vastly improve on the current procedure quality and overall effectiveness is substantial, but so are the challenges. The work produced over the duration of the project, even if the system itself is commercially unsuccessful, is likely to further science by introducing novel technologies and insights into this fast growing area.

1.3. PhD aim and contribution

There is undoubtedly significant motivation to research a technology such as this. The area of mobile *in vivo* robotics is still relatively new and so any novel technologies and technical insights developed herein could have an impact on both the medical and robotic fields, addressing fundamental questions such as “What challenges face the development of mobile *in vivo* robots?” and “Could devices such as these be a viable solution to future medical procedures?”

The aim of this work was to develop a mobile robotic device to traverse the length of a fluid-filled colon, providing a stable platform for the use of diagnostic and therapeutic tools². This included all aspects of development, including: mechanical design, fabrication, electronics integration and device control. The major steps taken to achieve this included:

- 1. Reviewing current literature** in order to better understand: the unique environment of the colon; the diseases affecting this region; current methods used to inspect and intervene in the colon and their limitations; the potential of a mobile robotic solution, including what has been done previously and what can be learnt going forward.

² The robot described in this thesis is one of two robotic devices that will be used in the CoDIR system. One developed at the University of Leeds and the other at the University of Dundee.

2. **Critiquing an existing concept (RollerBall)** that was generated in the CoDIR project – in light of the reviewed literature – and make necessary design modifications.
3. **Completing a detailed design** of RollerBall before **fabricating a working prototype**.
4. **Characterising the performance of the individual mechanisms** through theoretical calculations and a series of benchtop experiments.
5. **Exploring current methods of gaining traction on the colon** and developing a functional solution by considering literature and a robust empirical assessment of proposed solutions.
6. **Developing the electronics and software** required to control the prototype in a laboratory setting.
7. **Assessing the efficacy of the device** through a structured set of experiments.

The specific, technical contributions to the medical robotics community are:

- A novel method of achieving locomotion in the colon and a detailed assessment of its efficacy.
- Insight into the design and fabrication of small scale prototype, *in vivo* robotics.
- A functional method of gaining traction on the colonic lumen and a suggested optimal solution.
- Work on controlling a mobile robotic device in a synthetic colon environment.

1.4. Thesis structure

The individual chapters are summarised below:

Chapter 2 – Literature review

This presents relevant literature, including topics such as current procedures used to inspect the colon and various locomotion techniques that could be used on a mobile colonoscopy robot

Chapter 3 – Mechanical design, fabrication and characterisation

This introduces the RollerBall concept – a novel, mobile wheeled device. The design is described, as well as fabrication and benchtop characterisation of the key mechanical components.

Chapter 4 – Gaining traction in the colon

A critical requirement for a mobile device that uses the lumen to achieve locomotion is gaining sufficient traction on the low friction lumen. This explores the challenge in detail and a suitable tread pattern is proposed after empirically assessing multiple designs.

Chapter 5 – System Integration and Open-loop control

This includes work on manually controlling the robot. The associated hardware and software are developed and a series of tests to assess the efficacy of the control strategy and locomotion technique are carried-out.

Chapter 6 – Closed-loop control

This chapter builds on the previous, manual control and describes the development of more advanced, closed-loop control to improve usability, locomotion efficacy and safety.

Chapter 7 – Discussion and Conclusions

Here the key insights into topics such as locomotion efficacy and device usability are discussed before summarising the work in a series of conclusions.

Chapter 8 – Future work

The final chapter includes suggestions for future developments on the work presented in this thesis.

Appendix

An appendix provides further detail, including datasheets.

Chapter 2

Literature review

This chapter provides an overview of relevant literature on the research of mobile colonoscopy robots. The topics covered include: the anatomy of the colon; the need for investigating the colon and the procedures currently available; the potential of using a mobile colonoscopy robot and; a summary of various locomotion techniques that could be used. The goal of this chapter is to communicate the major clinical need for an effective method of directly accessing the colon and the challenges involved, before concluding what locomotion techniques are most suited to this unique environment.

2.1. The colon

The colon, or large bowel, starts at the ileocecal valve and can thereafter be divided into several sections (Figure 2.1), starting with the caecum and appendix, followed by the ascending, transverse and descending colon. The last section is the sigmoid colon (which is positioned before the rectum and anal canal). The colon is highly variable in its size and shape, with its length ranging between ca. 1.30 m and 1.88 m in adults [11] [12] (sigmoid colon (350 mm), descending colon (200 mm), transverse colon (390 mm), ascending colon (160 mm) and caecum (40 mm) [13] [12]). Diameters range from 105 mm in the caecum to as narrow as 16 mm in other regions of the colon [14] [15]. The shape has a number of flexures (bends): two are acute (the hepatic and splenic flexures) and, on average, 9.6 are moderate ($< 90^\circ$) flexures [11], all contributing to a highly variable, tortuous shape.

The colon is sacculated³ due to the colonic haustra; particularly noticeable when the colon is distended (insufflated). The colon is partially mobile, attached to the peritoneum⁴ via flexible mesocolons⁵. The lumen is between 0.7 and 1.5 mm thick [16] and is comprised of a series of distinct, concentric layers, including: the mucosa, muscularis mucosae, submucosa and muscle layers (Figure 2.1).

³ Comprising of a series of distinct “pouches” or “sacs”.

⁴ The membrane lining the cavity of the abdomen and covering the abdominal organs.

⁵ Flat tissue connecting the peritoneum to the colon - blood vessels, nerves and lymphatics branch through this.

The tissue's frictional characteristics have a huge impact on the design and locomotion efficacy of a mobile robotic device that uses contact based forms of locomotion. As is discussed in [17], a knowledge of the characteristics are useful to:

- Determine the required stroke length to achieve effective locomotion.
- Devise an efficient and safe method of clamping to the tissue to manipulate the friction forces.
- Control the device, where knowledge of how these characteristics change with varying parameters (such as speed and normal load) is useful for the control of the actuators.

The colon is highly lubricious as it is covered with a layer of shear-thinning mucus. The resulting frictional characteristics are complex and not well understood – this will be explored in more detail in Chapter 4.

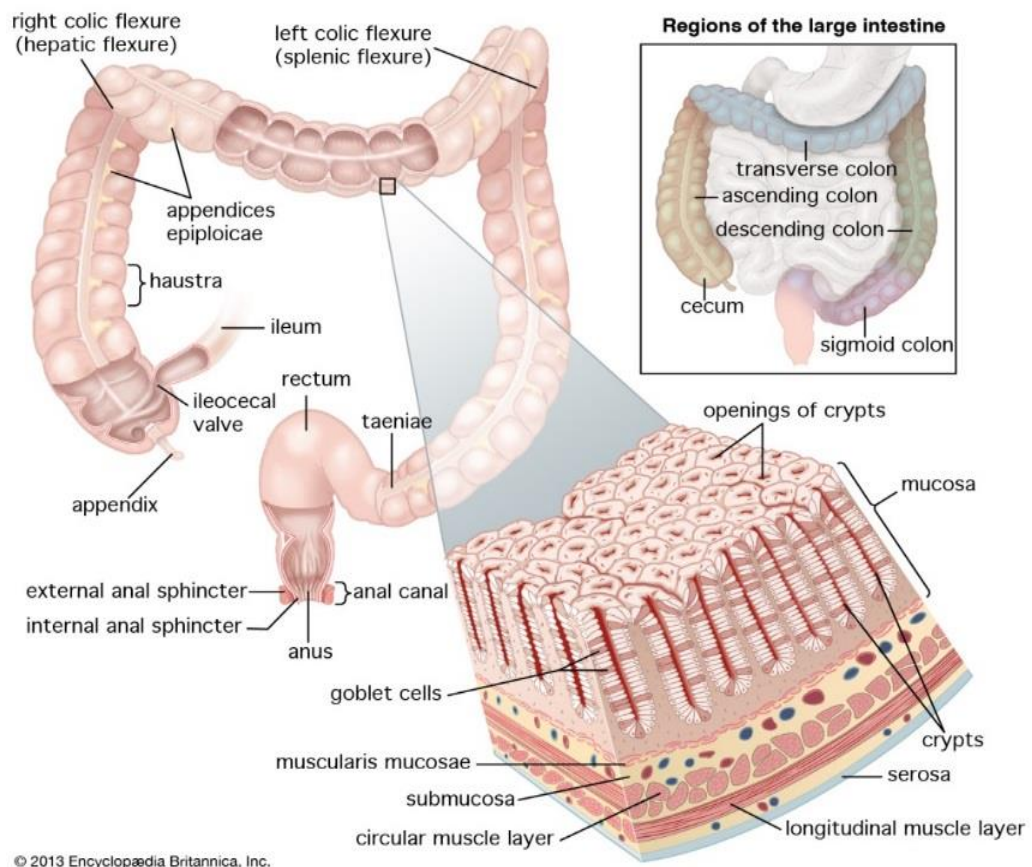


Figure 2.1 - A diagram of the large intestine (colon), showing its various segments and a cross-section of the multi-layered tissue. [18]

2.2. Colonic inspection and intervention

There are a number of diseases that can affect the colon, including inflammatory diseases such as ulcerative colitis and Crohn's disease, and the more deadly colorectal cancer – the world's 3rd leading cause of cancer related death [3]. These require diagnosis and treatment, with several different procedures available, ranging from completely non-invasive (such as computed tomography and faecal occult blood testing) to the more invasive and widely used conventional colonoscopy. These often come at significant economic cost. In Europe alone, the combined annual direct treatment costs for these are estimated at around €18 billion [1, 2]. More important than this is the effect these diseases have on quality and length of life. Worldwide, it is estimated that, annually, over 1 million individuals are diagnosed with colorectal cancer, with a mortality rate of nearly 33 % [19]. As it is with other forms of cancer, early diagnosis has a huge impact on mortality: If diagnosed at the latest stage, only 1 in 10 patients will survive longer than 5 years; if diagnosed at the earliest stage, this increases to 9 in 10 [5]. However, the physical properties of the colon and its inherent inaccessibility make directly inspecting and operating in this environment very challenging indeed. There are many factors that may lead to late diagnosis but to give an indication of the seriousness, a study of more than 1 million colonoscopies showed that 29 % of cancers were detected 'late' [20].

2.3. Current procedures

There is no doubt that having effective diagnostic and therapeutic procedures for the colon is important; the questions are whether direct access to the colon is required and if so, what is the best method of achieving that.

2.3.1. Virtual colonoscopy

If direct access to the colon is not required then Computed tomography colonography (CTC) or virtual colonoscopy may be the best solution to inspect the colon. It is one of the more modern, alternative techniques used and is specifically focused on colorectal cancer and the detection of adenomas/polyps. A virtual 3D model of the colon is produced using helical CT and advanced rendering techniques. It is then meticulously inspected by a specialist for abnormalities. Bowel preparation and colonic insufflation are both required [21].

This is an attractive procedure with seemingly few drawbacks due to its complete non-invasiveness. However, the newest, least invasive procedure is not always the most effective [22]. Table 2.1 presents the main advantages and disadvantages of CTC [21-24].

Table 2.1 - The advantages and disadvantages of Virtual colonoscopy (CTC):

Advantages	Disadvantages
Non-invasive procedure leads to significantly fewer complications and improved patient comfort/adherence.	Insufficient efficacy data. Currently, CTC has a lower sensitivity (ability to detect polyps), particularly with small polyps (< 6mm) ⁶ [21]. With polyp sizes < 6 mm, 6 – 9 mm and > 9 mm the sensitivity of CTC is estimated as 29%, 66% and 97% respectively. In comparison, the estimated sensitivity for CC is 80%, 88% and 91% respectively [23].
Bowel preparation often less intensive and sedation not required.	Poor detection of flat adenomas and general lack of histology information.
Effective at viewing entire colon, even in cases where there is severe narrowing of the colon.	Long term effects of radiation unknown, although one study estimates that there is still a risk (0.14%) of cancer post CTC [21].
Can detect extra-luminal abnormalities.	7-16% of patients who undergo CTC a conventional colonoscopy anyway [21, 23].
	Requires more frequent follow-ups.
	Is less cost effective in most cases.
	Can be time consuming due to the required collection and manipulation of data.

Although presenting some attractive advantages, two significant limitations of CTC, when compared to procedures that directly inspect/access the colon, are its inability to carry out therapeutic and robust diagnostic tasks such as polypectomies and biopsies (this is crucial for the treatment of colorectal cancer) [25] and its poor performance at detecting small or flat abnormalities (which would most likely be the case with early stage cancer). CTC is merely a diagnostic tool aimed at the detection of polyps and can augment but not replace the all-round, complete diagnostic and therapeutic procedure of something like the conventional colonoscopy.

It would appear that direct access (using a colonoscope, for example) is required the majority of the time. Some of the more common indications are listed in Table 2.2 [26].

⁶ The polyp size threshold determining whether or not a polypectomy is necessary is currently a controversial issue. Most experts recommend the threshold to be > 6 mm due to the prevalence of cancer in patients with diminutive adenomas being approximately 0.1%.

Table 2.2 - Colonoscopy indications [13]:

Colonoscopy indications
Evaluating an abnormality found using barium enema.
Evaluation of unexplained gastrointestinal bleeding.
Unexplained iron-deficiency anaemia.
Investigating the colon for synchronous cancer or neoplastic polyps.
Precise diagnosis of chronic inflammatory bowel disease.
Unexplained, clinically significant diarrhoea.
Diagnosis and treatment of colonic lesions.
Foreign body removal.
Excision of colonic polyp.
Decompression of acute nontoxic megacolon or sigmoid volvulus.
Balloon dilation of stenotic lesions.
Palliative treatment of bleeding neoplasms.
Marking neoplasms for localization.

It is easy to see why there are estimated to be more than 14 million colonoscopies carried out around the world each year [27]. Due to the nature of the procedure, there remain several contraindications to performing a conventional colonoscopy, the primary one being severe inflammatory bowel disease. In these cases, the colonic wall is particularly sensitive to perforation [13] and alternative procedures are required.

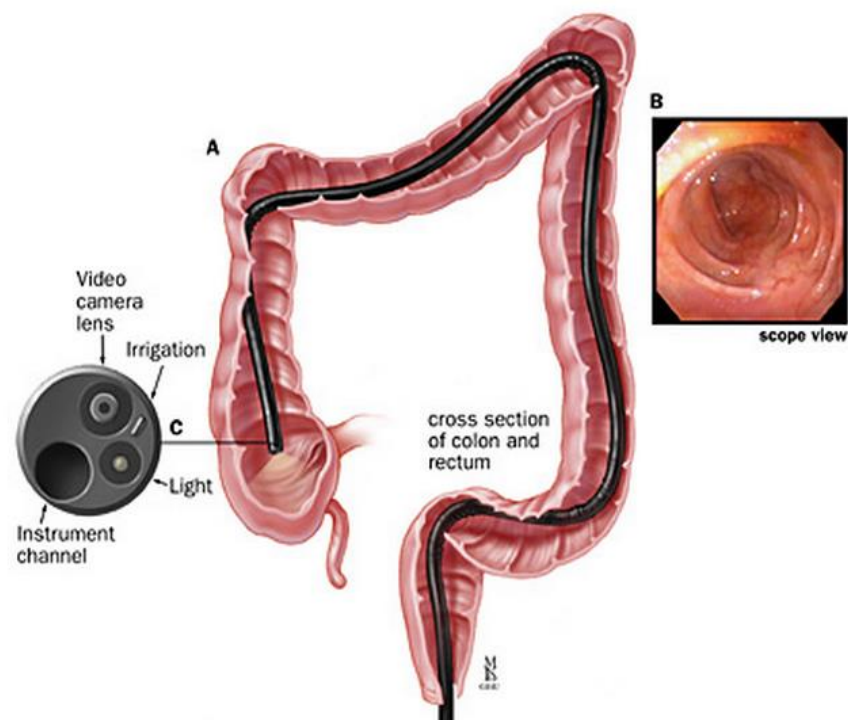
2.3.2. Conventional colonoscopy

By far the most common invasive procedure for inspecting the colon is the conventional colonoscopy; this is the benchmark that any alternative should improve on. The total colonoscopy is a procedure by which the entire colon can be inspected and, in some cases, allows for local therapeutic action. It was first described by Shinya and Wolff in 1969, bringing about the development of an effective means of diagnosing diseases and carrying-out small procedures, such as polypectomy⁷, *in situ*. Since then the colonoscopic procedure, and the equipment used, have improved significantly, resulting in it becoming the “gold standard” for the detection and prevention of colorectal neoplasms, as well as the diagnosis of a number of colorectal diseases [13].

⁷ Removal of an abnormal feature called a polyp.

2.3.2.1. Colonoscopy equipment

The conventional colonoscope is a flexible tube, 130-170 cm long and 1.3 - 1.5 cm in diameter. It is fitted with an actuated section at the distal end to facilitate passage around the tortuous colon. This can be bent in any direction using the steering controls. The core of the colonoscope usually contains a channel for tools and cables for the various lights and cameras present at the tip of the instrument (Figure 2.2). Additional equipment is required to carry out a colonoscopy, including a display for the real-time images from the colonoscope and a unit to regulate pressure within the colon.



A: Position of the colonoscope in the colon; B: endoscopic view;
C: detail of the colonoscope tip

Figure 2.2 - Colonoscope within the colon, including detail of the colonoscope tip. [28]

2.3.2.2. Outline of the current procedure

When required, a total colonoscopy procedure consists of four discrete phases: *bowel preparation*, *sedation*, *colonoscope insertion* and *colonoscope withdrawal* [13]. These are briefly described below:

Bowel preparation

Bowel preparation is an unpleasant but essential part of the colonoscopy, required to improve vision of the colonic mucosa. Most preparation methods involve the administration of an oral laxative the day before the colonoscopy in order to purge the colon of any residual matter. The intake of clear fluids during this period is highly encouraged to prevent dehydration. Most procedures involve the ingestion of PEG-ELS (a balanced electrolytic solution containing polyethylene glycol) or Phosphosoda (sodium phosphate). A strict dietary regime is then followed, with regular ingestion of the selected laxative and electrolyte solution. Antispasmodics are usually administered during the procedure as circular muscle spasticity is known to impair vision of the colon.

Sedation

Most colonoscopy procedures can be performed successfully without sedation but, endoscopists are encouraged to have a flexible attitude towards patient sedation. This is because of the anxiety understandably involved in the diagnosis of diseases, embarrassment due to the invasiveness of the procedure and pre-empted pain.

Colonoscope insertion

It is common for colonoscopists to perform a total colonoscopy hundreds of times and yet it remains a difficult technique to perfect. It is said that an average of 275 procedures are required before achieving competence [29]. The procedure is difficult because it involves the manual insertion of a flexible tube into a compliant, sensitive, tortuous-shaped and mobile colon using an external force. The exact technique used varies but what is clear is that the procedure requires significant expertise, “feel” and dexterous manipulation of the colonoscope.

In brief, a colonoscopy involves the insertion of a colonoscope into the anus with the aim of reaching the caecum and thus observing the whole colon. This requires the simultaneous controlling of the steering wheel controls with one hand and manual insertion of the colonoscope shaft with the other (Figure 2.3). The colonoscope advances when a combination of external force and internal tip steering is used. The external application of pressure⁸, and combined insertion and withdrawal movements, are used to control the buckling of the device and prevent undesirable loops forming. These loops often prevent completion of the procedure, can increase patient discomfort and can even result in perforation of the colonic wall (Figure 2.4). To aid in the advancement of the colonoscope

⁸ To the abdomen via the surgeon’s hand.

and visualisation of the tissue, the colon is distended using a pressurized gas (usually air or carbon dioxide). This distension often causes patient discomfort but performs an essential function (that warm water could also achieve).

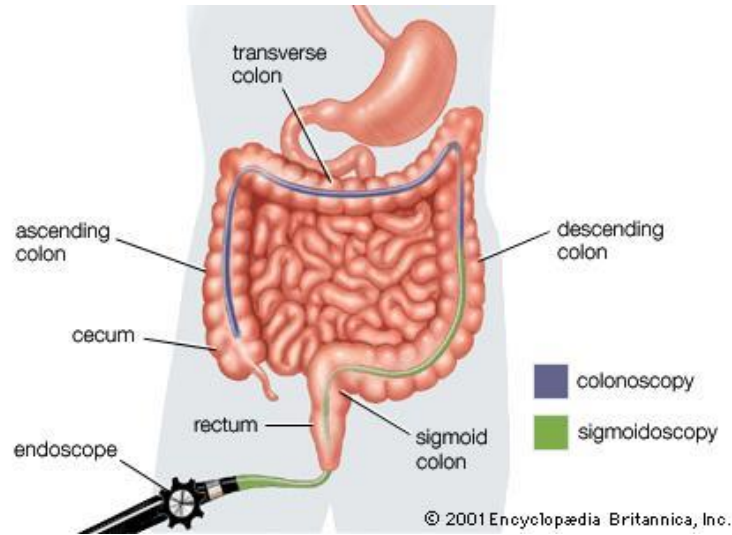


Figure 2.3 - Simplified diagram showing colonoscope insertion. [30]

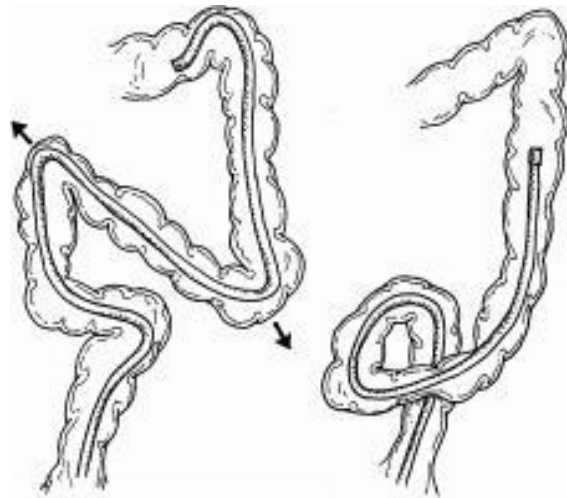


Figure 2.4 - Diagram showing the unwanted stretching of the colon due to lack of control of the colonoscope. [31]

Colonoscope withdrawal

In order to investigate all parts of the colon, every effort is made to reach the caecum. Although some diagnosis and intervention (such as biopsies and polypectomies) are carried out during the insertion of the colonoscope, most are carried out during withdrawal so that maximum attention can be given to diagnosis rather than colonoscope manipulation.

Meticulous inspection of every part of the colon is carried out to reduce the adenoma miss rate, a known indicator of procedure quality. Withdrawal time is expected to be in the region of 6 – 10 min [32] with strategies, such as changing the position of the patient, being used to improve vision of difficult to access areas. Areas that are particularly difficult to view include acute flexures and behind haustral folds.

2.3.2.3. Performance/efficacy

Colonoscopies are currently the best means of investigating the inside of the colon and have made a significant contribution to the reduction in deaths related to colorectal cancer. Although it is a well-established and widely practised procedure, it is far from perfect.

The quality of the procedure can be determined by the polyp miss rate and the caecal intubation⁹ rate [33]. On average, the polyp miss rate is in the range of 4-12% [3] for polyps greater than 6 mm in diameter, with some figures rising up to 22-27% for polyps less than 6mm in diameter, often resulting in the need for a back-to-back colonoscopy [34, 35]. Colonoscopy completion rates vary considerably. In a study of over 6000 colonoscopy procedures, 11% were considered incomplete [33]. That figure rises to 35% in another, larger study [36]. Although the completion rate is affected by factors such as insufficient bowel preparation, severe discomfort and presence of severe colitis [37], the difficulty of the procedure itself (and the associated level of experience required) is known to have a large impact [36] [38].

2.3.2.4. Complications

Despite the fact that no incisions are required to perform a colonoscopy, there are several types of complications can occur during the procedure.

Firstly, injuries to the colorectal surgeon performing the task can occur. In a study of 608 practicing colorectal surgeons, at least one injury or some level of pain was reported by 226 of the surgeons, supposedly due to carrying out colonoscopies. The estimated risk of injury, if more than 30 colonoscopies are carried out per week by a single surgeon, was approximately 47%. Injuries were mainly due to torqueing of the colonoscope during insertion and continuous use of the control dials. Some injuries were also caused by the posture of the surgeon during the procedure [39].

For the patient, a colonoscopy is uncomfortable and is sometimes considered painful. A study of 426 colonoscopies noted that 44.1% of patients reported some degree of pain [40].

⁹ Reaching the caecum with the colonoscope.

In one study, approximately 25% of patients reported bloating and 5-11% reported abdominal pain [41]. This discomfort is predominantly caused by air insufflation (bloating) and stretching of the colonic tissue when the colonoscope traverses flexures in the colon or during undesirable colonoscope looping; an indication of this discomfort is that one study reported 88.9% of procedures are performed under sedation [6]. In a large study carried out in Canada, the chance of a serious complication occurring was said to be 0.28%. Other studies have recorded much higher serious-complication rates of more than 1% [42, 43]. The most common of these was perforation of the colonic wall, the second being post-polypectomy bleeding. Again, the quality of the procedure, in this case measured by complication rate, was said to be dependent not only on the equipment but on how well practiced the colonoscopist is – because of the difficulty of the procedure [36, 41]. Perforation of the colonic wall is due to mechanical forces applied by the surgeon, acting on the tissue through the colonoscope [41]. The majority of applied forces have a magnitude of approximately 5 N, with torque values of ± 0.2 N.m [44].

It is clear that there is a great need to improve the current procedure due to its less than ideal performance and its numerous complications. This has been an area of significant research interest – Tapia-Siles et al. [25] found more than 200 related devices and novel alternatives. Some of these will be explored in the following sections.

2.3.3. Alternative colon distension: Hydro-colonoscopy

Hydro-colonoscopy involves the use of a warm, clear liquid for colonic distension in lieu of a gas (typically carbon dioxide). This technique was introduced to improve on the conventional colonoscopy by reducing patient discomfort in unsedated cases and by improving caecal intubation rate [45]. The advantages and disadvantages hydro-colonoscopy has versus carbon dioxide colonoscopy are shown in Table 2.3.

Table 2.3 - The advantages and disadvantages of Hydro-colonoscopy:

Advantages	Disadvantages
Reduced overall discomfort and therefore less sedation required [45-47].	Residual matter in the colon is suspended in the liquid thus obscuring vision [46, 48]. Longer procedure time, primarily due to the need for removing dirty liquid during the procedure [46, 47].
Increased caecal intubation rate in unsedated studies [45] (provided sufficient bowel preparation carried out [46]).	
Reduced post-procedure recovery time [49].	
Reduced elongation of the colon and less exaggerated angulations at the flexures (both present in some air insufflation procedures). This results in an increased ease of insertion (fewer abdominal compressions or patient position changes required) [47-49].	

Currently, the advantages far outweigh the disadvantages and therefore hydro-colonoscopy was a key inclusion in the CoDIR proposal.

2.3.4. Augmenting the colonoscope

Significant work has been carried out on the conventional colonoscopy procedure with the aim of maintaining the core concept but improving on its various drawbacks. Some of the current, major innovations include:

Double balloon enteroscope [50]

This is primarily used for investigation of the small intestine but can be used for difficult colonoscopy cases. A conventional colonoscope is fitted with an external balloon or “over-tube.” This over-tube can be inflated to distend the surrounding tissue and any undesirable loops in the colonoscope are subsequently straightened. This is an effective means of increasing caecal intubation rates in difficult colonoscopies but, it is associated with long procedure durations.

Colonoscope with adjustable stiffness [51]

This is essentially a conventional colonoscope with the simple inclusion of variable shaft stiffness. A low stiffness distal end allows negotiation of bends in the colon whilst a higher stiffness proximal end reduces the chances of loop formation. This has been shown to reduce patient discomfort and as a result, increase the caecal intubation rate.

Cap-fitted colonoscope [52]

Polyps are missed even with meticulous inspection of the colon, mainly because the tortuous shape of the colon and the presence of haustral folds. This innovation involves the fitting of a clear plastic cap to the tip of the colonoscope in order to flatten the surrounding haustral folds and improve mucosal exposure. This has been shown to improve polyp detection, particularly with polyps less than 6mm.

Third-eye retroscope [53]

This is another innovation aimed at improving polyp detection rates by improving vision of the tissue behind haustral folds. The conventional colonoscope is fitted with a “third-eye retroscope,” a camera that advances in front of the colonoscope and faces backwards. This allows visualisation of the blind-spot: the tissue immediately behind the colonoscope.

Although there have been a number of successful improvements to the colonoscope, they have not managed to completely alleviate the many factors that result in the colonoscopy’s complications and suboptimal performance.



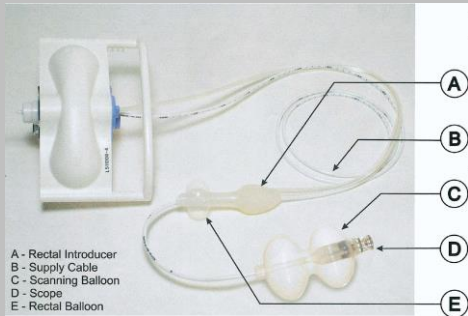
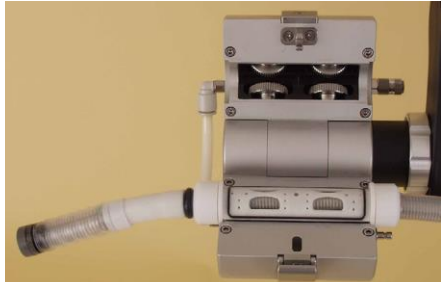
2.3.5. Robot-assisted colonoscopy

The use of robotic systems has become increasingly popular in many industries for a number of reasons, including their high position accuracy and movement repeatability. The use of robotics could significantly improve the colonoscopy procedure and there are a number of ways this could be done:

2.3.5.1. Automating the conventional colonoscope

Many of the drawbacks associated with the conventional colonoscopy can be attributed to the manual, external propulsion mechanism. The large forces and undesired colonoscope looping apply unnecessarily high forces on the colon. Having the colonoscope propel itself from within the colon, using the tissue as an anchor, could significantly improve the procedure as a whole [54]. Four such devices are described in Table 2.4:

Table 2.4 - Examples of automated / robotic colonoscopes:

Device	Description
<p>EndoCrawler [54]</p> 	<p>The EndoCrawler uses pneumatic bellows to propel the device through the colon. The inflated bellows extend sequentially backwards to push against the colonic walls, thus providing a propulsive force. This form of “inchworm” locomotion is inefficient as it relies on the bellows making contact with the tissue and for minimal slip to occur. Mobility around acute bends is also limited.</p>
<p>Device with “inchworm” [55]</p> 	<p>This device also uses an inchworm form of locomotion to traverse the colon. The device comprises of a steerable tip to bend around corners, a pneumatic bellow to extend the body and pneumatic clamps at either end to prevent the device slipping backwards during forward propulsion. This devices ability to traverse bends, as with [54], is limited and in this case the clamping mechanisms have been shown to damage the colonic tissue.</p>
<p>Aer-O-Scope [56]</p> 	<p>The Aer-O-Scope relies on a pressure differential inside the colon to advance the device. By controlling this differential, the direction and speed of the scope can be determined. A seal is maintained using double inflatable balloons at the end of the device. This device showed some success in traversing the colon but, there was a high level of pain recorded by some patients and the device itself can only be used for diagnosis as no biopsy channels are included.</p>
<p>Invendo SC20 [57]</p> 	<p>The Invendo SC20 is a computer-controlled device that uses an “inverted sleeve” mechanism to propel itself through the colon. An external driving unit advances the tip of the device by propelling a flexible inner sleeve. This rolls back on itself as it extends, resulting in the inverted-sleeve locomotion. The device currently works showing reduced patient discomfort, but it is an overall slow procedure and has a bulky actuation mechanism.</p>

While some of these devices succeed in reducing colonoscopy complications and improving other performance aspects associated with the procedure, they do not fully address the issue of patient discomfort and mobility within the colon. Furthermore, the size of the devices and the procedure duration still remain an issue.

2.3.5.2. Capsule endoscopy

One novel solution to the issues facing the conventional colonoscopy, and accessing the gastro-intestinal (GI) tract in general, is the use of capsule endoscopic technology, a solution many professionals believe to be the future of minimally-invasive GI screening [58]. In most cases this involves the passive¹⁰ locomotion of a small, wireless capsule through the GI tract, while *in vivo* images are recorded and subsequently inspected by an expert for abnormalities. This technology is an exciting area of development and, provided it can be refined, will “rapidly and significantly advance our ability to screen and survey the GI tract noninvasively” [58].

The primary advantage of capsule technologies is their minimally-invasive aspect [59]. This would significantly reduce patient discomfort and procedure related complications such as perforation of the colonic wall and could therefore increase patient tolerance. Additionally, due to their small size, these capsules could potentially increase intubation rates in difficult colonoscopies [60, 61]. Capsule technologies fall under two main categories: *Passive capsules* and *Active capsules*.

Passive capsules

Passive capsules (Figure 2.5) cannot be controlled but are instead swallowed and advance due to the natural peristalsis present in the GI tract. Although the simplicity of this type of capsule is attractive, it is unlikely to provide sufficient vision of all areas of the surrounding tissue because of the lack of movement control [58, 60], resulting in unreliable diagnosis in 20% of trials [61]. This is one of the most important aspects of a colonoscopic device because its primary function is the diagnosis of often difficult to identify colonic abnormalities, requiring precise control of the location and orientation.



Figure 2.5 - Pillcam, a common passive capsule used to investigate the GI tract (ca. 11 x 32 mm). [60]

¹⁰ Not requiring any foreign internal or external locomotion mechanism.

Active capsules

Active capsules aim to improve on the shortcomings of passive capsules by giving the endoscopist some control over the capsule's movement, thus giving them the potential to carry out therapeutic procedures and vision of specific regions. This control is achieved by incorporating a locomotion mechanism and other tools and sensing modules into a capsule like device (Figure 2.6) [61]. Active capsules can be divided into two subcategories: *External* and *Internal* locomotion techniques [59].

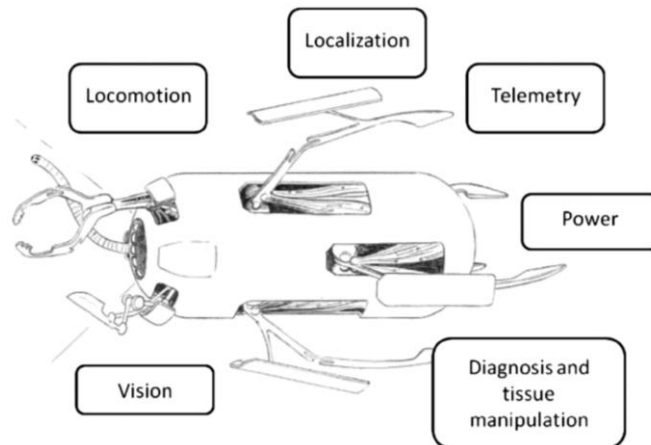


Figure 2.6 - Illustration of an active capsule platform showing key requirements [61]

External (magnetic) locomotion

This involves the use of an *ex vivo* magnetic force to move the *in vivo* capsule. The capsule shown in Figure 2.7 is an example of this. It contains carefully positioned permanent magnets within its chassis and is ingested by the patient. An externally based, 6-DOF robotic arm with a high strength magnet is then used to manipulate the position of the capsule inside the body by means of the magnetic field.

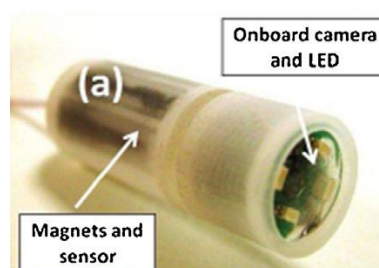


Figure 2.7 - A capsule controlled using an external magnet field [62]

This is a minimally-invasive, short duration procedure but has several issues [62]:

- The magnetic field is temperamental and may be weak with patients who have a high BMI.

- The presence of obstacles could result in locomotion inefficiencies and an overall loss of control of the device.
- It does not provide a stable platform (because it lacks an anchoring mechanism) and so the use of tools is presumably limited¹¹.

Internal locomotion

The limitations of passive capsules, and active capsules with a form of external locomotion, highlight the need for an even more advanced solution: a fully mobile, semi-autonomous diagnostic and therapeutic robotic capsule [61]. This is an attractive solution for combined colonic diagnosis and therapeutic intervention that could potentially alleviate most, if not all, of the drawbacks and limitations of current colonoscopic procedures.

Ideally, such a device would be: small; robust; extremely mobile; have an efficient, semi-autonomous locomotion mechanism and would provide a stable platform for the use of cameras and biopsy tools. The patient would feel little to no discomfort due to the relatively small forces needed by the device to propel itself, and the consequent lack of colonic straightening or stretching. These reasonably small forces may allow such a device to be used in patients who previously were unable to have a colonoscopy due to inflammatory bowel diseases. The colonoscopist would be able to fully control the device with relative ease, reducing physical stress and allowing more attention to be given to the diagnosis. Thus, the high mobility, small size and option of having both forward and rear facing cameras, could also significantly reduce polyp miss rates. The development of the fully active (conceptual) capsule shown in Figure 2.6 requires extremely small, complex mechanisms and electronics that exceed the limits of current technology. A more plausible approach is to not restrict the size and shape to a capsule. The resulting devices could simply be called “Mobile colonoscopy robots”.

2.4. A mobile colonoscopy robot

The development of a fully mobile, semi-autonomous diagnostic and therapeutic robotic platform could be a vast improvement on conventional colonoscopy. The use of a warm fluid (hydro-colonoscopy) could further improve colonic investigation by increasing caecal intubation rates and by reducing patient discomfort. The focus of the CoDIR project is to use a combination of these two methods to realise an optimum solution to colonic inspection

¹¹ In addition to this, the capsule will always be pressed against the side of the lumen nearest the external magnet, further reducing the efficacy of on-board tools.

and intervention. Below is a list of the general requirements of such a robotic device for use in a hydro-colonoscopy environment.

2.4.1. Device requirements and environmental challenges

The mobile robotic platform will be required to traverse a very unique and challenging environment. This is particularly true in the case of hydro-colonoscopies, where the device will not only be operating in a sensitive, compliant, tubular environment with varying shapes and sizes, but will also be fully submerged in a liquid. The device may use the surrounding tissue to push against or anchor itself. This will introduce new challenges considering the anatomy: the tissue is sensitive to perforation, extremely compliant, irregularly-shaped and has a low coefficient of friction due to a thick layer of mucus – the lumen giving rise to a complex set of frictional characteristics. Alternatively, the device could swim through the liquid medium with little to no contact with the surrounding tissue (provided there is sufficient colonic distension). A device operating in such an environment would have a number of requirements for it to be successful. The more important requirements with the reasons for each, are shown in Table 2.5 and continued in Table 2.6:

Table 2.5 - General requirements for a mobile robotic platform for hydro-colonoscopy.

Requirement	Description	Justification
Small size	Have a rigid diameter ideally less than 26 mm and a length less than 40 mm [8, 14, 15, 63].	Studies on the anatomy of the colon estimate a minimum colon diameter of 26 mm, giving an indication of the maximum width/diameter of a rigid robot. A short length would improve mobility around acute flexures.
High speed	Complete a standard colonoscopy in a one hour timeframe, preferably reaching the caecum in 6 – 8 min [63].	In order to be a viable replacement for a conventional colonoscope, a MCR should not lengthen the already time consuming procedure as this could increase procedural complications and costs.
High mobility	Traverse the full length of the large intestine; turning corners, stopping, starting and reversing its direction at the caecum [63].	Mobility is crucial in this case as it would directly affect the diagnostic performance of the device. The mobility is also crucial in ensuring successful caecal intubation.
Safe	Cause little to no damage to the surrounding colonic tissue [63].	The colonic tissue is sensitive, particularly in patients suffering from diseases such as diverticulosis. The interaction of the device with the colon, in terms of material chemistry and physical contact, must not cause damage to the tissue. As with all other <i>in vivo</i> medical devices, this is of paramount importance to this device.

Table 2.6 - General requirements for a mobile robotic platform for hydro-colonoscopy (Continued).

Requirement	Description	Justification
Be adaptable	Operate in a wide variety of patients.	In order to be successful, the device should be able to operate in patients with a large variability in colon diameter, shape and tissue surface features.
Provide a stable platform	Provide a stable platform for the use of cameras and biopsy tools.	In order to successfully view details of the colon with an on-board camera, a stable platform is required with a smooth locomotion technique. Additional therapeutic tools require a stable, anchored device in order to operate accurately and efficiently.
An effective locomotion technique	Have a robust locomotion mechanism and appropriate locomotion technique [63].	Locomotion is potentially the greatest challenge involved in designing such a device. The technique used should be appropriate to the unique environment of the colon; it must provide efficient and reliable locomotion <i>in vivo</i> (despite the tissue frictional characteristics and mechanical properties). The locomotion technique will determine the procedure length and overall effectiveness of the device [63].
Be robust	Overall robust device and if possible, an included failsafe.	Failure <i>in vivo</i> would have serious implications. A failsafe may have to be included to manage the potential risks of device malfunction.
Overcome tether drag (thrust)	The device should have the ability to pull a tether behind itself, achieving an average thrust of at least 1 N ¹² to overcome the associated drag.	Ideally, an <i>in vivo</i> device should be wireless as it would increase biocompatibility and device mobility. However, most devices include a tether as it simplifies on-board electronics, power supply and provides a means of manually removing the device in the event of a malfunction (failsafe).
Easy to use	The device should operate in the colon with minimal input from the user.	A significant cause of many of the drawbacks of colonoscopy is the difficulty of the procedure (and the required experience) [36] [38]. A procedure that is easy to perform will allow more attention to be given to important tasks such as diagnosis and surgical intervention.

These major requirements will be used to assess the effectiveness of current devices and the design of future concepts.

¹² This is an estimate from preliminary experiments conducted by researcher in the CoDIR group.

2.5. Locomotion techniques

It is clear that choosing an appropriate form of locomotion is crucial for the effectiveness of the device. It must take into account the unique geometry of the environment, as well as the tissue and lumen properties. Although there has been significant research focus on the design of active devices to traverse the intestine – using a number of different forms of locomotion – no device has fully succeeded due to the challenging environment. Furthermore, substantial work has been done on devices operating in a collapsed colon and less on devices designed to operate in a distended colon¹³. The tissue properties and colonic environment vary considerably between a collapsed and distended colon, therefore the design features will vary considerably too.

There are two broad classes of locomotion technique that could be used: *Contact-based* locomotion and *Swimming* in the liquid filled colon (having limited to no contact with the tissue). This section includes a number of designs that have been (or could be) used for an active, mobile colon-based device. The focus of this thesis is to design a device for use in a hydro-colonoscopy procedure and so the effectiveness of each design for use in this *specific* environment will be reviewed in the following format: Description of the technique; an example device and; whether it is feasible (when considering this context).

2.5.1. Swimming forms of locomotion

The use of a liquid to distend the colon during hydro-colonoscopy is a relatively new technique that has yet to be widely adopted. Consequently, no robotic devices purposefully built for swimming in the tortuous, fluid-distended colon currently exist. One of the primary advantages of hydro-colonoscopy is the reduced patient discomfort. Intuitively, if a device could be designed to swim within the colon with limited to no contact with the tissue then discomfort could be further reduced, as would other complications such as tissue damage. As there are currently no hydro-colonoscopy specific robots, general swimming techniques that are used, particularly in small robotic devices, will be investigated.

2.5.1.1. Conventional propeller

Description: Using conventional propellers to provide propulsion.

Example: Carta et al. [64] developed a propeller-based capsular device for use in the fluid filled stomach. The neutrally buoyant prototype capsule (15 x 40 mm), shown in Figure 2.8,

¹³ Additionally, no recorded work has been found on devices designed to operate in a fluid-distended colon (hydro-colonoscopy).

comprises of four propellers (3 mm diameter), each powered by a DC motor (4 x 8 mm, Didel MK04S-24).

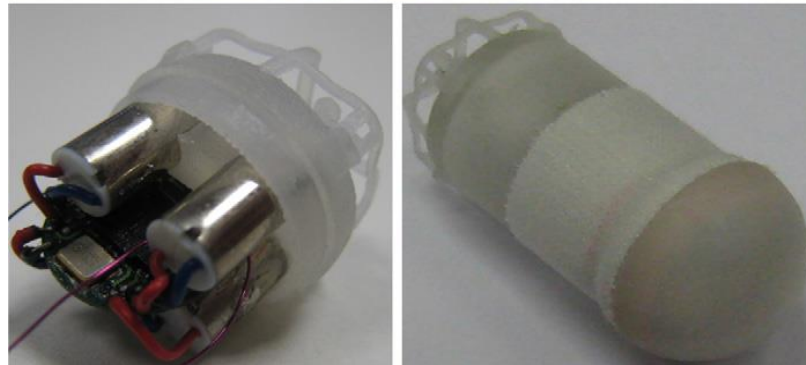


Figure 2.8 - A device powered by four conventional propellers. [64]

Feasibility: Tests showed “satisfactory results in terms of controllability” but “limited autonomy” with the operator controlling the device manually with a joystick [64]. Although this capsule originally had a different application, such a design could be used in a hydro-colonoscopy procedure. The small size and its controllability mean that it has great potential to traverse the tortuous fluid filled colon. However, limitations such as low thrust (likely preventing the use of a tether) and the restricted space for on-board tools suggest that it is not suitable for this specific application.

2.5.1.2. Ring thruster

Description: Replacing conventional propellers with ring propellers as a form of propulsion.

Example: Kennedy et al. [65] describe the design of a ring propeller, shown in Figure 2.9. This differs from a conventional propeller in that there is no central hub connecting the blades to the drive shaft. Instead, the blades are connected to an outer ring which is the rotor of an electric motor. A stator ring around rotor completes the propeller unit.

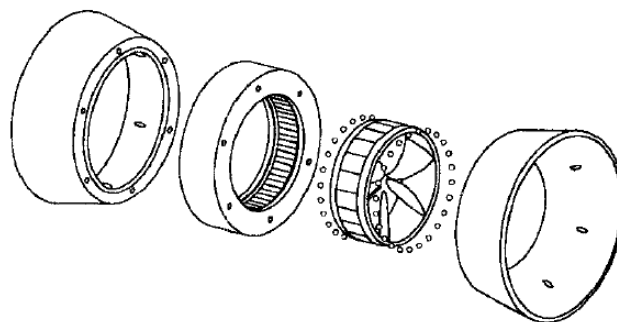


Figure 2.9 - An exploded view of a ring propeller. [65]

Feasibility: It was seen that these propellers were between 40 and 80% more efficient than alternative, conventional propellers. Other advantages of ring propellers include [66]:

- Compact mechanism due to the exclusion of gearing and drive shafts.
- Housing of the blades within the motor unit improves the safety aspect.
- The design allows for close proximity, counter rotating propellers.

Little work has been done on miniature versions of this type of propulsion. The manufacture would undoubtedly be challenging but, if an efficient motor can be manufactured and the thrust is scalable from the larger ring propellers previously tested, this offers a promising solution to propelling a colon-based capsule.

2.5.1.3. Rotating helix

Description: Rotating a helix will provide thrust as the thread-like structure pushes against the viscous fluid medium.

Example: Chen et al. [67] designed the device shown in Figure 2.10. It is designed for use in an endovascular environment and so must be very small (ideally < 3 mm). It has four rotating helices to propel and steer the device.



Figure 2.10 - Example of a device that uses rotating helices. [67]

Feasibility: These devices can be significantly miniaturized and use flexible tails/helices and so could provide an attractive, biocompatible solution to swimming within small, *in vivo* environments. Such devices do, however, have significant disadvantages, including: the predicted thrust force is very low and the propulsion is more effective in a viscous medium, not the watery medium present in hydro-colonoscopy. A device with a helix diameter of 5 mm has a thrust of approximately 6 mN at 200 rad/s [68], much too low for a tethered device.

2.5.1.4. Pressurized jet

Description: Using a simple, high pressure jet of water to produce thrust (from the inertial forces of the accelerated water).

Example: Mosse et al. [63] developed the device shown in Figure 2.11. This was more of an internally propelled colonoscope than a fully mobile capsule device, although the propulsion method could be used for a capsule device if a tether is included. Mazumdar et al. [69] designed and built the compact, highly manoeuvrable device shown in Figure 2.12. The robot steers itself by means of on-board centrifugal pumps. Although these are used for steering, they could also be used as a form of primary propulsion in a similar device such as that stated in [70], which has four eccentric rotor pump units based on the Downingtown-Huber design.

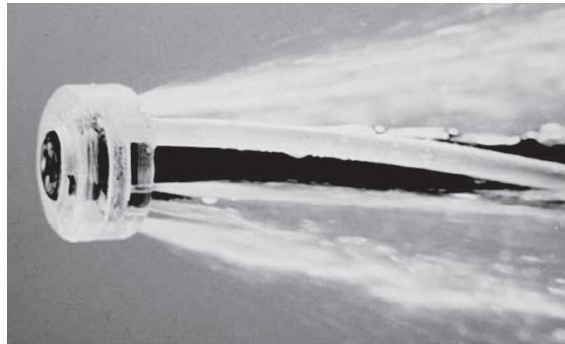


Figure 2.11 - An example of a device that uses a pressurized jet. [63]

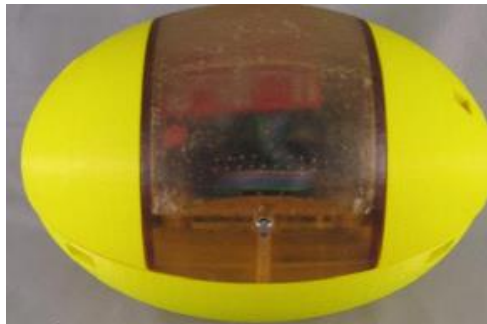


Figure 2.12 - A device that uses on-board centrifugal pumps. [69]

Feasibility: An attractive feature of using pressurized water jets for propulsion is that, like conventional propellers, they can be easily controlled in terms of direction and speed by using electronic valves. This in turn makes devices controlled by them highly mobile [69]. There is also an absence of external rotating parts, such as propellers, which is expected to improve the safety aspect. However, the difficulty of achieving sufficient thrust arises when such devices are scaled-down for use *in vivo* because of their inefficiency (50% [70]). The well-known fact remains that jet-propulsion is more suited to low speed applications, and propellers to high speed applications. Additionally, on-board pumps attain a relatively low

thrust for their size, with the 25 mm diameter pumps in [69] only achieving 0.125 N. An alternative is using a tether to transmit the pressurized fluid from an external pump to the device, as in [63]. This has the disadvantage of high drag from the tether (especially in the tortuous colon)¹⁴. Furthermore, the tether would have to be up to 2 m long whilst being as thin as possible. Having sufficient flow through such a tube would require a very high pressure. The device in [63] used 20 Bar and only managed to move a distance of 300 mm proximal to the anus before resistive forces became too large. Some minor tissue damage was seen and would be expected to worsen if the jet pressure was increased to the required amount.

2.5.1.5. Vortex rings

Description: Loosely inspired by the propulsion of squid and jelly fish, this involves the generation of traveling vortex rings using pulsed jets of water through a narrow orifice.

Example: This form of propulsion was investigated by Mohseni et al. [71], as well as a number of other authors. It is said that this form of pulsed jet is more efficient than a steady jet of equivalent mass flow rate, and so aims to improve on the previously mentioned pressurized-jet designs. A simple piston pump is used to firstly draw in water and then rapidly eject the water through the same orifice. As the stream of water travels out the orifice it wraps-up into a traveling vortex ring. This procedure is repeated in short succession to achieve a row of vortex rings and a positive net thrust (Figure 2.13).

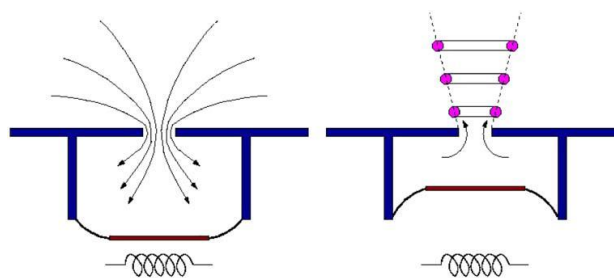


Figure 2.13 - The generating of vortex rings. [71]

Feasibility: This form of locomotion improves on the pressurized-jet's low efficiency, whilst maintaining the same advantages of control and biocompatibility. However, insufficient work has been carried on scaled-down versions of this propulsion method and as such, the achievable thrust is still relatively low compared to the propeller alternatives. In [72], a 25 mm piston, actuated using a voice-coil, produced a maximum thrust of approximately 70 mN. This value was expected to rise to approximately 250 mN if an improved voice-coil

¹⁴ A conventional tether containing thin electrical wires would likely have a smaller diameter and, potentially, lower stiffness (improved flexibility).

actuator was used. Therefore, significant work would need to be carried out in order to achieve the desired 1 N from a pump with a diameter less than 25 mm.

2.5.1.6. Fins (fish-like)

Description: Simple fish-like locomotion involving side-to-side movement of a fin. Some use a propulsive wave travelling down the length of the body and/or fin to provide a net forward thrust.

Example: Guo et al. [73] developed the device shown in Figure 2.14. It is designed to mimic the undulating swimming style of fish, where a propulsive wave is propagated down the body and/or fin. Ionic exchange Polymer Metal Composites (IPMC) actuators were used to achieve the motion. Wang et al. [74] developed a similar device, except Shape Memory Alloys (SMA) were used with an elastic energy storage mechanism to improve actuation efficiency (Figure 2.15). Takagi et al. [75] designed a robot to mimic the swimming style of rays (Rajiform swimming). They achieved this using multiple IPMC actuators positioned parallel to each other down the length of the fin (Figure 2.16). Actuating them sequentially produced a traveling wave which then resulted in a propulsive force. Kosa et al. [76] designed a swimming device that propels itself by means of a travelling wave, produced using piezo-electric micro-actuators (Figure 2.17).

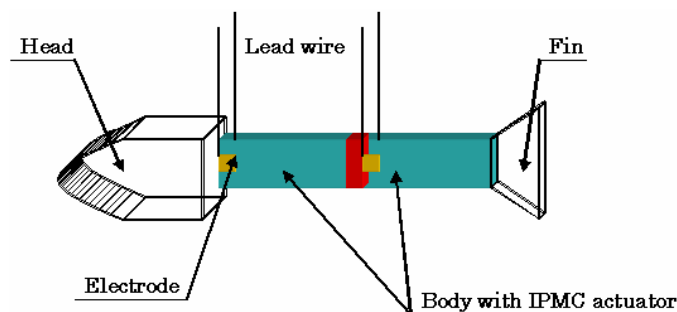


Figure 2.14 – Example #1 of a simple finned device using IPMC actuators. [73]

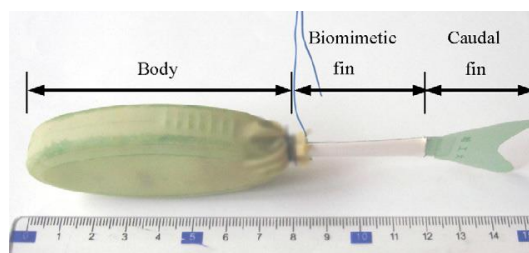


Figure 2.15 - Example #2 of a simple finned device using SMA actuation. [74]

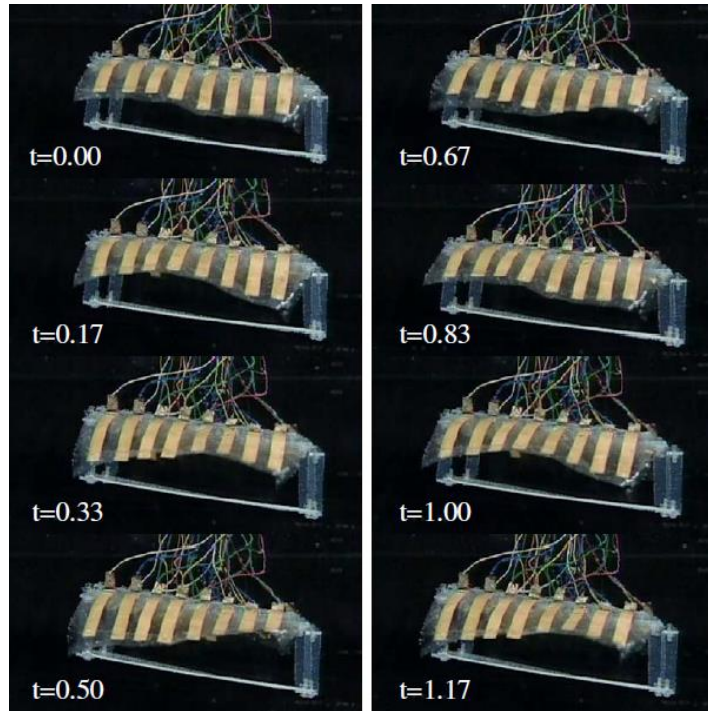


Figure 2.16 - Rajiform swimming using a flexible fin. [75]

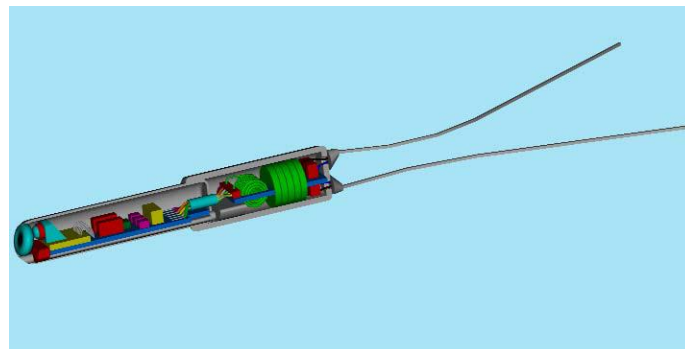


Figure 2.17 - Example #3 of a simple finned device. [76]

Feasibility: Fish-like propulsion is said to more efficient than propeller based propulsion, with the added advantage of a smaller turning radius [74] (a clear benefit for a device operating in the tortuous colon). The propulsion mechanism could be made to be simple and compact, potentially allowing these devices to be significantly miniaturized. Furthermore, the flexible nature of the devices means they would increase their feasibility for use in sensitive, constricted areas. However, swimming using a fish-like form of locomotion also has its drawbacks, the most notable is that, while recorded velocities were high (up to 112 mm/s in [74]), the propulsive forces of such devices are very low (3.75×10^{-4} N [73]). This severely restricts the possibility of tethered devices as they would most likely have insufficient thrust to overcome the associated drag. In hydro-colonoscopies there may be air pockets and/or stenosis of the colon and a swimming device would struggle in these cases, reducing its overall feasibility for practical use.

2.5.1.7. Summary – swimming forms of locomotion

Swimming devices designed for use in the colon would have a clear biocompatibility advantage as they would have limited contact with the sensitive colonic walls. This lack of lumen contact and potential for miniaturisation could result in high mobility and thus caecal intubation rates could be high. However, two critical issues currently remain with this form of locomotion:

1. *Generating sufficient thrust* – This seems to rule out fin-based methods as well as most pressurized jet methods, although pulsed vortex rings and propellers (both conventional and ring) seem more promising. The most capable methods could still struggle to achieve sufficient thrust to pull a tether.
2. *Carrying supplementary tools* – By their very nature, these devices are designed to be small, compact and do not include a means of anchoring themselves against the tissue for stability. This complicates the inclusion of on-board tools as they not only add weight and complexity but are more effective from a stable (fixed) platform.

These limitations point towards the use of the surrounding tissue for propulsion and stabilisation (anchoring).

2.5.2. Contact-based forms of locomotion

The two major issues present in swimming forms of locomotion could be solved by using the surrounding colonic walls as an anchor to push or pull against in order to propel the device. It would also provide a means of keeping the device stationary, allowing supplementary tools to be used. Relying on the tissue to propel the device does present some new challenges, including:

- Maintaining a high level of mobility whilst being in continuous contact with the tissue.
- Attaining sufficient traction and having a large enough stroke¹⁵ to carry out efficient motion in the flexible, low friction environment.
- Adjusting to the variable shape and size of the colon while achieving the above.
- Realizing all the aforementioned without damaging the sensitive colonic tissue.

¹⁵ Because of the inherent low friction there is likely to be a degree of slip during contact. When traction is made, the soft, elastic tissue needs to be deformed a certain degree before providing sufficient resistance for locomotion.

Below are some locomotion techniques currently used for colon-based devices, and others from different applications that could be adapted for use in this context:

2.5.2.1. Impact-driven

Description: This maintains the compact shape of a capsule and locomotion is achieved using the inertia of a moving mass to propel the robot forwards (Figure 2.18). This can be described as “vibratory locomotion” [77].

Example: The device designed by Carta et al. [77] uses an off-centre rotating mass to achieve vibratory locomotion. Because the mass is off-centre, a net forward force is produced and the capsule advances in small steps.

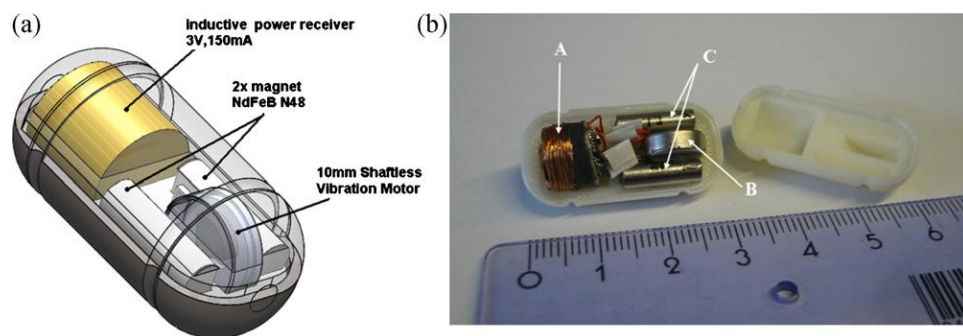


Figure 2.18 - Impact-driven capsule device. [77]

Feasibility: This form of locomotion is most effective on hard surfaces and so would be extremely inefficient in the mobile and compliant colon [77] – the energy from the vibrating mass would be dissipated through deforming the visco-elastic tissue. Furthermore, although the capsule is compact, the lack of fine movement control, lack of device steering and anchoring mechanism would not allow the housing and effective use of supplementary tools.

2.5.2.2. Elongated toroid

Description: This is a unique form of locomotion designed to mimic the cytoplasmic streaming ectoplasmic tube found in amoebae Figure 2.19, a.

Example: Hong et al. [78] designed the “whole-skin locomotion device” shown in Figure 2.19, b. It aimed to mimic the natural system by contracting one end of a mobile toroid. This results in the extending of the opposite end of the device as the toroid turns itself inside-out

(Figure 2.19, a.). Activating the appropriate ring actuator (eg. 1a, 2a or 3a in Figure 2.19, a.) as it reaches the end of the toroid results in a continuous forward motion.

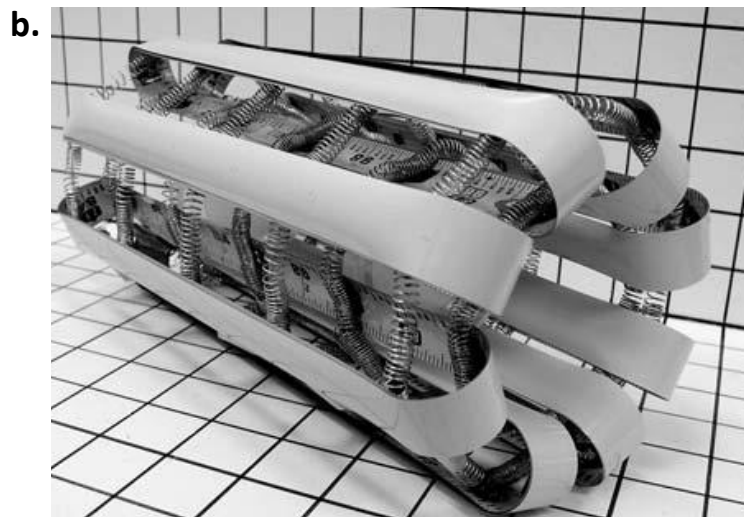
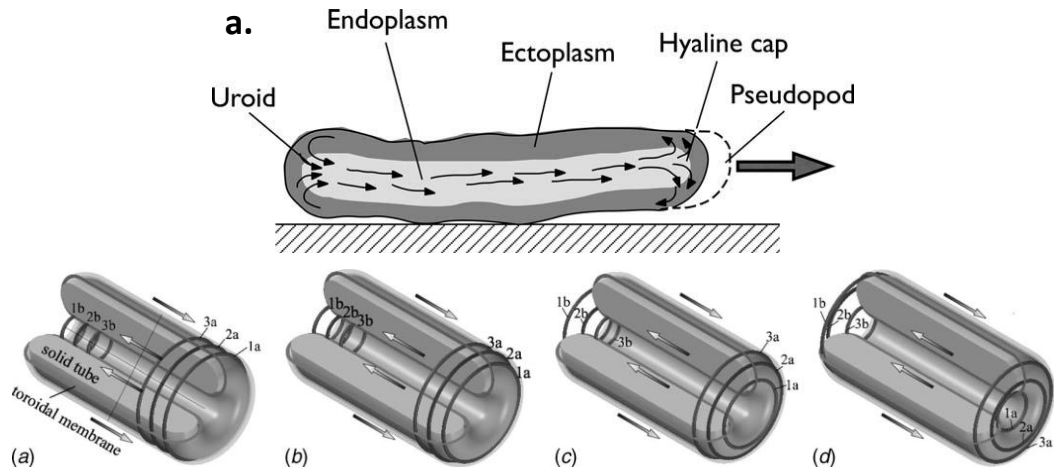


Figure 2.19 - Elongated toroid form of locomotion. a. The locomotion technique. b. An example of such a device. [78]

Feasibility: This has the potential to effectively move inside the colon as the whole body generates traction whilst the front advances¹⁶. It has the additional advantages of reduced tissue damage and having a compact shape which could result in high caecal intubation rates. However, this is a complex locomotion mechanism that has not yet been fully developed or tested *in vivo*. Furthermore, the lack of fine steering control and the fact that the actuation mechanism dominates the composition of the body reduces its ability to house

¹⁶ This could also exploit the larger magnitude static friction.

additional tools and cameras. It also does not have a means of actively changing its diameter which may limit its use in a distended colon (due to less device-tissue contact).

2.5.2.3. Wheeled/tracked

Description: This involves the use of conventional wheels or tracks, spaced evenly around the body, to propel the device through a tubular environment. Some form of extension mechanism is often used to ensure the wheels/tracks remain in contact with the surface as the diameter of the tubular environment changes.

Example: Sliker et al. [79] developed the tracked device shown in Figure 2.20, a. This device has a track on each side to provide propulsion, with a textured track surface to improve traction. It was designed for use in the small bowel, but is not constrained to it. During one study, it was tested and deemed suitable for natural orifice transluminal endoscopic surgery (NOTES) and for use in the colon.

Kwon et al. [80] designed and built the pipeline inspection robot shown in Figure 2.20, b. Although not designed for use *in vivo*, such a design could be implemented due to its ability to adapt to varying diameters (advantageous for maintaining traction within the colon). A similar device was developed by Park et al. [81]. This comprises of a single module which has the ability to adapt more easily to changing diameters and has improved mobility around bends (Figure 2.20, c.). Liu et al. [82] used wheels instead of tracks, with a flexible, modular layout to improve mobility around bends (Figure 2.20, d.).

Lambrecht et al. [83] show how an alternative to both wheels and tracks, Wegs™, could be used to improve mobility over uneven terrain (Figure 2.20, e.).

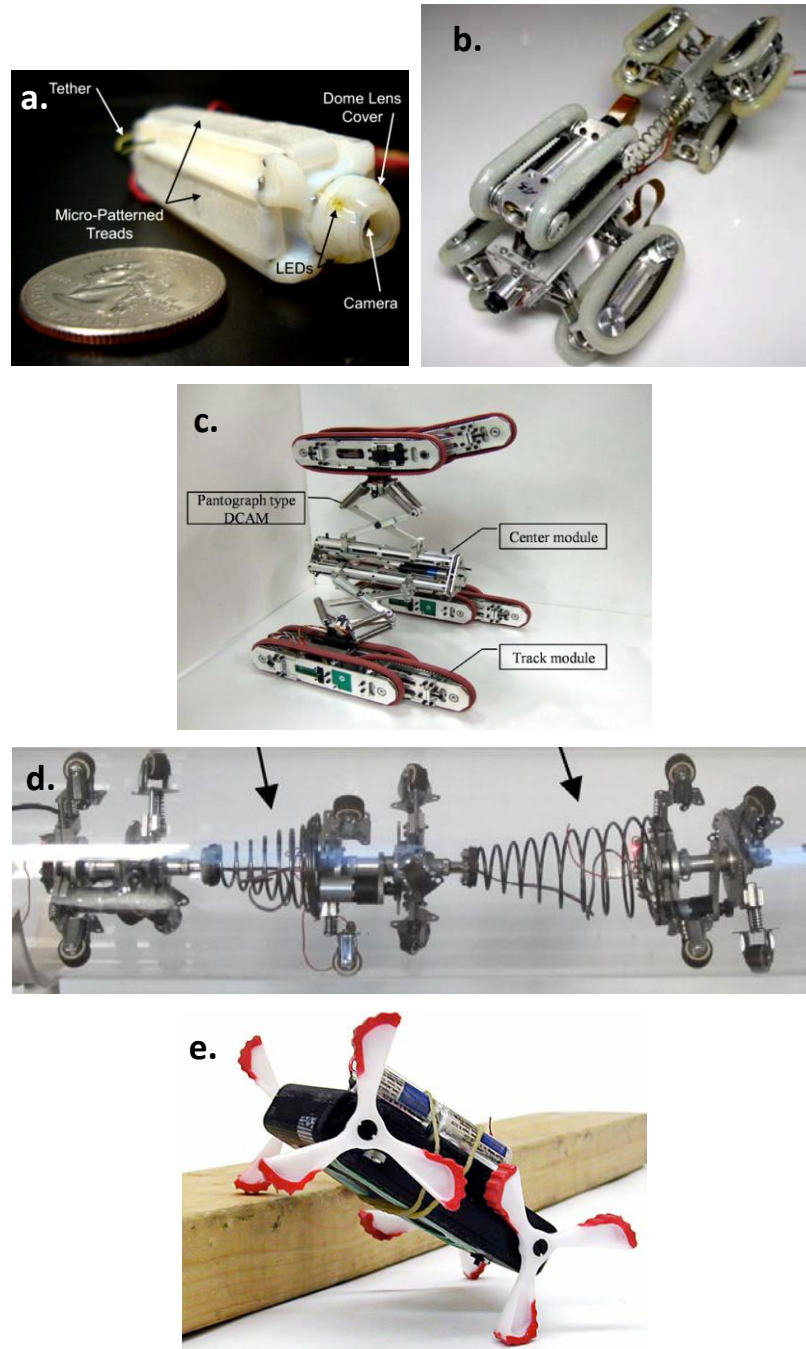


Figure 2.20 - Various wheeled / tracked devices. a. – c. Tracked devices. [79], [80], [81] d. Pipe inspection, wheeled device. [82] e. Device using Whegs. [83]

No such device has currently been designed to replace a colonoscope and to be used in a distended colon, particularly one that is fluid filled. Therefore, some general assumptions will have to be made on the feasibility of such devices.

Feasibility: In one study, the robot described in [79] was successful in achieving locomotion *in vivo*, but the tests highlighted some common issues with using such devices, namely the difficulty in miniaturizing the complicated actuation mechanism and the often slow

movement speeds due to high torque requirements. In terms of mobility around tortuous bends, tracked devices would theoretically perform badly due to their slip-steer approach, and their long and inflexible tracks/bodies. Modular wheeled devices such as that described in [82] are more promising in this regard, due to their smaller contact areas and more flexible bodies.

A major concern with wheeled devices is attaining sufficient traction on the compliant, slippery and uneven colonic lumen. Pipeline inspection robots adjust their diameter to maintain contact with the surrounding surface. A similar approach could be used to improve traction in the colon. Tracks are known to have higher traction than wheels but due to their drawbacks of high complexity and inflexibility, an alternative approach would be advantageous. One approach is the use of Wegs™ - these combine the obstacle traversing ability of legs with the simplicity and high rotational speeds of wheels [83]. It is hypothesized that the higher contact pressure of the individual legs will help to improve traction in the colon by deforming the tissue surface and penetrating the slippery mucus layer to reach the higher friction mucosa surface. Combining the features of diameter adjustment seen in pipeline inspection robots with an optimum wheel design may be a promising solution to a mobile colon-based device.

2.5.2.4. Screw thread

Description: A rotating, spiral-shaped structure is used to provide propulsion. As the thread interlocks with the surface a net force is generated in the axial direction (Figure 2.21, a.).

Example: Kim et al. [84] describe a novel solution to propelling a device within the colon. Locomotion was successful after several aspects of the design were optimized including component mass, dimensions, rotational speed and spiral shape (Figure 2.21, b.).

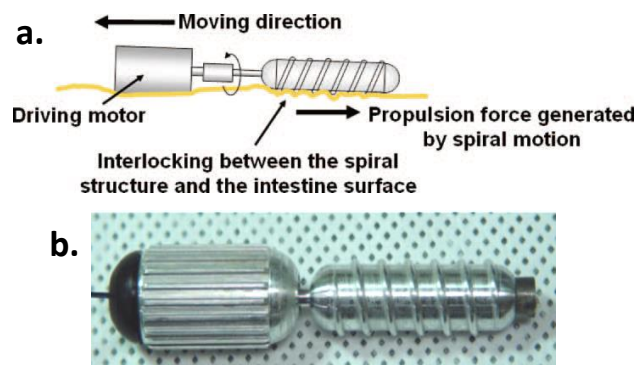


Figure 2.21 - Screw thread-based locomotion. a. The locomotion technique. b. An example of a device. [84]

Feasibility: This device has a significant advantage of reduced complexity and so could be easily miniaturized. However, a fundamental issue with this design is the high probability of twisting the colonic tissue, causing both tissue damage and inefficient locomotion. Furthermore, the device does not have the ability to be steered and would not provide a fully controllable, stable platform for surgical tools.

2.5.2.5. Snake-like

Description: These devices use serpentine locomotion to propel themselves. In smaller snakes, this involves the movement of an S-shaped horizontal wave down the length of the body to push against obstacles or against the ground itself. In larger snakes, a form of peristalsis is used, similar to the inchworm form of locomotion. A combination of both forms could be used.

Example: Crespi et al. [85] designed and built an amphibious, snake-like robot that successfully achieved both ground and water based locomotion (Figure 2.22).



Figure 2.22 - Amphibious, snake-like device. [85]

Feasibility: The amphibious nature of this device and its relatively small diameter are attractive features. However, it is not suitable for use in the colon because of the space required to carry out serpentine locomotion - the device would likely struggle around acute flexures and restricted diameters. It also could result in patient discomfort and tissue damage due to its size and form of locomotion (causing potentially large deformations of the colon – ie. stretching the sensitive (innervated) mesocolons).

2.5.2.6. Inchworm

Description: This is one of the most popular forms of locomotion developed for use in the human GI tract, due largely to its simple mechanism and compact shape (similar to that of a worm) [86]. In its simplest form, this locomotion technique involves the positive displacement of the device by a actuating a central “extensor” and the control of friction using some form of clamp at either end of the device [63]. Therefore, these devices operate most effectively in a small diameter lumen.

Example: Phee et al. [87] describe the design of a prototype inchworm device that uses expandable body segments and a mechanical clamp at either end to propel itself within the colon (Figure 2.23). Wang et al. [88] use a similar design except the mechanical clamps are replaced with a high friction, full-bellow skin (Figure 2.24). Other methods, such as expandable bellows and directional friction, have been used to achieve the required friction control, with similar success attained. The device shown in, Figure 2.25 [89], uses extendable arms as anchors. The “feet” have specially designed pads to increase friction against the colon lumen.



Figure 2.23 - Example 1 of an inchworm device. [87]



Figure 2.24 - Example 2 of an inchworm device. [88]

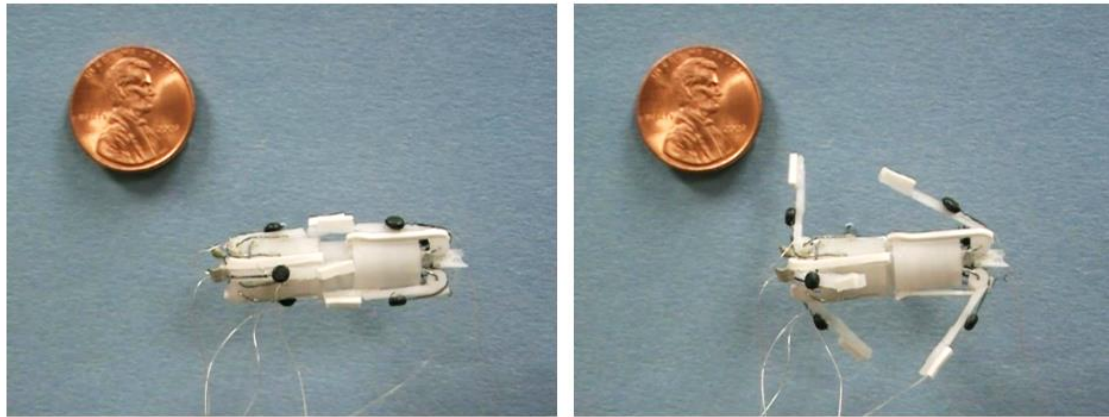


Figure 2.25 - Example 3 of an inchworm device, showing a novel method of controlling friction. [89]

Feasibility: The success of these devices in a fluid-distended colon is unknown but assumed to be poor due to the consequent lack of traction (reduced tissue contact). Many studies have been carried out in collapsed colons. In these studies, a large stroke (sometimes greater than 100 mm) is required to achieve effective locomotion, significantly deforming the colon and requiring a long body. This introduces several problems: Firstly, there is an “accordion effect” where the tissue is deformed during a forward movement without the device achieving a positive displacement, resulting in very inefficient locomotion. Secondly, the stretching of the tissue could be uncomfortable for the patient and could potentially cause tissue damage, particularly if a mechanical clamp is used to anchor the device¹⁷. Lastly, this type of locomotion is not particularly well suited to the acute flexures due to its long length and the aforementioned accordion effect. The inefficient locomotion technique may result in a poor caecal intubation rate, may not allow it to be used in patients with weakened colonic walls and may prolong procedure time. A general lack of fine movement control and mobility adds to its ineffectiveness and furthermore, reduces its ability to house supplementary tools.

2.5.2.7. Legged

Description: Using varying shaped legs, foot design and walking gait to achieve locomotion. This requires the synergy of both: achieving contact with the tissue (so that a force can be transmitted) and the displacing of those contact points to achieve locomotion [90]. This type of locomotion has been widely researched as it is expected to achieve higher locomotion efficiency than the inchworm technique [91, 92].

¹⁷ A mechanical clamp is often used to ensure sufficient traction in the slippery colon.

Example: Li et al. [91] designed a device that aims to mimic the movement of the natural mucus-cilia system (Figure 2.26). This is a very simple device with legs that have only a single degree of freedom and a gait that avoids the accordion effect. Valdastrri et al. [92] present a 12-legged device designed to be swallowed and then distend the tissue while advancing with a simple walking gait. Traction was achieved by using hook-shaped feet and a large number of legs (ie. contact points - allowing for reduced individual contact forces) (Figure 2.27).

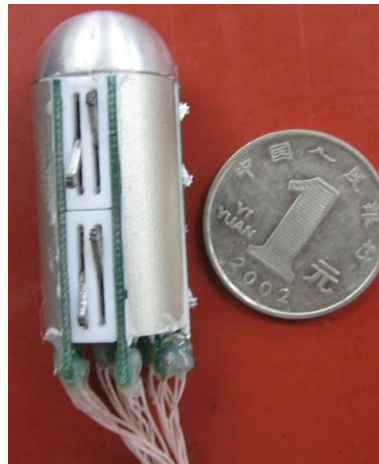


Figure 2.26 - Example 1 of a legged device. [91]

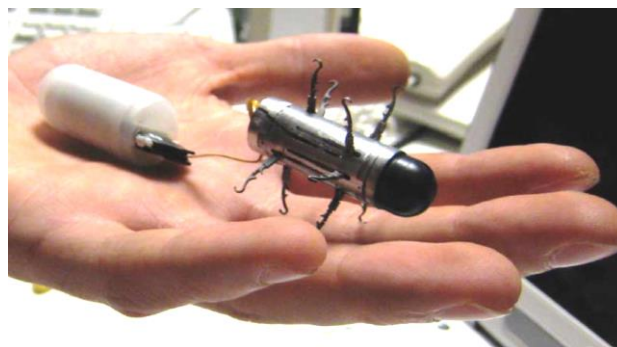


Figure 2.27 - Example 2 of a legged device. [92]

Feasibility: Legged devices are often chosen because of their adaptability to challenging surfaces and environments. They also have the ability to avoid critical areas and so could reduce tissue trauma. The actuation mechanism used and the lever effect of the legs often results in a large stroke length, advantageous in the mobile colon. Traction could also be optimized by varying the foot design and increasing local tissue deformation at each contact point [90]. One of the main issues with legged devices however, is the high complexity which adversely impacts miniaturization. This could be addressed by using a gait that can be simplified to a basic, alternating sweeping action with a single degree of freedom. This will result in a technique similar to the “moving anchor” described below. It could increase the possibility of miniaturization and increase the robustness of the device.

Another issue with legged devices is their effectiveness in a distended colon. This requires long legs in order to make contact with the tissue and would consequently introduce a new problem: the increased overall size of the device and the resulting reduced effectiveness in small apertures. Finally, in order for a legged device to be feasible, the foot design must be optimized. The previously mentioned devices utilize a relatively small foot size and high rigidity material. Although some thought has gone into biocompatibility, these devices could still potentially damage the sensitive tissue at the highly deformed contact points. This suggests the need for soft, compliant limbs with additional consideration into the use of less destructive traction/adhesion mechanisms.

2.5.2.8. Simplified legged (moving anchor)

Description: This is a simplified legged form of locomotion and involves the moving of an anchor point down the length of the device. This could be achieved, for example, by the moving of legs down the length of the body in waves (similar to a millipede) or, by the linear movement of a clamp/anchor.

Example: Kim et al. [93] designed the device shown in Figure 2.28. The robot extends its arms out to make contact with the tissue of the collapsed colon before moving the anchor backwards to achieve a forward step.

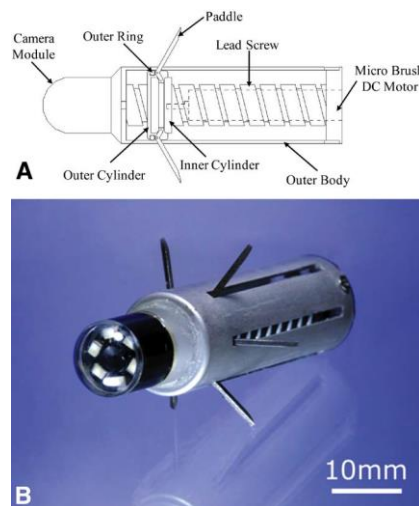


Figure 2.28 - Example of a device using a "moving anchor." [93]

A. shows the mechanism and B. the prototype and scale.

Feasibility: This form of locomotion has the primary advantage over other legged devices of being compact and simple. Its main drawbacks, when considered for use in hydro-colonoscopy, are its presumed ineffectiveness in a large diameter (distended) colon. This issue, as with conventional legged-devices, is due to the relatively short extendable arms

which would not make complete contact with the tissue in large apertures and would therefore have low traction. They could be lengthened but this would then require them to have a complex mechanism to adjust their length for narrow apertures and negate the original advantage of simplicity.

The arms in Figure 2.28 are rigid and sharp in order to produce a reliable anchor. This could seriously affect the overall biocompatibility due to a high risk of perforation of the colonic tissue. This form of locomotion also requires a large stroke in order to overcome the “stretch” in the tissue and so requires a relatively long actuation mechanism in the device’s body. It also has some limitations when considering the mobility, as there is no steering mechanism and the paddles’ traction is most effective in one direction only.

2.5.2.9. Summary - Contact-based locomotion

When compared to swimming methods of locomotion, the contact-based forms of locomotion show great potential in the area of propulsion force and ability to house surgical tools (due to their stable, anchored platforms). The primary concern with this type of locomotion is achieving sufficient traction while maintaining both mobility and safety. This is where most of the current designs fall short. The devices that seem to achieve the highest traction are the ones that deform the tissue, for example the legged designs. However, these clearly have a higher risk of causing tissue damage due to high contact pressures. The most promising solutions in terms of mobility are simple legged devices and varying diameter wheeled devices. These have the ability to steer around flexures in the colon and the high stroke length (or continuous rotation in the case of wheels) could produce effective locomotion by increasing traction and reducing the “accordion effect”. It is clear that significant work is still required to produce an effective diagnostic and therapeutic robotic platform for hydro-colonoscopy. Due to the requirements of having a tether and the ability to house surgical tools, contact-based locomotion seems most suitable. The design of such a device is challenging and requires the optimizing of both mobility and traction, while ensuring a very high level of biocompatibility.

2.6. Conclusions from literature

There is considerable motivation to develop an effective procedure for the direct inspection of and intervention in the colon. The CoDIR project could significantly improve the current colonoscopy procedure by replacing the colonoscope with a small, mobile robotic platform. The development of this platform presents a number of challenges mainly due to the complex environment. This is particularly true with hydro-colonoscopy, as the entire colon is filled with a liquid. With respect to the anatomy, the tortuous shape and varying diameter

suggest a small, highly mobile device is required and the locomotion technique must also be highly adaptable. The sensitivity of the tissue suggests a soft interface is needed as well as a robot structure that adapts to the environment rather than one that adapts the environment to itself; this will be challenging to achieve due to the properties of the colon. And finally, the low friction mucus layer highlights the need for finding a method of achieving sufficient traction while causing minimal tissue damage.

A number of mobile robotic devices were reviewed. The inclusion of a tether is advantageous in easing the challenge of developing on-board electronics and can provide a means of manually retrieving the device in an emergency. Although a swimming device would be beneficial in terms of trauma, the thrust generated by these devices is very small and would struggle to overcome the tether drag. Furthermore, such a device does not provide a stable platform for the use of surgical tools. For these reasons, a contact-based device has been deemed most suitable. Various locomotion strategies were then investigated and it was concluded that wheeled and legged devices are most feasible for use in this unique environment. Of these two, wheeled locomotion was chosen as the technique to explore further. This decision was based on a number of advantages of this method:

- The continuous rotation of the wheels may favour the low friction, visco-elastic and low modulus tissue. Legged and inchworm-like locomotion are limited as they require long stroke lengths and complex mechanical linkages: they first must make contact with the lumen and then overcome the stretch in the tissue to produce a net forward movement.
- Wheels can be highly modified to suit their environment, including their shape, material and surface texture. A specialised wheel could be designed to have high traction and low trauma in this unique context.
- The continuous contact with the lumen (contact-based locomotion) results in a stable, anchored platform and could make the use of diagnostic and therapeutic tools more effectively¹⁸.
- Actuation of wheels (e.g. using DC motors) is well understood in terms of mechanical transmission and electronic control. It can also provide both high torque and rotational speeds.

¹⁸ However, one caveat of this is the need for a mechanism to alter the size of the robot (workspace) to suit the varying diameters of the colon.

Chapter 3

Mechanical design, fabrication and characterisation

This chapter introduces the RollerBall concept – a wheeled robot conceived prior to this PhD. A series of design refinements to this core concept are then described before going into the detailed design of the device. Specifics on the fabrication and assembly of the full working prototype are then given before the chapter concludes with a full benchtop characterisation of the key mechanisms of the robot.

3.1. Specifications of a mobile colonoscopy robot

Major requirements of a mobile colonoscopy robot were proposed in Table 2.5 and 2.6 in Section 2.4.1. These were used to inform the design of the robot presented in this thesis and to evaluate its performance. To add to this, Table 3.1 includes the major design specifications that were derived from the requirements.

Table 3.1 – A list of the major specifications of a mobile colonoscopy robot.

Requirement	Specification	Notes
Small size	Diameter less than 26 mm and length not more than 40 mm.[8, 14, 15, 63]	These values consider average diameters of the colon reported in literature.
High speed	A linear speed of at least 3.85 mm/s.	Assuming a colon length of 1.85 m [11] [12] and 8 mins to reach the caecum [63].
High mobility (including effective locomotion technique)	Move in forward and reverse directions through a flexible lumen. Traverse a range of corners from 30 ° to 120 °	The majority of flexures are less than 90 °, with two on average being larger [11].
Overcome tether drag (thrust)	Greater than 1 N gross thrust.	This was a value proposed after preliminary investigations by the CoDIR group on the expected tether drag.
Safe	Maximum pressure at wheel interface less than 3 Bar [94, 95]. No mechanical induced trauma beyond mucosal	Pressures in the order of 3 Bar are said to be required to perforate the colon [94, 95] therefore, contact pressure should not exceed this. As described by Lee et

	layer after 10 s of continuous slip.	al., trauma confined to the mucosa could be considered acceptable as it is the underlying submucosa that contains blood vessels and lymph nodes [96].
Be adaptable	Working diameter of 26 mm (required diameter) to ca. 62 mm.	Based on the expected diameter ranges in the colon [97] [8].
Provide a stable platform	Able to fix the robot position and orientation (fixed platform).	Provided the device is adaptable, it should have a stable, fixed structure to provide a platform for the use of surgical tools.
Be robust	Last at least 10 hours of continuous, manual handling and normal operation (locomotion) without failure.	In a clinical setting, parts of the device may be disposable and so only require a short lifespan, while others should not fail after many hours of use. This value was chosen as a preliminary target for the current, 3D printed prototype and will allow it to be used for all the bench top tests.

The subsequent pages include the design and fabrication of a robot to meet these specifications.

3.2. RollerBall: a mobile, wheeled robot

There are a number of different locomotion techniques and potential robot designs that could be conceptualised for this application. A review of current literature suggested that a wheeled robot could be a promising candidate for the CoDIR project because of a number of strengths summarised in the previous chapter.

As with any contact-based form of locomotion, gaining traction is crucial to the device's efficacy. A number of authors have shown that using a tread pattern can greatly increase the friction on the intestine [96, 98, 99] and so it was assumed that this would allow the effective use of a wheeled device such as that presented here¹⁹. The limited literature available on the design of such devices and the inherent complexity of the environment means that there are a number of questions on the efficacy of a robot concept that can only be determined empirically.

3.2.1. Concept overview

A wheeled robot called "RollerBall" was conceived prior to the start of this PhD. Figure 3.1 illustrates the major design features that it comprises of:

¹⁹ This challenge of gaining traction on the colon is explored in great detail in Chapter 4.

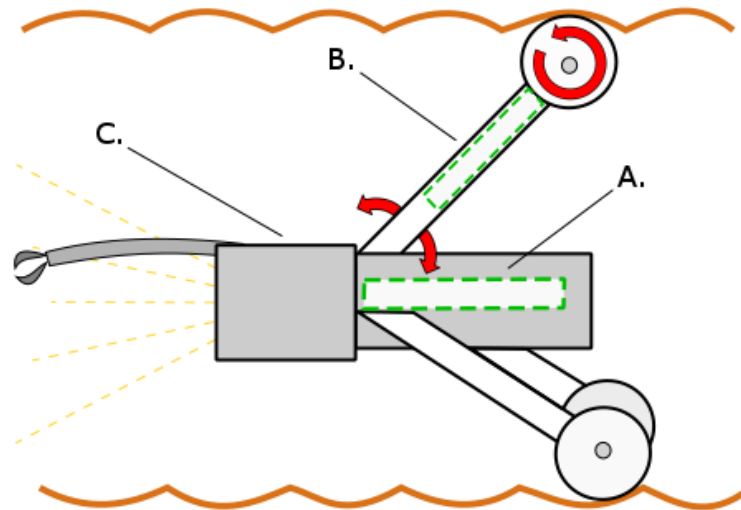


Figure 3.1 - An illustration of the core RollerBall concept.

This figure shows: A. Central chassis with an *Expansion mechanism* to provide a stable platform in varying diameter lumens; B. *Wheel mechanism* to provide tractive effort and; C. The stable platform allows it to house on-board diagnostic and therapeutic tools to provide similar functionality to a colonoscope.

At the heart of the design is a central chassis from which extend three radially distributed, expandable arms. An *Expansion mechanism* (Figure 3.1, A.) is used to ensure the wheels are always in contact with the lumen as the diameter changes. At the end of each of the arms is a wheel, rotated by a *Wheel mechanism* within the arm itself (Figure 3.1, B.). Driving the wheels produces a net forward or backward movement, and adjusting the individual speeds steers the device. The contact-based locomotion and ability to adjust the angle of the arms means the robot can provide a stable platform for the effective use of on-board diagnostic and therapeutic tools (such as a camera, light source and biopsy tool – Figure 3.1, C.).

RollerBall went through three prototype iterations before the start of this PhD. The different versions are shown in Figure 3.2.

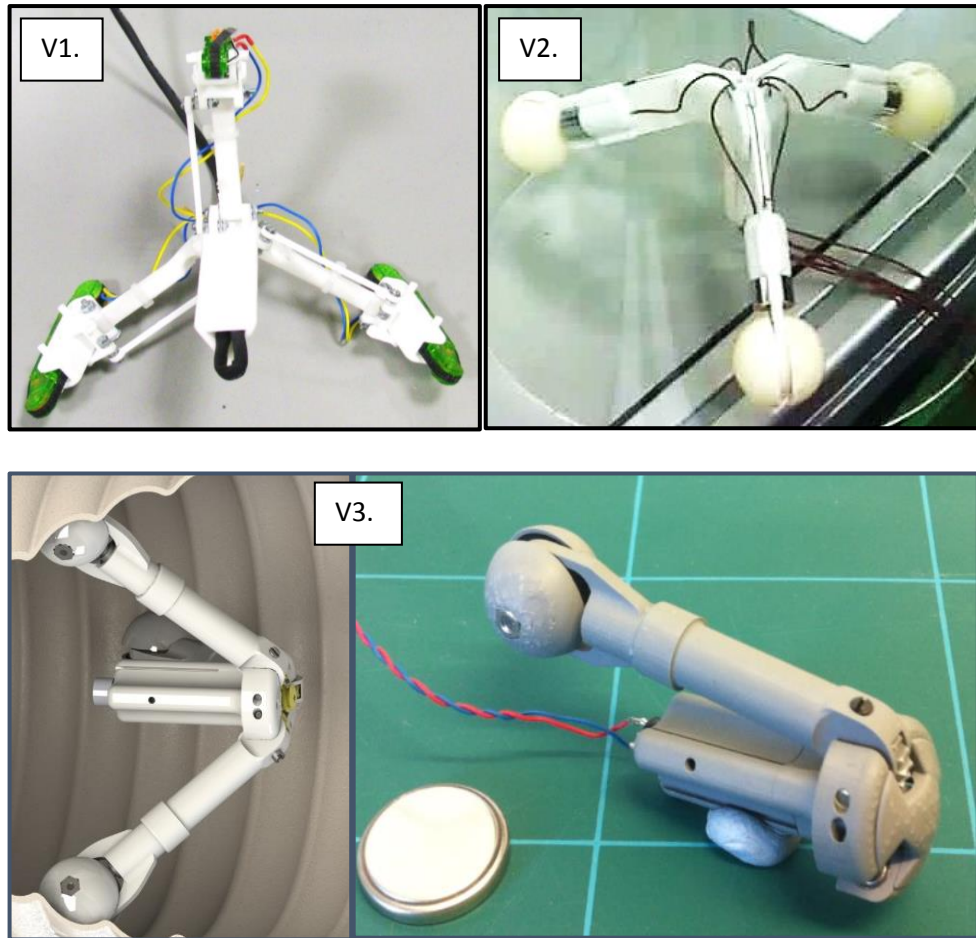


Figure 3.2 - The various iterations of RollerBall, from the start of the CoDIR project - V1 - to the concept adopted at the start of this PhD - V3.

The concept began by using tracks for locomotion (Figure 3.2, V1) – chosen for the presumed increase in traction. This was later switched for spherical wheels because tracks require a complex and bulky actuation mechanism which could seriously restrict miniaturization. Spherical wheels are not only simple to actuate, but they are also compact, an atraumatic shape and are likely to have good traction as a larger proportion of the wheel surface can make contact with the thin, low modulus lumen (Figure 3.3).

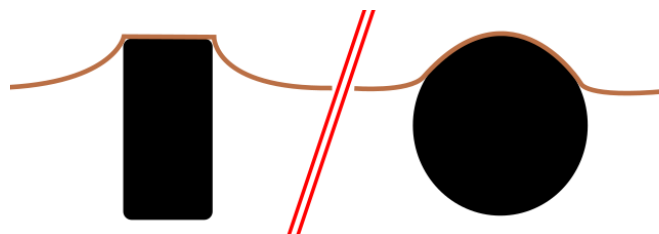


Figure 3.3 - An illustration of how spherical wheels offer a more functional, less traumatic solution in the intestine.

Concept V1 and V2 in Figure 3.2 used a passive mechanism to expand the arms. Although adding complexity, it was thought that more control over the angle of the arms and the

amount of force they apply to the lumen is required – this is the main development from V2 to V3. From this stage onwards the arms are actuated by an expansion mechanism in the central chassis which allows the device to *actively* adapt to the size of the surrounding lumen.

The V3 concept was fabricated but not fully assembled (as can be seen in Figure 3.2) or empirically assessed prior to this PhD; details such as how to package on-board electronics, control the device (including both hardware and software components) and information on how the device performs as a whole, were lacking. Preliminary tests on robot V1 – 3 showed that the RollerBall concept had potential but had a number of necessary refinements. It was decided that the main focus of this PhD should be on characterising, refining and testing of this core concept with the aim of advancing it to a full working prototype.

3.3. RollerBall V4

The development of RollerBall V1 – 3 highlighted a number of missing features and significant challenges. The resolving of these makes up the majority of the work in this thesis and are summarised in Table 3.2.

Table 3.2 - A summary of the major changes made to RollerBall and the work carried-out to progress it to a working prototype.

Issue/Challenge	Solution	Addressed in...
Integration of electronics into the prototype.	An electronics module at the front of the robot was designed.	Current chapter
Potential stability issue with V3 due to offset location of Centre of Mass (Hereafter: CoM).	Methods of stabilising the device were proposed.	Current chapter
Minor issues with arm design including axle play/alignment, a bulky wheel hub and lack of force feedback.	The arm was redesigned to improve axle alignment, reduce the profile of the wheel hub and include a method of force sensing.	Current chapter
Wire routing and device encapsulation.	Preliminary work was done on the efficient routing of the wiring. This and the design of the electronics module were done with encapsulation in mind.	Current chapter
Material selection, fabrication and assembly of a robust prototype.	A material was chosen and then fabrication and assembly were	Current chapter

	refined to produce a functional, robust prototype.	
Gaining traction in the colon.	An in-depth review of literature and an empirical evaluation of a number of tread designs was carried out.	Chapter 4
System development and control	The the control and its associated electronics hardware were developed iteratively from open-loop to a more advanced closed-loop system.	Chapter 5

The following pages elaborate on some of these major changes made to the concept to progress it from V3 to V4 (Figure 3.4).

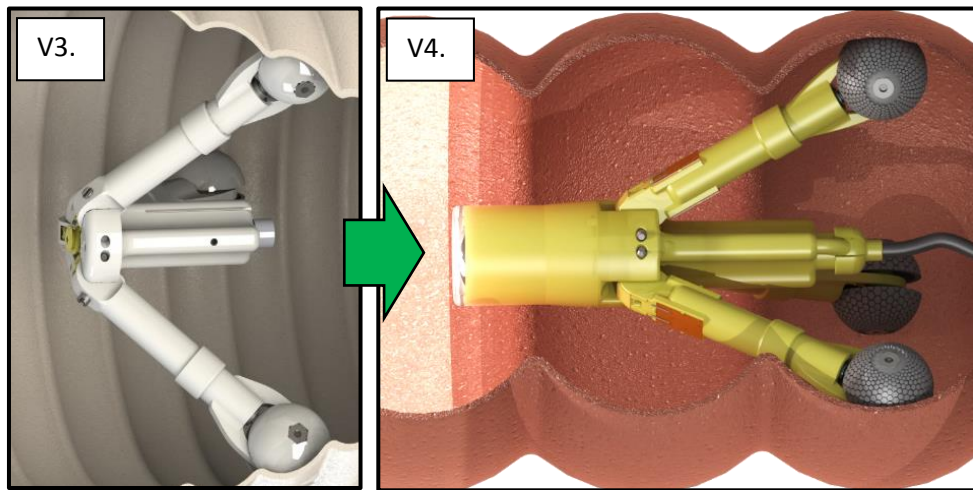


Figure 3.4 - Renders showing the advancement of the RollerBall concept from V3 to V4 made during this PhD.

3.3.1. Electronics module

The main motivation for having a device like RollerBall (which is able to maintain a fixed, stable position in the colon) is the effective use of diagnostic and therapeutic tools. To achieve this, the first major design modification was the inclusion of an electronics module. This could be placed at a number of different locations around the robot however, the position of the arms makes it intuitive to place the electronics in a module at the front of the device (as was illustrated in Figure 3.1, C. and Figure 3.4). This module is designed to be replaceable, anticipating the usefulness of having different functionality based on the patient and the context - for example: a simple, low cost module that contains only a camera and light source could be used for mass screening. This could be switched for a more complex, higher cost module containing on-board therapeutic tools for targeted treatment in an individual patient.

3.3.2. Stability considerations

Ideally, RollerBall should be able to maintain a central position within the colon lumen (such as that shown in Figure 3.4) while allowing the orientation (or pose) to be adjusted.

NB: Orientation refers to the angular position of the robot's longitudinal axis relative to the axis of the lumen. The orientation shown in Figure 3.4 and Figure 3.5, B. - where the robot and lumen axes are aligned - is hereafter considered the desired "idle" orientation.

Initially, the location of the CoM of the robot (positioned in front of the wheels) seems to present a potential issue with this stability. This was confirmed in preliminary tests, where the prototype was unable to maintain the desired, central orientation.

Referring to Figure 3.5, B: The weight of the device produces a torque (T_{mg}) between the wheel contact points²⁰ that acts to rotate the robot (destabilising it). This torque is proportional to the weight of the robot (mg) and distance L_1 . L_1 is inversely proportional to the angle, a , therefore this torque is most pronounced when the arms are closed (in a narrow diameter lumen). In air, the only forces opposing this are friction forces F_{Fr1} and F_{Fr2} .

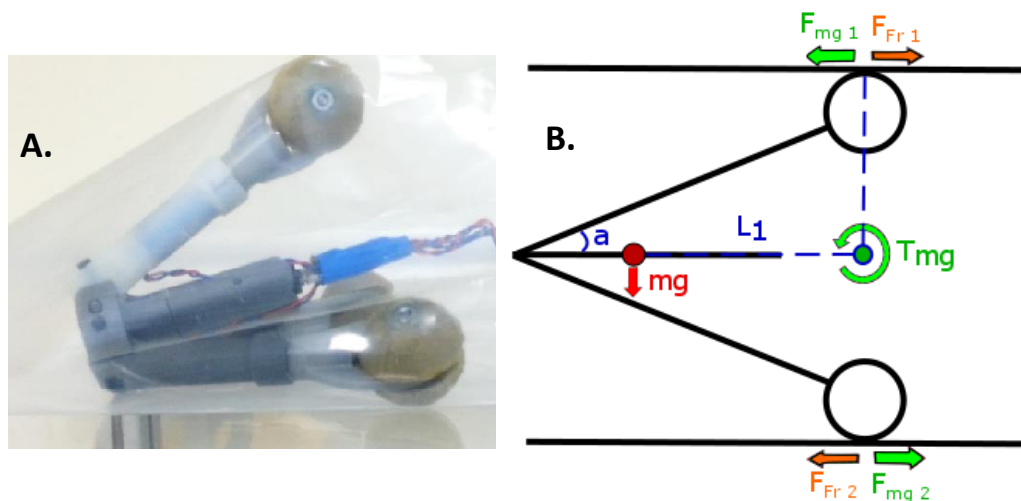


Figure 3.5 – Considering RollerBall's stability.

A. Testing an early prototype in 'flat-pack' plastic highlighted the issue of this offset CoM – A central, horizontal orientation was difficult to maintain. B. A Free-body diagram showing the major forces affecting the stability of RollerBall. mg is the weight of the robot, acting from the CoM; T_{mg} is the resulting torque, perpendicular to the wheel contact points; a is the angle of the arm (which determines L_1); F_{mg} are the forces produced by T_{mg} at the wheel-tissue interface and; F_{Fr} are the friction forces that oppose these.

²⁰ The FBD is simplified, in reality there are three wheel contact points: one at the top, two at the bottom, with the two lower wheels sharing F_{Fr2} and F_{mg} .

The intended use of water to distend the colon (included in the scope of the CoDIR project) could alleviate this issue. The electronics module is positioned at the front of the device (ie. furthest from the wheels) and therefore, the module could be designed to include sufficient buoyancy to counteract, or at least assist with, the offset CoM (weight). Nevertheless, a practical limitation during laboratory testing of the prototype is that this solution is completely dependent on the support of the fluid and this could complicate testing. Two temporary alternatives were explored:

1. *A passive spring mechanism at the front of the robot to support the offset CoM.*

This was realised by incorporating a simple spring element into the electronics module and designing it to deform from two main force vectors (represented by arrows in Figure 3.6, A.): approximately front-on (e.g. a haustral fold) and from below (e.g. the weight of the device (mg) and narrowing diameters (elastic restoring forces from the tissue)).

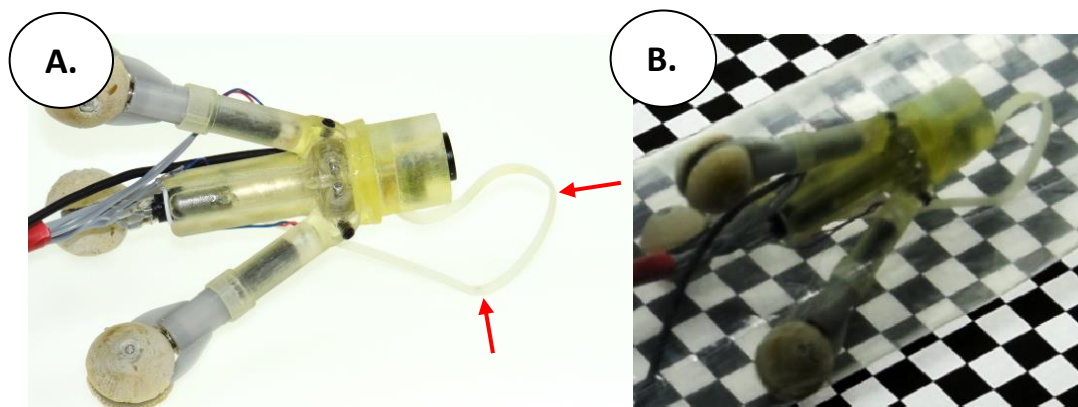


Figure 3.6 – Integrating a passive spring element.

A. An early RollerBall prototype with integrated spring element to support the front of the robot (offset CoM) – the arrows show the directions in which the spring is designed to deform. B. The device being tested in ‘flat-pack’ plastic.

Preliminary tests in a ‘flat-pack’ plastic tube showed that the spring element could effectively support the device (Figure 3.6, B.) and deform over obstacles however, a crucial limitation halted further use of this option: the spring element (a physical protrusion) severely restricts the workspace of the robot’s tip.

2. *An artificial environment that allows RollerBall to gain large amounts of traction.*

The second option assumes that if there is sufficient traction between the wheels and the lumen, the friction forces (F_{Fr} in Figure 3.5, B.) combined with the tractive effort from the wheels could oppose the offset CoM and help to maintain the robot’s orientation. The

absence of any protrusions (such as the spring in Option 1) also allows the orientation to be adjusted in any direction and hence more closely represent the intended use/performance. This high traction option was used for the remainder of the work presented in this thesis, with various soft silicone tubes being used as the test environments in Chapter 5 and Chapter 6.

3.3.3. Arm design

A number of modifications were made to the robot arm. Referring to Figure 3.7: The profile of the wheel hub was reduced to ensure maximum wheel contact occurs²¹; two ball bearings were included to reduce the axle play and improve alignment; the base of the arm was redesigned to incorporate force sensors (a half-bridge strain gauge circuit) and lastly, the efficient routing of the motor and sensor wires was considered.

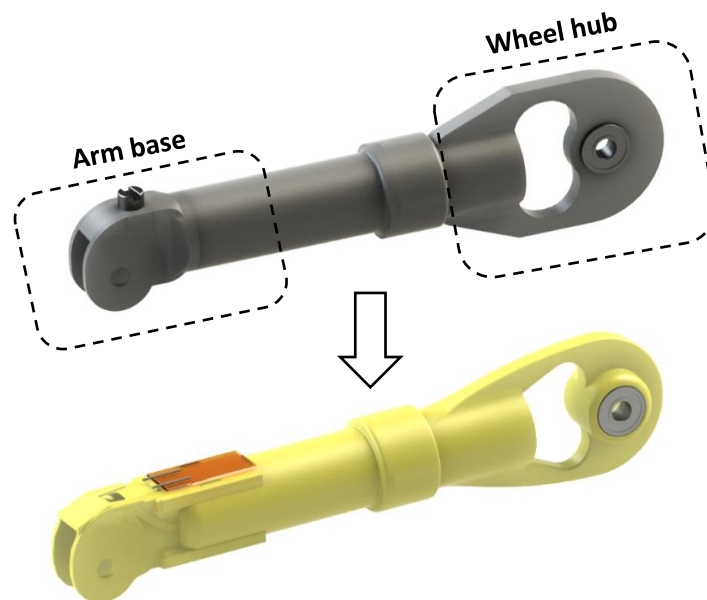


Figure 3.7 – Renders showing the design progression of the arm (wheel mechanism).

3.3.4. Preliminary encapsulation considerations

The scope of this project did not include major factors associated with commercialization, such as: mass manufacture and assembly; unit cost (including whether whole or part of the device would be disposable); biocompatibility (in terms of the materials used) and; complete encapsulation and ability to be re-sterilised. However, two preliminary steps were taken:

²¹ In a narrow diameter lumen (arms “closed”), tissue will likely contact the outer surface of the arm and increase drag. The highest point on the arm is the wheel hub; the size of the wheels could be increased to be protrude much further than this point, but this would also increase the overall diameter of the robot and restrict its use in small apertures. Currently, the best solution is to reduce the profile of the wheel hub as much as possible to ensure maximum tissue-wheel contact.

1. The previously mentioned, detachable electronics module groups the sensitive electronics in a housing that would be easier to seal than if the components were distributed across the robot.
2. The routing of the wires, including details of how the tether attaches to the rear of the robot and how the expansion motor (previously exposed in V3) is covered, were carefully considered.

3.3.5. Fabrication and assembly

RollerBall V1-3 highlighted the challenge of fabricating and assembling small, intricate robots. At this scale, the small parts are fragile and require careful selection of the tolerances used between push-fit components. The prototype needs to function properly while being robust enough to carry-out a number of potentially long duration, challenging benchtop tests without failure. If parts do fail, they need to be remade and replaced with relative ease so as to not slow prototype development. A precise and accurate 3D printing technique was used to manufacture the individual parts from a durable resin. These were post processed by hand to ensure a suitable tolerance and surface finish before assembly.

3.4. Detailed design

This section provides a full description of RollerBall (V4) and is approximately divided into three subsections based on the key components: The *Wheel mechanism* (Figure 3.8, i.), the *Expansion mechanism* (Figure 3.8, ii.) and the *Electronics module* (including wire routing and tether coupling) (Figure 3.8, iii.):

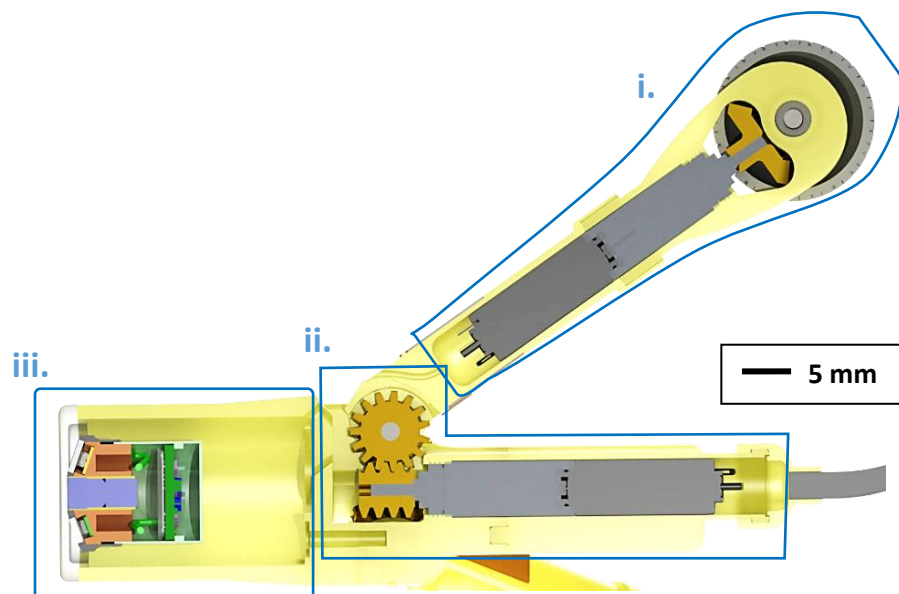


Figure 3.8 – A cross-sectional view of RollerBall V4 showing the three main components.

i. The wheel mechanism; ii. The expansion mechanism and; iii. The electronics module.

3.4.1. Wheel mechanism

The net speed and direction of the robot can be controlled by adjusting each of the three wheel speeds independently. This setup also allows the robot to turn on-the-spot (ie. adjust its orientation while stationary).

Referring to Figure 3.9: Each wheel is actuated by its own high power DC motor located in the arm. The motor rotates the wheel via a 1:1 bevel gear assembly that is contained within the spherical wheel. This split wheel arrangement is an efficient use of space and ensures a compact arm/wheel mechanism (as can be seen in the cross-sectional view). One of the bevel gears is fused to one half of the wheel and then the axle is fused to both wheel halves (therefore, transmitting the torque to the whole wheel). The wheel and axle assembly is supported by two 5 mm ball bearings.

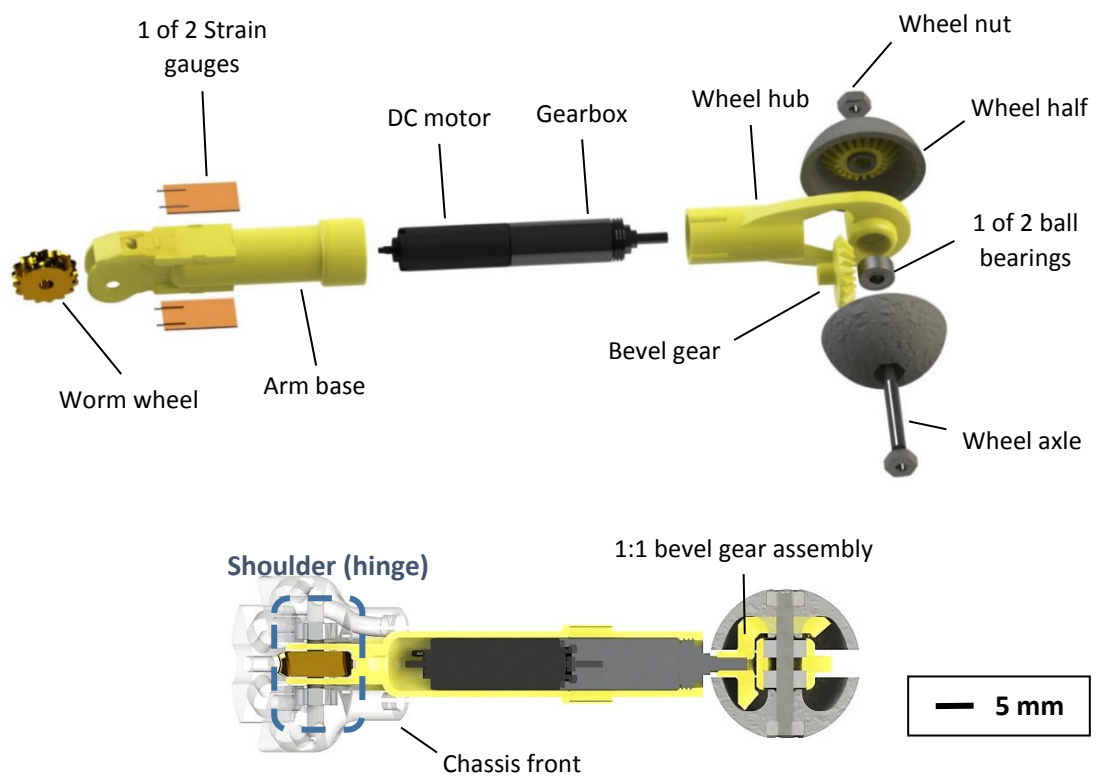


Figure 3.9 – The wheel mechanism of the robot.

An exploded view of the various components and a cross-sectional view of the assemble arm. A 5 mm scale bar is included for both.

The requirements in Chapter 2 suggest that RollerBall should perform at least as well as the colonoscopy. This means it should be able to reach the caecum in 6-8 mins – a linear speed²² of at least 3.85 mm/s; the wheels are 17.25 mm in diameter therefore giving a rotational speed of ca. 4.3 rpm (assuming no slip). This is a relatively low speed in the context of DC motors and so a high torque motor assembly could be used to ensure the motors do not stall during normal operation. At the initial stage of development when the motors were selected, it was difficult to predict the degree of slip that the robot would encounter and the required tractive effort (torque). Therefore, a 6 mm *Maxon RE6* with a 221:1 reduction gearbox was selected as it provided a good balance of speed and torque (See Appendix A. for the motor and gear box data sheets).

3.4.1.1. Force sensing

The ability to measure the force applied by the arms (from the expansion mechanism described in the next section) is useful to prevent trauma, ensure wheel-tissue contact and control traction. The DC motor greatly increases the strength and stiffness of the arm, meaning low strain levels are present at the range of forces the robot can apply – this was confirmed visually (qualitatively) and from Finite Element Analysis (*Solidworks Simulation*) (Figure 3.10). Therefore, this setup was deemed suitable for using conventional strain gauges (GF series, foil gauges by TML, bonded with a cyanoacrylate plastic adhesive). The arm design and motor position were modified to locate the maximum stress/strain in a suitable position for the strain gauges: In-other-words, far enough from the shoulder joint to give space for the sensor leads, with the gauges positioned over the region of maximum strain to improve signal output (annotated on Figure 3.10). A half bridge circuit (compressive and tensile strain gauges) was used to further amplify the strain gauge output signal and provide some temperature compensation. A detailed description of the force sensing (including performance and calibration aspects) is provided in Chapter 6.

²² 8 mins to traverse a 1.85 m colon.

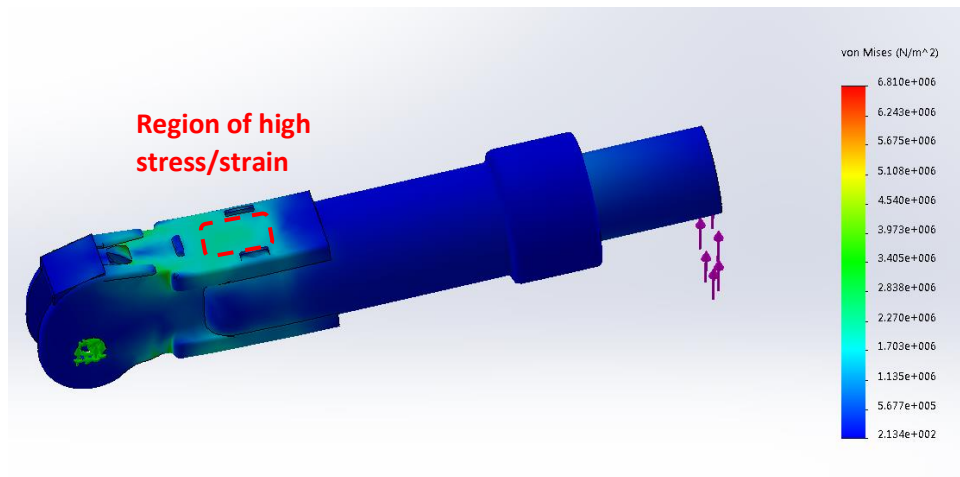


Figure 3.10 – A screenshot of the simple FEA carried out on the arm.

A force of 2 N (greater than the maximum force applied by the expansion mechanism, described in the next section) was applied to the end of the motor (modelled as a steel cylinder). The region of high stress/strain is located approximately in the centre of the strain gauge mounting.

3.4.2. Expansion mechanism

The expansion mechanism is used to adjust the angle of the three arms. This has two purposes: to secure the robot in position by ensuring the arms are always in contact with the lumen (ie. a stable platform) and; to apply a force normal to the lumen to both provide and control traction.

Referring to 3.11: A worm gear assembly is used to convert the motor shaft rotation into an angular displacement of the arms. All three arms are connected to a single worm gear therefore, all are adjusted simultaneously.

Ideally, the arms should be independently controlled. This would allow each arm to apply the same amount of force to the lumen and remain stable in all robot orientations. With the current setup, high friction between two of the three arms (or an obstacle) could stall the expansion mechanism motor before the third arm has applied sufficient force to the lumen to gain traction. A further limitation is that the expansion mechanism is not back-drivable and so needs to be continuously controlled to avoid trauma and maintain the desired force. However, the mechanism required to actuate each arm independently would be significantly more complex (and harder to miniaturise) and so was not included in the scope of this PhD.

As with the wheel mechanism, it was difficult to determine the exact amount of torque required from this motor. Intuitively, high torque is needed to ensure sufficient force can be applied at all three wheel-tissue interfaces and considering that a single motor is the only source of actuation. A high speed may also be required to ensure the arms can rapidly alter

the force (to either increase traction or avoid trauma). The same Maxon 6 mm motor (221:1 gear reduction) was used for a balance of speed and torque, however, a further 20:1 reduction was chosen for the worm gear assembly as the torque requirements are greater in this mechanism.

The motor was screwed into the chassis front and locked in place by a flat 'key' in the chassis rear. A steel axle, supported by two 5 mm ball bearings, was used as the hinge of the arm (shown in Figure 3.11).

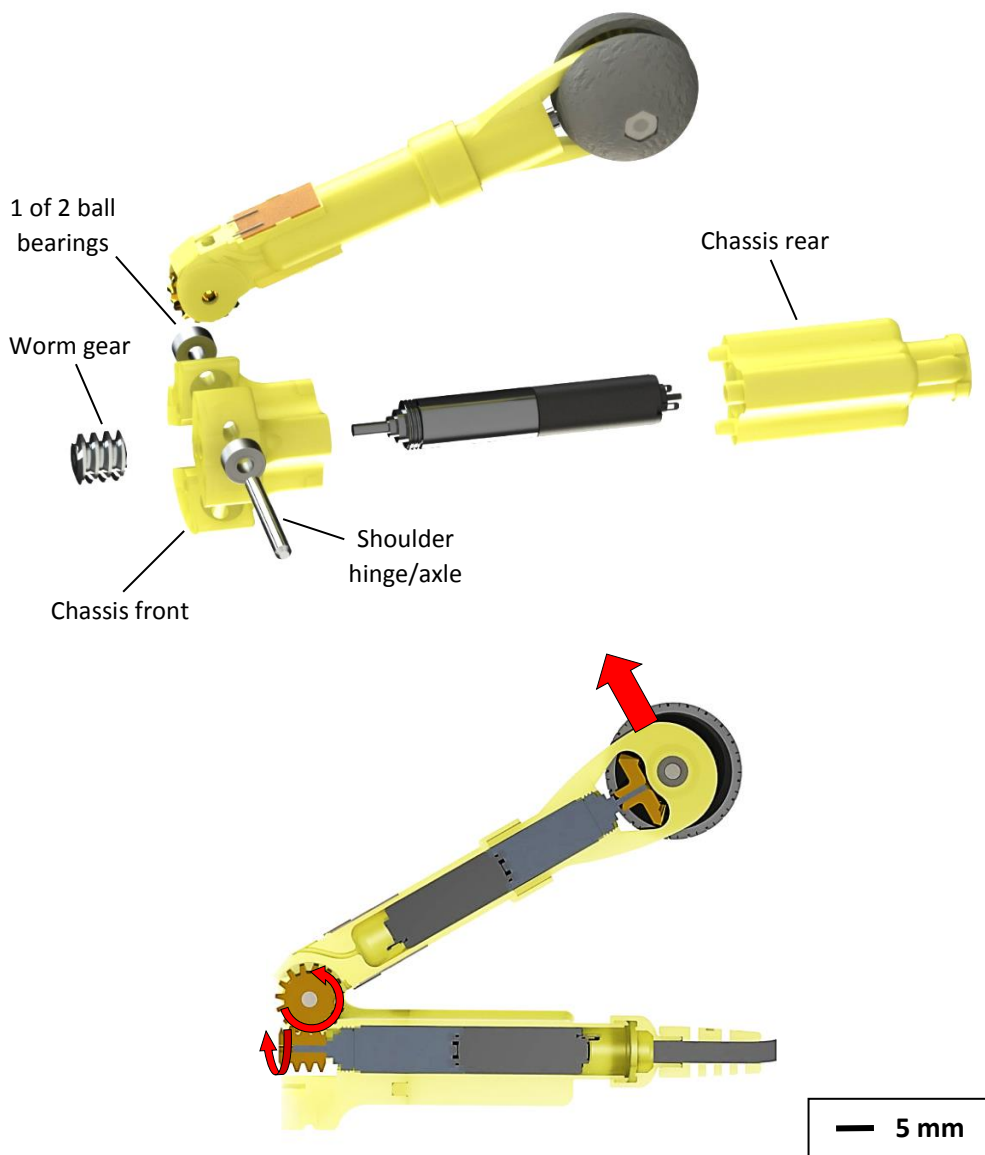


Figure 3.11 – The expansion mechanism of the robot.

This figure includes an exploded view of the various components and a cross-sectional view of the assemble mechanism showing the compact arrangement and details of the transmission. A 5 mm scale bar is included for both.

3.4.3. Electronics housing and cable routing

An electronics module was designed for any on-board electronics²³, containing them and helping to reduce the complexity of future encapsulation.

Referring to Fig. 3.12: The module is screwed onto the front of RollerBall (chassis front) and includes a transparent cap for the camera. As mentioned in the stability considerations, this could be used in future developments to provide buoyancy and help counteract the offset CoM.

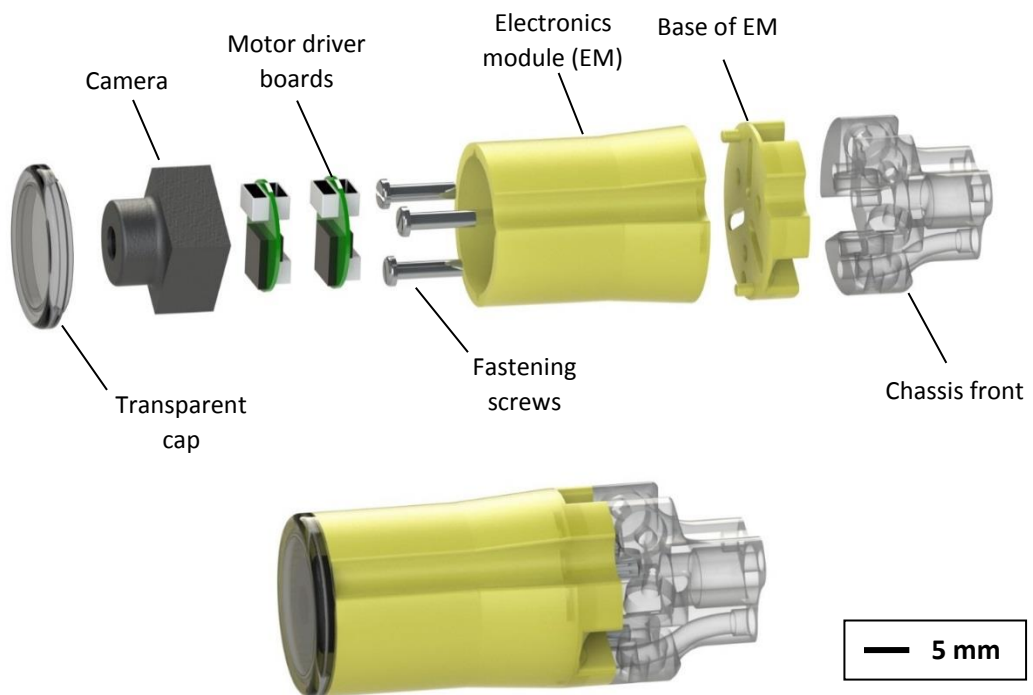


Figure 3.12 – The electronics module.

This figure includes an exploded view of the various components and a view of the assembled unit. A 5 mm scale bar is included for both.

Referring to Figure 3.13: A 3 mm outer diameter, 24-core, flexible tether was used. The insulation was stripped from the end section before threading the bundled wires through the enclosed channel to the front of the robot and into the electronics module. The individual wires were then separated and threaded back through slots in the module to their respective locations.

²³ This currently just includes a camera however, the motor driver boards shown in Figure 3.12 were designed by the collaborators (University of Dundee).

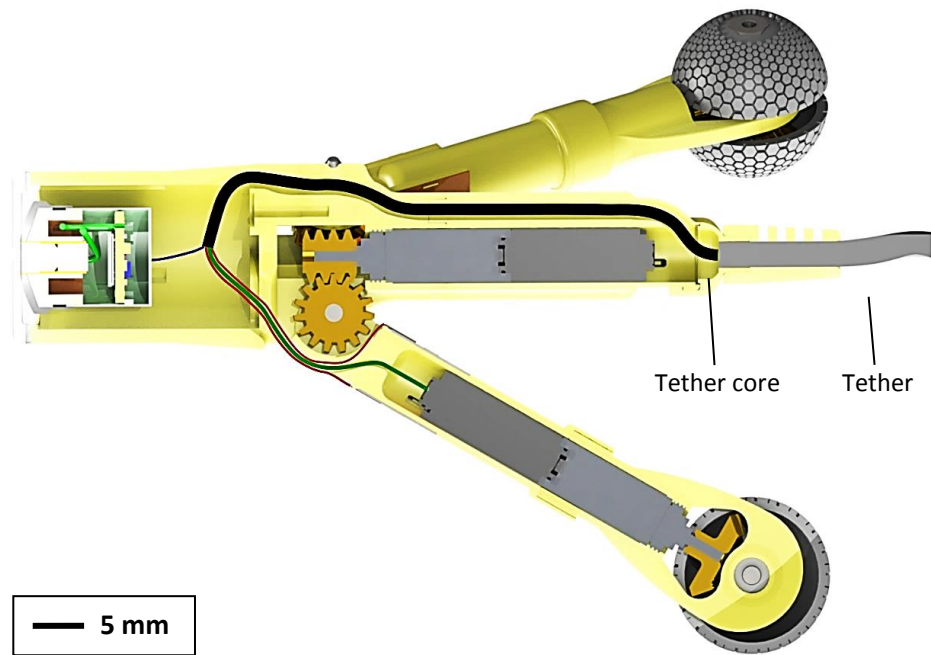


Figure 3.13 – A cross-sectional view showing the route of the tether core.

The individual wires are then fed back through the electronics module to their respective components. A 5 mm scale bar is included.

Referring to Fig. 3.14: An end cap was then placed around the tether to seal the back of the robot. This is fixed to the chassis rear via a ridge and is itself held together by a cable strain reliever – securing the tether in place using friction.

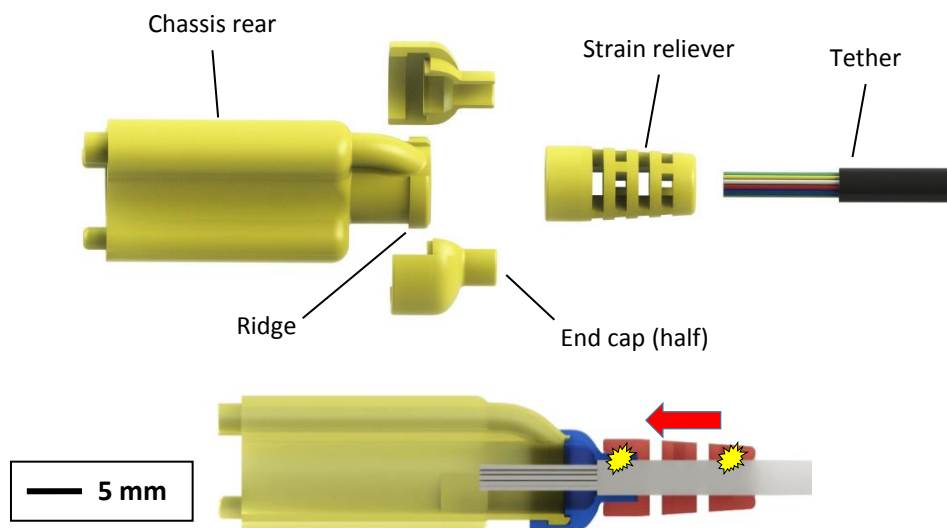


Figure 3.14 – The tether attachment comprising of an end cap and strain reliever.

The cross-sectional view shows how the individual components press together with a tight push-fit tolerance. A 5 mm scale bar is included for both.

3.5. Prototype fabrication and assembly

3.5.1. Fabrication

The manufacture of the small, complex parts that make up RollerBall is well suited to 3D printing. This is especially true with the manufacture of the prototype presented in this thesis as multiple small iterations and replacement components were required. Because of the small feature size on some of the parts, an in-house DLP (Digital Light Projection) printer was used (*EnvisionTEC, Perfactory 3 mini, multi lens*). This had a resolution between 15 and 60 μm , and could accurately reproduce the parts from CAD models with a smooth surface finish. The most durable resin available was used – LS600 (*EnvisionTEC*; the data sheet can be seen in Appendix B.). Despite the high precision and accuracy of the printer, many of the parts that had a push-fit tolerance had to be manually sanded-down to remove support features. All parts were 3D printed, with the exception of the following high load, high wear parts: the 2 mm wheel axles and arm shoulder axles (which were machined from stainless steel); the 5 mm ball bearings (commercially available, metal) and the worm and wheel gear assembly (which were custom made from steel and brass respectively).

The prototype was designed with dimensions that exceeded the requirements but that were considered to be suitable for laboratory based testing. A smaller prototype could have been fabricated using commercially available 4 mm motors, giving the potential to reduce the overall dimensions by ca. 30 %²⁴ (an image of this is included in the Future work, Section 8.1). However, the fabrication would have been even more convoluted and the plastic resin may not have given the small features the required strength. The larger scale used also meant that further modifications and repairs were less complex to perform and the robust prototype could be extensively tested on.

3.5.2. Assembly

Once the parts had been manufactured, assembly was completed in the following steps:

Referring to Figure 3.15:

Step 1 – Strain gauges

The strain gauges were first bonded to the prepared, flat surfaces of the arm base. These were then covered in silicone to provide some wear protection. The strain gauge leads were then threaded through the arm base and soldered to a contact that was bonded to the arm.

²⁴ Since they make up a large proportion of the device, this magnitude reduction is calculated assuming that the motors are the governing factor in the overall size of the device.

Insulated wires were then soldered to the contact and the worm wheel fixed into the arm using superglue. The finished part is shown in Figure 3.15, A.

Step 2 – Robot arms

The bevel gear was held in position before screwing the DC motor into the wheel hub. Loctite™ 243 (thread locking adhesive) was used as a non-permanent method of preventing the motor from unwinding itself in high torque situations. The two bearings were then placed into the wheel hub with a push-fit tolerance – the assembled motor, gear and bearings are shown in Figure 3.15, B. The axle (which is bonded to one half of the wheel) was then inserted into the bearings before screwing the two wheel halves together; again, Loctite™ was used to fix the wheels to the axle and prevent them from unwinding. The arm base could then be inserted over the motor and wheel hub with a push-fit to complete the arm assembly. Steps 1 and 2 were repeated for all three arms (Figure 3.15, C.).

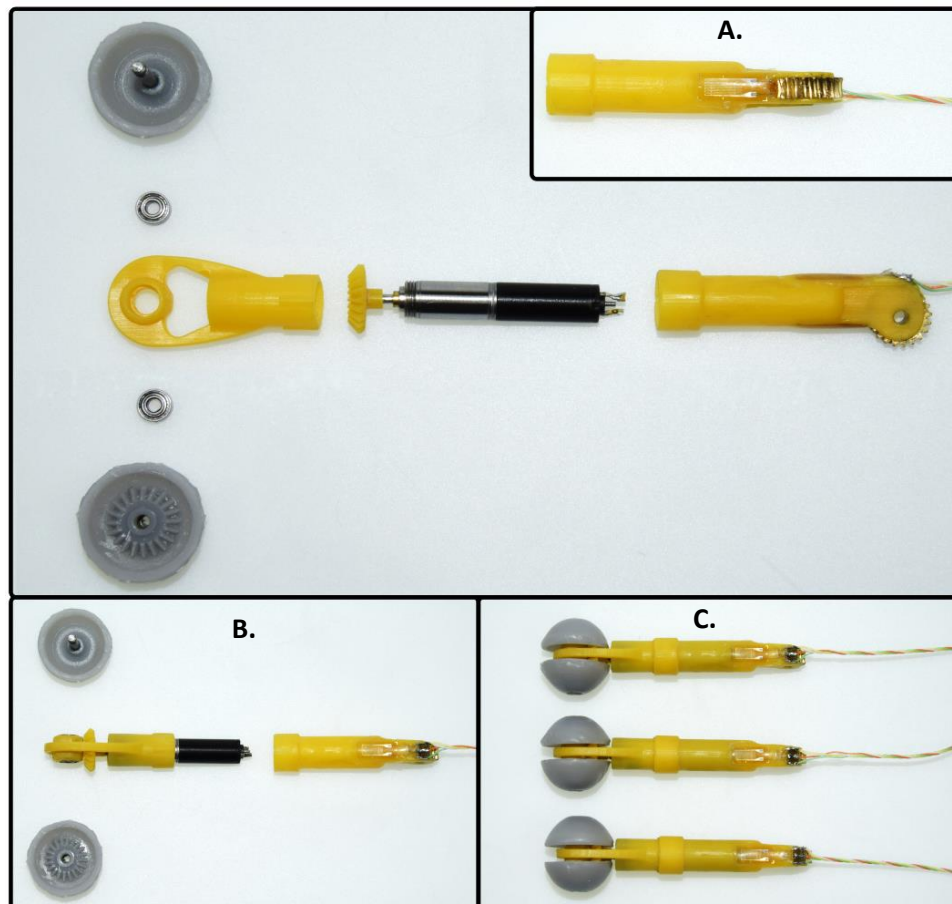


Figure 3.15 – A sequence of photos taken during the assembly of the three arms.

Referring to Figure 3.16:

Step 3 – Robot chassis

Six ball bearings were inserted into the chassis front and then a DC motor with an epoxy-bonded worm gear was screwed into position. The chassis rear was then slid over the motor and inserted into the chassis front with a push-fit. The finished chassis is shown in Figure 3.16, A.

Step 4 – Inserting the wires and electronics module

The next step was to thread the bundled wires from the rear of the chassis to the front of the electronics module, via the route described in Section 3.3.3. The individual wires were then threaded back through their respective slots (one for each arm) as shown in Figure 3.16, B.

Step 5 – Soldering

The prepared arms and camera were then soldered to their respective wires on the chassis (Figure 3.16, C.). The excess length of wire from the individual components was then pulled back into the electronics module before inserting the camera with a push-fit. The arms were then inserted into their respective shoulders before being held in place by inserting the axles (hinges).

Step 6 – Tether attachment

The final step involved neatening the wires (eg. any slack still present) before fixing the tether in place using the two halves of the tether end cap (Figure 3.16, D.). This end cap was itself held together by the tether strain reliever, pressed over the cap with a tight push-fit. The finished prototype is shown in Figure 3.16, E.

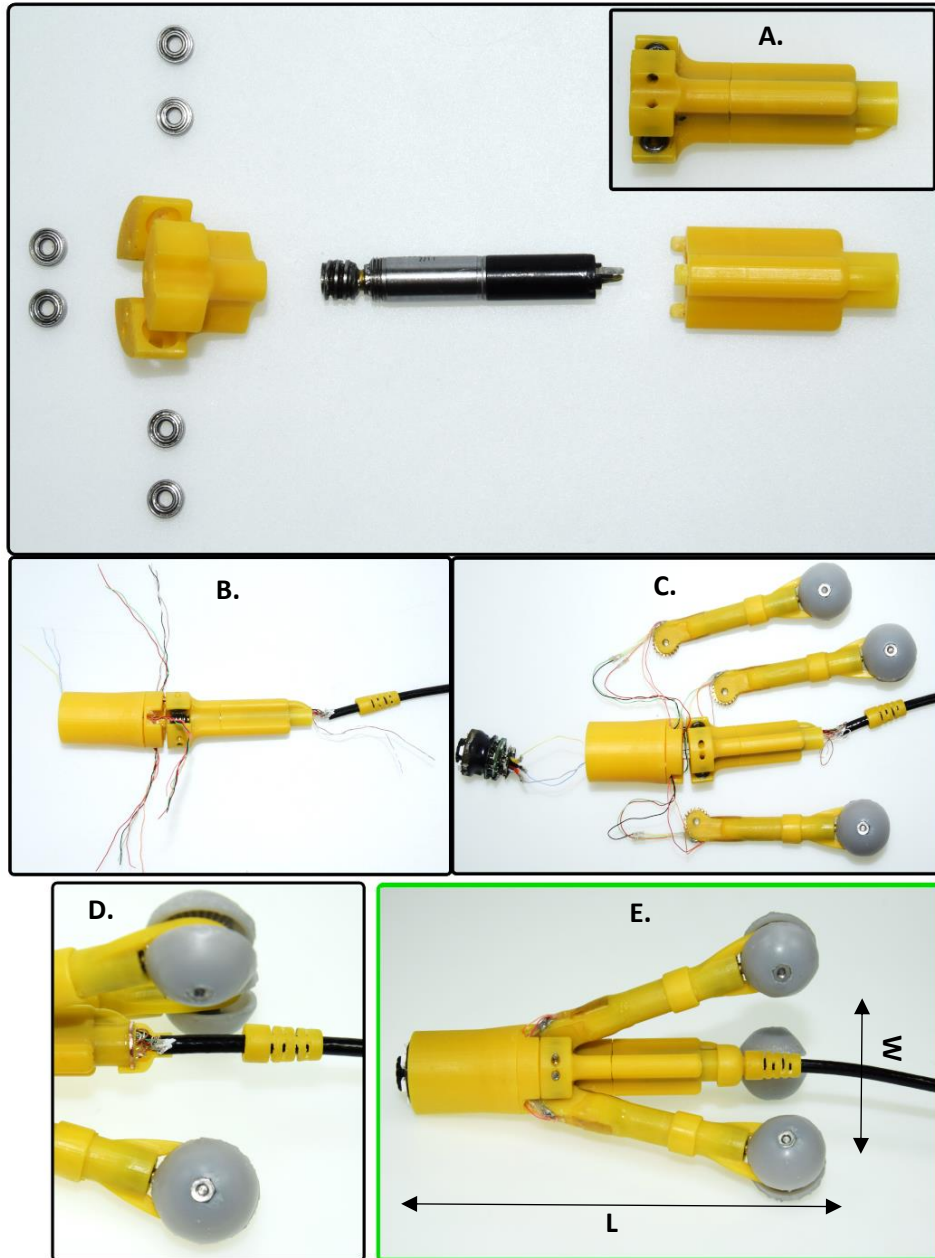


Figure 3.16 – A sequence of photos taken during the assembly of the chassis and rest of the prototype.

The final prototype is shown in E. and includes overall dimensions (when the arms are collapsed fully) of $L = 95$ mm and $W = 35$ mm.

3.6. Benchtop characterisation

This section describes the theoretical and actual performance of the individual wheel and expansion mechanisms through calculations and benchtop experiments.

3.6.1. Theoretical performance

3.6.1.1. Wheel mechanism

Assuming low friction, the theoretical maximum wheel velocity (ω_M) (no load) was calculated as 84.2 rpm (8.82 rad/s) using Equation 3.1:

$$\omega_M = \frac{\omega_{NL}}{n_G} \quad (3.1)$$

where ω_{NL} is the no load speed of the motor (18600 rpm)²⁵ and n_G is the gear reduction (221).

The theoretical maximum tractive effort²⁶ (TE_M) was calculated as 3.74 N using Equation 3.2:

$$TE_M = \frac{\tau_m \cdot n_G \cdot \eta_g \cdot \eta_b}{r} \quad (3.2)$$

where τ_m is the motor's maximum torque (0.000485 Nm), n_G is the gearbox reduction (221), r is the radius of the wheel (0.0086 m), η_g is the efficiency of the gearbox (0.6) and η_b is the efficiency of the bevel gears (assumed to be 0.5 because of the rough plastic gears used).

3.6.1.2. Expansion mechanism

The arms can be adjusted with a theoretical maximum angular velocity (ω_A) of 4.21 rpm (0.44 rad/s), calculated using Equation 3.3:

$$\omega_A = \frac{\omega_n}{n_G \cdot n_W} \quad (3.3)$$

where ω_n is the maximum speed of the motor (18600 rpm), n_G is the gearbox reduction (221:1) and n_W is the worm gear reduction (20:1).

²⁵ The efficiency of bevel gears is typically high and so total friction in the wheel mechanism was expected to be low and hence no load speed was used.

²⁶ Or force applied to the substrate.

The length of the arms (54.5 mm) and the diameter of the wheels (17.24 mm) means that RollerBall has a large workspace, able to operate in diameters ranging from ca. 35 mm (arms approximately closed) to 137 mm (arms perpendicular to chassis – fully open).

The arms actively apply a force perpendicular to the arm (F_A) that is proportional to the motor torque. The theoretical maximum force per arm was calculated as 4.47 N using Equation 3.4:

$$F_A = \frac{\tau_m \cdot (n_G \cdot n_W) \cdot \eta_g \cdot \eta_b}{L \cdot N_A} \quad (3.4)$$

Where τ_m is the motor's maximum (continuous) torque (0.000324 Nm), L is the length of the arm (from the shoulder joint to the wheel axle) (0.0545 m), n_G is the gearbox reduction (221:1), n_W is the worm gear reduction (20:1), η_g is the efficiency of the gearbox (0.6), η_b is the efficiency of the worm gear assembly (assumed to be 0.85) and N_A is the number of arms (in this case, 3).

The inclusion of force sensors (that record cantilever bending force, ie. normal force) and the fact that normal load is used to control traction (based on Coulomb's law) means that it is important to know how much of the arm force is applied normal to the lumen at different arm angles (Figure 3.17).

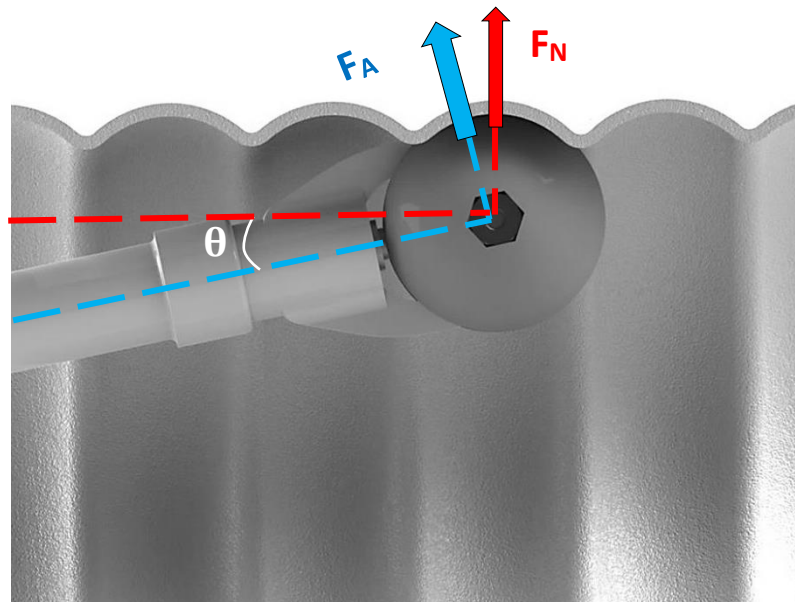


Figure 3.17 – The relationship between the Arm force (F_A) and the resulting Normal force (F_N).

Assuming the robot axis is aligned with the lumen axis, the normal force applied by the arm (F_N) is proportional to the arm force and the cosine of the arm angle, as shown in Equation 3.5.

$$F_N = F_A \cdot \cos(\theta) \quad (3.5)$$

where F_A is the arm force and θ is angle between the arm and the chassis. Therefore, when the arms are fully closed, 100 % of the force is applied normal to the lumen. When the arms are fully open (perpendicular to the chassis), 0 % of the force is applied to the lumen and any force from the elasticity of the tissue is applied parallel to the arm axis and so not registered by the strain gauges. In-other-words, the expansion mechanism and force sensing become less effective in larger diameter lumens.

3.6.2. Actual (Benchtop) performance

Simple benchtop experiments were carried out to assess the functional performance of the wheel and expansion mechanisms with the aim of characterising their outputs and identifying any potential limitations in their performance (or function).

3.6.2.1. Method - Wheel mechanism

To measure the rotational speed, a visible mark was placed on the wheel before it was filmed rotating at maximum speed for 5 revolutions (visually assessed). The time taken per revolution was then used to calculate the rotational speed. A total of 5 repetitions were carried out.

To measure the maximum tractive effort, a single arm of RollerBall with a high friction tread pattern was pressed (F_N) into a block of silicone to prevent slip (Figure 3.18). This silicone was placed on a linear bearing slide, which in turn was connected via a steel rod to an in-line load cell. The current to the motor was then increased to the maximum rated current and the resulting tractive effort (TE) was transmitted to and measured by the load cell (this test rig is described in more detail in Chapter 4). Variance was high and so a total of 10 repetitions were carried out.

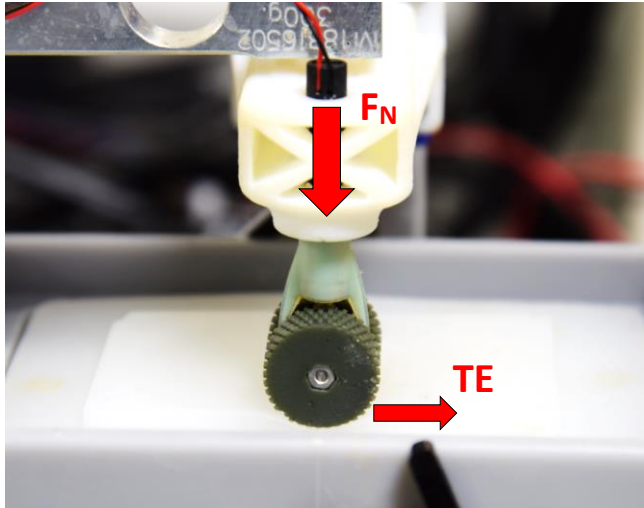


Figure 3.18 – A close-up view of the test rig used to measure the maximum tractive effort of the wheel mechanism.

A preload (F_N) is placed on the arm to increase the friction between the wheel and silicone to a level that stalls the motor. The tractive effort (TE) is subsequently measured.

3.6.2.2. Method - Expansion mechanism

The angular speed of the arm(s) was also measured visually. A single arm was attached to the robot chassis which itself was secured in position. The arm was then filmed expanding at maximum speed, from fully closed to fully open. A backdrop with angle increments was used to determine when the arm reached 90° (fully open) (Figure 3.19). The time taken was used to calculate the angular speed and a total of 5 repetitions were carried out to find the average.

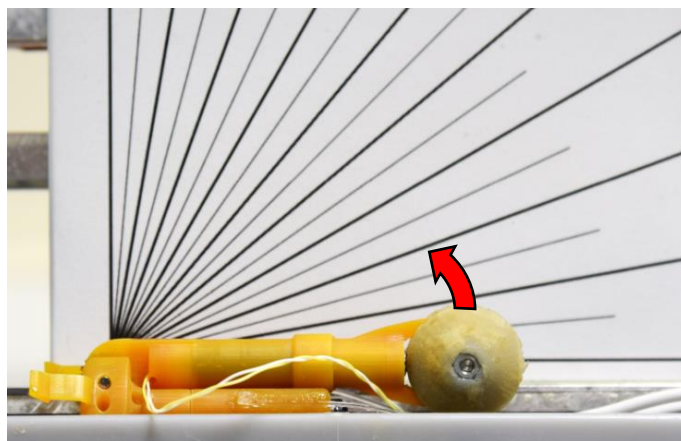


Figure 3.19 – A close-up view of the test rig used to measure the maximum expansion speed of the arm.

The chassis is secured in place and angle increments are used to visually assess when the arm has reached the desired angle.

To measure the maximum expansion force, the prototype was kept in the configuration shown in Figure 3.19 and a beam load cell was lowered down to make contact with the

wheel and block its expansion. Current to the motor was then increased to the maximum rated current of the motor and the peak force recorded²⁷. A total of 10 repetitions were carried out due to high variance seen in the results.

3.6.3. Results and discussion

Table 3.3 summarises the theoretical performance of the individual mechanisms and the results from the benchtop assessment.

Table 3.3 - The theoretical and actual performance of the wheel and expansion mechanisms.

Parameter	Theoretical	Benchtop
Wheel velocity (rpm)	84.2	90 ± 0.85 (n = 5)
Wheel tractive effort (N)	3.74	2.98 ± 0.71 (n = 10)
Arm angular speed (rpm)	4.21	9.47 ± 0.42 (n = 5)
Arm force, per arm (N)	4.47	1.47 ± 0.16 (n = 10)

The actual wheel speed slightly exceeds the theoretical value. This is presumably due to inaccuracy in the applied voltage (the driver board could have applied a larger voltage than desired). This speed will likely drop to ca. 25.7 rpm when in continuous slip against the lumen²⁸. This still exceeds the minimum required speed of 4.3 rpm mentioned in the requirements in Chapter 2. The actual tractive effort was significantly lower than the theoretical value. Again, this could be attributed to an inaccuracy in the applied current and the value used for the efficiency of the bevel gears (0.5) which was clearly overestimated²⁹. Despite the high losses in the wheel mechanism, the available tractive effort is still large and is likely to exceed requirements.

The measured angular speed of the arm was significantly higher than the theoretical value. This further supports that there was an inaccuracy in the voltage applied by the driver board. Conversely, the actual force per arm (1.47 N) was much lower than the theoretical value. This is presumably from the high static friction at the many interfaces (including: worm gear assembly, motor gears and between the arm shoulder and the chassis) and requires further attention in future developments.

²⁷ In future developments, this was achieved by using strain gauges on the arms.

²⁸ Assuming the motor rotates at the nominal speed (5670 rpm).

²⁹ Logically, friction loss in the plastic gears will be high. From the experiments, efficiency of the bevel gears is in the order of 0.4.

3.7. Summary

The RollerBall concept was chosen for this PhD because of the possible advantages of using wheeled locomotion in this context and the potential seen in the development of V1 – 3. Provided traction can be made, the use of wheels may suit the low modulus tissue because of the continuous, high rotational speeds achievable. The individual motor speeds can also be easily and precisely controlled to perform small, precise movements of the robot – useful for the effective use of tools. Commercially available DC motors also provide a high power to size ratio, increasing the ease of miniaturisation. The adjustable arms could ensure that the device provides a stable platform in varying diameter lumens which will also be crucial for the effective use of on-board diagnostic and therapeutic tools.

A number of refinements were made to the design of the pre-existing V3 concept:

1. A module was designed to house the electronics.
2. The stability (CoM) was considered and a solution presented.
3. A number of minor design changes were made to the concept and more major modifications made to the arm design.
4. Preliminary encapsulation considerations were made.
5. A suitable fabrication technique (using a durable material) was found. Step-by-step assembly was then carried-out to produce a robust prototype.

A large proportion of the prototype parts were 3D printed from a durable resin. The overall size of the device (with the arms in a ‘closed’ position) was approximately 95 x 35 mm. This exceeds the requirements suggested in Chapter 2, however, it was deemed a suitable scale for the first fully working prototype and the planned laboratory work. Encapsulation was considered during the designing and fabrication of the prototype however, it is not currently water-tight and would therefore not be suitable for repeated use in a flooded or unhygienic environment. The robustness of the prototype was evident in handling (during and post fabrication) however, whole device tests are needed to show this.

The individual mechanisms functioned as intended in benchtop tests. The wheel tractive effort and rotational speed exceeded requirements. The requirements of the expansion mechanism are not well established at this stage and will need to be assessed in whole device tests. Two potential limitations of the expansion mechanism may hinder the performance of the robot: the high damping in the expansion mechanism and the lack of independent arm actuation.

Further work is required to address two major necessities:

1. Gaining traction on the colon lumen.
2. Development of the whole robotic system, including electronic hardware and control software.

As mentioned at the start of this chapter - despite the clear advantages of using wheeled locomotion and the successful fabrication of a prototype - it will be necessary to test the device as a whole before being able to comment on the concepts overall efficacy as a mobile colonoscopy robot.

Chapter 4

Gaining traction in the colon

This chapter explores the feasibility of gaining traction in the colon – critical to the overall efficacy of RollerBall. Literature is first reviewed, covering topics such as the properties of the colonic mucosa, previous attempts to characterise the friction and existing work on designing tread patterns for a biological substrate. Literature shows that the frictional characteristics are extremely complex and so a robust empirical approach was then used to investigate the performance of a number of 3D printed, patterned wheels. These were assessed both in terms of traction and trauma, with the goal of choosing a suitable tread pattern for RollerBall.

4.1. Introduction

Achieving functional levels of traction is crucial for the effective locomotion of wheeled devices as it allows forces (be it propulsive, resistive or stabilising) to be transmitted to the surrounding environment. It is also important to understand the specific frictional characteristics of the wheel-substrate contact as it allows the forces to be predictably controlled [17]. This is particularly challenging for RollerBall as the colon is arguably one of the most difficult biological substrates to gain traction on because of its unique properties and inherently low friction characteristics. Ideally, the wheels should provide sufficient traction with minimal normal force being applied to the tissue (high friction coefficient) – reducing the demands on the mechanical system and helping to minimise mechanically induced trauma due to excessive pressures. There are a number of intuitive ways to control friction on the colonic lumen, including: *Suction* – using a vacuum to adhere to the soft tissue; *Muco-adhesives* – exploiting the adhesive interaction between a synthetic muco-adhesive and the biological mucus layer and; *Tread patterns* – increasing resistance by the physical interaction of the tread and the tissue substrate.

A muco-adhesive is a polymer based adhesive that, as the name suggests, interacts with the mucus layer of the colon. It can be described by combining a number of theoretical mechanisms, including: *the electronic theory* – attractive forces present due to the build-up of electrical charges at the interfaces; *the absorption theory* – comparatively larger forces arise from the formation of hydrogen and van der Waals bonds; *the wetting theory* – stating

that interfacial energy should be considered as it is an important factor in muco-adhesion and; *the diffusion theory* – the penetration and physical entanglement of the molecules in the mucus and adhesive provides further adhesion [100, 101]. This has been used for local drug delivery, where capsules are coated with a muco-adhesive to adhere to the tissue and slowly release a drug. It could also be used on a mobile robotic platform to gain traction against the low friction mucus. Dodou et al. [102] looked to develop this method and static friction was seen to increase by a factor as high as four, demonstrating its effectiveness at adhering to the mucus layer. No tissue damage is caused as the adhesive bonds to the mucus layer itself. This is a huge advantage of muco-adhesives however, there are a number of issues with using this method to gain traction: Firstly, the static friction is high but once the bonds are broken the friction reduces significantly [103]. Secondly, and similarly, once the bond is broken and the hydrogel has swollen, the muco-adhesive is no longer effective and will not adhere as it did initially. A means of renewing the muco-adhesive layer is required for repeatable adhesion. Lastly, muco-adhesives often require some time to form a bond and so the movement speed of the device will be restricted [100, 102-104].

Octopuses use suction cups to effectively increase resistance on a number of different surfaces underwater; actively adhering to the surface, increasing contact area and friction between their rough-textured³⁰ pads and the substrate [105]. A passive sucker, such as that presented in [106], could be designed for the colon to increase adhesion and improve friction at the same time. However, considering the context of a mobile wheeled robot: suckers can create strong attachment forces but their uncertain efficacy at resisting shear, combined with the relatively complex mechanism required to create and control the vacuum, means that this form of increasing friction is most suited to applications requiring a static, long duration hold and not the rapid or continuous shear present in mobile robots. This challenge is shown in work by Patronik et al. [107], where friction was only considered satisfactory when a textured (tread) surface was added. Similarly, the drawbacks of using muco-adhesives suggest they are also suited to such (low shear) applications. Therefore, the comparatively simpler mechanism of using tread patterns – which is most often used in mobile applications – will be the focus of this work.

The aim of this Chapter is to find a suitable tread pattern for Rollerball, which has high traction and yet imposes low trauma at the levels of normal force required. The substrate is first described in detail before the current theory of gaining traction on soft biological

³⁰ This is a key feature to improve friction.

substrates is presented. There are a huge number of factors contributing to traction in this context, as an illustration, Figure 4.1 shows some of the most significant.

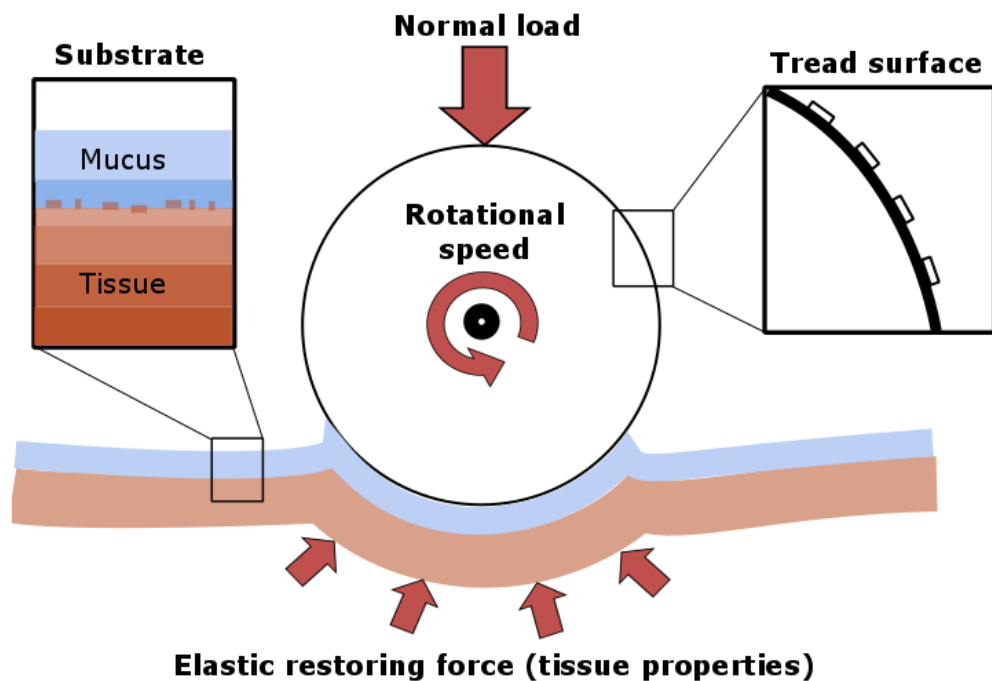


Figure 4.1 – An illustration of *some* of the many factors contributing to the overall traction achieved by a wheel on colonic tissue.

Main factors including: *normal load* (affecting contact area, elastic restoring force and fluid thickness); *rotational speed* (affecting the properties of the mucus and tissue and overall hydrodynamics); the underlying *tissue properties* (dissipating energy and determining factors such as contact area); the *tissue substrate* (which is multi-layered, has a surface roughness and a non-Newtonian mucus layer) and; the *tread surface* (including its surface roughness, tread geometry, scale and surface chemistry).

The complexity means that it is questionable whether a suitable model could be created to accurately predict how a tread will perform, particularly since the substrate is likely to change from individual to individual. As a result, this chapter explores previous successful tread designs used in this (or similar) context and uses that to provide further insight into the mechanisms involved. The knowledge gained is then applied to a comprehensive experimental study on the performance of various macro-scale, 3D printed tread patterns, the results of which contribute to a better understanding of how to achieve high traction on the colon. Lastly, a wheel tread candidate for RollerBall and optimum solution are proposed.

4.2. The colonic mucosa

Tread patterns are extensively used to improve traction between two surfaces. The geometry, scale and material properties of the tread are largely chosen based on the substrate. On hard, dry and rough substrates (tarred roads, for example) this is a somewhat simple task where traction is increased by increasing road-tyre contact using a soft rubber compound and a large, smooth tyre. In comparison, the mechanisms involved in the tribological interactions between soft, wet biological tissue and a relatively harder surface are less described in literature. To explore the mechanisms involved, the substrate should first be well defined. The colon was described in Chapter 2 - Section 2.1, as being thin, soft and lubricious; this section adds to it by including details on the mucosa that are relevant to traction.

The human intestine has an extremely low friction lumen. Work by Lyle et al. [108] highlights this, reporting friction coefficients ranging from 0.0004 (between smooth steel and small intestine) to 0.018 (between micro-patterned PDMS and small intestine) – these values could be even lower on the colon. Three features contribute greatly to this: the properties of the underlying tissue; the substrate features/roughness and; the properties of the mucus.

4.2.1. Tissue properties

Intestinal tissue is extremely soft and there is little documentation on the mechanical properties of human colon, particularly *in vivo*.

Under tension, the maximum stress and destructive strain of the colon vary between 0.87 - 0.9 MPa and 62.8 - 180 % respectively [109, 110]. The tissue is viscoelastic, with higher strain rates yielding higher stress. Higa et al. [111] showed that the absolute stress under compression varied from 14.7 kPa to 204.8 kPa, with a change in compression rate from 0.02 mm/s to 5 mm/s. If stressed in different directions, the multi-layered structure of the colon results in the mechanical properties shown in Figure 4.2.

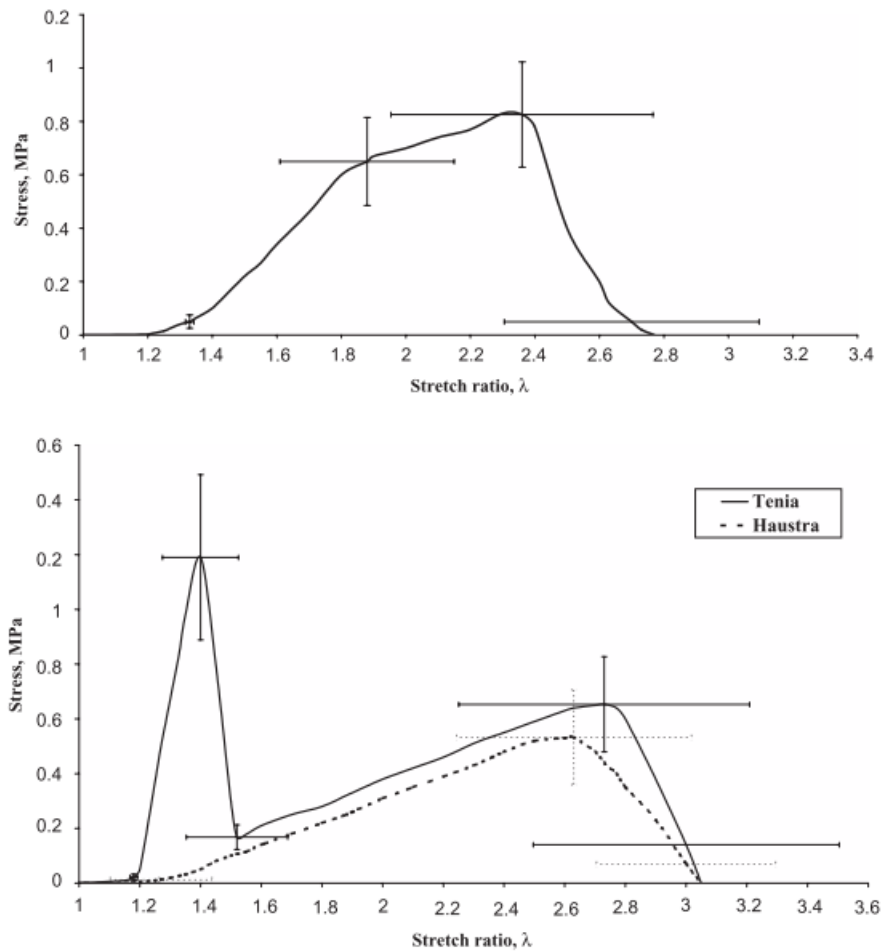


Figure 4.2 – The stress-strain curves of two colon specimens (large bowel) under transversal and axial tensile loading. [109]

4.2.2. Surface features

When laid flat, the colonic lumen is comprised of millimetre-scale creases or ridges. These are likely to differ greatly from individual to individual and also based on colon regions however, as an example, Buselli et al. [99] reported them ranging from 0.72 mm to 1.18 mm in amplitude. The surface is smooth on the micro-scale, comprised largely of tube-shaped crypts which are separated by connective lamina propria (with a single layer of epithelial cells near the lumen) – the overall appearance is described as honeycomb-like and the features said to be in the order of hundreds of nanometres [112].

4.2.3. Mucus layer

The lumen is covered by mucus that consists of two distinct layers: a firmly adhered layer and a loose, mobile layer. The average overall thickness varies greatly, ranging from 135 μm [113] to in excess of 200 μm [114]. The thickness is determined by the balance between secretion and degradation rates [113]. In humans secretion occurs at ca. $240 \pm 60 \mu\text{m/h}$

therefore, if not degraded, a thickness in excess of 700 μm could occur [114]. The mucus is non-Newtonian, with a viscosity ranging from 0.16 – 1000 Pa.s as shear rate is decreased from 100 to 0.01 rad/s. This can be qualitatively described as changing from a gel-like substance to water [113, 115]. The presence of this thick mucus blanket and its two distinct layers is crucial to the frictional characteristics of the colon. On a high level, it creates a “slippage plane” where a body that contacts the colon surface shears the mobile mucus layer and the adhered layer remains unstirred (ie. direct contact with the epithelium is not made) [113].

4.2.4. Summary of properties

Because of the relatively few studies on the specific topic of frictional characteristics, some studies on the small intestine have also been included. As a way of comparison, Table 4.1 presents the major features of both.

Table 4.1 - A comparison of the small and large intestine.

Attribute	Small intestine	Large intestine
<i>Mechanical properties</i> ¹	0.83 MPa (at 88% strain), ca. 138% yield strain [109].	0.65 MPa & 0.83 MPa (at 88% & 136% strain). ca. 177% yield strain [109].
<i>Tissue thickness</i>	1 – 3 mm (depending on distension) [116].	0.7 – 1.5 mm [16].
<i>Surface features</i>	Villi, Roughness of 150 μm [117].	Crypt cells, 30 – 670 nm roughness [112].
<i>Mucus layer</i>	119 – 527 μm (13 – 37 μm of which firmly adhered) [118].	200 – 940 μm , replenished at ca. 240 $\mu\text{m}/\text{h}$ [114]. (65 – 167 μm of which firmly adhered) [118].
<i>Mucus properties</i> ²	0.063 – 5 Pa.s [115].	0.16 – 1000 Pa.s [115].

¹Max stress in transversal direction (cadaveric tissue).

²Apparent dynamic viscosity of porcine mucus (0.01 – 100 rad/s shear rate).

The differences shown in Table 4.1 do not detract from the major similarities: they are both soft, visco-elastic and covered in a lubricious mucus layer.

4.3. Frictional regime

The most common and well known friction model involves two dry surfaces contacting each other with a normal force. The resulting friction force approximately follows Coulomb's law, where friction increases linearly with normal load as the degree of asperity-asperity contact is increased – direct contact must be made for this form of resistance to take place. Total friction force is proportional to the degree of contact (which is proportional to normal load), the surface roughness and the material properties (as asperity deformation provides resistance). Contact is improved by matching the surface roughness of the tread with the substrate and thus maximising asperity-asperity interlocking [99]. However, it is clear that the friction model in the intestine is more complex and does not follow this law because of the many factors involved (illustrated in Figure 4.1). Obvious indicators of this are the presence of an adhesive force at zero load [17] and a nonlinear dependence of the friction coefficient and normal load [119].

As Lyle et al. [120] have emphasised, a number of authors have studied this subject but the frictional characteristics of the colon (or intestine as a whole) are still not well understood. Interpreting the results from studies that use different experimental designs and control different variables (such normal load, contact area, velocity etc.) is challenging, with the individual effect of each variable and the complexity of the biological substrate having differing, sometimes contradictory, results.

There appear to be a number of factors affecting resistance to motion in this environment and so the frictional characteristics could be described by combining them [121]:

1. *Micro asperity-based (Coulomb) friction* – There may be direct contact between the asperities of the two surfaces and a resulting friction force that approximately follows Coulomb's law. Zhang [121] and Lyle et al. [108] have shown that this is a very small component of the total resistance and in fact, as will be discussed later, it is unclear whether direct contact is actually made. Therefore, the component of the friction force that is load dependent (and hence said to approximately follow Coulomb's law) may in fact arise not from direct, micro-scale asperity-asperity contact, but from *Environmental resistance*.

2. *Environmental resistance* – Sometimes referred to as “edge-effects” [120] or hysteresis losses [122], this resistance is from the visco-elastic deformation of the intestinal tissue. This can occur at different scales, including: the global deformation of the surrounding tissue by the robot or robot’s appendage and the multiple, localised deformations of the lumen created by individual features of a tread pattern. The magnitude of this is proportional to the tissue modulus (or elastic restoring force which provides resistance to deformation), the tread groove volume (or volume of tissue squeezed) and the tread geometry (as the tread face must provide an effective obstruction during shear) [17, 98, 122]. Since the tissue is visco-elastic, this resistance increases with increased velocities (shear rates) [111, 119, 121].

3. *Viscous friction* – This results from the adhesive and viscous properties of the mucus. While the contact is static³¹, the tacky mucus provides an adhesive force. Then, during movement, resistance comes from the viscosity which provides resistance to shear [120]. Therefore, this force should largely be dependent on: the surface area in contact with the mucus (including the contact angle, ie. surface chemistry) and the apparent viscosity (which is dependent on mucus thickness and inversely proportional to shear rate). Intuitively, this resistance should therefore decrease with velocity however, literature is unclear on this and the results are sometimes contradictory [17, 115, 121].

The convoluted frictional characteristics and the unclear mechanisms involved suggests there is still a need for further investigation. This will be reported in the subsequent sections, including: exploring how nature optimises traction and whether this could be applied to the intestine (Next section); reviewing others previous work on the use of tread patterns on biological tissue (Section 4.5) and in the experimental assessment of various macro-scale tread patterns (Section 4.7).

4.4. Looking to nature

As it is often with other areas of research, nature may help in finding an elegant solution to gaining traction in the colon. Tree frogs have a remarkable ability to both adhere to (and gain traction on) a wide range of surfaces including smooth and wet substrates. Their toe pads have hexagonal pillars 10 – 15 μm wide, separated by ca. 1 μm channels³² [123]. Each

³¹ Or at very *low* velocities.

³² Hexagonal pillars are most common however, a number of other geometries (including 4, 5 and 7 polygons) are also present.

pillar is then covered in smaller, 10 - 40 nm pillars (Figure 4.3). One reason hexagons may be used in nature is that they can be very efficiently packed into a given space. This gives rise to both a high contact area and a large drainage channel area. The mechanical properties of the toe pads are also key: the surface of the pad (the micro and nano-scale pillars) are keratinised with a modulus similar to silicone rubber (5 - 15 MPa) – thought to provide a conformable surface that is also wear resistant. The underlying toe pad has a much lower stiffness of 4 – 25 kPa (on par with some of the softest known biological structures) [124]. These functional surfaces increase traction and/or adhesion through a number of mechanisms, including: increasing real contact (as the pattern conforms to the substrate and the micro-scale pillars interlock with the substrate asperities); encouraging the displacement and even distribution of thin fluid layers on the surface of the substrate, reducing fluid film lubrication and increasing the effect of capillary forces (adhesion) and lastly; exploiting van der Waals forces that arise from the intimate contact between the pillars and the substrate [123, 125-130].

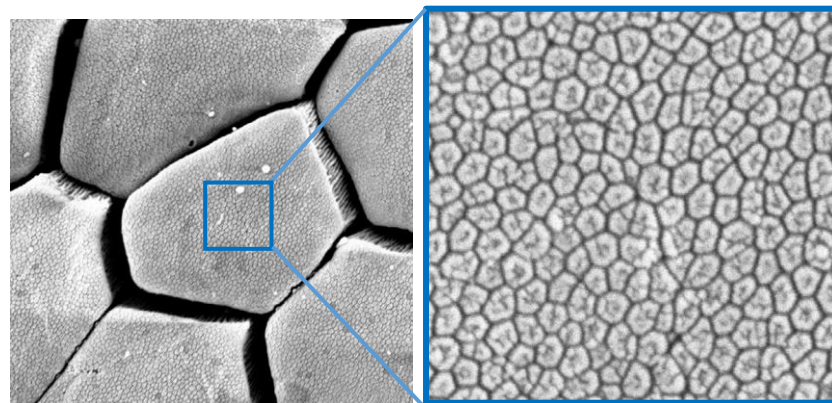


Figure 4.3 – The hierarchy of features on a tree frog toe pad, modified from [130].

Researchers have attempted to mimic these functional surfaces with a similar, but slightly larger, scale and geometry. The work showed that a surface with this pattern is much more effective on a wet substrate than a surface with no pattern. The following was also noted [125-128]:

- A micro-patterned tread produced less stick-slip as the individual pillars can deform and so maintain contact during shear.
- Crack propagation³³ is hindered.

³³ As the two interfaces are pulled apart, the crack (separation) releases strain energy that encourages the propagation of the separation. The pillars slow this by deforming and ensuring the interfaces stay in contact for as long as possible.

- Elongated pillars (orientated with the long edge perpendicular to the direction of shear) result in higher friction.

A similar tread pattern could be used on the colon to improve traction however, the efficacy of a tree frog's toe pad on an intestinal substrate (that is comparable in stiffness and has a thick mucus layer) has yet to be investigated.

4.4.1. Considering hydrodynamics

The toe pads of tree frogs are highly specialised to effectively handle fluid at the interface. Hydrodynamics should be considered in the context of RollerBall because the colon has a layer of mucus and in some cases may be flooded; RollerBall also uses wheeled locomotion and so high shear rates (90 rpm, ca. 81 mm/s) and a rolling contact are present. A fluid layer drastically reduces friction (as the fluid is much easier to shear than the underlying tissue) and in some cases may completely prevent the direct contact of two surfaces. A rapid de-wetting of the surface (displacing excess liquid) increases the degree of tread-surface contact, providing resistance sooner and to a greater degree. These are both desirable for a wheeled robot which should gain traction in a short time with little slip – improving locomotion efficiency and controllability.

Hydroplaning occurs when the hydrodynamic pressure of the contact zone matches the wheel contact pressure and the wheel is then supported by the fluid film. This fluid film can shear much more easily than the substrate and so traction is reduced [131]. Tyre treads are known to delay hydroplaning by providing channels for this fluid to escape [131, 132]. Hydroplaning is greatly affected by the viscosity (and density) of the liquid and the relative velocity; a more viscous liquid (such as the mucus in the colon) and a high speed resulting in a much larger hydroplaning risk [130, 133]. However, despite the high viscosity of the intestinal mucus, it is uncertain whether conventional hydroplaning could occur in this context because of the presumed low net speed of the robot. In saying this, it is worth speculating that the firmly adhered mucus layer could still entirely support the tread surface if the contact pressure and feature height are not great enough to penetrate it.

If the tread surface is not completely supported by the mucus layer, a very likely issue is the presence of trapped “liquid islands” between the wheel and substrate. These can smooth the substrate surface and therefore reduce asperity-induced viscoelastic deformation of the tread (or tissue in the case of the colon) [133] - friction is reduced presumably on both the micro and macro scales. Logically, this effect is could be pronounced on the soft, visco-elastic colonic surface as some of the energy put into displacing the fluid will be lost deforming the

underlying tissue instead. Regardless of the exact state and its effect on traction, the fluid layer between the tread and substrate should be displaced as quickly and completely as possible.

Gupta et al. [134] investigated what effect micro pillars had on hydrodynamic repulsion (force required to displace the liquid between two approaching surfaces). The work showed that pillars effectively reduce hydrodynamic repulsion by providing channels for fluid to flow through when the fluid layer is thin. Referring to Figure 4.4: The distance (h) at which fluid flows through the channels is h_0 and is seen to be dependent on channel depth – ie. the channels have no effect when $h > h_0$. When $h \ll h_0$, the channels again have no effect as fluid is displaced radially from the individual pillar surfaces.

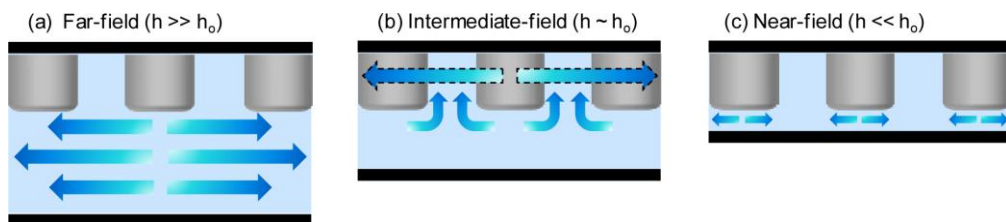


Figure 4.4 – A sequence of images showing out-flow of fluid from a patterned surface.

When the fluid thickness (h) is greater than a critical thickness (h_0), the channels have no effect. When the critical thickness is reached, fluid flows through the channels and helps to reduce hydrodynamic repulsion.

When the thickness drops significantly below the critical thickness, the channels again have no effect.

Persson et al. [130] showed similar results: Channels assist in drainage because they increase the effective separation between the surfaces. For optimum squeeze-out speed, a hierarchical distribution of channels should be used, as highlighted in work done on tree frog toe pads. In order to increase both adhesion and friction, the tree frog must rapidly remove excess liquid during each toe strike. The dense array of hierarchical channels is said to provide a means for the liquid to flow out of, reducing hydrodynamic repulsion at multiple fluid thicknesses because of the hierarchal structure. As the fluid is displaced, it first flows through the larger channels and then as the fluid layer reaches a critical thickness, it flows through the smaller channels until an extremely thin layer remains. This more intimate contact increases friction and the extremely thin fluid layer increases adhesion [130, 134]. A higher channel volume and channels perpendicular to the direction of travel have been shown to be most effective in the automotive industry [132]. It is unclear if this is from enhanced de-wetting, but elongated pillars have also been shown to improve friction on a wetted surface (in the axis perpendicular to the direction of shear) [128].

4.5. Tread patterns for biological use

A number of authors have researched the use of tread patterns on biological tissue to increase traction (or adhesion) and minimize trauma. In this chapter, these are broadly separated into two classes: “micro-treads” and “macro-treads” – where micro-treads have a feature scale less than 200 μm . The aim is to provide further insight into the frictional characteristics of the intestine and help direct the design and testing of a suitable tread for RollerBall.

4.5.1. Micro-treads

These treads tend to assume that direct contact will be made with the intestinal lumen (specifically, the underlying epithelial cells). Therefore, the tread feature dimensions are chosen in an effort to match the roughness of the substrate and so increase real contact and resistance from the interlocking of the tread features with the substrate asperities [99].

Buselli et al. [99] explored the use of circular pillars, with diameters ranging between 15 and 180 μm , on porcine colon. A height of 100 μm was maintained and the spacing varied between 11.5 and 135 μm . The use of pillars was shown to increase the friction coefficient from a range of 0.17 - 0.4 (control) to 0.23 – 0.75 (pillars). Similarly, Glass et al. [135] tested an array of circular, 140 μm diameter, 140 μm high and 105 μm spaced pillars, this time on small intestine. The tread pattern increased the friction coefficients from a range of ca. 0.09 - 0.25 for a flat surface to ca. 0.15 - 0.4 for the pattern surface (the variation being from normal load).

Lee et al. [96] tested patterns that included: a control (smooth), square-shaped pillars, parallel grooves (to direction of shear), perpendicular grooves, pyramid-shaped pillars and bottle-shaped pillars. Although geometrically different, the relative heights, widths and spaces between the features were kept constant (approximately 65 μm high, 85 μm wide and spaced 65 μm apart). Parallel grooves were shown to give the highest friction coefficient (exceeding unity and increasing the coeff. by ca. 158% compared to the control). This was closely followed by Perpendicular grooves. Tread geometry was said to have less of an effect on friction at higher normal loads due to resistance being dominated by edge-effects.

Chen et al. [123] assessed the efficacy of hexagonal shaped pillars (as well as other shapes) as the interface for surgical graspers. Elongated hexagons (parallel to the direction of shear, ca. 100 μm long, 50 μm wide and 30 μm high) performed best on wetted liver, with a friction coefficient between 0.7 and 0.9. It is unknown how these geometries perform on intestinal tissue at either micro or macro scale.

***NB:** The majority of these tests were carried out at relatively low velocities (sometimes less than 1 mm/s) and low normal loads (typically less than 1 N).*

4.5.2. Macro-treads

Macro-treads rely on the physical squeezing or deforming of the tissue between tread features to provide resistance – exploiting environmental resistance [121]. The other components (Coulombic and viscous) contribute, but less significantly.

Accoto et al. [122] looked solely at a smooth coupon and a coupon with rectangular grooves 2 mm wide (spaced 4 mm apart). The flat surface had a friction coefficient in the order of 0.001 and the rectangular grooved surface a value of ca. 0.47. Wang et al. [17] used a metallic, flat coupon (control) and compared it to coupons with triangular, cylindrical and rectangular-shaped features (each feature approximately 1.5 mm wide). Surface geometry was shown to have a significant effect on the friction coefficient, with the control having the lowest (approximately 0.15) and the triangular surface the highest (approximately 0.875). Gao et al. [98] investigated a number of less conventional, more complex tread patterns. The patterned grooves all had a depth of 0.5 mm and a width of either 0.5 mm or 1 mm. The following patterns were tested: Smooth (control), array of circular holes, ring-shaped holes, perpendicular grooves (to direction of shear), perpendicular wavy grooves, square-shaped holes and oblique or diamond-shaped holes. The oblique grid performed best, followed by the square grid indicating that a more complex groove pattern with both multi-orientation grooves and a high groove area/volume is important. In this work it was stated that friction force is related more to tread channel volume rather than tread surface area (ie. environmental (deformation), not Coulombic (asperity contact)). The friction coefficients exceeded unity, most likely due to the inclusion of a Carbopol polymer used to increase muco-adhesive forces. Lastly, Kim et al. [117] tested various end-effectors with either rounded, flat or hollow-tipped tubes and with varying number of protrusions – focusing almost entirely on environmental resistance. A single, flexible, flat-tip tube had a friction coefficient of 1.17, whilst a rigid flat-tip had a coefficient of 0.52. Generally, the use of multiple tubes gave better traction than single tubes as they have a higher chance of interlocking and generating a stable contact. An optimum design included 9 flexible, 2 mm long, 0.76 mm diameter (0.25 mm bore) tubes (coeff. of 1.46).

4.6. Literature summary and discussion

Superficially, micro-scale tread patterns seem to be an attractive option. They could be designed to closely match the scale of roughness of the colon which would theoretically maximize contact area (asperity-asperity contact) and result in high friction. The micro-scale of the tread would also ensure less trauma is inflicted on the tissue as stress is evenly distributed across the many micro features/treads. Furthermore, if there were sufficiently high stress concentrations to pierce the mucosa, the micro-treads cannot physically penetrate far enough to reach the submucosa. However, to achieve this high friction, the treads must contact the surface and the surface should ideally be a comparable stiffness, if not higher than the tread - this would ensure the deformation of the asperities provides resistance. The presence of a mucus layer, and the low stiffness of the tissue, may hinder this for the following reasons:

Firstly, the mucus layer must be displaced before the treads can contact the underlying tissue epithelium. It is likely that very little real contact will be made because the mucus is comparatively thick. This is particularly true in the colon where the firmly adhered mucus layer would require significant force to displace and can be in excess of 150 μm thick [118]. Thus, there is likely to remain a thin layer of mucus between the tread and the tissue epithelium (particularly under low loads)³⁴ and resistance is likely to come almost entirely from the mucus. At low velocities, this resistance is from the adhesive bond between the mucus and the contacting surface. While shearing does break these bonds, if the velocity is low enough, stress relaxation in the tissue may allow them to reform [119, 120]. At higher velocities, resistance comes from the shear forces within the mucus [120]. This may explain the seemingly high friction coefficient at low normal loads and velocities – sometimes exceeding unity - because resistance from the mucus is not dependent on load but on adhesion, and these bonds can reform. At high normal loads, the very little to no direct contact between the two surfaces would result in a low friction coefficient as resistance due to the properties of the mucus are expected to remain relatively constant regardless of load.

Secondly, the tissue has an extremely low mechanical modulus. On the micro-scale it is therefore assumed that, even if asperity-asperity contact could be made, resistance from the micro-scale deformation will be low as the low volume of tissue is easily displaced by the relatively stiff tread features. The seemingly poor scalability (of traction with normal load

³⁴ It is true that a tread pattern, including micro-pillars, can reduce hydrodynamic repulsion and promote the displacement of liquid from a contact however, a micro-scale tread will have little effect on a mucus layer that can be thicker than 500 μm with a firmly adhered layer as thick, or thicker, than the height of the pillars.

and speed) of micro-treads is highlighted by the fact that the friction coefficient is shown to decrease greatly with normal load. The friction coefficients of the micro-scale patterns mentioned in this paper were seen to reduce by ca. 43 – 69 % with an increase in normal load. As mentioned previously, this is likely due to the fact that the source of resistance is changing from the muco-adhesive forces (non-load-dependent and so a high value) to the comparatively lower forces from shearing the mucus. Another possible explanation for this reduction is that mucus is progressively squeezed out of the crypts on the intestine surface as load increases, enhancing lubrication [119, 122], smoothing the substrate and further reducing (or likely preventing) real contact [130]. Finally, when considering the practical use of these treads, it is intuitive that they are easily flooded by thick fluid layers and the features can be clogged by small debris. The micro scale means the individual pillars/treads are also susceptible to damage and their fabrication complex. Therefore, micro-scale tread patterns seem to be very effective at low sliding speeds and low normal loads however, their appropriateness for a functional wheel under high speeds and loads is questionable.

Under higher normal loads and speeds, the dominant form of resistance on intestine is from environmental resistance, which can increase net resistance by an order of magnitude compared to the other forms of resistance [108]. It is less dependent on contact area and more on tread groove volume (ie. the volume of tissue squeezed/displaced between the tread features). High stress concentrations are favoured as they deform the tissue greatly and therefore more tissue is 'squeezed' [17]. Any protrusion will deform the tissue and provide resistance (as was emphasised by the simple features used in [117]) however, tread geometry has been shown to have a significant effect. For example, ridges with a triangular cross-section outperform ridges with a rounded cross-section [17]. An array of circular holes is outperformed by a grid of square holes which in turn is exceeded by a grid of diamond-shaped holes [98]. Environmental resistance requires tissue to deform into the tread grooves before the tread face can provide an obstruction during shear [17]. Having a large groove volume to surface area ratio (and thus high stress concentrations) is one part of the solution; the other must be the orientation of the grooves (tread faces) as elastic restoring force is applied to any edges that deform the tissue during shear and is applied in the direction of shear. Therefore, perpendicular-lined grooves should give the highest level of resistance as the tissue cannot deform around it (as it would with circular pillars for example [98]). However, this may present a problem during shear since tissue may not successfully re-enter the tread grooves and could instead pile-up only at the leading edge – particularly at high velocities where stress relaxation does not occur fast enough (Figure 4.5).

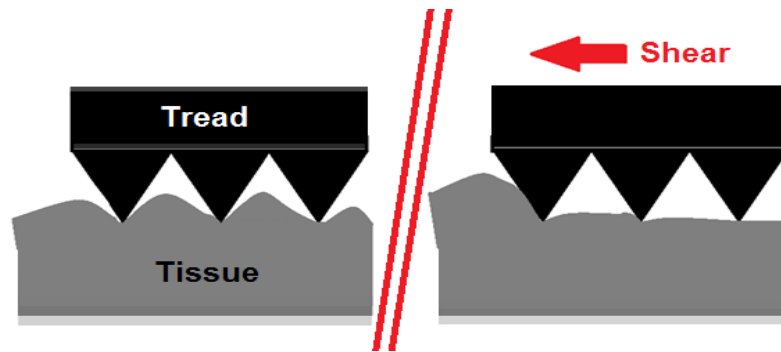


Figure 4.5 – An illustration of how tissue deforms into perpendicular (to shear) tread features.

Perpendicular treads may perform badly during shear – they could behave as a single surface with one gripping edge (effectively negating the presence of multiple grooves).

On-the-other-hand, parallel-lined grooves provide less obstruction to the tissue during shear however, the soft tissue readily enters into the tread. It is therefore logical that the front edges of diamond-shaped grooves [98] (or the similar shaped hexagonal pillars) provide a combination of these two requirements: they are angled in such a way that they both simultaneously encourage the ingress of tissue *and* provide an edge to resist the elastic restoring force. This may be why they performed best in literature.

The friction coefficient of macro-scale tread patterns should be less dependent on normal load as the mucus and surface roughness have less of a significant role in resistance. As a result, these treads appear to favour applications with higher sliding speeds and normal loads. Literature supports this with coefficients - although generally lower than those achieved with micro-scale treads – reducing only slightly (ca. 6 % [17, 122]) with increasing normal load. The implication of this is that friction forces could be effectively controlled by adjusting normal load. The reduced need to match the colon roughness and the simple mechanism of gaining traction could also mean that these treads function well on all regions of the colon. However, one significant drawback of using them is the potential for high trauma from the exploitation of high localised forces. And so, in summary:

- Despite the advantage of low trauma and high friction coefficients, micro-scale treads do not appear well suited to the colon – particularly under higher normal loads and shear rates.
- Macro-scale treads seem most appropriate as they exploit the dominant form of resistance (environmental) and are generally more robust and scalable. They are also easier to manufacture.

- Tread geometry has an effect on macro-scale friction coefficients. Parallel and perpendicular-lined treads show promise, as does an array of elongated hexagonal-shaped pillars.
- A compromise may have to be made between the robust, scalable traction of macro-scale treads and the delicate, low trauma interface of micro-scale treads.

4.7. Experimental work

The reviewed literature emphasises the challenge of gaining traction on a colonic substrate. Although there have been a number of groups that have successfully shown the efficacy of tread patterns on some biological substrates, including the colon, there has been little on the functional performance of macro-scale patterns specifically. Furthermore, most have focused on the sliding of a flat coupon as opposed to a wheel undergoing slip³⁵. Results have also varied greatly and in some cases are contradictory – such as the extent to which normal load affects friction coefficient, the effect of surface area and velocity (shear rate). Lastly, there has been no real attempt to quantify the trauma caused by tread patterns on the colon (beyond a basic qualitative description). The main desired outcomes of this experimental section are to therefore:

1. Gain a better understanding of the efficacy of macro-scale tread patterns on colonic tissue (under relatively high normal loads and rotational speed - slip).
2. Determine the effect tread geometry has on traction performance.
3. Attempt to quantify the trauma caused by such treads.

Four steps were planned to achieve these outcomes:

Step 1 – Design³⁶ (including geometry, scale and aspect ratio) and fabricate the tread patterns.

Step 2 – Empirically assess which of the patterns (including a control) results in the highest traction; both in a static and dynamic (continuous slip) case.

Step 3 - Modify the aspect ratio and scale of the best performing tread in an attempt to optimise it further.

Step 4 – Place each tread pattern under a range of loads and continuous slip and observe tissue trauma.

³⁵ The impact the mucus has in this situation is therefore unclear.

³⁶ Based on intuition, preliminary tests and the reviewed literature.

Literature reports experimental results with few repetitions and often high variance. This is expected as these tests are laborious (with many control variables) and generally, biological substrates are renowned for high variability. A total of 16 repetitions per condition was therefore chosen to give more robust results and allow statistical significance to be considered. To avoid an excessive number of repetitions, the contact area, velocity and material properties of the tread were not varied and focus was maintained on tread geometry and its effect on traction and trauma.

4.7.1. Tread design and fabrication

4.7.1.1. Tread design

A number of geometries of tread have been tested in literature. One that consistently shows promise, and is hence the focus of this work, is a tread consisting of closely spaced hexagonal pillars (or similar diamond-shaped pillars [98, 123]). The large surface area can effectively distribute force and so has the potential to reduce trauma; the interlocking channels are effective at rapidly de-wetting a surface and promoting an intimate contact between the two surfaces and; the multifaceted shape of the pillars may also provide high environmental resistance on soft substrates, as shown by the use of a similar pattern in [98, 123]. Using elongated hexagons has been shown to improve friction results however, the best orientation is unclear in literature [123, 128] and therefore both orientations have been included in this study. To better understand the role of tread geometry, a number of other simple treads were also included. These were: A control (smooth) tread, parallel lines (to the direction of shear) and perpendicular grooves - both shown to be effective by Lee et al. [96].

A feature width of 750 μm , depth of 500 μm and aspect ratio (*Feature width : Space between features*) of 1:1 was chosen and maintained for all the treads. This was based on preliminary experimental work and on a range of successful macro-scales reviewed in literature which tends to consider the average thickness of the mucus layer³⁷. In an attempt to optimise the chosen tread pattern (in terms of traction and trauma – *Step 3*), the width and depth of the features were then reduced to 500 μm and 330 μm respectively, and a 2:1 aspect ratio also explored. This scale was selected as it approaches the limit of the fabrication technique used

³⁷ A tread height exceeding the average mucus thickness is desirable as it improves the likelihood of the mucus being effectively displaced and real contact made. A high channel volume would also squeeze more tissue, providing greater environmental resistance.

and is close to (but larger than) the chosen point at which a tread is considered micro-scale in this work (200 μm). All the tread geometries and relative scales are shown in Figure 4.6.

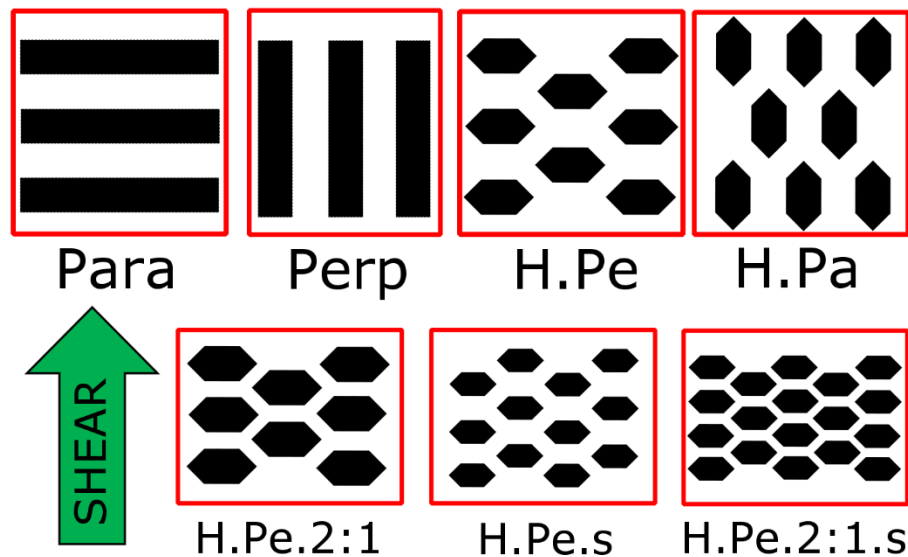


Figure 4.6 – The geometric patterns assessed in this experimental work and their given names.

Para = Parallel ridges; *Perp* = Perpendicular ridges; *H.Pe* = Hexagonal pillars (arranged perpendicular to shear);
H.Pa = Hexagonal pillars (arranged parallel to shear); *H.Pe.2:1* = Hexagonal pillars spaced closer together;
H.Pe.s = Hexagonal pillars of a smaller scale (500 vs 750 μm); *H.Pe.2:1.s* = Hexagonal pillars of a smaller scale,
spaced closer together.

This selection will allow the hypothesis that perpendicular orientated, elongated hexagonal pillars provide superior traction (compared to simple lined treads) - particularly during shear³⁸. It will also give some indication of whether both traction and trauma can be optimised by adjusting the scale and aspect ratio.

4.7.1.2. Material selection

With rubber wheels on rough road surfaces, friction is due to viscoelastic deformation of the rubber tread³⁹ [130]. On a very soft substrate, the opposite must be true: friction is primarily due to the viscoelastic deformation of the substrate by the much stiffer tread pattern (Environmental resistance). To reduce trauma *in vivo* the compliance of the two contacting bodies could be matched to reduce interfacial stress concentrations [136]. This is a challenge

³⁸ More specifically, it will confirm that resistance occurs primarily along perpendicular, gripping edges (which should be very evident when comparing the parallel lined tread with the perpendicular lined tread) and that the presence of both perpendicular and parallel grooves/channels found in hexagonal tread will help to maintain these gripping edges during shear (as tissue ingress is encouraged and a long edge/face is provided to resist the elastic restoring force).

³⁹ “substrate asperities generate pulsating deformations of the tread material that increase friction”

as colonic tissue is extremely soft and so even materials such as silicone will be significantly stiffer. A soft material is also expected to conform more closely to the substrate, increasing real contact area and thus increasing normal friction. Furthermore, previously mentioned research has suggested that a pattern that can deform increases friction because the patterns remain in contact with the substrate longer. Crucially, however, if environmental resistance is indeed the main source of resistance on tissue, deformation of the substrate is required and so a very soft tread pattern may not be as advantageous as expected. In fact, a soft tread may reduce friction as mucus is less effectively displaced and the tissue surface is smoothed (by the presence of liquid islands). Nature uses a combination: The surface of a tree frog's toe pad is hard wearing and relatively stiff compared to the incredibly soft underlying tissue [124]. This allows the bulk of the toe pad to conform to the surface while the surface structures provide resistance (by displacing the liquid and interlocking with the surface asperities). It is clear that a balance is required. Too stiff a material and trauma could be large; too soft a material and friction due to environmental resistance *may* be minimal. As a starting point - and to simplify fabrication - a rigid material was used to guarantee tissue deformation and tread feature integrity.

4.7.1.3. Tread fabrication

The wheels were fabricated out of a plastic resin (*HTM140, EnvisionTEC*) using a 3D printer (*EnvisionTEC, Perfactory 3 mini, multi-lens*). This had a resolution between 15 and 60 μm and could accurately fabricate the wheels from CAD models (Figure 4.7). A by-product of this was the build lines (orientated perpendicular to the wheels direction of shear – Figure 4.8), giving a surface roughness (R_z) of the Control that is in the order of the colon: 6.4 μm . This was measured using a contactless profilometer device (*Alicona Infinite Focus*). To simplify the tread design, a cylindrical wheel shape was used⁴⁰ with similar dimensions to the spherical wheels used on RollerBall (including: a width of 7.25 mm and diameter of ca. 17.25 mm). The exact real contact area was expected to vary slightly from repetition-to-repetition because of the high variability of the underlying substrate, and so would be difficult to measure/calculate. The global contact area of the wheel was also expected to vary but on average was measured as ca. 36 mm².

⁴⁰ As opposed to the spherical shape used on RollerBall. A sphere would require the tread scale to vary across the surface of the wheel in order to maintain the aspect ratio used.

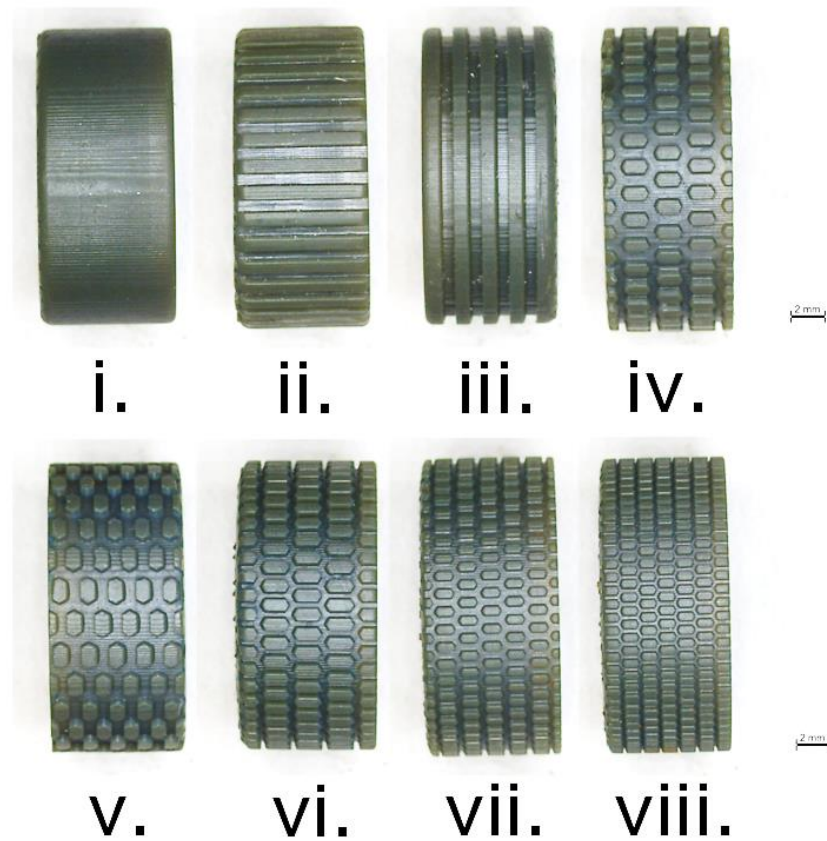


Figure 4.7 – The 3D printed tread patterns.

i. Smooth (control); ii. Parallel ridges (*Para*); iii. Perpendicular ridges (*Perp*); iv. Hexagonal pillars (arranged perpendicular to shear, *H.Pe*); v. Hexagonal pillars (arranged parallel to shear, *H.Pa*); vi. Hexagonal pillars spaced closer together (*H.Pe.2:1*); vii. Hexagonal pillars of a smaller scale (500 vs 750 μm , *H.Pe.s*); viii. Hexagonal pillars of a smaller scale, spaced closer together (*H.Pe.2:1.s*).

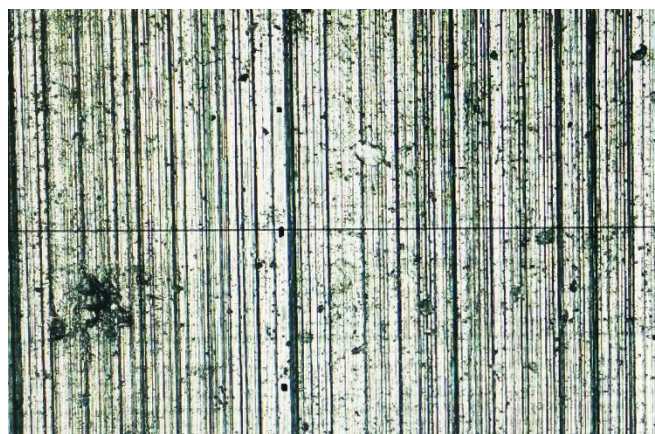


Figure 4.8 – A microscopic view of the “smooth” surface of the control.

This figure gives an indication of the regular, lined features produced in the 3D printing technique used. Surface roughness (R_z) is 6.4 μm .

4.7.2. Test apparatus

There were a large number of potential experimental variables, some relating to the mechanics (eg. Speed, degree of slip, normal load and contact area), some to the substrate used (eg. age of the tissue, source and region of colon used, how it is secured to the rig (backing and amount of tension), mucus condition (hydration) and tissue temperature) and others to the tread itself (eg. tread geometry, scale, aspect ratio and material used (mechanical properties)). The test conditions were simplified to avoid excessive test duration and complexity by considering what the most important variables were (partly chosen from literature and partly from preliminary studies) and then controlling them as accurately as possible using a custom made test rig. The test rig (shown in Figure 4.9) had the major requirements of:

- Applying a repeatable, accurate normal force to the wheel.
- Applying a torque to the wheel tread.
- Using a realistic (biological) substrate.

As the purpose of this work was to determine the *functional* performance of various 3D printed tread patterns, where possible, worst case conditions were used. These included:

- **A strained substrate** – This was done for a number of reasons: firstly, and most significantly, to more closely represent the conditions during a colonoscopy (an insufflated colon)⁴¹; secondly, to flatten the substrate; and lastly, to squeeze-out mucus from the mucosa (increasing lubrication).
- **A thick mucus layer** – The mucus layer is highly variable and is likely to have one of the most significant effects on traction. The distal part of the colon was used as this is expected to have the thickest mucus layer.
- **A flooded substrate** – Liquid may be present in the colon (especially in the case of hydro-colonoscopy), flooding the substrate ensures the mucus layer remains hydrated (low viscosity) and shows the treads' ability to rapidly displace liquid during slip. Yoshida et al. [137] state that the tissue (mucus) hydration plays a key role in reducing friction. A partly de-hydrated mucus could greatly increase traction because of the high viscosity, while a diluted mucus layer may give traction values less than those found *in vivo* (ie. a naturally hydrated mucus).

⁴¹ Lyle et al. also suggest that placing the tissue under stress may be a more “natural representation of the tissue mechanics *in vivo*”.

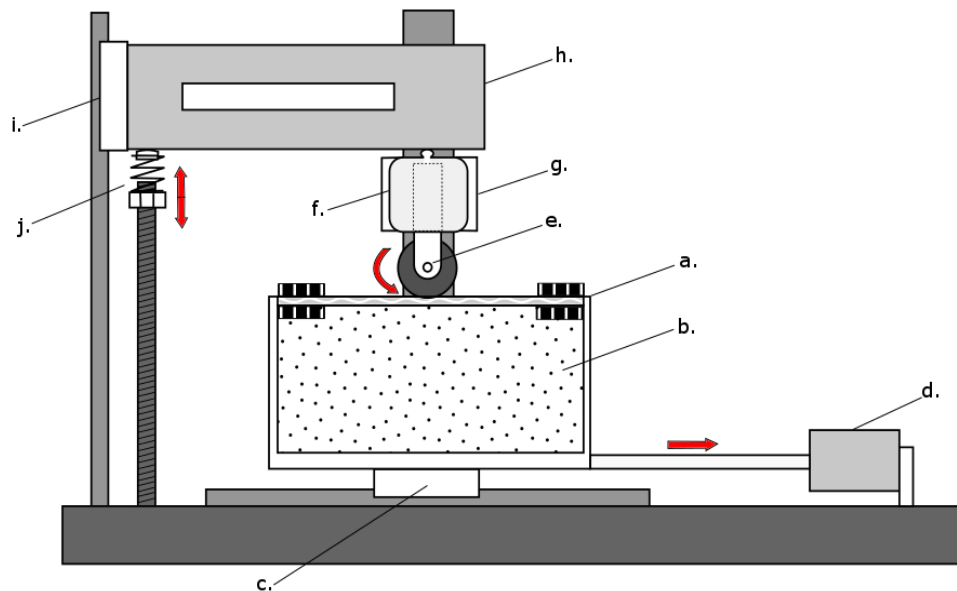
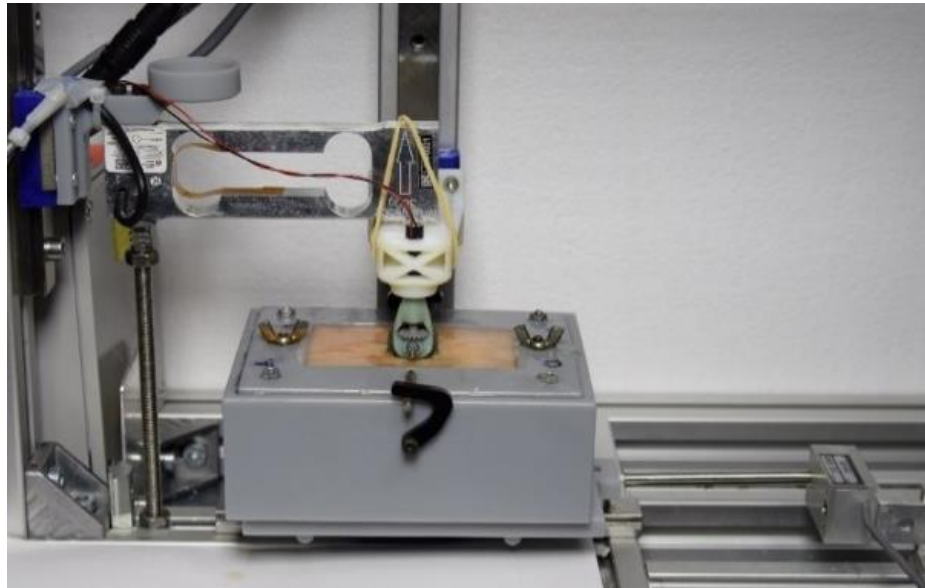


Figure 4.9 – The traction rig and key components.

a. Tissue clamp; b. Silicone base; c. Linear guide rail; d. Bed load cell (traction); e. Robot wheel; f. Lightweight motor bracket; g. Linear guide rail; h. Beam load cell (normal load); i. Linear guide rail and j. Counter balance spring mechanism.

Referring to Figure 4.9: A clamp (a.) was used to hold the colon tissue sample on top of a block of soft silicone (b.) (Shore 00-30). The clamp was placed on a low friction linear ball-bearing slide (c.) and was connected to the bed load cell (*Transducer Technique, GS0-150*) (d.) via a rigid steel rod. This setup allowed any shear force applied to the tissue to be precisely measured by the load cell with minimal losses. To assess the functional

performance of the tread patterns, the drivetrain from the actual robot prototype (e.) was used to rotate the wheel. A stiff, lightweight bracket (f.) secured this assembly to a separate linear ball-bearing slide perpendicular to the substrate (g.). This allowed the wheel assembly to be lowered onto the surface and any torque applied by the motor to be isolated from the beam load cell. The beam load cell (h.) was secured to a third linear ball-bearing slide (i.), in-line with the wheel and bed load cell. The wheel bracket was coupled to the end of the beam load cell using rubber cord (thus maintaining contact - and hence normal load - between the two, while allowing rotation from wheel torque). The combined mass was applied as a normal, passive load (weight) to the tissue. An adjustable spring (j.) opposes this and was used to set the desired amount of normal load applied to the substrate. A motor controller (*ESCON 24/2*) was used to supply and control the desired motor current (torque) and a compact RIO (*National Instruments, cRIO-9024*) was used to acquire all the data.

4.7.3. Tissue preparation

Fresh pig colons were acquired from an abattoir on the day of testing. The pigs were all 5 – 6 months old and the distal 1 m of the colon was used. The tissue was gently washed with water to remove any residual matter before being placed in a container of room temperature, phosphate buffered saline solution to prevent dehydration and degradation. All tests were completed within 5 hrs (below the 10 hrs recommended by Kim et al. [117]). When required, a 120 mm long sample was cut from the colon, opened flat and pierced onto one side of the tissue clamp in a longitudinal orientation. A mass of 193 g⁴² was then hung from the opposite side of the sample to gently stretch the tissue in the longitudinal axis before being clamped in place (Figure 4.10). The sample was then placed onto the silicone base and immediately hydrated with a ca. 2 mm deep layer of saline solution.

⁴² The calculations for this are shown in Appendix C.

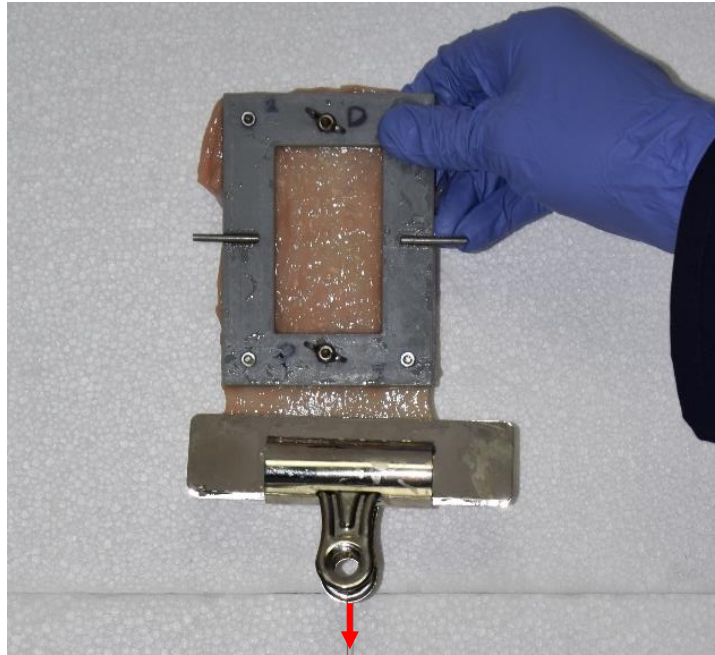


Figure 4.10 – A tissue sample clamped in a pre-tensioned state.

Tension is applied by hanging a mass in the longitudinal axis (red arrow in the figure).

4.7.4. Traction test protocol

Each wheel was washed in IPA to remove any residue before being attached to the motor assembly for testing. The beam load cell and wheel assembly were then lowered onto the centre of the tissue sample and the desired normal load applied by adjusting the spring mechanism. To evaluate the initial treads (750 μm scale), two normal loads were used: 25 gf and 50 gf⁴³. Pressures in the order of (and sometimes exceeding) 3 Bar are said to be required to perforate the colonic tissue [94, 95], therefore these are well within this limit and the force available from the expansion mechanism (102 gf). After ca. 20 s, demand current to the DC motor was increased linearly from zero to 120 mA (half the rated current of the motor) over 20 s. At this point the current was maintained for 5 s before decreasing at the same rate to 0 mA. Increasing the current linearly allowed the maximum static traction to be measured. The nominal operating voltage of the motor was maintained throughout therefore, during continuous slip, the estimated speed was 90 rpm (corresponding to ca. 81 mm/s linear shear rate, based on the nominal speed of the motor). The bed load cell recorded the tractive effort while the beam load cell recorded the normal load. After one repetition, the beam load cell and wheel assembly were raised and the tissue clamp and bed load cell slid a set distance forward to align with a new area of tissue. The next repetition was then carried out. This was done for a total of four repetitions per tissue sample, with

⁴³ During tests with the modified scale and aspect ratio, only 50 gf was used as the purpose was only to compare them to the preliminary treads, not assess their load dependence.

four tissue samples being used for each tread (two from the distal end of the colon segment and two from the proximal end), resulting in a total of 16 repetitions per tread pattern/load combination. Table 4.2 summarises the number of repeats per condition.

Table 4.2 - A matrix showing the total number of repetitions carried out in the traction tests.

		Condition			
		25 gf Normal load		50 gf Normal load	
		Proximal colon sample	Distal colon sample	Proximal colon sample	Distal colon sample
Tread pattern	Sm	8	8	8	8
	Perp	8	8	8	8
	Para	8	8	8	8
	H.Pa	8	8	8	8
	H.Pe	8	8	8	8
	H.Pe.s	-	-	8	8
	H.Pe.2:1	-	-	8	8
	H.Pe.2:1.s	-	-	8	8

4.7.5. Data analysis

A typical traction profile from a single repetition consists of two distinct features (Figure 4.11): a sharp increase to a peak traction value (*Static traction*) (Figure 4.11, a.) followed by a return to a lower magnitude (*Dynamic traction*) (Figure 4.11, b.) - where the wheel is in a continuous slip regime. The results were simplified into two traction coefficients that were used to describe the overall performance of the tread: The *Static traction coefficient* (μ_s) was calculated by dividing the static (peak) traction by the corresponding normal load at that instant; and the *Dynamic traction coefficient* (μ_d) was calculated by dividing the average traction over a steady-state five seconds of the run by the mean normal load over the same five seconds.

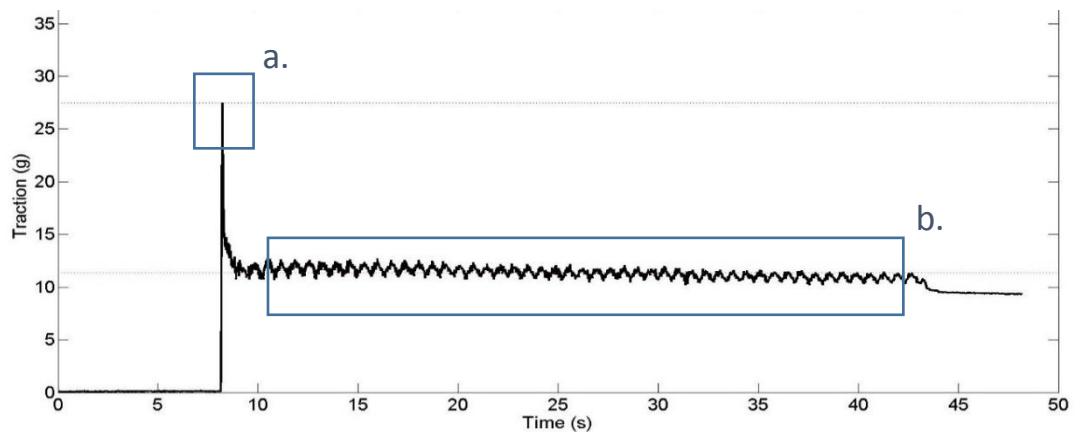


Figure 4.11 – A typical traction profile from one repetition.

The plot in this figure shows two distinct features: a. The static case and b. The dynamic case, where the wheel is in continuous slip.

4.8. Results and discussion

Similar to literature referenced in this chapter, the results showed a high level of variance – particularly evident in the static case (Figure 4.12). This made obtaining statistically significant results challenging. In the dynamic case (Figure 4.13), variance was considerably less, indicating that the traction mechanism is much more consistent and predictable. The reason for this is uncertain however, one explanation could be that while static, there is high variability in: the degree of direct contact (and the thickness of the underlying mucus layer); the volume of tissue squeezed between the treads and, although every effort was made to avoid it, the length of time from the wheel making contact with the substrate to the start of the test (affecting degree of stress relaxation in the tissue). The implication of these could be a highly variable magnitude of resistance. During continuous slip, these variabilities could even out resulting in less overall variance between repetitions.

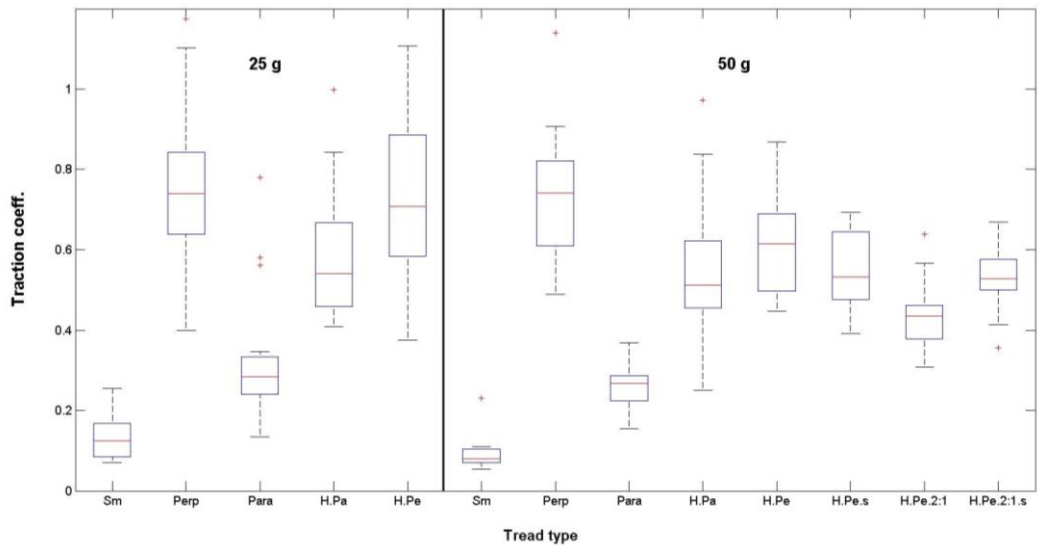


Figure 4.12 – A boxplot showing the traction coefficients from the static condition.

Plot shows tests under 25 and 50 g loads. Each box has n = 16 repetitions.

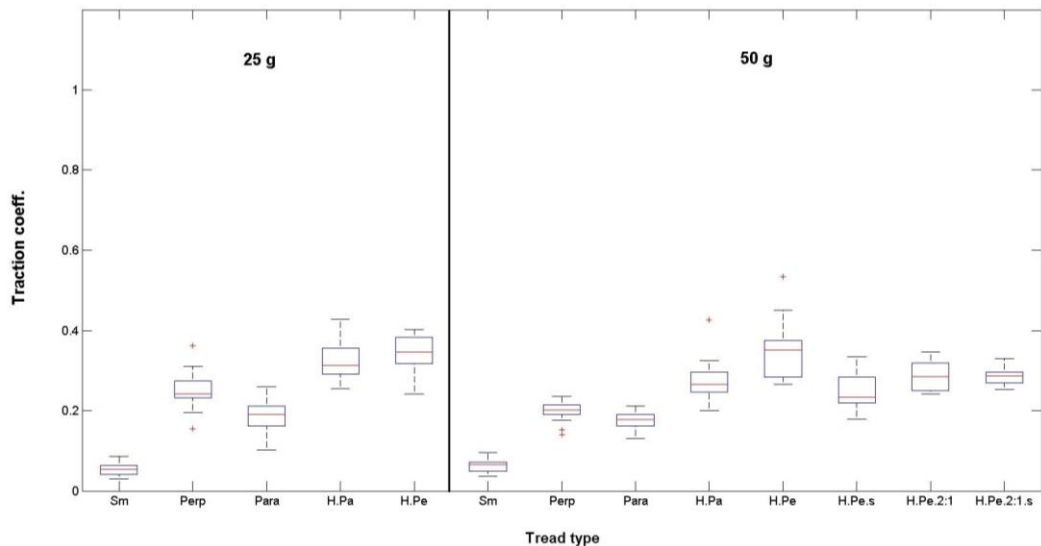


Figure 4.13 – A boxplot showing the traction coefficients from the dynamic condition.

Plot shows tests under 25 and 50 g loads. Each box has n = 16 repetitions.

4.8.1. Effect of Colon and colon region used

As was highlighted in the literature review: the size, shape and properties of the colon can be highly variable from individual to individual and so will give varying traction results. Because of the limited size of the tissue specimens and the fact that a new contact patch was used for each repetition, many different colon specimens (from multiple pigs) were used to obtain all the results. Comparing results from different colons and regions (testing them against the null hypothesis that they are not from the same group), it was seen that the majority (10/13) of the results showed no statistical significance ($p > 0.05$) between traction

coefficients from the same tread on different colons and colon regions. In the dynamic condition (slip), 7/13 of the results showed no statistical significance. The lack of significance and the differing results between static and dynamic cases is likely due to the opposing variances in the results⁴⁴. This, in addition to the requirement of having a tread pattern for all regions of the colon and the use of a macro-scale tread, suggested that the results from each tread pattern could be combined (regardless of colon and region) to give an overall indication of how each tread performs generally – this is how the results are displayed in Figures 4.12 and 4.13.

4.8.2. Effect of tread geometry

Referring to Figure 4.12, Static case: The tread geometry was shown to greatly affect the traction coefficient. The control had a mean coefficient of 0.112 ± 0.068 (averaged across both loads, $n = 32$). The highest coefficient was seen by the 750 μm scale perpendicular tread (0.755 ± 0.264), closely followed by the 750 μm scale H.Pe tread (0.676 ± 0.248). A perpendicular orientation in the tread patterns was a clear advantage as the coefficients for Perpendicular tread and H.Pe were greater than their parallel counterparts.⁴⁵

Referring to Figure 4.13, Dynamic case: As one would expect, the dynamic traction coefficients were significantly lower than in the static condition. Interestingly, the performance of the Perpendicular tread greatly decreased when slip was introduced. In this case, H.Pe had the highest coefficient of 0.348 ± 0.084 , closely followed by H.Pa which had a coefficient of 0.300 ± 0.0731 (compared to 0.058 ± 0.021 of the Control).

The control had a higher traction coefficient than similar controls in literature. This was attributed to the micro-scale build features that result from 3D printing fabrication (in this case, lines perpendicular to the direction of shear). This highlights two things: the commonly unwanted rough surface finish from 3D printing may be advantageous in this case, resulting in a hierarchy of tread features that improve de-wetting and; the overall poor performance of micro-scale ridges/grooves on the colon due to no direct contact with the tissue epithelium. A further reason for this comparatively high friction coefficient could be manufacturing inaccuracies: it was seen that the wheels were slightly misaligned and this caused vibrations during continuous slip that could have increased resistance from hysteresis losses in the tissue.

⁴⁴ Lyle et al. found similar, non-statistically significant results when looking at friction coefficients on different intestine regions.

⁴⁵ The results for the Hexagonal treads under 50 g load were not statistically significant.

The outperforming of the perpendicular compared to parallel-lined treads confirms the hypothesis that resistance is produced largely at perpendicular gripping edges. Furthermore, the subsequent poor performance of perpendicular lined treads during shear confirms the hypothesis that the combined perpendicular and parallel grooves found in H.Pe and H.Pa provide a more ideal condition where tissue can squeeze into the channels and maintain contact with the perpendicular gripping edges (as opposed to the scenario shown in Figure 4.5, Section 4.6).

4.8.3. Effect of scale and aspect ratio

Reducing the scale of the tread and the distance between features (2:1 aspect ratio) reduced the traction coefficients. This supports the theory that environmental resistance (tread groove volume and high stress concentrations) has a more dominant effect than tread surface area. Of these altered treads, the 500 μm scale, 1:1 aspect ratio H.Pe tread had the highest static traction coefficient of 0.553 ± 0.099 and the 500 μm scale, 2:1 aspect ratio H.Pe tread had the highest dynamic traction coefficient of 0.287 ± 0.023 .

4.8.4. Effect of Normal load

It was evident in literature that the friction coefficient decreases with an increase in load. The exact reason for this is unclear but it is suggested that one of the causes is the increasing load squeezes out mucus and water from the mucosa [119, 122] another may be the altering of the mucus properties [138] and another still is the transition from one form of resistance to another. The results in this study somewhat support this, showing the traction coefficient of the majority of the tread geometries⁴⁶ decreasing slightly as normal load doubles (although, with limited statistical significance). In the static case, as expected, the control showed the greatest reduction of 30.5 % ($p < 0.05$). Parallel, Hexagonal (perpendicular), Hexagonal (parallel) and perpendicular showed reductions of 21.2 % ($p > 0.05$), 16.8 % ($p > 0.05$), 6.0 % ($p > 0.05$) and 4.0 % ($p > 0.05$) respectively. In the dynamic case, the control and hexagonal (perpendicular) showed an *increase* in the traction coefficient of 16.1 % ($p > 0.05$) and 1.4% ($p > 0.05$) respectively. Perpendicular, parallel and hexagonal (parallel) all showed a reduction in the coefficient of 21.1 % ($p < 0.05$), 4.3 % ($p > 0.05$) and 14.8 % ($p < 0.05$).

4.8.5. Limitations

Firstly, it is also important to emphasise the limitation of the literature values referenced in this chapter (including tissue and mucus properties, and friction coefficients). Animals are often used in lieu of humans in research. There are obvious anatomical differences and the

⁴⁶ Except H.Pe and the Control in the dynamic case (the results were not statistically significant, however).

properties are said to be fairly similar by some [94, 139] and quite different by others [110] – a further indication of the complexity involved. Work referenced in this thesis included data from all sources (cadaveric and animal; *in vivo* and *in vitro*). For example, cadaveric tissue is said to lose its tone, having a lower stiffness than living tissue. A comparison of *in vivo* and *in vitro* mechanical properties of goat colon showed that, at a low compression rate, the tissue is stiffer in-vitro [111]. There is also expected to be variability in mechanical properties from individual to individual due to the complexity and uniqueness of biological organisms.

The most significant limitation from the experimental work was the environment, with the obvious limitation being the use of porcine colon in lieu of human. Because it was decided to carry-out a high number of repetitions, a compromise was made on the complexity of the tests and test rig. The temperature of the tissue was kept relatively constant at room temperature - from dissection to traction tests. The tissue properties are different as a result of this reduced temperature and the lack of blood supply [120]. Saline solution was also used to flood the substrate. This would have altered the properties of the mucus, with the viscosity expected to be lower than *in vivo* due to dilution [113, 137]. However, traction from the macro-scale treads is expected to be less dependent on the mucus properties and so this should not be an issue (it is also unclear what effect the saline had on the tissue water content and hence mechanical properties). Lastly, because the deformation of the tissue is key to the traction coefficient, a compliant backing was used and the properties of this are expected to only loosely represent those found *in vivo*. Because of the experimental complexities, including the worst-case, unique conditions used (eg. strained substrate), it is difficult to say whether results over or underestimate the friction response. In situ tests were shown to give lower friction coefficients (presumed to be due to higher tissue temperature, muscle tone, mucus replenishment and maintained blood flow to the area) by Lyle et al. [120]. Despite these uncertainties, the high number of repetitions used in this study, combined with the repeatable experimental method used, enable an informed selection of tread pattern for functional use and a better understanding of the friction mechanisms on this unique substrate.

4.9. Trauma assessment

A significant motivation for developing a device like RollerBall is the potential for greatly reduced patient discomfort and procedure complications. The use of rigid, macro-scale tread patterns – which are designed to gain traction by deforming/squeezing the substrate – presents an obvious danger of causing trauma on the sensitivity of the tissue. This section uses the same experimental setup used in the traction work but this time explores the trauma caused by the treads when placed under higher loads and continuous slip.

4.9.1. Method

Similar conditions to the traction tests were used. In this case, however, the wheel was placed into continuous slip for 10 seconds using a step current input. Higher normal loads of 50 g, 100 g and 200 g were used as no trauma was visible during the 25 g traction tests. A single repetition was carried out per load and tread type, resulting in a total of $n = 24$. The contact patches from each repetition (often visible to the naked eye) were stained with black India ink, excised and then placed in individual test tubes to be fixed over 24 hrs using formaldehyde. The small, thin tissue samples were held flat using thin, flexible and permeable plastic filter paper. The samples were then moved to and stored in a 70% solution of ethanol. Histology⁴⁷ was carried out on each sample to assess mucosal trauma. It was difficult to ensure the slice was taken from a suitable site therefore, three slices were taken across the sample to increase the probability of acquiring a representative cross-sectional view of the trauma caused (an illustration of this is shown in Figure 4.14).

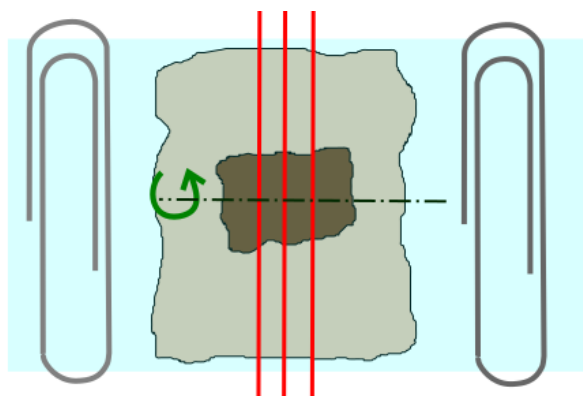


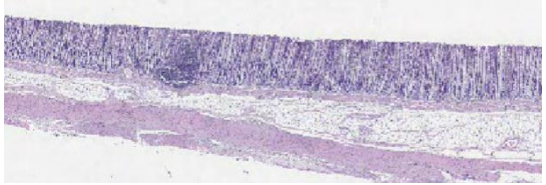
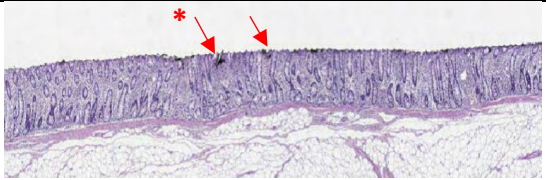
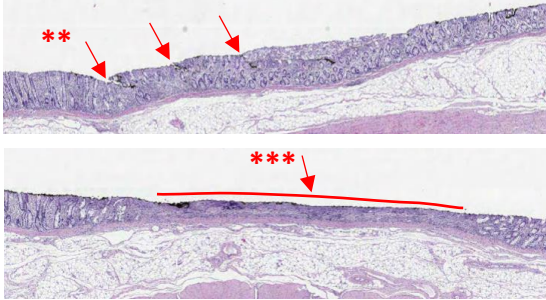
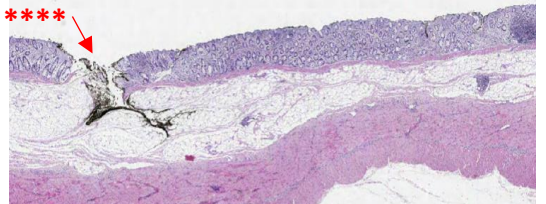
Figure 4.14 – An illustration showing one of the prepared tissue samples pre-histology.

The small tissue sample is held flat between two permeable plastic filter membranes (and paper clips). Three slices were then taken across the region of interest, as shown by the red lines. The wheel rotation (green arrow) was about the axis shown by the black dotted line.

⁴⁷ A preserved tissue sample is embedded in wax and then thinly sliced. These slices are then imaged using standard light microscopy.

Each histology slice was carefully inspected for abnormal, mechanical induced features and the slice with the greatest amount of trauma was chosen and ranked using Table 4.3. This degree of trauma, and the maximum load at which no major trauma was seen, were used to assess each tread pattern.

Table 4.3 - A summary of the features used to rank the tread trauma.

Degree of trauma	Description	Example slice
0	No features visible (mucosa intact, no abnormalities detected)	
1	Very small features	
2	Small features	
3	Large features (eg.)	

*Very small features, considered an abnormally rough surface or very small cuts⁴⁸.

**Larger cuts but well within mucosal layer.

***Distinct eroding or compressing of mucosal layer.

****Cuts through, or complete erosion of, mucosa.

⁴⁸ Unclear in some cases but included as potential trauma.

4.9.2. Results and discussion

Despite a well-developed, repeatable protocol and standard histology methods, it was found that this process was difficult to precisely control and the results from the study were unclear in many cases. This was attributed to the method used to collect the data and the obscure nature of the images:

Firstly, the storing of the samples may have caused two noteworthy issues: The membrane used to keep the sample flat may have caused once visible features (eg. a lesion) to close and eroded (or deformed) sections of tissue to flatten-out, making their detection difficult. The latter was particularly evident with the parallel tread which displayed distinct (to the naked eye) grooves post-test (Figure 4.15). During the histology investigation, these features were no longer visible – suggesting that they could have in fact been dents rather than cuts. Secondly, slicing the sample in the correct region also proved difficult because of the embedding process (in which the tissue is embedded in wax) – the region of interest becomes less visible, obscured by the opaque wax. The inclusion of 3 slices spaced evenly apart from each other (shown previously in Figure 4.14) was chosen to increase the probability of slicing the contact patch (region of interest). To further improve this, the tissue samples were kept as small as possible, with the region of interest kept repeatedly in the centre of the sample.

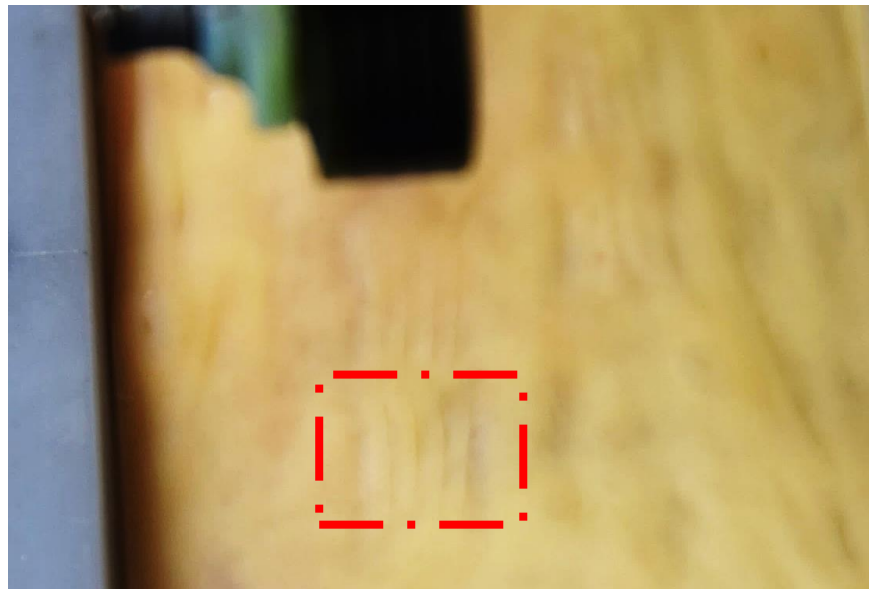


Figure 4.15 – Visible grooves or ‘dents’ seen post-test (Parallel tread, 50 g load).

The decision to select the slice with the worst trauma for each tread and load condition was deemed the most accurate method of assessment available. Trauma confined to the upper region of the mucosa was considered acceptable as this can heal effectively as it does not contain vasculature. The results are summarized in Table 4.4:

Table 4.4 - Tread trauma results showing the degree of trauma seen and the load it first occurred at.

Tread:	<i>Sm</i>	<i>Para</i>	<i>H.Pe.2:1.s</i>	<i>H.Pe.s</i>	<i>Perp</i>	<i>H.Pe.2:1</i>	<i>H.Pe</i>	<i>H.Pa</i>
Trauma:	0-1	0-1	1-2	1-2	2-3	3	3	3
Max Load (g):	200	200	200	200	100	50	50	< 50

Trauma was less than expected, considering how stiff the tread patterns are compared to the tissue. The control, parallel, H.Pe.s and H.Pe.2:1.s all caused what was thought to be acceptable levels of trauma, even up to loads of 200 gf. This may be because the dual mucus layer creates a “slippage” plane [113] and effectively protects the underlying tissue. The perpendicular tread showed acceptable levels of trauma up to 100 gf of normal load but clearly eroded the mucosa at 200 gf. H.Pe, H.Pa and H.Pe.2:1 all showed significant levels of trauma above loads of 50 gf.

4.10. Traction and trauma conclusions

Literature suggests that, for applications requiring high shear rates (velocities) and functional levels of traction, a macro-scale tread pattern may be most suitable for the colon for the following reasons: ease of manufacture (and reduced chance of tread contamination); scalability (less dependent on the presence of mucus and surface roughness) - meaning traction can more effectively be controlled using normal load and the performance is unlikely to change significantly from region to region; and environmental resistance is a dominant form of resistance against the soft substrate. Outcomes from the experimental work included:

- A macro-scale tread pattern greatly increases the traction coefficient compared to a control (micro-scale features).
- Tread geometry has a significant effect on the traction coefficient, with H.Pe and Perp treads resulting in the highest coefficients in the static case. During slip, the more complex, H.Pe and H.Pa had the highest traction coefficients.

- Reducing the scale and the spacing between the pillars reduced the traction coefficient, indicating that resistance is primarily from environmental resistance.
- The large scale hexagonal tread patterns caused significant trauma, while the other geometries and the smaller scale hexagonal patterns caused less.

The H.Pe.2:1.s was chosen for use on RollerBall as it may provide the best performance, balancing traction and trauma. If this tread were to be used with 50 gf normal load and if slip is controlled, RollerBall could produce ca. 27.5 gf of tractive effort per wheel (82.5 gf net propulsion) - this could be improved in future work.

4.10.1. An optimum tread for the colon?

In light of the experimental work presented here and the literature reviewed, an optimum tread pattern for the intestine (and other wet, biological substrates) could include the following bio-inspired, hierarchical design:

- *A macro-scale, elongated hexagonal tread pattern made from a very low modulus, visco-elastic material (approaching that of the colon and surrounding tissue).*

This could improve friction as the tread conforms to the substrate and helps to reduce trauma by limiting peak stress concentrations. The visco-elastic deformation of the tread may increase hysteresis losses [130], while also helping to reduce crack propagation (maintaining contact with the tissue for longer, thus prolonging static friction). A high channel volume should be used, meaning deep and wide spaces between pillars (such as that used in the experimental work). This will ensure tissue can be effectively squeezed into the spaces and fluid readily displaced.

- *The surface of these macro-scale pillars could be covered with a higher stiffness array of micro-scale hexagonal pillars, treated with a hydrophobic layer [128].*

While the underlying low modulus, macro-scale features improve contact, exploit environmental resistance (including losses in the tread itself) and displace thick fluid layers effectively - the micro-scale pillars produce a hierarchy of features that will improve de-wetting of the contact further. This will increase the likelihood of the stiffer, micro-scale features making direct contact with the surface asperities and will maximise coulombic and viscous friction.

Chapter 5

System Integration and Open-loop Control

This chapter describes the steps taken to advance RollerBall from the pure mechanical device described in Chapter 3, to a fully mobile and controllable prototype. This includes the development of the electronics hardware and the associated control software. A series of laboratory-based, whole-device experiments are used to direct the development of the control and test the overall efficacy of the robot.

5.1. Introduction

Chapter 3 introduced the design and fabrication of the RollerBall concept. It then showed that the individual mechanisms function as intended by characterising their performance in a series of calculations and benchtop experiments. Chapter 4 then addressed the essential requirement of gaining traction in the colon and the results indicated that substantial traction could in fact be acquired, with the potential for further, significant improvements to be made in future work. These chapters justified the further development of the concept to a fully operational prototype; this required consideration of the desired functionality and intended use of the device (System requirements), and then the development of both the electronic hardware and software control. It was expected that this would be a significant challenge and may bring to light fundamental limitations of the concept therefore, the goal of this work was to simultaneously progress the prototype from an open-loop stage to a more advanced, closed-loop stage while assessing its overall efficacy.

5.1.1. System requirements

RollerBall is designed to traverse the length of the colon with a number of desired attributes that will ultimately determine the robot's functionality and overall efficacy as a colonoscopy procedure. General requirements of a mobile colonoscopy robot were suggested in Chapter 2; Table 5.1 considers what the specific, ideal control attributes are based on these, and their associated software requirements.

Table 5.1 – The major (ideal) control attributes.

Desired control attribute	Description	Software requirement
<i>High mobility</i>	Stop, start, traverse corners, adjust orientation while stationary and adapt to changing diameters.	A method of mapping user inputs to motor outputs that result in the desired movement(s).
<i>Safe to use</i>	Prevent trauma and discomfort caused by the robot, and potential damage to the robot itself.	Include feedback and software limits to control the amount of force applied to each arm.
<i>Simple to use</i>	Minimal input from the operator and intuitive, accurate control.	Incorporate a simple method of controlling the device and viewing feedback. Automate as many processes as possible.

To achieve these at the prototype stage, there are a number of requirements that are specific to the hardware used (Table 5.2):

Table 5.2 – The major requirements of the electronic (control) Hardware.

Hardware requirement	Description
<i>Simple user interface</i>	Use an intuitive controller and a graphical user interface for viewing data (feedback) and setting parameters. This would help to improve usability.
<i>Low latency communication and data processing</i>	Rapid acquiring, processing and displaying of data to achieve smooth robot control with minimal errors (which may cause damage to the robot or surroundings). This would help both the mobility and safety control aspects.
<i>Robust and scalable (adaptable)</i>	Able to incorporate various future add-ons, such as: visual feedback (camera) and force sensing. Allow the modifying and replacing of parts to be carried out easily. This is crucial to this, prototype-stage of development.
<i>Flexible tether</i>	A tether should be used to simplify the on-board electronics and as a fail-safe (manual method of retrieving the robot). This would also help to simplify the electronics development at this stage.

5.1.2. System development strategy

The aim of this chapter (and the next) is to develop the hardware and software required to achieve the desired control summarised in Tables 5.2 & 5.3, while simultaneously assessing the efficacy of the concept. A number of objectives were planned to achieve this:

1. Design and build the system hardware and associated communication architecture.
2. Develop an initial (open-loop) method of processing the user inputs to control the net speed and orientation of the robot, and angle of the arms.
3. Design and build a test environment for the robot that will allow the software to be developed in a controlled, iterative manner.
4. Assess the performance of the open-loop system before progressing further.
5. If open-loop tests are successful, develop a closed-loop method of controlling the robot – improving safety, locomotion efficacy and usability.
6. Assess the performance of the closed-loop system and conclude on the robot's overall locomotion efficacy and usability.

5.2. Hardware

Emphasis was placed on understanding and developing the core concept and facilitating multiple iterative changes to the system. Consequently, the hardware (the majority of which is shown in Figure 5.1) was chosen and developed with this in mind.

At the heart of the system is the robot (Figure 5.1, a.). Power and data communication is transmitted to the robot via a thin (3 mm) and flexible tether (Figure 5.1, b.). Initially just eleven wires of the available twenty four were used: two per DC motor and three for the camera. The motor wires were connected directly to four DC motor driver boards (Figure 5.1, c.) and the camera wires to a USB video grabber. Control signals (speed and direction) were sent to the individual driver boards by a *myRIO-1900* controller (*National Instruments*) with USB interface (Figure 5.1, d.). This has a powerful embedded processor (Dual core Xilinx Z-7010; 667 MHz speed and 256 MB non-volatile memory), a number of digital and analogue input/outputs and was used for high priority processing and transmitting of data. The DC motor driver boards were powered via a benchtop power supply unit (Figure 5.1, e.). An Xbox 360 games console controller (*Microsoft*) was used as the primary method of user input, chosen for its intuitive layout (Figure 5.1, f.). A laptop computer (Figure 5.1, g.) was used as a graphical user interface and to integrate the myRIO, Xbox controller and any other additional hardware used in future developments.

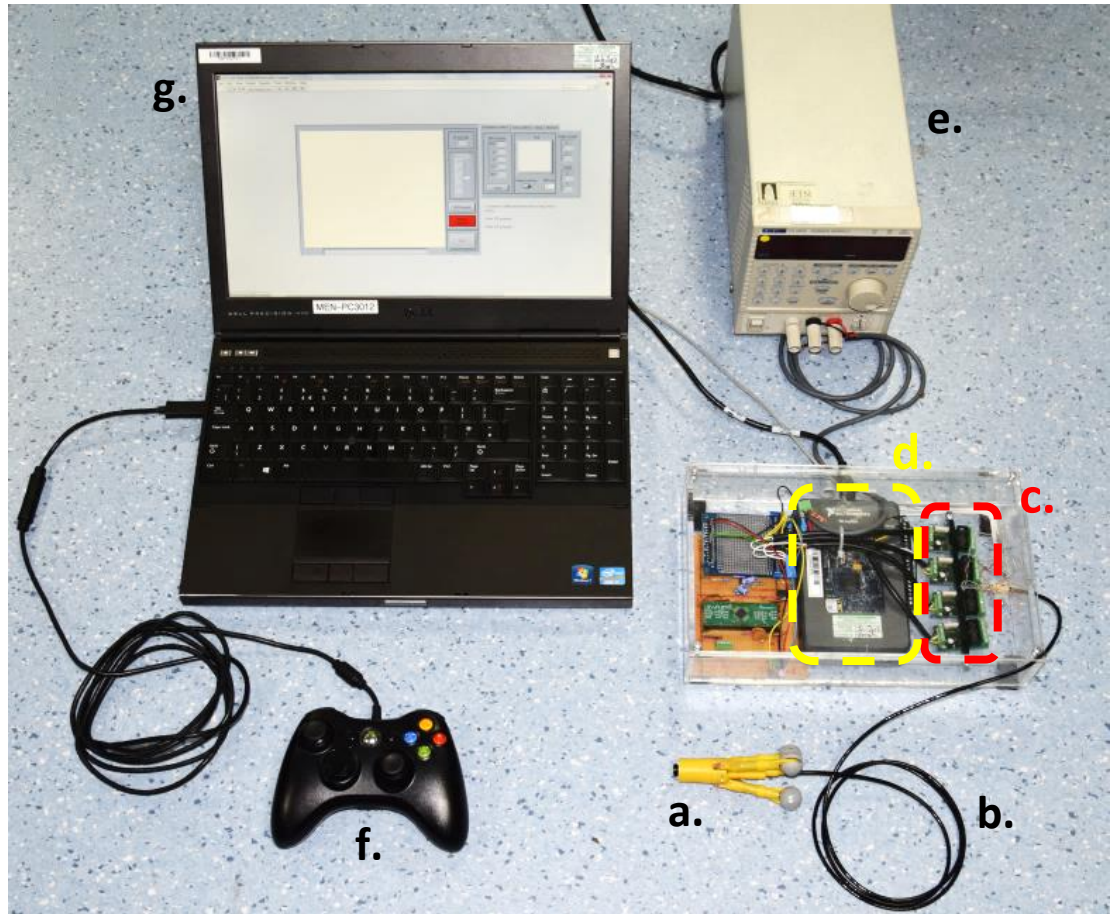


Figure 5.1 – The majority of the components that make up the RollerBall platform.

a. The prototype; b. Tether; c. DC motor driver boards; d. *myRIO* controller; e. Benchtop power supply; f. Xbox controller and; g. Laptop PC

This setup satisfies the requirements set out in Table 5.2. It is robust and allows for the modification of each stage of the communication process, with for example, the inclusion of different sources of feedback. The PC provides a large display for the GUI and multiple ports for connecting to the various hardware used. Processing is shared between the *myRIO* and Laptop to reduce latency and improve reliability.

LabVIEW (*National Instruments*) was used as the programming language for the robot control. This was decided for two main reasons:

1. The intended use (and availability of) *National Instruments* hardware, including the *myRIO* (and *cRIO* used in Chapter 4). LabVIEW is particularly effective at communicating between these (and other hardware) and a PC. This allows for the natural integration and parallel running of multiple programs on different processing units.

- The desired development of a graphical user interface (GUI) is well suited to the graphical programming style of LabVIEW which has a library of various front panel controls and indicators.

5.3. Open-loop control strategy

The first stage of development involved an open-loop control strategy where the user controlled every aspect of the robot, with only visual feedback of the state of the device⁴⁹. This work was used to establish the control algorithm used to map the user inputs to the motor outputs and more generally, to assess basic usability and locomotion efficacy before increasing the control complexity.

The schematic in Figure 5.2 summarises the core⁵⁰ control strategy used for the open-loop system.

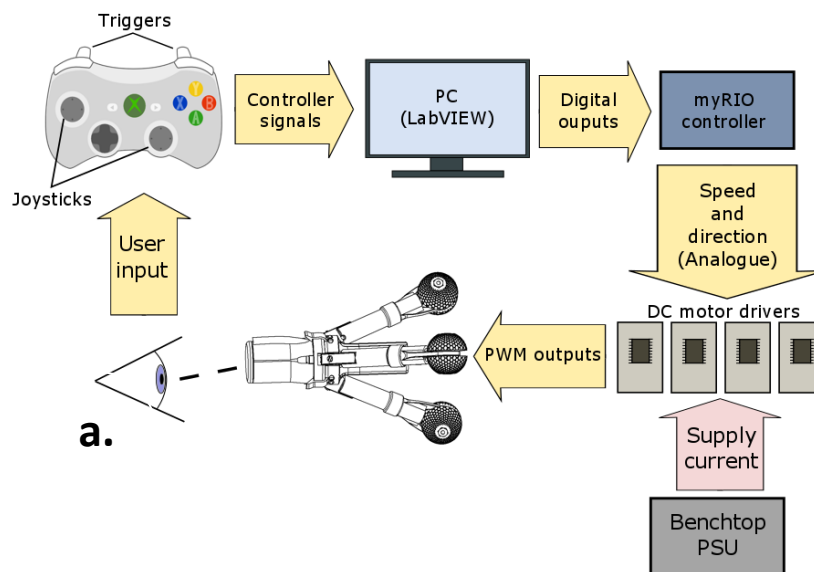


Figure 5.2 – A schematic of the core RollerBall system communication architecture.

Note: The only source of feedback is the direct view of the robot.

Referring to Figure 5.2: Starting from a., the user visually checks the position and orientation of the robot. A judgment is then made on what movement is required next. This is applied to the Xbox controller inputs which are acquired and processed by the laptop. The

⁴⁹ This control is called open-loop because the robot does not include any sensor feedback. However, in reality, the loop is closed by the user who receives visual feedback of the device and provides adjustments based on their intuition.

⁵⁰ Slight modifications will be made to this in subsequent sections.

commands are then output to the *myRIO* controller which calculates the required motor speeds to achieve the desired movement (using the dedicated embedded processor for consistent performance). The motor speeds and direction are then output to each of the motor driver boards which are powered by a benchtop power supply unit. The driver boards output the corresponding PWM signals to the motors via the tether, resulting in a change in either the position, orientation or arm angle of the robot (or all simultaneously). The whole process is repeated continuously.

All processing could have been carried-out on the PC however, to increase performance, the *myRIO* processor was dedicated to time critical aspects of the control, such as: acquiring signals, calculating motor speeds with minimal latency and handling potentially fatal errors (ie. minimising potential damage caused by or to the robot). The next section describes this use of resources and the major programs that make up the system.

5.3.1. System architecture

The hardware was shown previously in Figure 5.1 and the open-loop control strategy was shown in Figure 5.2. Figure 5.3 combines the two and shows an overview of the main hardware, control programs, resource use and communication flow.

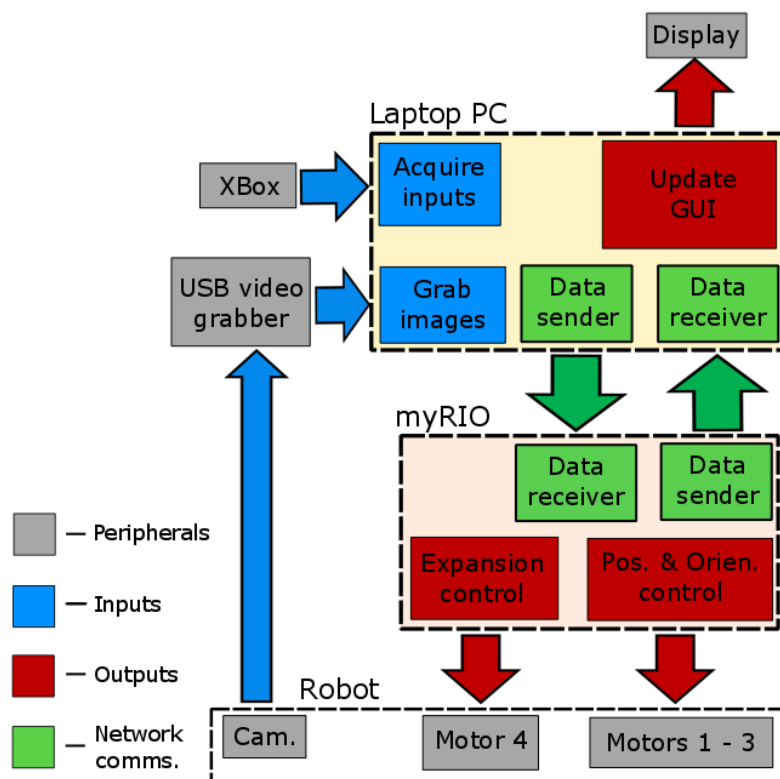


Figure 5.3 – The RollerBall system architecture showing the distribution of the peripheral devices, the main programs and flow of data.

For reference, the distribution and naming of the hardware in the robot is shown in Figure 5.4.

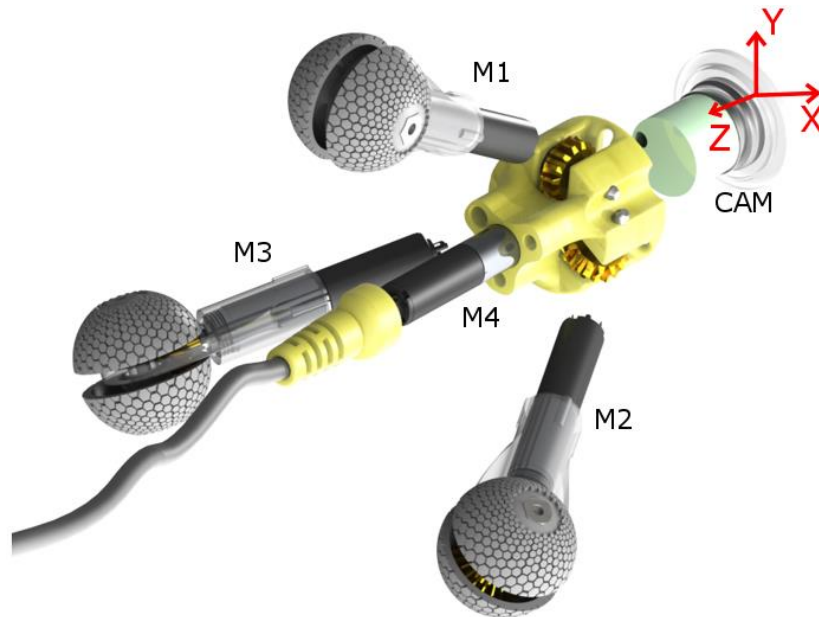


Figure 5.4 – A modified render showing the location and naming of the four DC motors (M1 – 4) and camera (CAM). It also shows the coordinate frame used.

Referring to Figure 5.3: The Xbox controller is connected directly to the Laptop PC via USB. A simple program (“Acquire inputs”) is used to acquire the data and distribute it to its dependents. The camera (Analogue video (AV) output) is connected to the Laptop via a USB grabber. A program (“Grab images”) is used to acquire the images and another program (“Update GUI”) is used to display this and other data (including the Xbox values) on the GUI (Laptop display). Relevant data (such as the Xbox values) is sent over a “Network stream” (a *National Instruments* method of inter-device network communication) to the *myRIO*. Here, a program called “Expansion control” is used to control the angle of the arms (actuated by Motor 4, Figure 5.4.) and another, as the name suggests, is used to control the position and orientation of the robot (determined by the relative speed and direction of Motors 1 – 3, Figure 5.4).

The localisation of the robot can be split into two tasks: the *Expansion control* (arm angle) and the *Position and orientation control* (wheel speeds). These are the two main programs that control the robot and will be discussed in subsequent sections.

5.4. Expansion control

Control of the angle between the robot arms and the chassis is required to adapt the size of the device to changing lumen diameters, and thus maintain traction and a stable platform. At this stage control is relatively straightforward: driving the expansion motor in the robot chassis at a defined rate will adjust the angle of the arms proportionally. The motor driver boards have two inputs: *Speed* (an analogue voltage, 0 – 2.5 V) and *Direction* (a digital input). They have one output: a *PWM* signal of defined amplitude, frequency and duty cycle. The rate of expansion, and the direction (expand or contract), can therefore be altered by simply inputting these two variables.

A program, running on the Laptop, was first written to acquire all the data from the Xbox controller. The Xbox triggers were then used to intuitively control the speed and direction of the arms; Figure 5.5 shows the location of these on the controller and their movement direction.

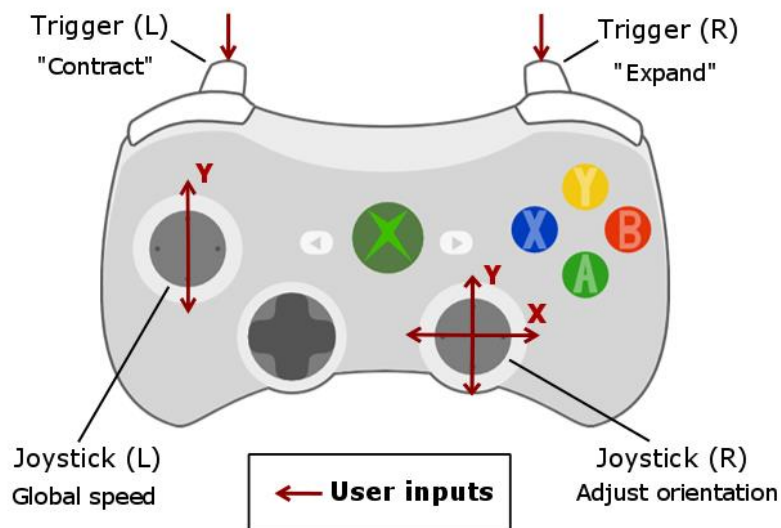


Figure 5.5 – An illustration of the Xbox controller showing the inputs used.

Each trigger has a potentiometer and so the degree of depression of each could be measured by the Laptop and converted into a 0 – 2.5 V range. A separate program, running on the *myRIO*, was then written to operate as illustrated in Figure 5.6.

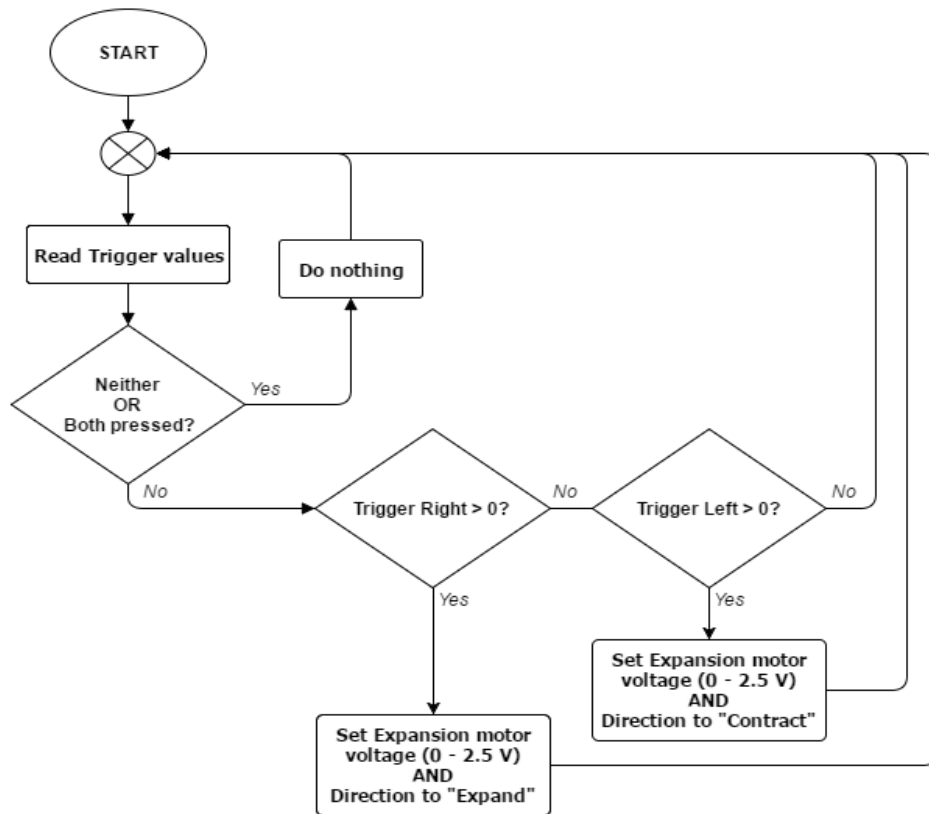


Figure 5.6 – A flow chart of the open-loop expansion control.

Motor voltage is proportional to Trigger depression, ie. 2.5V is trigger fully depressed.

This gives the user full manual control over the position (angle) of the arms and the rate at which it is altered by squeezing the associated trigger.

5.5. Orientation and position control

When the three arms of RollerBall are pressed against the lumen by the expansion mechanism, the device is held in position. Then the orientation of the robot's longitudinal axis can be placed and maintained in-line with the axis of the lumen in a central, idle position. From here, the orientation could be adjusted in any direction to either navigate a corner or line-up with a target. This will suit the use of diagnostic and therapeutic tools well, giving the operator a view of the whole lumen and the ability to position the tip of the robot as desired. Figure 5.7 and 5.8 define the coordinate system and the direction of the forces used to move the robot.

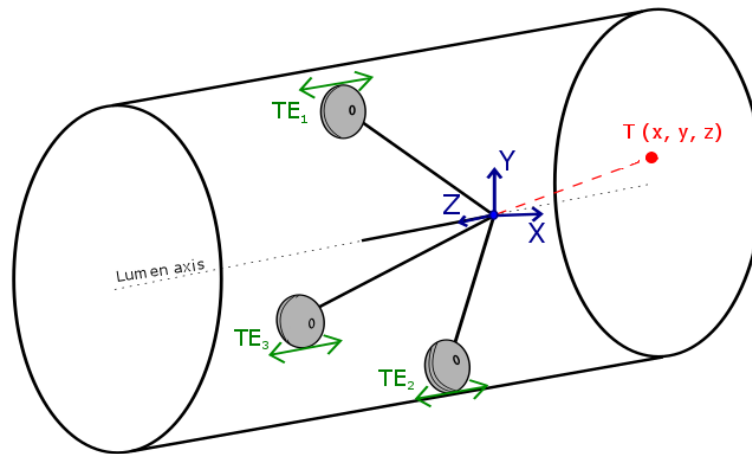


Figure 5.7 – An isometric, free body diagram of RollerBall in a lumen

A Cartesian coordinate frame is fixed to the tip of the robot. The three wheels apply a tractive effort (TE) to the lumen and are used to move the robot towards a target (T) in 3D space.

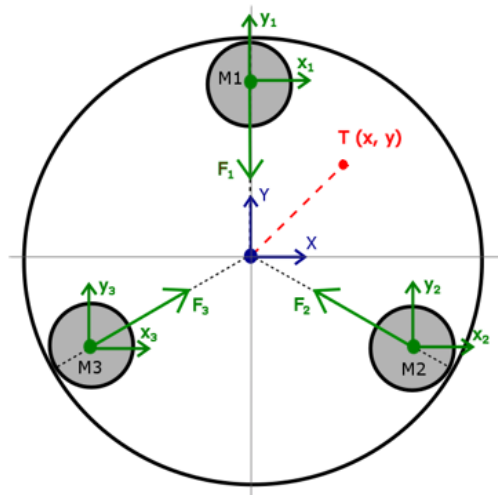


Figure 5.8 – A 2D (x-y plane) view from the rear of RollerBall showing the even spacing of the three wheels/motors (M1 – 3).

In this plane, the tractive effort of each wheel results in a force towards the centre of the robot ($F_1 - F_3$). Adjusting the relative speed of each of the motors can be used to turn the robot towards the target (T).

Currently there is one source of feedback – the visual position of the robot – determined by looking at the device itself (a perspective similar to Figure 5.7). The desired functionality (previously mentioned in Table 5.1) is to have control over the net speed and direction of the robot (the global position), and the ability to adjust its orientation either while moving - to navigate a corner - or while stationary - to observe a region of interest. Assuming the robot orientation is central (as shown in Figure 5.7), a net forward or backward movement could be achieved by simultaneously driving all three wheels at a fixed speed and direction. Introducing a differential speed in the wheels would cause the robot to turn as it moves and,

if the speed and direction of the appropriate wheels are adjusted correctly, the orientation could be adjusted while the global position of the robot is fixed (ie. rotating on-the-spot). One of the main tasks of the control software is to use an algorithm to map some user inputs onto each individual motor, setting its speed and direction to perform the requested movement.

5.5.1. Motor speed control

The Xbox controller has two analogue joysticks: left and right. These were chosen to control the position and orientation of the robot with the user inputs shown in Figure 5.5. Each has two potentiometers; one registers movement in the 'x' axis and the other in the 'y' axis therefore, the Cartesian position of the joystick can be defined. The desired mobility control was achieved at the user (input) level by having the 'y' axis of the left joystick control the gross forward or backward speed of the robot (a movement in the 'z' axis in figures 5.7 and 5.8). The right joystick is used to make adjustments to the orientation (ie. introduce a differential speed in the wheels – a movement in the x-y plane in Figures 5.7 and 5.8).

***Example:** Moving just the left joystick forwards will move the robot straight forwards at a speed proportional to the 'y' position of the joystick – all motors turn at the same rate. Moving just the right joystick up and to the right will adjust the orientation of the robot such that the tip (front) is facing up and to the right (also at a rate proportional to how far the joystick is moved). Combining the two joystick movements would cause the robot to move forwards while turning up and to the right.*

Practically, the left joystick defines a variable called the *Global speed* (ω_{Global})⁵¹. The right joystick defines the *Target* variable – the requested position of the robot tip in the x-y plane. An algorithm uses this *Target* to calculate the required *Turning (differential) speed* and direction of each motor ($\omega_{Turning(n)}$, where 'n' is the motor number: M1, M2 or M3 in Figure 5.4)⁵². The *Global speed* is then added to the Turning speed to define the overall speed and direction of each motor ($\omega_{M(n)}$, Equation 5.1), where the sign defines the direction of rotation and again, 'n' is the motor number.

$$\omega_{M(n)} = \omega_{Turning(n)} + \omega_{Global} \quad (5.1)$$

⁵¹ Global or 'gross' speed refers to the user defined forward or backward speed of the robot through the colon, where the sign of ω_{Global} is the direction.

⁵² Turning speed refers to the differential speed of each motor that results in the required movement direction.

The summation of the individual motor speeds determines the movement direction and net speed of the whole robot⁵³ (ω_{Net} , Equation 5.2):

$$\omega_{Net} = \omega_{M(1)} + \omega_{M(2)} + \omega_{M(3)} \quad (5.2)$$

The user defines the *Global speed* and direction by adjusting the ‘y’ axis value of the left joystick. The potentiometer value is converted to a -50 to +50 % range – ie. joystick fully back sets the *Global speed* to -50% and joystick fully forward sets the *Global speed* to +50%. On-the-other-hand, the *Turning speed* ($\omega_{Turning(n)}$) is calculated by passing the user input (*Target*) through an algorithm that converts it into a speed for each motor.

As previously mentioned, the *Turning speed* is set using the right joystick. The potentiometer analogue values are acquired and the position naturally defined in the Cartesian plane as shown in Figure 5.9. This x-y plane of the joystick can be superimposed onto the x-y plane defined in Figure 5.8, such that moving the joystick up (+y) will move the tip of the robot up.

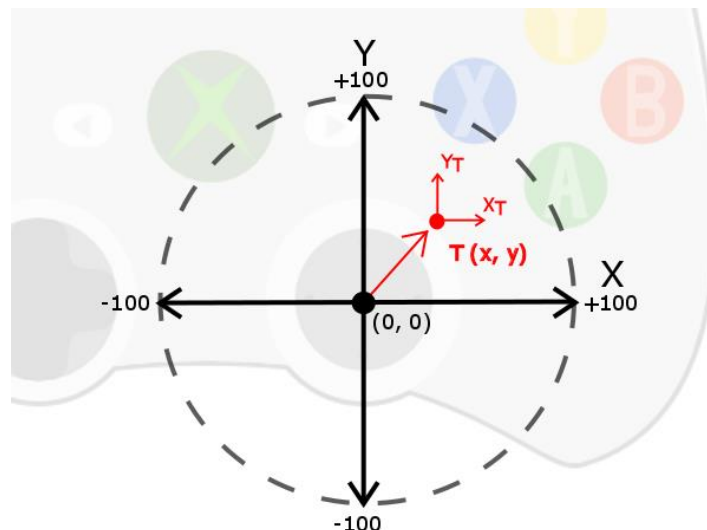


Figure 5.9 – The right joystick is used to set the desired *Target* (T) which is defined in the x-y plane.

The algorithm calculates the required speed and direction of each motor ($\omega_{Turning(n)}$, a range of -50% to +50%) that would move the tip of the robot towards the *Target*. The *Global speed* is added to this to determine the speed and direction of each motor ($\omega_{M(n)}$, a range of -100% to +100%). This sequence of steps is summarised in Figure 5.10.

⁵³ The net speed of the robot is similar to the global speed set by the user, but takes into consideration the turning component (a differential speed in the individual motors/wheels)

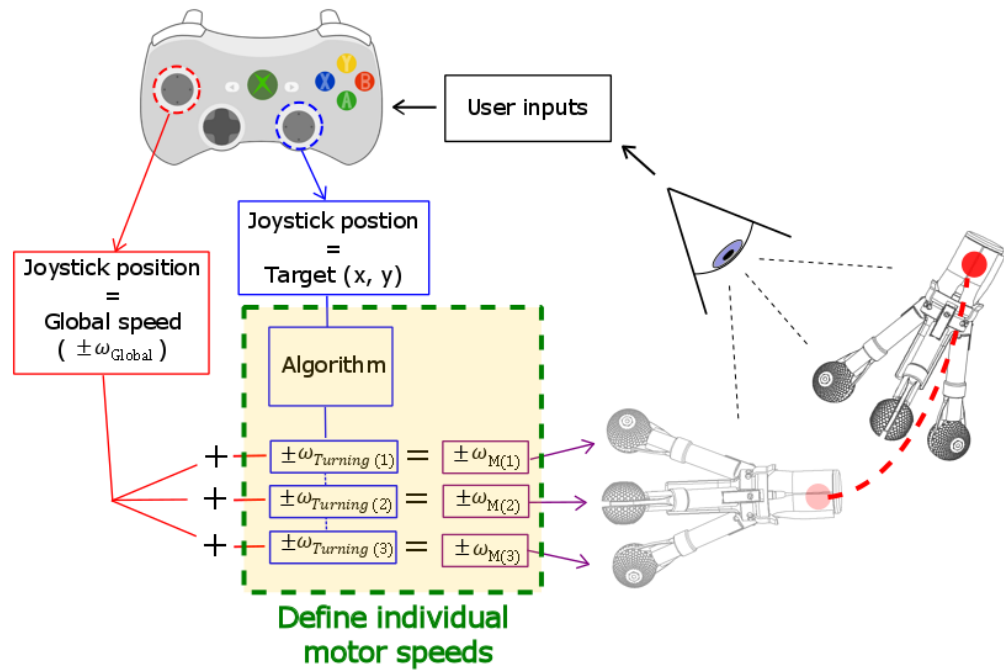


Figure 5.10 – A schematic summarising how the user inputs are mapped onto the motor outputs which move the robot.

5.5.1.1. Defining the individual motor speeds

When considering the x-y plane of the robot (shown previously in Figure 5.8 and in more detail in Figure 5.11), each wheel can only apply a force in-line with the centre of the robot. Therefore, to orientate the robot towards a target, the relative speed of each of the wheels needs to be adjusted, with the individual speeds from each wheel being summed to produce a resultant vector that moves the tip in one direction.

To calculate the relative speeds of each motor, the Cartesian coordinate system (x, y) was first converted to a Polar coordinate system (r, θ) (where r and θ are in the ranges of $0 - 50\%$ and $0 - 360^\circ$ respectively). This plane is comprised of three sectors ($S1 - 3$, Figure 5.11), created by the arm arrangement. The effect adjusting each wheel speed had on the robot orientation was then considered:

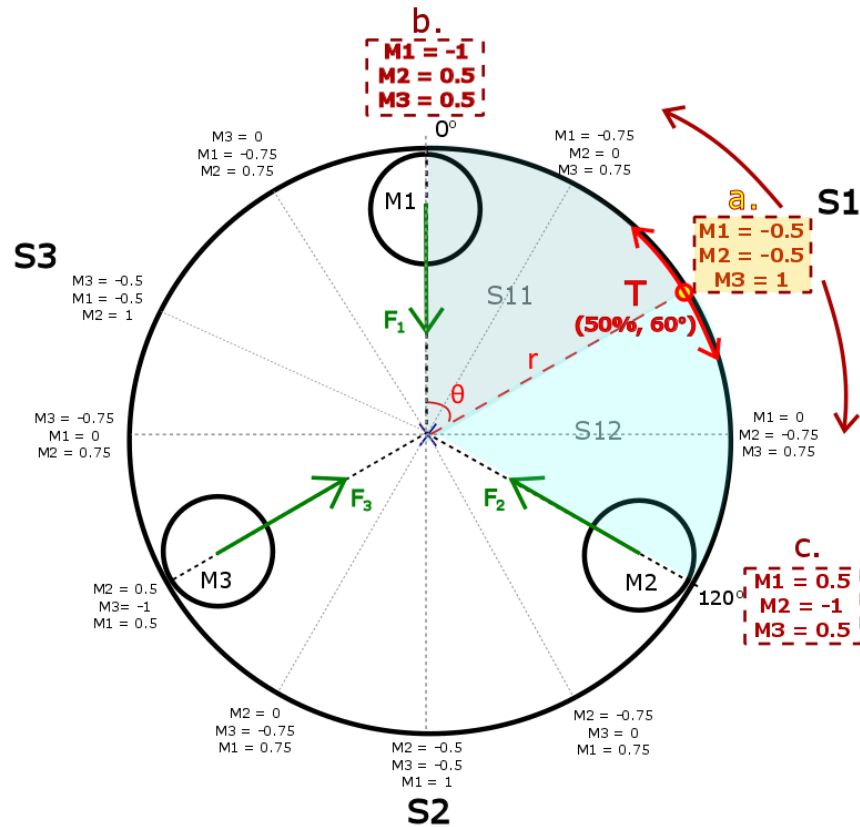


Figure 5.11 – A schematic showing how the relative motor speeds are assigned using the angle of the Target.

S1 – 3 are the three sectors created by the three wheels/motors (M1 – 3). Each sector is then split into two further sub-sectors (eg. S11 and S12). The Target (T) is defined in the polar coordinate system (r, θ), where the angle can be used to determine what sector the Target is in. Knowing the sector and sub-sector is important as it determines the relative motor speeds required to move in that direction. a. – c. are three examples of the relative motor speeds at each Target angle of 0° , 60° and 120° .

Referring to Figure 5.11: Moving to the *Target* in S1 (polar coordinates: $50\%, 60^\circ$) is most efficiently achieved by increasing the velocity of M3 ($\omega_{R(3)}$). This is because force F_3 is directly in-line with this angle and so any applied force moves the robot tip in the correct direction (ie. not requiring any input from M1 or M2 to achieve the motion). The robot could turn in this direction by driving M3 only, however, reversing M1 and M2 (which both have component forces in-line with F_3) could further assist with turning. So, when the *Target* is at this angle (60°), M3 is given a maximum relative velocity of 1 and M1 & M2 are rotated in the opposite direction at a lower relative velocity of -0.5 (Figure 5.11, annotation a.).

NB: The exact magnitude used for these relative velocities is not crucial. The motor in-line with the current Sector (M3 in the example) is given a higher value because it is the primary source of movement force. The motors either side of the current Sector (M1 and M2 in the example) are assisting rather

than solely driving the motion and so are given a lower relative velocity, in this case a relative velocity of -0.5 was chosen (the negative sign denoting a reversed rotation). What is most important is the difference between the individual motor speeds as this determines the resulting movement direction - and this is explicitly set using the input angle.

Continuing with the example (*Target* at 50%, 60°): as the angle of the *Target* is reduced to 0° (ie. into S11), it begins to align with the force applied by M1 and so this motor is given the highest relative velocity. In the case where the *Target* is at 0°, M1 is given a relative velocity of -1 and M2 & M3 given slower relative velocities of 0.5 (Figure 5.11, annotation b.). Similarly, as the angle of the *Target* is increased to 120° (ie. into S12), it aligns with the force applied by M2 and therefore, M2 is given the highest relative velocity of -1 and M1 and M3 relative velocities of 0.5 (Figure 5.11, annotation c.). Since the arms are symmetrical, this same relationship the *Target* has to the individual relative velocities in S1 (S11 & S12) could be applied to S2 and S3.

The angle is used to determine what Sector (S1 – S3) the *Target* is in and then Equations 5.3 – 5.5 are used to calculate the relative velocities at that specific angle.

Equation 5.3 is the relative velocity of the motor in the first subsector (eg. S11, M1 in Figure 5.11):

$$\omega_{R(Sn1)} = -1 \left(0.5 + 0.5 \left(1 - \frac{\theta}{60} \right) \right) = -1 \rightarrow 0.5 \quad (5.3)$$

Equation 5.4 is the relative velocity of the motor in the second subsector (eg. S12, M2 in Figure 5.11):

$$\omega_{R(Sn2)} = +0.5 \left(1 - \left(\frac{\theta}{30} \right) \right) = -1 \rightarrow 0.5 \quad (5.4)$$

Equation 5.5 is the relative velocity of the motor opposite the current Sector (eg. M3 in Figure 5.11):

$$\omega_{R(S)} = 0.5 + 0.5 \left(\frac{\theta}{60} \right) = 0.5 \rightarrow 1 \quad (5.5)$$

Multiplying the relative velocity of each wheel ($\omega_{R(n)}$) by the radius of the *Target* (0 – 50%) gives the *Turning speed* of each wheel ($\omega_{Turning(n)}$). As mentioned previously, this *Turning speed* is then added to the *Global speed* and the resulting value and sign determines the

final speed and direction of each motor (ie. Equation 5.1). This whole process is carried out by the *Position and Orientation Control* program and is described further with the supplementary Figure 5.12.

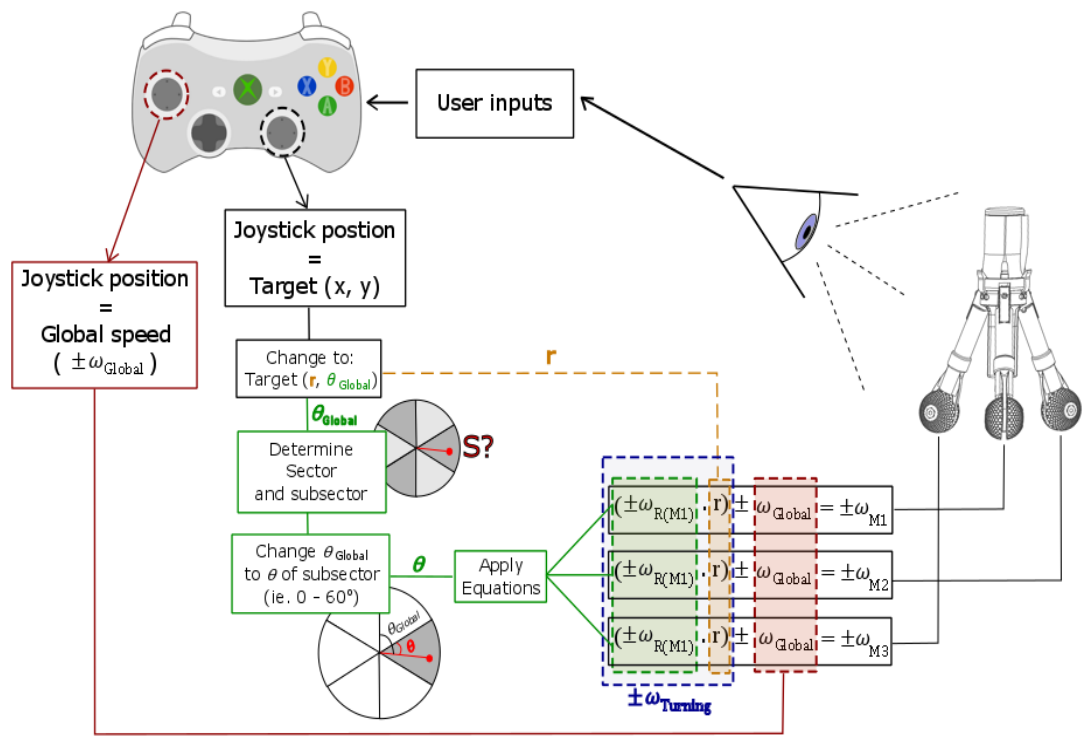


Figure 5.12 – An overview of the *Position and Orientation control* program.

5.5.2. Summary

To control the movement of RollerBall, simultaneous control over the angle of the arms and the position and orientation of the device is required. The angle of the arms is adjusted using the two triggers and a manual *Expansion control* program that was described in Section 5.4. The two joysticks are then used to control the position and orientation of the robot in a separate program. A method to map the user (joystick) inputs to the motor outputs was explored; this used a Polar coordinate system, with the angle and radius of the target being used to calculate the *Turning speed* of each motor by means of three equations (Equations 5.3 – 5.5). The *Turning speed* is added to the *Global speed* to define the net speed of each motor and the requested movement is performed. These programs were written and simulated in LabVIEW. To assess the efficacy of this control method, the associated programs and the prototype in general, a test environment was next required.

5.6. Test environment

The colon is a complex environment and one that presents a particular challenge to mobile robots. Advanced control is crucial to the success of the RollerBall concept and like many development processes, this requires multiple iterations of testing and refining. If carried out in a biological, hydro-colonoscopy environment, this would present significant issues:

1. It would require the use of many tissue specimens that need to be carefully prepared, positioned, secured and distended with fluid. This would undoubtedly result in the iterative process being slow.
2. Human colon is difficult to acquire, with the most common source being thiel cadavers (where the structure and properties have been altered by the preserving process [109]). Animals, such as pigs and dogs, are often used as a substitute (eg. in Chapter 4, pig colon was used) however, they are anatomically different – in Chapter 4 the pig colon was seen to have more pronounced haustral folds and a generally smaller diameter than human values stated in literature. Therefore, if this animal substitute was used, the size and shape of the *ex vitro* colon environment would be limited by the anatomy of the animal and would result in an inefficient use of the tissue (with some parts unusable due to their small diameter or unrealistically pronounced haustra).
3. The fact that the RollerBall prototype is a complex device and is not fully encapsulated means that the electronics could be damaged by the biological fluids and sterilisation would be extremely difficult, if not impossible. This would mean that a new prototype would be required for each subsequent test – especially if the colon was distended with fluid.
4. A biological environment would present a unique limitation to the development of the control: the visibility of the device as it moves inside the tissue is restricted. This is important as a clear view of the prototype orientation, arm angle and general physical state is required to assess the control and provide insights as to how to improve the performance.

What is required is an environment that is robust, reusable and does not compromise the sensitive electronics, allowing the prototype to be used over many iterations. Furthermore, the environment should ideally allow the individual control aspects (such as cornering ability or adjusting the arm angle) to be visually assessed in a controlled, isolated setting. Then, more specifically the environment should include the following features to broadly represent the colon:

- Varying diameters.
- Multiple corners of different angles.
- A thin and flexible lumen.
- Partial support that allows the lumen to move and expand.
- Obstacles to represent the haustra.

It would be nearly impossible to recreate the biological colon out of synthetic materials and satisfy all of these requirements and therefore, a compromise had to be made on how realistic the environment was. The traction work was carried out on a biological substrate and it was shown that substantial traction can be acquired using a tread pattern (with further improvements possible). This outcome suggested that the frictional characteristics could be excluded from this environment as it was already assessed separately. A higher friction substrate could be used, reducing the complexity of the environment and allowing the orientation of the robot to be adjusted in all directions because the offset CoM (mentioned in Chapter 3, Section 3.2.2) could be overcome by the available tractive effort.

Two synthetic tubes were designed to meet the aforementioned requirements. One included no corners but a diameter that varied from 90 mm to 40 mm over its length⁵⁴ (the schematics are shown in Figure 5.13). This would allow the control of RollerBall's orientation and arm angle to be investigated, as well as straight line speeds. The second tube included multiple corners but a fixed, 60 mm diameter lumen. This would allow mobility around corners to be assessed, with the combination of the two tubes giving an indication of overall usability and locomotion efficacy. Clear silicone (*Smooth-on, Sorta Clear*), with a Shore hardness of 40A, was used to provide a flexible and durable lumen. This was painted onto a machined and treated foam mould. Multiple coats were applied to build-up a layer thickness of approximately 1 mm. The tubes were durable enough to then be rolled off of the moulds

⁵⁴ The diameters were chosen to represent the average diameter of the human colon but at a slightly larger scale since the prototype does not yet meet the size requirements.

before gluing nylon tabs onto the tubes with silicone adhesive. These tabs were used to suspend the tubes from an aluminium support frame using thin nylon line.

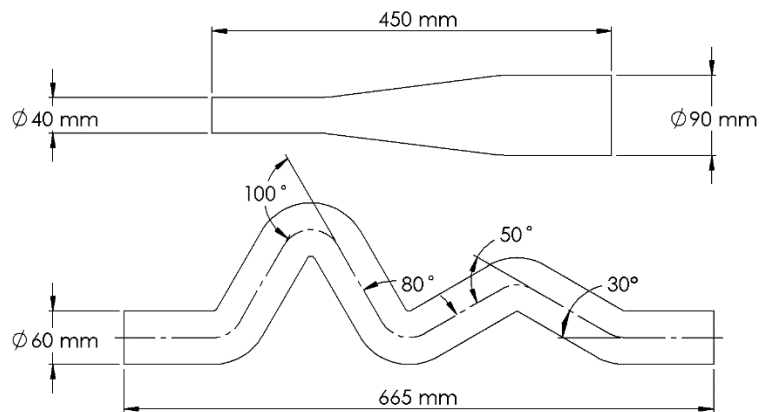


Figure 5.13 – A schematic showing the geometry and dimensions of the two main tubes used to evaluate RollerBall.

Suspending the tubes, such as that shown in Figure 5.14, ensured the shape of the colon was maintained while allowing the free expansion of the lumen and partial mobility of the tube during tests.



Figure 5.14 – The silicone tube with multiple corners, suspended by thin nylon line from an aluminium frame.

This environment was used for the majority of the work in this chapter⁵⁵. The following pages describe the development of the control software and the assessing of the overall efficacy of the RollerBall concept.

5.7. Open-loop system evaluation

A series of laboratory-based experiments were carried out to assess the efficacy of the open-loop control system and the general locomotion efficacy of RollerBall.

5.7.1. Method

The complete RollerBall system (including the hardware in Figure 5.1, the system architecture described in Figure 5.3 with the individual control programs described in Sections 5.4 and 5.5) was assembled. A prototype without a camera was used and so the only source of feedback was the visual state of the device in the transparent lumen (provided by the user). Two groups of experiments were then carried out, one in each tube: *Group 1* used the tube with changing diameters to assess RollerBall's ability to adapt to narrowing apertures and adjust its position and orientation. *Group 2* used the tube with multiple corners to further assess RollerBall's mobility, this time around corners. Both tubes were used to assess the locomotion efficacy and qualitative usability.

5.7.1.1. Group 1 – Changing diameter tube

The tube with changing diameters was suspended from the aluminium frame in a similar way to that shown in Figure 5.14. During one repetition, the prototype was first inserted into the large end of the tube before the arms were expanded to make contact with the lumen. The expansion of the arms was adjusted “by eye” – with the angle being increased until the wheels had deformed the lumen and there was sufficient traction for the robot to maintain a central/level orientation (Figure 5.15).

⁵⁵ A third tube, similar to the varying diameter tube, was fabricated to include multiple haustra-like obstacles and was used to assess the closed-loop control of the arm angle (*Expansion mechanism*). This is described in more detail in Chapter 6.

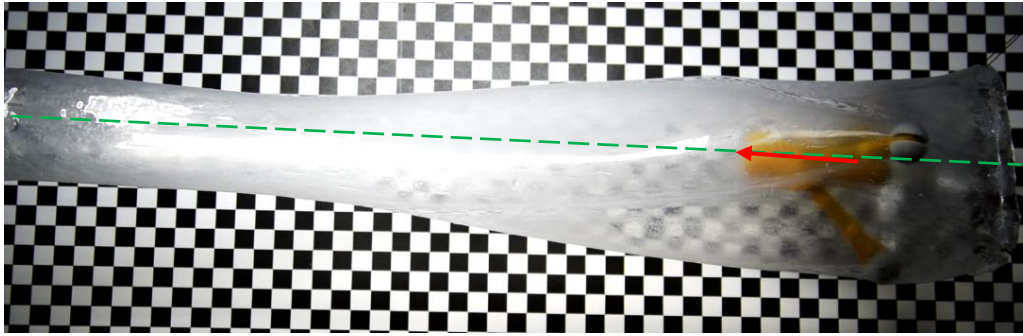


Figure 5.15 – The idle/starting position of RollerBall in the changing diameter tube.

The longitudinal axis of the robot (arrow) was aligned with the longitudinal axis of the lumen (dotted line). The checkered boxes are 1 cm square.

From this starting position, the user then attempted to traverse the length of the tube; this required the simultaneous adjusting of the arm angle (as the diameter narrowed), the orientation (to maintain a central/level pose) and the global position (ie. the *Global speed* and direction). Each test was videoed from above and the recordings used to calculate max speeds (in constant diameter sections) and the average movement speed across the length of the tube. One practice run was taken before completing a total of five repetitions.

5.7.1.2. Group 2 – Tube with multiple corners

The silicone tubes were switched. During one repetition in this next tube, RollerBall was inserted in the end with the smallest angle bend and the arms expanded to stabilise the robot in the idle position (Figure 5.16).

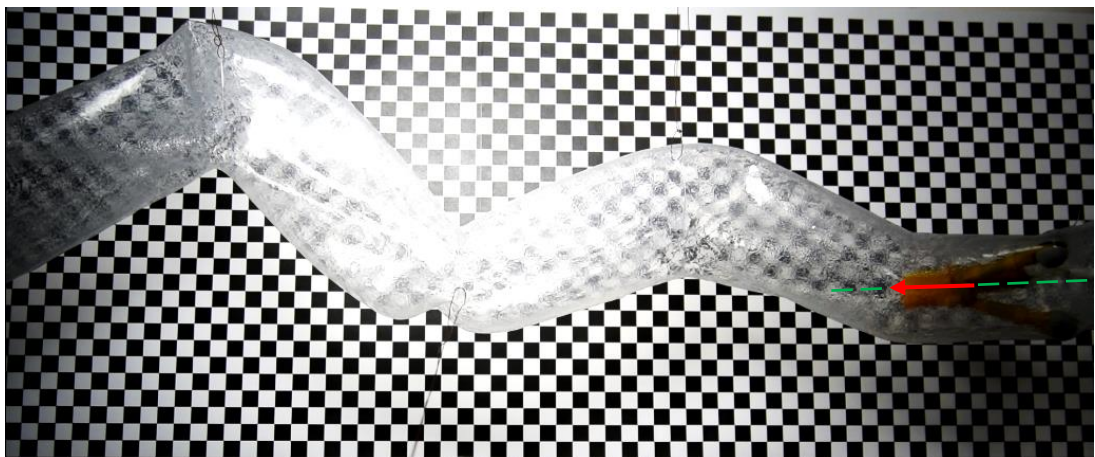


Figure 5.16 – The idle/starting position of RollerBall in the tube with multiple corners.

The longitudinal axis of the robot (arrow) was aligned with the longitudinal axis of the lumen (dotted line). The checkered boxes are 1 cm square.

From the starting position, the user then attempted to traverse the corners in order of increasing acuteness. Again, this required the simultaneous adjusting of the arm angle (this time mainly to control traction), the orientation (to navigate a corner) and the global position (ie. the *Global speed* and direction). The tests were videoed from above and the recordings used to calculate the average movement speed across the length of the tube. One practice run was taken before completing a total of five repetitions.

5.7.2. Results

The entire length of the narrowing diameter tube was successfully traversed in all five repetitions (a sequence of images from one repetition is shown in Figure 5.17, a.). The average speed while doing so was calculated as 4.9 ± 1.7 mm/s ($n = 5$) from the video recordings. Maximum speeds in the order of 22 - 29 mm/s were also recorded in the constant diameter sections of the tube, where the arm angle did not need to be adjusted. The orientation of the device could be adjusted on-the-spot in both wide and narrow apertures (wide aperture shown in Figure 5.17, b.).

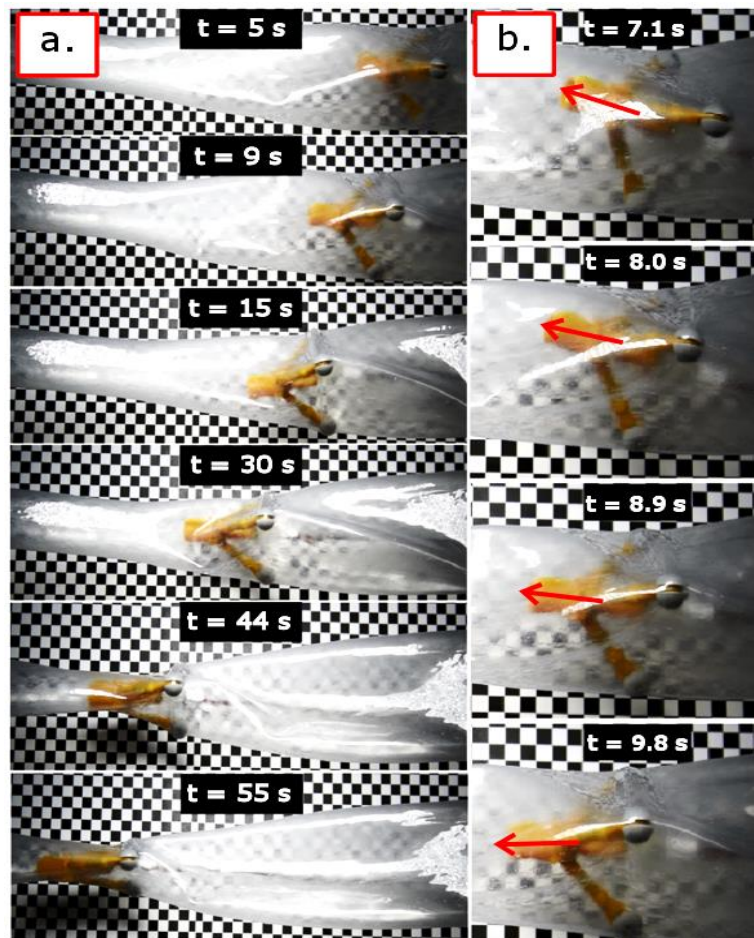


Figure 5.17 – A sequence of images from one repetition in the changing diameter tube tests.

a. One complete repetition and b. Adjusting the orientation.

RollerBall was successful in traversing the majority of the corners during tests in the second tube. A sequence from one of the repetitions is shown in Figure 5.18.

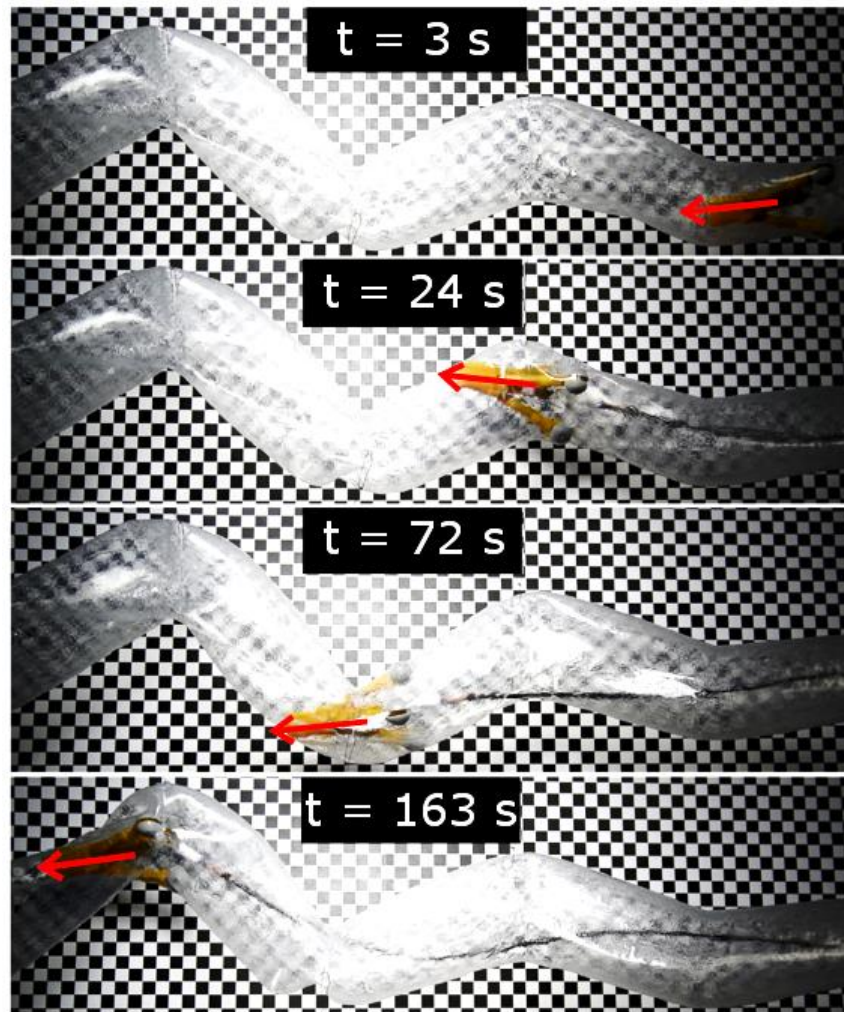


Figure 5.18 – A sequence of images from one repetition in the tube with multiple corners.

The success rate for each corner of the tube (from all 5 repetitions) is shown in Table 5.3:

Table 5.3 – Cornering success rate.

Corner angle	30°	50°	80°	100°
Success rate (n=5) (%)	100	80	60	60

The average speed from one complete repetition of the tube (traversing all corners) was measured as 3.6 mm/s.

5.7.3. Discussion

Tests in the variable diameter tube showed that the orientation of RollerBall can be controlled in both an expanded and collapsed robot state. Maintaining a central, “level” orientation in the tube during tests was required to prevent the front of the device from catching on the lumen and stopping progress. This required the user to make frequent, small adjustments to the orientation during forward locomotion. The controllability - particularly when adjusting the orientation - showed the efficacy of the method used to control the individual motor speeds.

The lack of force feedback meant that it was difficult to assess when to alter the angle of the arms. In order to maintain a stable platform and traction, while moving from one aperture to another, the user had to monitor the degree of lumen distension around the wheels. The force sometimes reached a level large enough to stall the motors in the expansion and wheel mechanisms – likely to cause damage *in vivo* and to the prototype if repeated many times. Despite the simple approach used to control the arms, the tests showed that RollerBall can use the expansion mechanism to operate in varying apertures.

Tests in the second tube further demonstrated the mobility of RollerBall and efficacy of the locomotion technique as it successfully traversed multiple bends. Unsuccessful cornering was attributed to the length of the prototype and the high friction between it and the silicone tube; if the angle of approach was suboptimal, the device became wedged in the corner (Figure 5.19) and required considerable manoeuvring to free it.

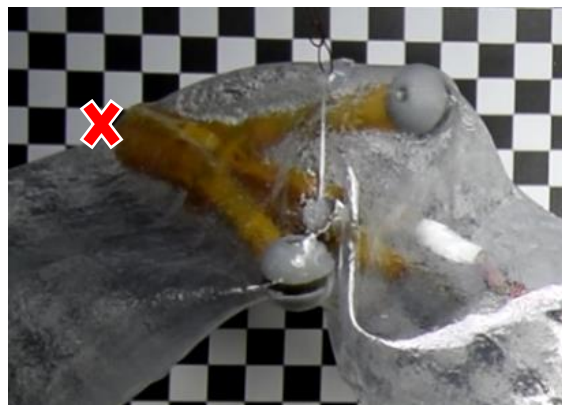


Figure 5.19 – An image of RollerBall stuck in a corner.

The use of DC motors and the control strategy employed meant that very precise movements could be made by intuitive adjustments of the analogue joysticks and triggers. However, the fact that the user was required to simultaneously control speed, orientation and arm angle meant that controlling the robot, particularly around bends, was challenging. Precise, manual control is particularly difficult when the device rolls because this changes

the user's axis of reference⁵⁶. The issue of the lack of automation is highlighted by the slow average movement speed in both tubes: 4.9 ± 1.7 mm/s ($n = 5$) in the first tube and 3.6 mm/s ($n = 1$) in the second tube, compared to the peak speeds of ca. 22 – 29 mm/s when little user input was required (in a straight section of tube, for example). Despite these low values, the speed broadly meets the requirements for a colonoscopy procedure.

5.7.4. Conclusions

Preliminary tests of the open-loop system revealed the following:

- The system architecture functions as intended, allowing the prototype to be controlled robustly.
- The prototype itself is robust and can be handled and tested with no part failures. The individual mechanisms functioned as intended and provided sufficient performance for the required movements in the silicone tubes.
- The control strategy used, and the programs developed, were effective in manually controlling the robot with intuitive user inputs. Tests in the silicone tubes showed the efficacy of the locomotion technique; the device can adapt to varying diameters, provide a stable platform, adjust its orientation and navigate a range of corners.
- Control was less intuitive once the robot had rolled about the lumen axis; an on-board camera could improve usability by maintaining a fixed view/reference for the user.
- The length of the device restricted movement around acute bends as it was greater than the bend radius. Similarly, the silicone tubes were effective at providing a reusable environment and high traction, however, high friction between the body of the robot and the lumen further hindered progress in some cases.
- The average speed of the device meets the requirements however, it could be greatly improved with more advanced control; the user inputs, despite being intuitive, were cumbersome as multiple tasks needed to be carried-out simultaneously. Furthermore, the lack of force feedback meant that control of the arm angles was difficult and excessive force may have been applied.

The success of these tests encouraged the further development of RollerBall. They suggested that the inclusion of embedded force sensors and a camera may greatly improve

⁵⁶ Steering the device using the image from an on-board, forward facing camera will likely alleviate this problem as the view (image) is fixed to the axis of the robot.

mobility, usability and safety; they could also permit the automated closed-loop control of arm expansion and device orientation. Automation is expected to significantly reduce the demand on the user and greatly increase the overall movement speed. A forward facing camera and force feedback would also mean that the robot could operate in a non-transparent tube. The pursuit of automation is the main theme of the next Chapter.

Chapter 6

Closed-loop control

This chapter concludes the control development and evaluation of RollerBall. Force sensing is first included on each arm to permit the arm force (and so angle) to be adjusted autonomously. A forward facing camera was then included and the image feedback used to automate the adjusting of robot orientation. The effect this automation had on locomotion efficacy and usability was then assessed in a series of experiments before finishing with a test showing the feasibility of semi-autonomous control of the entire robot.

6.1. Closed-loop control system

The rigid arms connected to the *Expansion mechanism* via a non-back-drivable mechanism and the method of locomotion used by RollerBall (continuous control of wheel speeds) means that advanced, automated control is not only desirable but may be a necessity to ensure its efficacy as a colonoscopy procedure. The manual, open-loop experiments showed that the device could be controlled intuitively but it needs several advancements, namely:

1. Force feedback from each arm to ensure a safe threshold is not exceeded.
2. A method of automating the arm actuation, maintaining a desired force range for acquiring traction in changing diameters and ensuring a stable platform.
3. The integration of a forward facing camera to - apart from the obvious requirement of visualising the colon - improve usability by giving the user a fixed view of the robot orientation.
4. A method of automating the orientation control to assist in maintaining a desired pose.

This section explores these advancements and ends with whole device tests to validate them and the overall efficacy of RollerBall.

6.2. Expansion control

Active control of the arm angles is required to maintain traction and a stable platform; it is also necessary to limit the applied force to avoid damaging both the colon and the robot itself. The stiff arms, described in Chapter 3, were each fitted with a half bridge strain gauge circuit close to the shoulder joint where strain is highest.

6.2.1. Instrumentation

The setup shown in Figure 6.1 was used for the force sensing. A Wheatstone bridge circuit was used to measure the strain of each arm, with half of the bridge active (two strain gauges on the arm) and the other half passive, placed separately to the robot on a conditioning board. A change in voltage is measured from the changing resistance of the strain gauges during arm flexing. The analogue voltage signals from the strain gauges are transmitted via the tether to a conditioning board. The conditioning board also included voltage regulators for the bridge excitation and a PSoC 3 (Programmable system-on-chip) to condition the signals, including: amplification using the embedded OP amps, analogue to digital conversion and transmitting of the strain signals via I2C at a rate of 200 Hz. The *myRIO* acquired the I2C data and was also used to power the conditioning board via an internal, regulated voltage source.

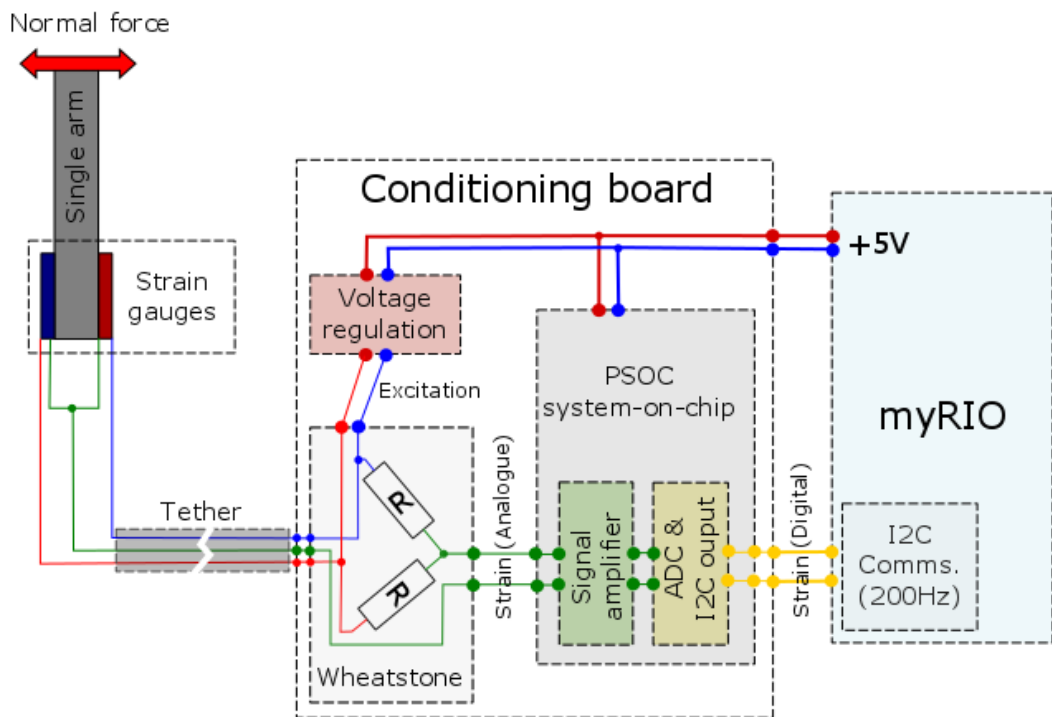


Figure 6.1 – A schematic of the force sensing system.

This shows only the major components to the system. Only one of the three arms is shown.

The conditioning board was fabricated and the strain gauges integrated into the prototype. The next step was to characterise the output and calibrate it to measure force.

6.2.2. Characterisation

The resistance of strain gauges changes proportionally with the amount of strain placed across them; this resistance can then be measured as an analogue voltage. The strain, and how it changes with different loads, is determined by the material properties of the arm. Ideally, strain is proportional to the input load (and so constant with a constant input). Therefore, the system is stable and a calibration coefficient can be used to determine the load from the raw strain signal. The strain gauge setup described in the previous section was put through a number of tests to characterise the force sensing system.

A simple test was first done to validate the signal acquisition over time. To do this, the system was powered-up and the raw strain signal data collected for ca. 30 min. The system was then left on for ca. 2 hours before collecting raw data for another 30 mins. This was done to assess whether the system needs to be “warmed-up” before being used. The results showed that, as expected, there is some noise in the signal. This could be from a number of sources but was not considered an issue as it is small in comparison to the strain values measured during normal use. Initial trials showed that a 100 g mass resulted in a strain output greater than 1000. The noise is therefore only 2% of what would be considered a high input load given the expansion mechanism capabilities. It could easily be filtered-out in the software using a low-pass filter. While the system was “cold”, the strain value was seen to decrease slightly over time (from a value of 2 to -16 over 30 mins – presumably from the increase in temperature and resulting change in resistance/perceived strain). Once warm, the strain value remained relatively constant over the 30 min duration (with a standard deviation of 2.5), thus indicating that the system is stable once warmed-up.

To characterise the force sensing, the output strain profile that results from a step load input was investigated. With a perfectly elastic, linear material, the output profile should closely match the input profile, with straight edges and a constant steady-state output; this is required for both calibration and acquiring accurate force readings.

6.2.2.1. Characterisation method

The entire RollerBall system was switched-on and left to warm-up for approximately two hours. A single arm of RollerBall was fixed at the shoulder in a horizontal orientation - measured using a small spirit level. A known mass was then hung, instantaneously, from the end of the arm and left for approximately 30 seconds while the strain data was measured at 200 Hz by the *myRIO* and logged at 100 Hz. The mass was then removed and the arm left unloaded until the strain reading returned to zero. A different mass was then hung from the arm in the same way. This was repeated for three different masses (11.2 g, 51.0 g and 101.2

g)⁵⁷ and three repetitions per mass. The entire process was carried-out on all three arms of RollerBall.

A typical strain output from these experiments, including a superimposed ideal step input, is shown in Figure 6.2. It is clear that the output is not ideal; most noteworthy is an increasing strain over time. The latter was attributed largely to the 3D printer resin used to fabricate the arms which is not purely elastic and creeps under constant load (this was confirmed with a long duration test, the profile of which is shown later in Figure 6.3). The former attributed to both the material properties and the method used to apply the load.

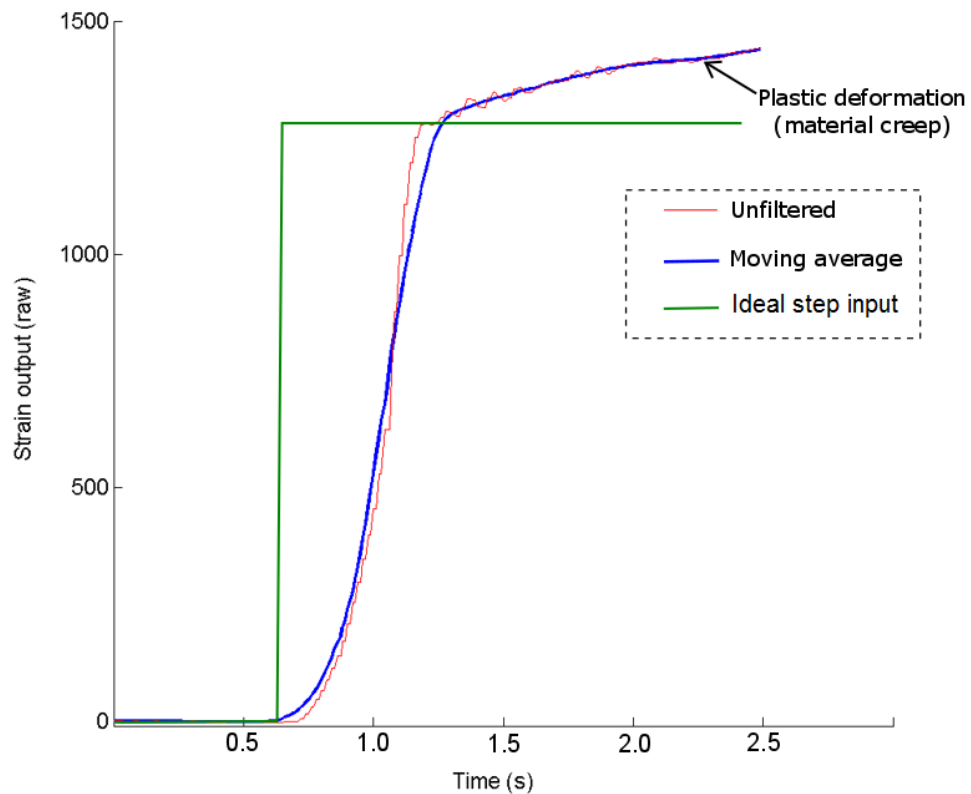


Figure 6.2 – A plot showing the first 2.5 seconds of the collected strain data.

This figure highlights the suboptimal response from the strain gauges: material “creep” (increasing strain over time).

The collected data was processed to characterise this non-linear behaviour and assess the repeatability of the strain readings. It was later used to calibrate the sensors.

⁵⁷ These were values were chosen based on the available force from the expansion mechanism and were measured accurately using a KERN digital scale (PCB 1000-2) with a resolution of 0.01g.

6.2.2.2. Data processing

A number of steps were required to process the strain data:

1. Find the point at which the material begins to creep (ie. separate the linear and non-linear regions of the strain profile).
2. Determine a robust method of measuring an accurate strain value that can be used for calibration and subsequent force readings.
3. Model the creep behaviour of the material.

A MATLAB script was written to process the data and achieve the three points mentioned above. It first locates the point at which the strain output begins to increase over time (material creep). This was found by searching for the peak second derivative of the strain output in the first 250 ms of data acquisition (Figure 6.3, annotation 1.).

***Hypothesis:** When the mass is first placed onto the arm, the strain output rapidly increases in the first few milliseconds (almost instantaneously). The rate of change of the gradient in this region is very small as the output is approximately linear – an elastic response. When the full mass has been placed onto the arm and the arm has undergone the majority of its deformation, there is a spike in the second derivative as the arm transitions from elastic to plastic deformation (material creep).*

This point in time signifies the end of the (approximately) linear response and is the point of interest (POI) (Figure 6.3, annotation 2.).

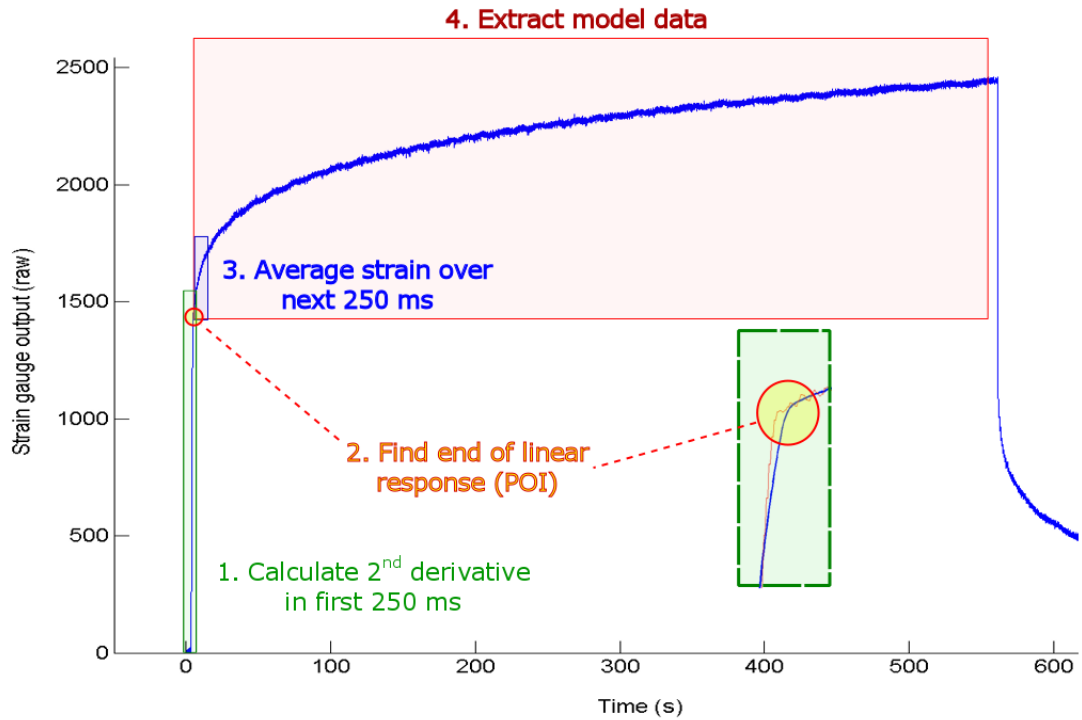


Figure 6.3 – An annotated plot showing a strain response from a long duration step input.

This figure shows that the material creep occurs over a long duration and includes annotations showing how the data was processed.

From this POI, the next 250 ms of strain data was averaged and stored as the strain value for that mass (later used for calibration) (Figure 6.3, annotation 3.). A model was then fitted to the data, from the POI to the end of the non-linear region (Figure 6.3, annotation 4.). This was done using the curve fitting tool in MATLAB (*cftool*). This script was run for all data sets collected.

6.2.2.3. Results and discussion

The data processing script was successful in repeatedly locating the POI. This allowed the subsequent 250 ms of data to be averaged to find a strain value for each specific mass. The average strain data from all three strain gauges is shown in Table 6.1.

Table 6.1 – The average strain outputs for all Strain gauges and multiple loads.

	SG1	SG2	SG3
Mass (g)	Strain (Avg., n=3) \pm std	Strain (Avg., n=3) \pm std	Strain (Avg., n=3) \pm std
11.2	145.2 \pm 1.64	120.9 \pm 1.96	127.43 \pm 1.51
51.0	654 \pm 4.05	535.4 \pm 4.00	568.85 \pm 5.05
101.2	1308 \pm 4.64	1060.6 \pm 0.87	1134.4 \pm 7.91

The low standard deviation seen in the strain values indicated that the strain gauges are robust and give repeatable readings. There are a number of factors that could account for the slight deviation, including: inaccuracies in the data processing, variability in the force sensing system (eg. temperature or noise) and most significantly, the method used to apply the load. The latter was seen as disturbances in the linear region of the strain profile and may have also increased the *apparent* damping in the system⁵⁸.

The remaining non-linear region of the strain profile, under all loads, was then successfully described (Equation 6.1) with a time-dependent, two-term power series model ($R^2 > 0.95$) using the curve fitting tool in MATLAB:

$$f \varepsilon(t) = a \cdot t^b + c \quad (6.1)$$

Where c is the strain at the start of the model and a & b are the coefficients that determine how the strain increases over time. Interestingly, a & c have a linear relationship ($R^2 > 0.99$) with mass and b is relatively constant. The constant value of b suggests that it relates to the material properties (constant over all loads). The coefficients of the model, from a single strain gauge, are shown in Table 6.2.

Table 6.2 – The average model coefficients from different masses (SG2).

SG2			
Mass (g)	a (Avg., n=3) ± std	b (Avg., n=3) ± std	c (Avg., n=3) ± std
11.2	27.6 ± 1.8	0.21 ± 0.00	103 ± 3.1
51.0	107 ± 5.5	0.22 ± 0.01	466 ± 3.4
101.2	221 ± 15.3	0.21 ± 0.01	916 ± 14.7

Some variation was seen in the model coefficients, although they were considered acceptably low. This is most likely from the human error associated with the load application, mentioned previously. The linear relationship of a and c with mass, and the constant value of b suggests that this material creep could be predicted and compensated for. The previous Figure 6.3 shows the material creep over a period of approximately 25

⁵⁸ The masses were applied by hand, hung from the arm by a thin nylon line. The masses had to be gently released so as to not introduce added force from the inertia of the falling mass. The release of the mass (over a few milliseconds), combined with the expected stretch in the nylon line, may have slowed the strain response – ie. increased apparent damping – and introduced variability.

minutes. This duration was chosen as whole robot tests could take this length of time. Assuming the robot arms are under 100 gf of load, the creep will introduce a significant error of ca. 67 % after 25 minutes. There are three possible solutions for this:

1. Compensate for the material creep (ie. apply a time varying offset to the output).
2. Use a different, purely elastic material for the arms.
3. Keep the length of time the arms are under load to a minimum.

6.2.3. Calibration and validation

The average strain values displayed in Table 6.1 (found post-processing) were used to determine the calibration coefficients for each strain gauge. The average values were plotted and a linear fit applied. The R^2 was greater than 0.99 for all strain gauges, indicating that they could be used to accurately measure force. The gradient of each plot was calculated and used as the calibration constants (Table 6.3).

Table 6.3 – The calibration constants for all strain gauges.

	SG1	SG2	SG3
Coefficient	12.93	10.45	11.19

To validate the calibration and determine the accuracy of the force sensing (excluding the material creep), two random masses (28.7 g and 68.5 g) were hung from a randomly selected arm (in this case, SG2). The collected data was processed using the MATLAB script. The average strain value was divided by the calibration coefficient and the force (gf) calculated. Table 6.4 shows the results.

Table 6.4 – Force sensing validation.

Expected force (gf)	Measured force (gf) (Avg., n = 3) ± std
28.7	29.8 ± 3.8
68.5	69.9 ± 2.1

The average percentage error was calculated as ca. 2.9 % across the two loads. Without human inaccuracies in the force application, this could be significantly lower and suggests that, provided the material creep is dealt with, the force sensing system is effective.

6.2.4. Material creep compensation – feasibility trials

The low variance in the model coefficients (Table 6.2) and their linear relationship with mass meant that it may be possible to compensate for the material creep. The relationship between the model coefficients and mass was first determined by calculating the corresponding gradient of the linear regression. The previous MATLAB script was then modified to have the following functionality (Figure 6.4):

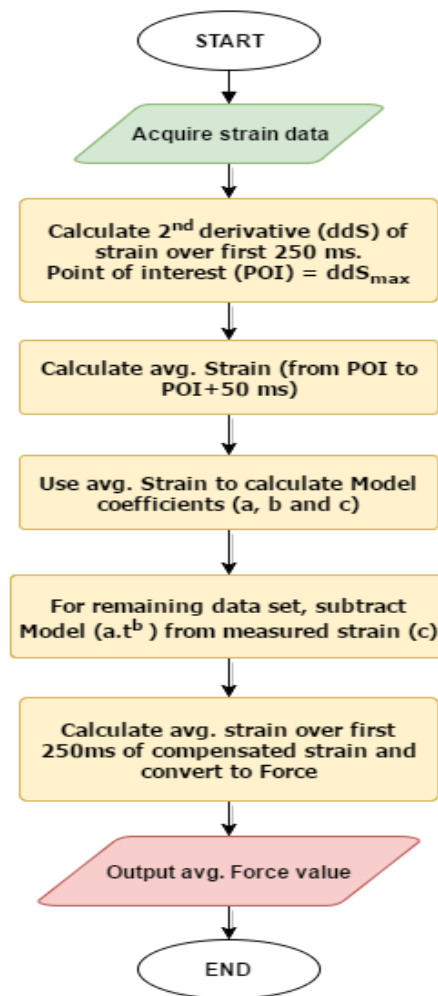


Figure 6.4 – A flowchart showing the various stages used to compensate for the material creep.

An example output plot from this compensation program is shown in Figure 6.5.

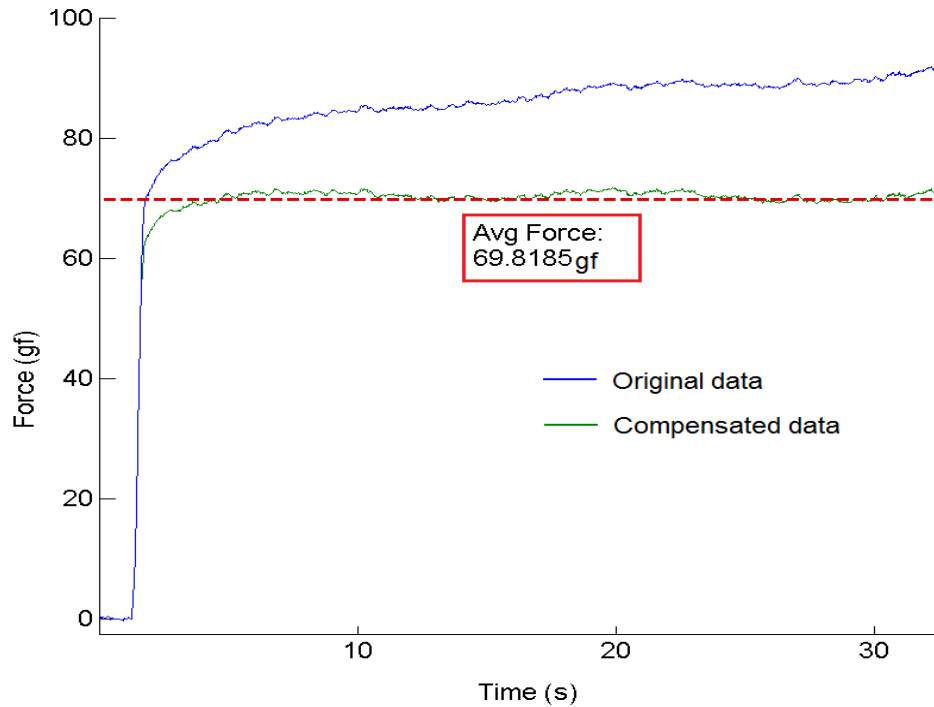


Figure 6.5 – An example output from the material creep compensation program.

Applied load = 68.5 g

Figure 6.5 demonstrates that the program could successfully compensate for the material creep, giving an approximately steady-state strain/force output close to the value of the actual applied load. However, this program was developed for post-processing the data and was not suitable for real-time processing of the strain data. Such a task would require a more complex program that tracks the force history and applies the appropriate constants to the model in real-time. This work was not justified as the material used (resin) is specific to the prototype and future devices are likely to use more linear, elastic materials. Therefore, it was decided that the material creep would not be compensated for and the duration of each test on the prototype would instead be kept to a minimum; if within one minute, the error would be ca. 20 %. This was considered suitable for the current application as a safe force range (rather than a very specific, accurate force) could be maintained to avoid damage to the robot.

6.2.5. Summary – Force sensing

Half bridge strain gauge circuits were used to measure the force applied to each arm of RollerBall. The sensing system was robust and could measure instantaneous force with only minor variance. The strain data required post processing to calculate this applied force but

could do so accurately (ca. 2.9 % error). The material used for the prototype (a 3D printed resin) exhibited a non-linear strain response during prolonged loading, expected to be from the plastic deformation (creep) of the material. This was accurately modelled and it was demonstrated that, given more time and further development, this could be compensated for in real-time. Other alternatives suggested were: using a different, purely elastic material for the arms and; not compensating for the creep but instead keeping prototype testing duration to a minimum. The latter was chosen based on the intended use of different materials in future developments.

6.2.6. Expansion control strategy

Tests on the open-loop system highlighted the demanding task the user has to control the robot smoothly. Reducing the remand on the user is a desired requirement for this procedure and automating parts of the control will also likely improve the locomotion efficacy (eg. speed). The first task to automate is the arm angle (Expansion control). This needs to be adjusted frequently to maintain traction in a lumen that is highly variable in diameter along its length.

6.2.6.1. Closed-loop force control

Each arm is fitted with a half bridge strain gauge circuit that can effectively measure the normal force applied to it. This was initially included to ensure a “safe” force threshold was not exceeded however, it could also be used to control the arm angle by keeping the force within a desired range.

As the lumen narrows, the elastic force on the arms increases and is measured by the strain gauges. The *Expansion mechanism* could then compensate for this by contracting the arms under closed-loop (PID) control - using the strain gauge feedback - to maintain a desired force. This is a complex problem as there are a number of different factors affecting the control system, including:

1. The inertial load on the motor from the five stage gearbox, worm gear assembly and three robot arms. Given this setup, the inertia is expected to be high.
2. High friction load on the motor from the gearbox, worm gear assembly and shoulder joint. The static friction in particular is expected to be very high. This was seen in the benchtop characterisation where the actual force was only ca. 30 % of the theoretical output.
3. The non-linear properties of the arm and lumen material. This includes the material creep mentioned previously and hysteresis losses.

4. The combined backlash of the worm gear assembly and motor gearbox.
5. The presence of two scenarios: contracting the arms (little resistance) and expanding the arms (high resistance – deforming the lumen).

These factors will have some predictable, negative effects:

1. The inertial load, high friction and non-linear material properties (including hysteresis losses) will introduce significant damping into the system and greatly increase the rise time (reduce responsiveness). The damping of the material was seen in the force sensing characterisation.
2. Backlash, and the transition from expanding to contracting, could introduce instability as the force may suddenly change. This could manifest as high frequency oscillations as the control attempts to compensate with equal, unattainable brevity. This will make the use of the Integral (I) and Derivative (D) constants in the PID both crucial and challenging, as they are both time dependant.

The complexity of the system suggested that the automation should be developed empirically (eg. using intuition and manual PID tuning) with the ultimate goal of assessing whether keeping the maximum arm force within a desired safe range is possible with the current mechanical setup. Two programs were written to achieve this force control and are summarised in Figure 6.6.

Referring to Figure 6.6: Given that all three arms are actuated by a single motor and safety is paramount, it was decided that the max force value (F_{max}) from all three strain gauge pairs ($max(SG1-3)$) should be used for the closed-loop control of the force and resulting angle of the arms.

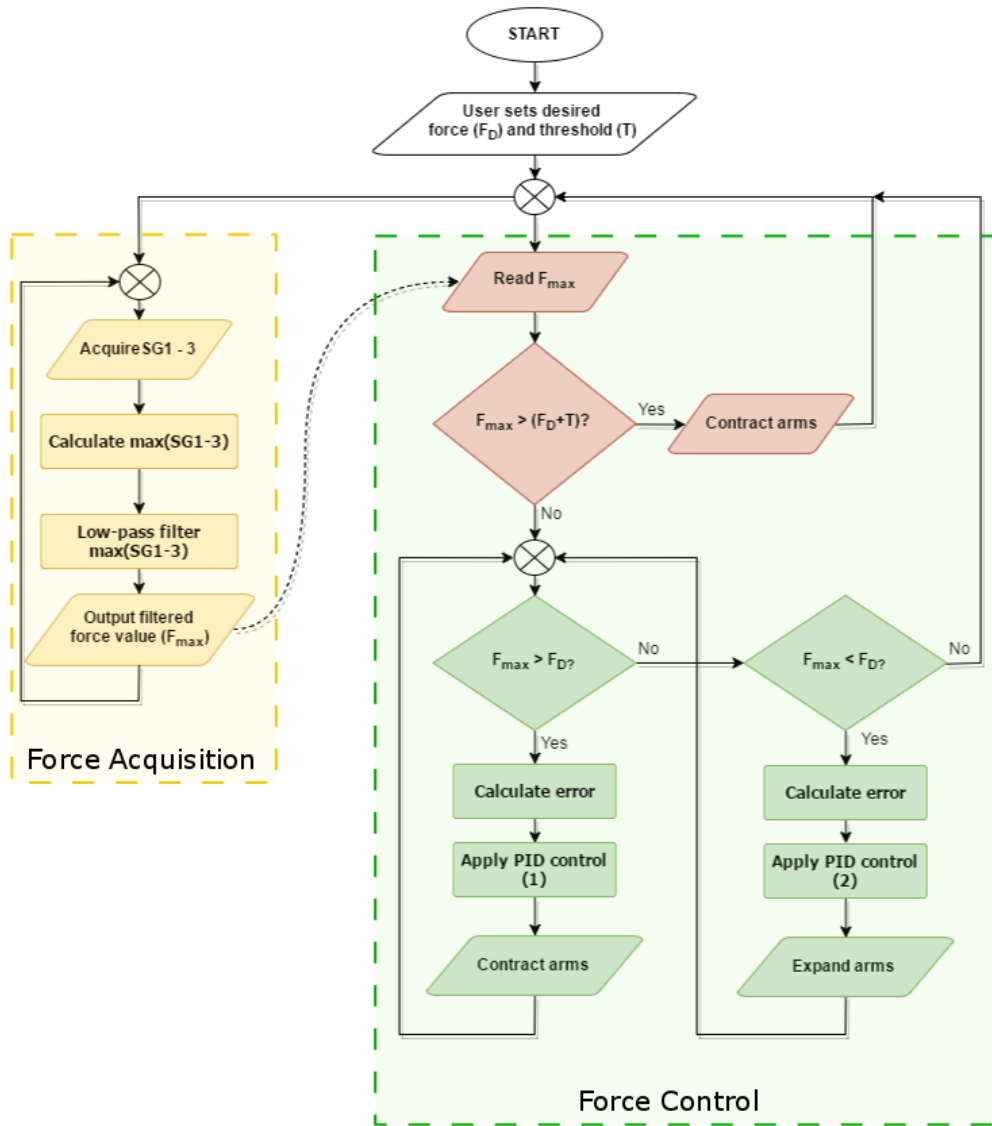


Figure 6.6 – A simplified overview of the closed-loop force control programs.

The individual forces were monitored continuously in a dedicated, high loop-rate (200 Hz) program and filtered using a low pass filter. The conditioned value was then sent to a separate program to adjust the force using conventional PID control. The first stage of this automated force control, and so having the highest priority, was to check whether a safety threshold had been exceeded. If so, the arms were immediately contracted before PID control was considered. If the force was within safe limits, the current F_{max} value was used to adjust the arm angle using two separate PID constants; one for contracting the arms and the other for expanding the arms.

Two sets of constants were required as the two tasks are likely to have different characteristics:

1. During expansion, the arms will be in contact with the lumen and so need to deform the material, adding extra damping and slowing the system down (increasing the output rise time).
2. During contraction, the arms are not obstructed and in fact may be assisted by the elastic force that is applied to the wheels by the stretched lumen. This could have the effect of reducing rise time.

To tune the PID controllers, the prototype was inserted into a straight silicone⁵⁹ tube, supported by a rigid frame (Figure 6.7). The arms were then expanded to make contact with the lumen and apply a small force of ca. 15 gf.

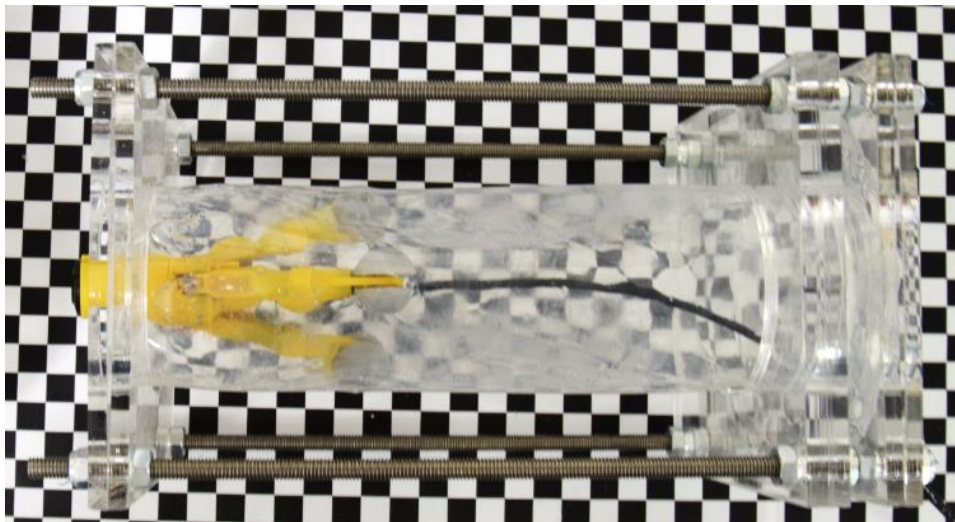


Figure 6.7 – The silicone tube and support frame used to secure RollerBall during closed-loop force control tests.

Very small PID constants were then applied to both controllers before a desired force was set and the automated force control engaged⁶⁰. The prototype and force output were observed while the PID constants were slowly increased. This began with increasing the Proportional (P) constant to achieve the required force and rise time without the system becoming unstable (oscillating uncontrollably). The Integral constant (I) was increased if there was a steady-state error and lastly, the Derivative constant (D) was slowly increased to reduce the overshoot.

⁵⁹ The same silicone was used as previous tests (Shore hardness of 40 A).

⁶⁰ The included safety threshold ensured that the prototype was not damaged during tuning.

To validate the automated control, the desired force was cycled through a number of different values (ca. 20 gf, 50 gf and 80 gf), alternating between high and low forces. The slow responsiveness of the system limited the value of P that could be used. Too high a value and the arms oscillated – ie. the force value changed much faster than the *Expansion mechanism* (arm velocity) could compensate for. This was seen to place the system into continuous oscillation (Figure 6.8).

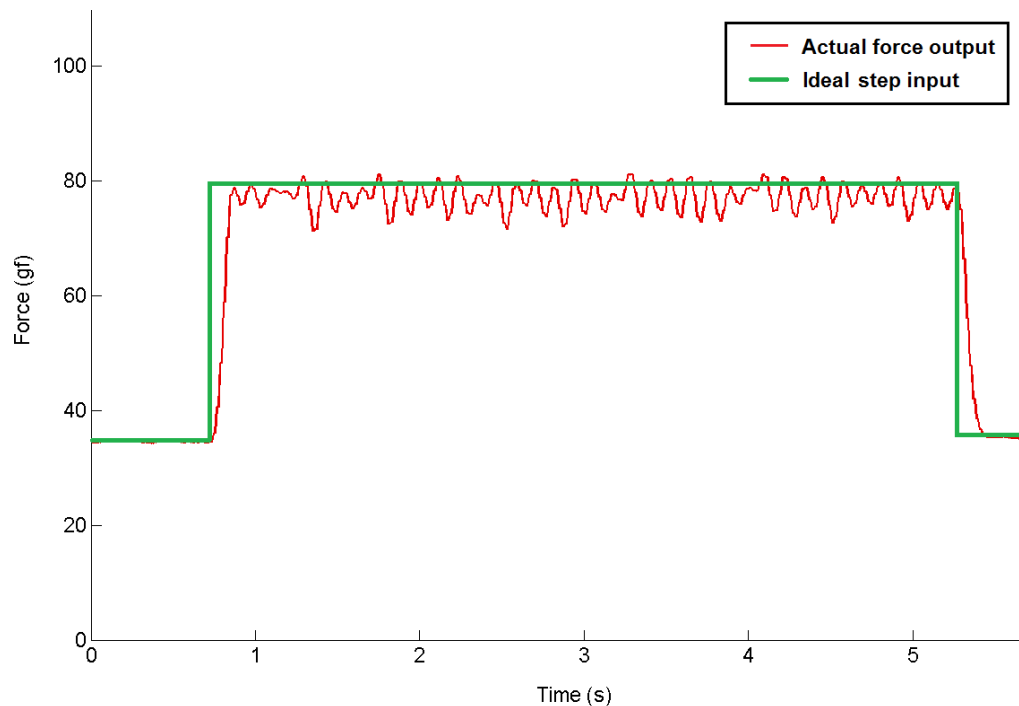


Figure 6.8 – A plot showing the undesirable continuous oscillation present when the Proportional (P) constant was too high.

The presence of backlash was expected to augment this issue and also restrict how much D could be used to reduce the settling time and overshoot. When the “slack” in the system is taken up by the *Expansion Mechanism* (or a disturbance), the force changes unrealistically fast in that instant. Since the D constant is proportional to the rate of change, the system can over compensate if D is too large. The I constant was also ineffective in this system; likely causes are the presence of backlash and the added error over time from the material creep - even an extremely small (ca. 0.0001, compared to the value of P used – ca. 0.15) value resulted in continuous oscillation. The result of these limitations was that a compromise had to be made on the performance: A lower than ideal P value was used to avoid oscillations, and because D could not be used to a large enough extent. I was not used.

The output, shown in Figure 6.9 was tuned to be slightly underdamped in order to reduce rise time and achieve maximum responsiveness.

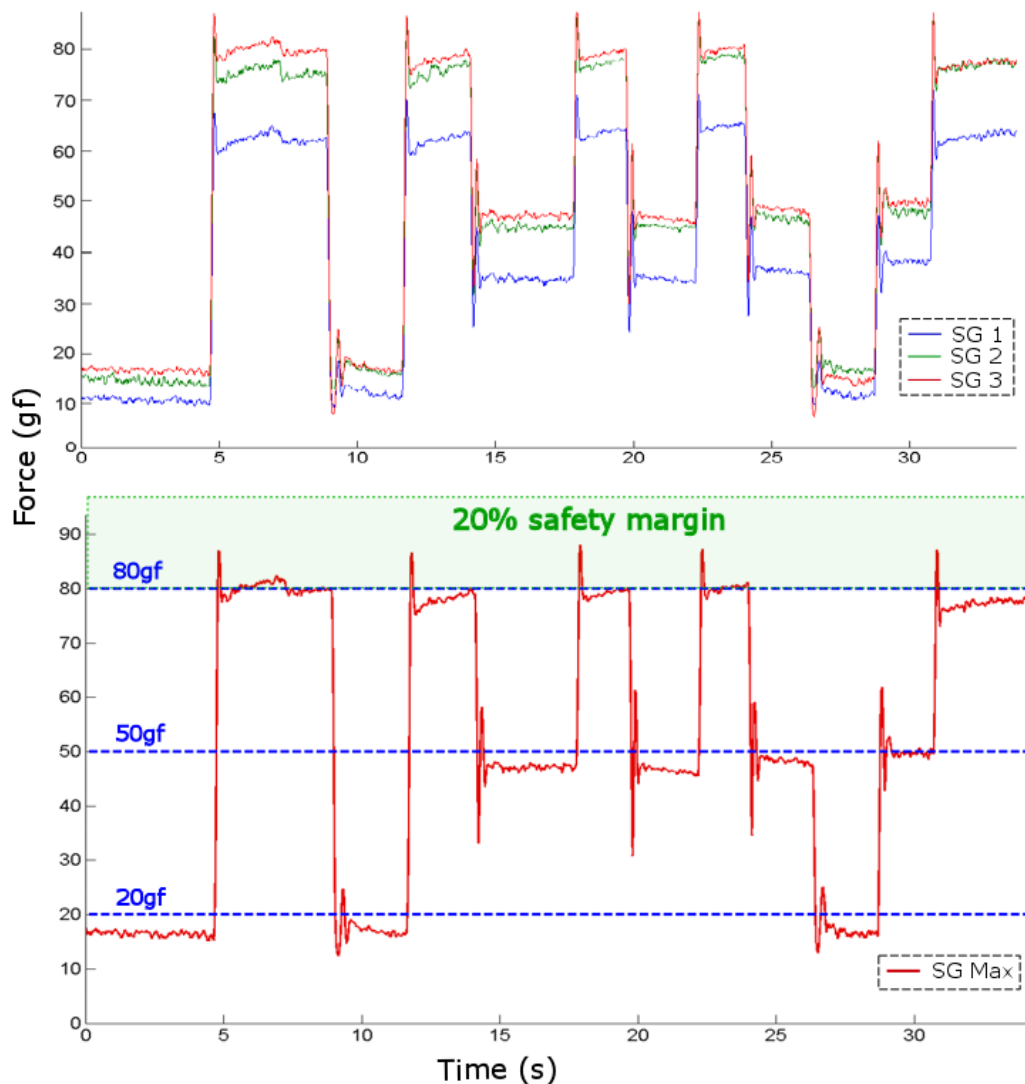


Figure 6.9 – Two plots showing the force response from a series of set point changes by the user.

The first plot shows the raw force output from all three arms. The second plot shows just the maximum force measured (as this is what the controller uses). The various user input levels are shown by the blue dotted lines. A 20% safety margin was considered acceptable.

A larger P value was used for the contraction constants, as safety (avoiding high forces) was prioritised over traction (expansion): the arms could be expanded at a rate of ca. 4.3 gf/ms and contracted at a rate of ca. 6 gf/ms. The first plot in Figure 6.9, showing the output from all three arms (strain gauges), highlights a further limitation of the *Expansion Mechanism*: the lack of individual arm control. The force on SG 1 is considerably lower than SG2 and 3 because of gravity (the mass of the robot is placed across SG2 and 3). This will likely remain

when there is a subsequent increase in the demand force as the controller uses only the max force (ie. SG 3 in this case).

There was some error in the magnitude of the force output, particularly at low loads. This was attributed to both the low P value (insufficient force to effectively make small arm angle adjustments) and the lack of I control. The significant overshoot and underdamped response was a result of the inability to effectively use D control. At higher loads, this overshoot was within the 20% safety margin and so was not considered an issue.

6.3. Orientation control

The orientation of RollerBall required continuous user input to control. This was necessary to counteract the offset CoM when stationary and to maintain the desired pose during movement (ideally a horizontal, forward facing orientation).

For example: as Global speed was increased, any slight difference in the wheel speeds (from the joystick Target coordinates) resulted in RollerBall moving at an angle. To avoid colliding with the lumen and to maintain the tip of the robot in the advantageous central location, the user had to advance in a series of small movements, alternating between advancing (by increasing the Global speed) and updating the orientation (by reducing the Global speed and adjusting the Target – joystick coordinates). This was seen in the open-loop tests and will be shown again in the tests in subsequent sections.

The “pulsating” (stop-start) movement highlighted the necessity of having advanced control with this concept.

6.3.1. Conceptual control strategy

Hypothetically, RollerBall could include both automated arm control (as shown in the previous section) and some form of automated orientation control. This orientation control could have the user interface illustrated in Figure 6.10 and the functionality shown in Figure 6.11.

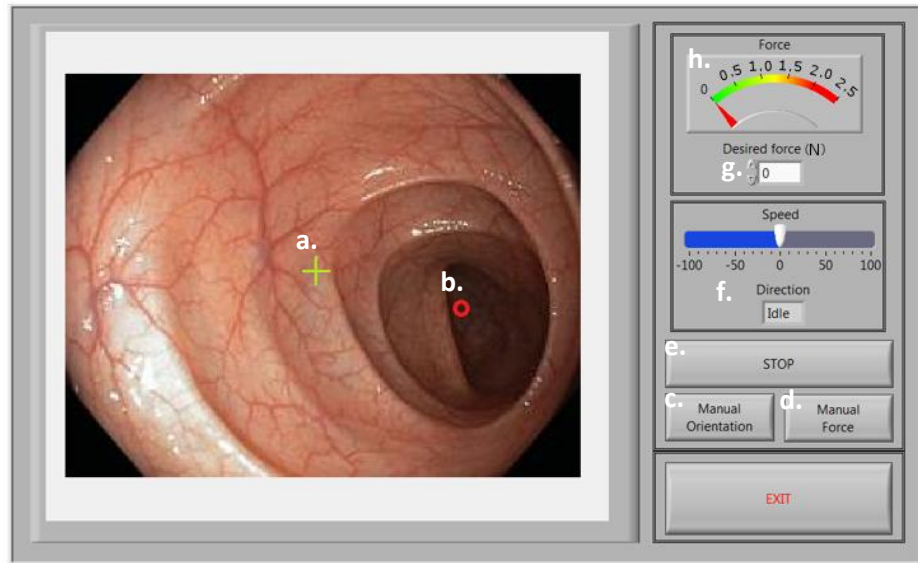


Figure 6.10 – The actual GUI, modified to represent the hypothetical functionality.

a. The centre of the robot view; b. The tracked Target (lumen centre); c. – e. Buttons are used to switch between manual and auto control; f. The user sets the speed and direction; g. The user also sets the desired force application and; h. A force gauge displays the force data.

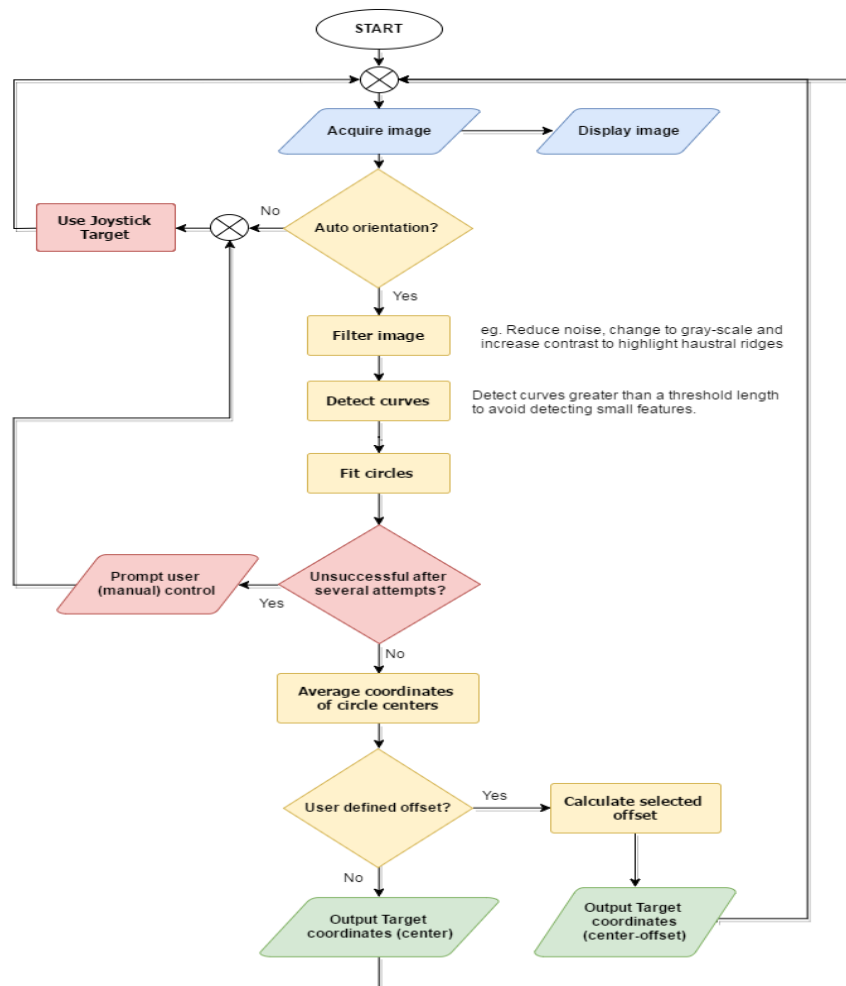


Figure 6.11 – A flowchart showing an overview of the hypothetical orientation control.

Referring to Figure 6.10 and 6.11: While in auto-pilot (“Manual Orientation” and “Manual Force” buttons deselected), the arms will expand to make contact with the lumen and apply a force set by the user (“Desired force”). This force will be displayed to the user on the force gauge. The images from the forward facing camera could then be processed to extract the distinct ellipses of the haustra. Mathematically finding the centre of these ellipses and then averaging them will give a point (Target) approximately in the centre of the lumen and towards the direction of the bend (Figure 6.10, b. and with steps summarised in Figure 6.12). This Target could be used to adjust the orientation in real-time. If the user would like to move the orientation to point the robot at a region of interest, then simply “clicking” the point on the image could send the pixel coordinates to the controller which then adds this offset to the Target found from the haustra (ie. using the lumen centre as a reference). This level of control would require the user to simply select the desired movement speed and direction. If the centre of the haustra cannot be found, the program would automatically turn on “Manual Orientation” and prompt the user to control the robot.

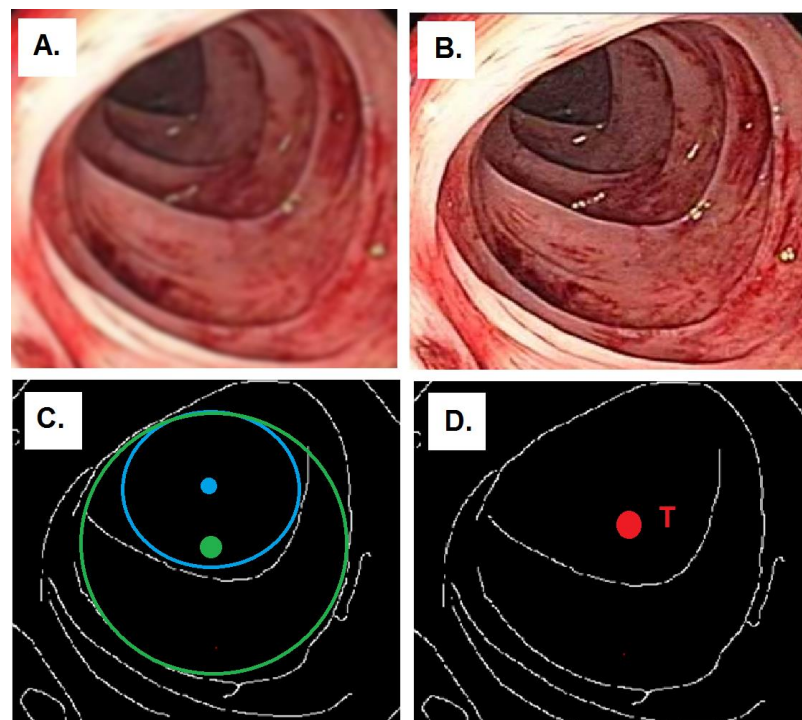


Figure 6.12 – An example of the image processing steps likely required.

A. The original image. B. Sharpened image with higher contrast. C. Use edge detection to detect haustral ridges. Use function to fit circles to large curves and find their centres. D. Average the circle centres to find the Target coordinates – approximately in the centre of the lumen.

This method of orientation control is unique in that it does not require additional sensors that would add further complexity and cost to the device. It is also independent of gravity; the 3D trajectory required to traverse the colon limits the use of on-board IMU's to control orientation. This software could feasibly be developed in LabVIEW as it has the necessary image processing functions required to carry out the steps shown in Figure 6.12. However, given the current low frame-rate of the camera (30 fps) and the limited processing power of the myRIO, it may not be possible to achieve effective closed-loop control as it requires high frequency operation. An intermediate, simplified alternative was explored to validate the feasibility of this control concept.

6.3.2. Preliminary development

Detecting the haustral ridges is likely to be the most demanding part of the control, requiring significant software development, a high frame rate camera and large processing power. To demonstrate the potential of the automated orientation control, the goal was modified to track a simple object (of defined colour and shape) and use this as the *Target* for the *Position and Orientation controller* (which was previously developed to use Joystick coordinates). The program used to track the image and acquire the Target coordinates is summarised in Figure 6.13.

Referring to Figure 6.13: After acquiring a single image, the program first checks whether a Target template⁶¹ exists. If it doesn't (on the first run of the program, for example) then it waits for the user to select the live camera feed on the User interface (UI). Selecting an object on the camera image will save a rectangular region of interest (ROI) around the mouse coordinates. The program then learns the specific pattern of pixels contained within it – the *Target template*. A new image is acquired before it and the *Target template* are input to a LabVIEW function called "IMAQ: Match Color Pattern." This function searches for the Target template within the given image. If a successful match is found, the coordinates of the match in the image are extracted and displayed as a dot on the UI. If no match is found, the user is notified and the coordinates "0, 0" are output to the *Position and Orientation control program* – ie. no differential speed is applied to the motors.

⁶¹ A saved image (Region of interest - ROI) containing the Target object, eg. a red circle.

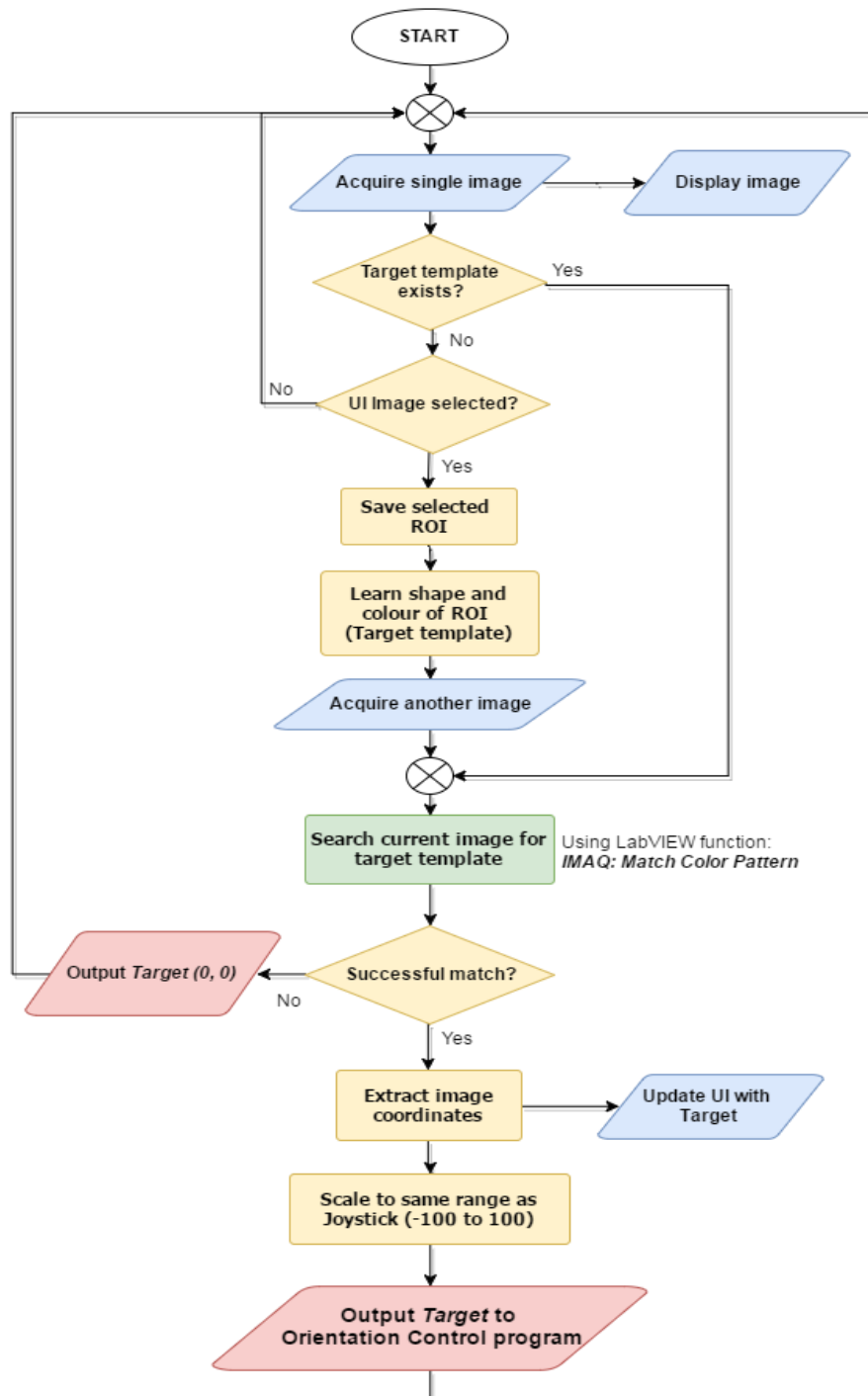


Figure 6.13 – An overview of the preliminary closed-loop orientation control program.

The successfully tracked coordinates are then converted to the same output range as the Joystick (Figure 6.14) so that they can be used in the pre-existing *Position and Orientation control program*.

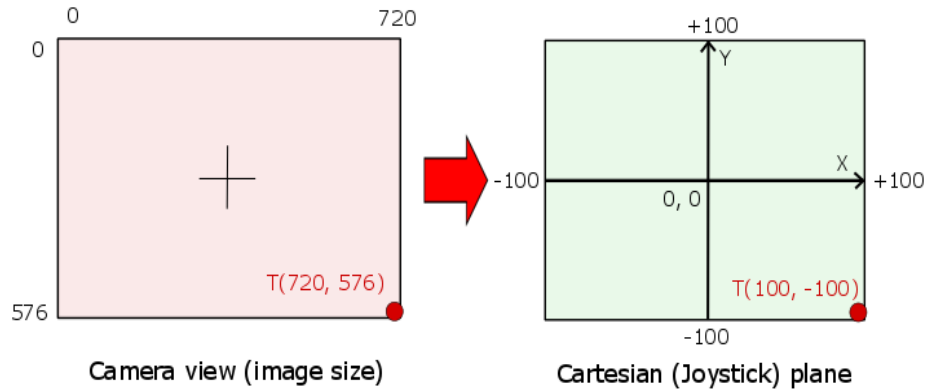


Figure 6.14 – A diagram showing the coordinate conversion.

The *Position and Orientation control program* was then modified to use the coordinates of the tracked object (Target) and closed-loop PID control to automate the orientation adjustment; this is summarised in Figure 6.15.

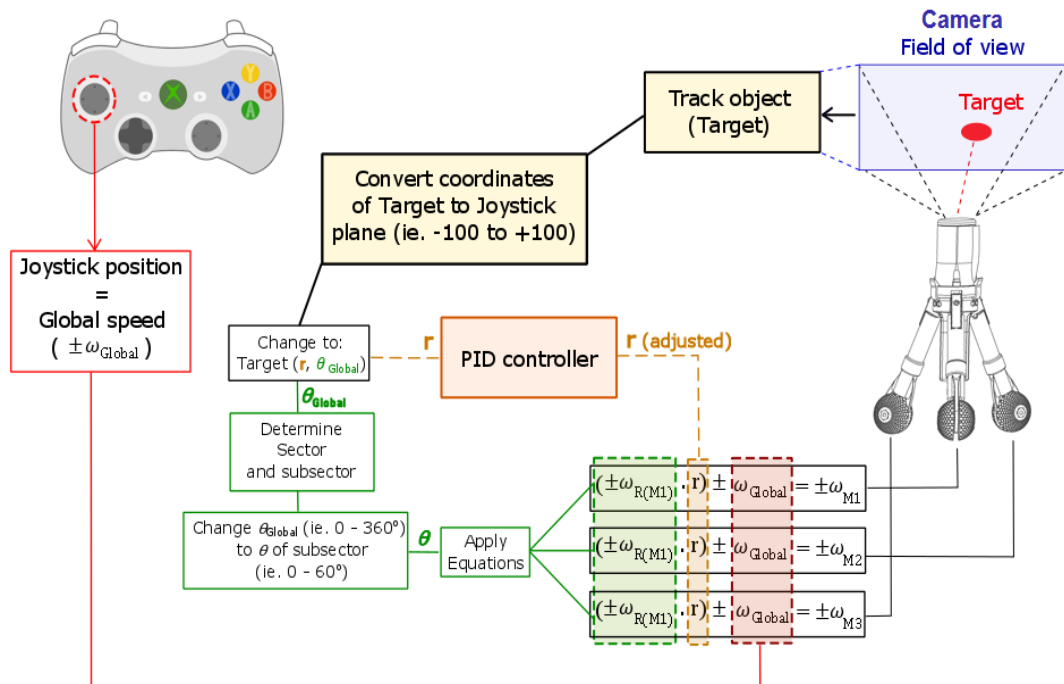


Figure 6.15 – A schematic showing an overview of the closed-loop orientation control strategy/program.

This program could successfully track a target and output the correct coordinates. One limitation, however, was the frame rate of the camera used (30 fps). PID control requires a high frequency process variable (Target) so that it can update the output to the plant (wheel motors) at a high rate. This ensures that there is sufficient time for the plant to adjust to the

new error (which, in this case, is the distance from the Target to the centre of the robot). Currently, the image updates, a target is found and then sent to the *Position and Orientation control program* which calculates the new motor speeds. The robot moves in a set direction and at a potentially high speed. During this movement the image and image tracking could remain unchanged and hence, by the time a new Target has been acquired, the robot may have overshoot. The PID controller will detect an extremely fast rate of change in the error as this new Target is found and could compensate however, a higher loop rate is required.

6.3.2.1. Tuning the closed-loop Orientation Control

As with the Expansion control, this system was tuned manually. Before this however, a solution had to be found to the issue of the slow image frame rate and latency due to image processing. The PID controller ideally needs to operate at a high frequency, thus requiring a high frequency process variable (error input). To achieve this, the image acquisition, image processing and automated (PID) Orientation control were separated and run in parallel, with the communication flow shown in Figure 6.16

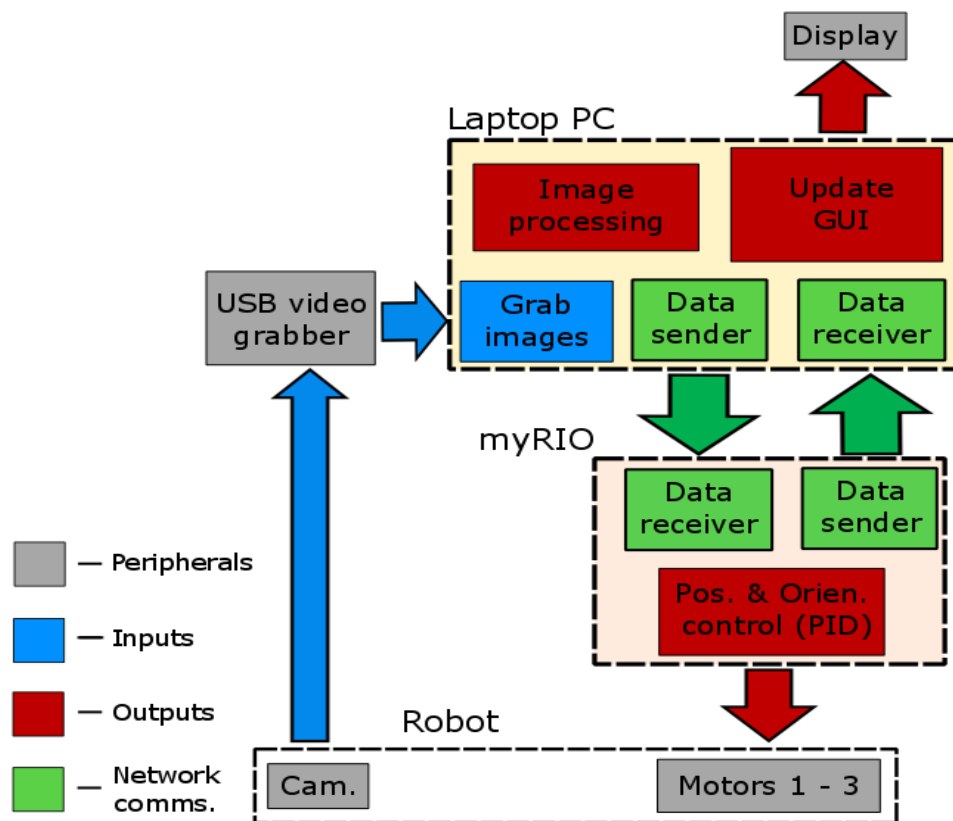


Figure 6.16 – An overview of the system architecture, showing just the items associated with Orientation control.

Image processing is carried out on the Laptop for high processing power. Position and Orientation control (calculating the wheel speeds) is carried out on the myRIO for consistent performance.

The *Image processing* required significant processing power and so was carried out on the Laptop. The acquired images and tracked target were updated on the GUI. The Target was then sent to the myRIO where the PID control took place. The myRIO was used for a consistent, highly robust loop rate. To accommodate for the difference in loop rates between the image grabber (ca. 30 Hz or 30 fps) and the PID controller (ca. 200 Hz) - and to smooth the Target coordinates - the Target was put through a moving average filter at the higher rate.

A moving average introduces lag in the output data equal to half of the sample width (span) - this is usually unwanted. In this case, the lag is desirable as it has the effect of delaying rapid changes in the tracked Target. Because of the slight imperfections in the Image processing and the slow camera frame rate compared to the robot movement speed, the Target coordinates could change significantly, regardless of sampling rate; this means filtering based on frequency will not be as effective. Control issues result when a new Target is acquired that has a large error (distance from the centre of the robot to the Target) as the PID controller output would be large and the movement speed great (thus likely to overshoot). Therefore, the error was used as the moving average span and hence, when a new Target is found far from the current robot position, the moving average span is large and the output value slowly increases to the actual value. As the robot moves towards the Target, the error reduces and so does the moving average span. This increases the responsiveness for the final small adjustments necessary. So, despite the low Target refresh rate and potentially high variance, this provides a smoothed, high frequency output for the controller.

To tune and evaluate the image tracking and automated orientation control, a separate test rig was developed. This had two components: the first was a short, straight section of tube to house the robot. The second component was a target with objects for the software (and robot) to track. The objects needed to move in a repeatable way to allow for multiple iterations to be carried-out and compared. A straight section of silicone tube was secured in a rigid frame, with two supports at either end to hold the lumen open. Opposite this was placed a round target with multiple LEDs arranged in a circle around the centre. These LEDs were controlled using the *myRIO* and permitted a repeatable sequence to be executed. The setup is shown in Figure 6.17

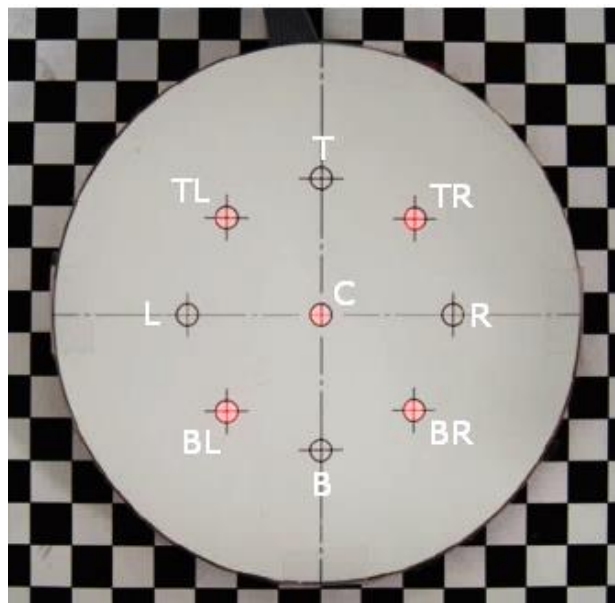
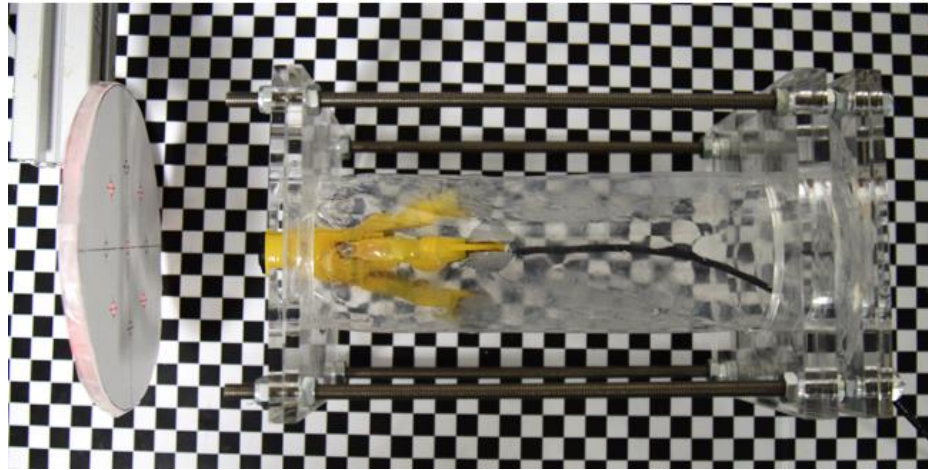


Figure 6.17 – An overview of the system architecture, showing just the items associated with Orientation control.

The LEDs in the array are named: top (T), top right (TR) etc.

To automate the LED sequence, a program was written to control the LED array based on the location of the current Target (tracked image). This had the functionality described in Figure 6.18.

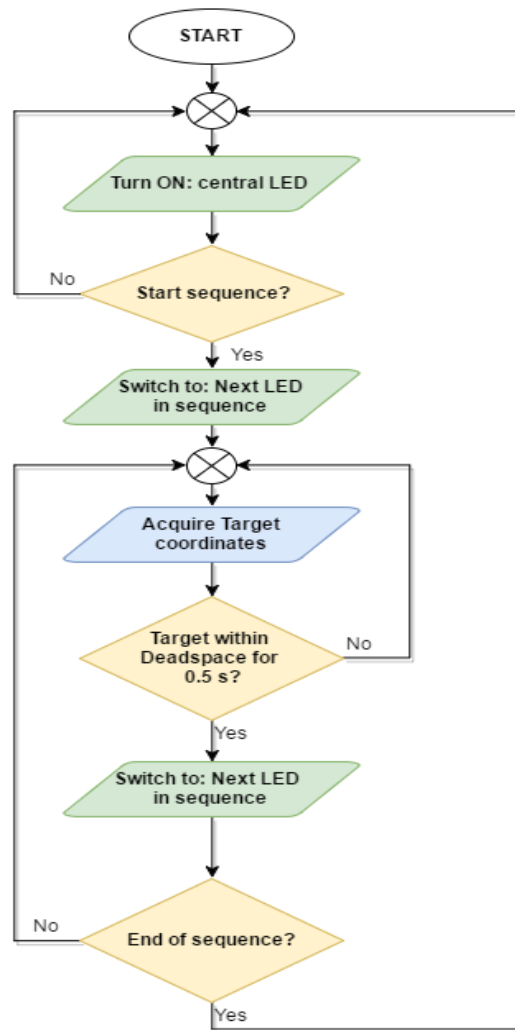


Figure 6.18 – An overview of the control program used for the LED array.

Starting from the central LED, the orientation is adjusted to align the robot (centre of the camera view) with the current illuminated LED. The image tracking returns the Target (tracked LED) and if it is within the dead-space (ie. approximately in the centre of the camera image \pm several pixels) for 0.5 seconds, the program considers the Target successfully reached and it turns on the next LED in the sequence.

Individual LEDs were switched on and the PID constants adjusted manually until the system was stable and had satisfactory performance; stability (low overshoot / overdamped) was desirable. The control was then validated by completing the following sequence autonomously for three repetitions: C – TL – C – TR – C – BL – C – BR – C (ie. an “X” shape). The automated orientation control was shown to successfully adjust RollerBall’s orientation to point at each LED in the sequence, in all three repetitions. The results from one repetition are shown in Figure 6.19:

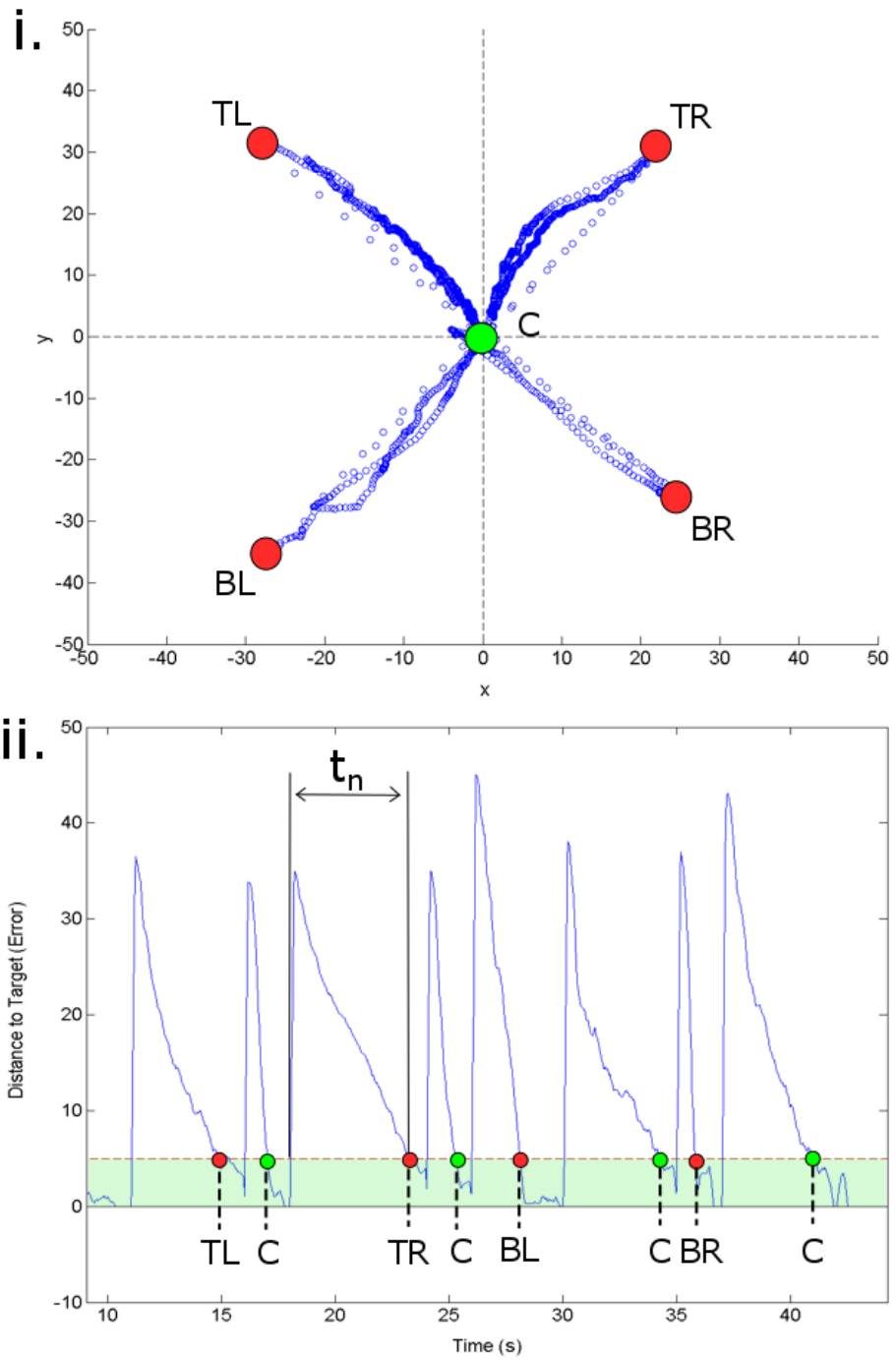


Figure 6.19 – The results from one repetition of tuning the automated orientation control.

i. is an x-y plot showing the tracked coordinates of the Target (the Targets are annotated) – a close grouping of coordinates (darker trace) indicates a slower movement. ii. is a plot showing how the error (distance from Target) changes over time. There is a rapid increase as the tracking detects the new LED and then a decrease as the robot moves toward it. When the Target is within a dead-space of 5 (green region on the Error plot) for more than 0.5 s, a new LED/Target is turned on. t_n is therefore the time taken to move to a Target.

Referring to Figure 6.19: The first plot (i.) shows the coordinates of the tracked Target (LED). Starting from C, a new Target appears (eg. TL at coordinates (-30, 30)) and the robot slowly moves towards it. As the robot moves, the tracked Target coordinates approach the centre of the camera view (ie. 0, 0)⁶². This movement direction is shown in the second (ii.) plot: when LED TL is switched on there is a spike in the error (ie. the image tracking detects the target far from the robot centre). The robot then starts to move towards the Target and so the error (distance between it and the robot centre) decreases. When the Target reaches the centre of the camera view (an error of less than 5) and remains there for 0.5 s, a different LED (Target) is switched on and the process repeats.

All Targets (eight orientation adjustments in total) were reached in an average total time of 22.8 ± 0.5 seconds ($n=3$), found by summing the individual times to each Target (eg. “ t_n ” in Figure 6.19, ii.). The variance in the time taken to reach each Target indicates that there is an imbalance in the motor speeds and the robot moves faster in some directions than others. This is also shown by the dense array of Target coordinates leading from LEDs TL and TR – the robot moved comparatively slower than the Target was acquired.

6.4. Closed-loop system evaluation

The experiments on the open-loop (manual control) RollerBall system in Chapter 5 showed the efficacy of the locomotion technique but highlighted the great need for automation. This section evaluates the more advanced, closed-loop RollerBall system, which includes: a forward facing camera view, automated expansion (force) control and automated orientation control. This work was carried out in three stages:

- 1) To evaluate the need for automation, the robot was manually controlled through silicone tubes in both forward and reverse⁶³ directions. The maximum force and user input speed (*Global speed*) were recorded. The forward facing camera was also included; this was done to assess whether giving the user a fixed point of view (reference) would help with orientation adjustment.
- 2) Tests were then carried out with fully automated *Expansion control*. This was expected to improve usability and locomotion efficacy (especially speed) by allowing the user to give more attention to the position and orientation control. It should also ensure traction is always maintained and normal force does not

⁶² The plot shows the movement of the Target relative to the fixed reference of the centre of the camera image, not the robot relative to the Target

⁶³ This was not assessed previously.

exceed unsafe limits (where trauma to the lumen or damage to the robot could occur⁶⁴). A third test environment was introduced; one that has multiple rings down its length to simulate the haustral bands.

- 3) The final tests evaluated the automated orientation control. A purpose built test rig was used to assess how the automated orientation control compares to manual orientation control. This was done to assess the feasibility of incorporating lumen tracking in future developments. If this could be done then the user would need to only input the desired speed, direction and force and the robot is controlled autonomously.

6.4.1. Test environments

Four synthetic colon environments were used in this experimental work. The two previously developed (one straight with a varying diameter and the other fixed diameter but with multiple corners) were included. The open-loop tests revealed the issue of having a lumen with too high friction: the robot body easily catches on the tube and hinders progress. Talc powder was used as it provided some friction reduction but maintained enough for the robot to be able to maintain a central orientation (ie. counteract the offset CoM). The thin layer slightly obscured the view of the robot however, it was still visible and encouraged the use of the forward facing camera for orientation feedback.

A third tube was developed to more thoroughly assess the Expansion control. The biological colon has global changes in lumen diameter as well as local changes (such as haustra) – the arms must adapt to both. A straight, varying diameter tube was fitted with thick silicone bands on the outer surface. This maintained a smooth lumen internally, while presenting RollerBall with local regions of higher stiffness (simulating ridges). These three tubes were individually hung from an aluminium frame by thin nylon line and all are shown in Figure 6.20.

⁶⁴ Even if tissue damage does not occur, excessive normal force on the arms was seen to stall the wheel motors in the manual control tests and should be avoided.

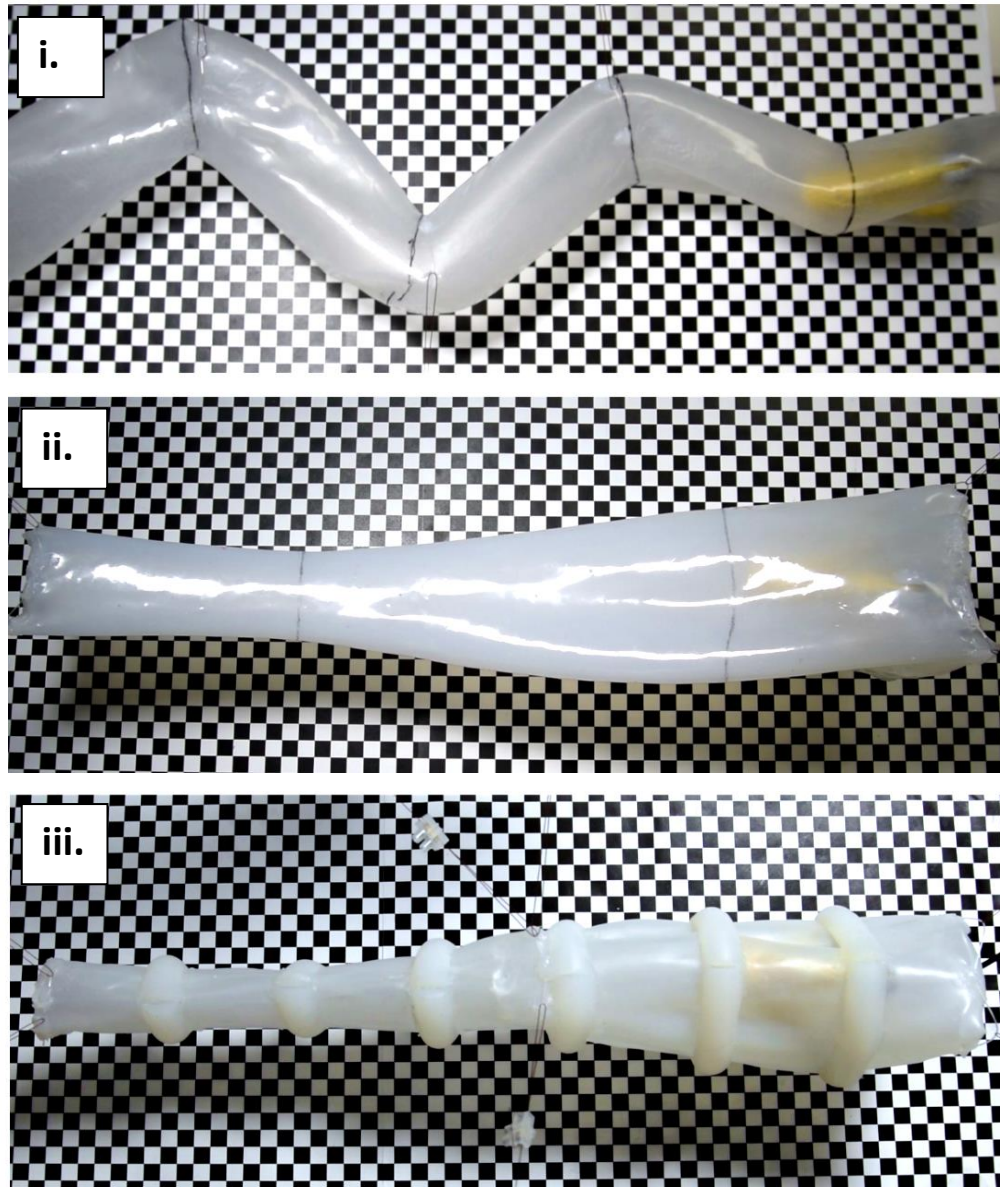


Figure 6.20 – Three of the silicone tubes used to test the closed-loop control of RollerBall.

The talc slightly obscures the view of the robot. i. The tube with multiple corners (each marked with a black line). ii. The tube with changing diameter. iii. The tube with changing diameter and local regions of high stiffness (creating obstacles – local regions of changing diameter).

The test rig described in Section 6.3.2.1. (Figure 6.17) was used for the orientation control tests.

6.4.2. Method

Although Manual control tests have been carried out, each of these subsequent group of tests have a manual control included for comparison. This will also factor-in the user's increase in ability from practice over time.

6.4.2.1. Force sensing and camera feedback

The robot was first placed into one end of the tube (either Figure 6.20 i. or ii.) and the force sensors reset. The arms were then expanded to make contact with the lumen and apply a force just below the user defined safe limit⁶⁵. The user then attempted to traverse the length of the tube before reversing back to the start. The main source of feedback was the camera view and the maximum force reading; both displayed on the GUI (Laptop). The goal was to traverse the tubes as fast as possible whilst maintaining control of orientation (ie. moving in a controlled manner) and avoiding excessive deformation of the lumen (ie. excessive force). The maximum force, *Global speed* input and camera feeds (from the robot and an external camera view of the entire tube) were recorded. This method was completed for the following repetitions:

- One practice and then five repetitions in the changing diameter tube at a force limit of 150 gf.
- One practice run and then five repetitions in the tube with multiple corners at a force limit of 100 gf.

These test results were used to more accurately describe the level of user input required and the need for automation. They were also used to assess the locomotion efficacy when reversing and when using the forward facing camera view as orientation feedback.

6.4.2.2. Automated force control

These tests were carried out in tubes i. – iii. (Figure 6.20) with the automated expansion control activated (repetitions under full manual control were also included for comparison). Tests under full manual control were done first: The robot was placed into the tube and the force sensors reset before expanding the arms to contact the lumen with approximately 100 gf of force. A large force limit of 200 gf was set to give the user more control over the force (ie. avoiding the automated force limit overriding the control). The user then attempted to traverse the length of the tube before reversing back to the start. As the goal was to assess

⁶⁵ Different force limits were used to assess the importance of arm force on mobility.

force control, during these tests, more emphasis was placed on maintaining a central orientation and fixed force of 100 gf than *Global speed*. The maximum force and camera feeds (from the robot and an external camera view of the entire tube) were recorded. This was completed for three repetitions in all three tubes shown in Figure 6.20 (with an additional practice run included when transitioning to a new tube).

The tests were then repeated but this time, automated expansion control was engaged and a desired force was set⁶⁶. Again, the tubes were traversed before reversing back to the start, with emphasis being placed on maintaining a central orientation and controlled movements during locomotion. The maximum force and camera feeds (from the robot and an external camera view of the entire tube) were recorded, and three repetitions per tube completed.

These tests were carried out to assess the efficacy of the automated expansion control; whether it could adjust the arm angle continuously to maintain a desired force range. The effect this had on locomotion efficacy and usability was also considered.

6.4.2.3. Automated orientation control

The final tests had two stages, both carried out with automated orientation control (and manual control included for comparison).

Stage one: RollerBall was placed into the straight tube opposite the LED array in the configuration shown previously in Figure 6.17, Section 6.3.2.1. The automated expansion control was then activated to secure the robot in a central orientation – ie. centre of camera view aligned with the central LED. The LED sequence program was then run; this displayed a new object to which the user attempted to move the robot tip towards manually. Aligning the centre of the camera image with the illuminated LED for more than 0.5 seconds activated the next target. A different sequence to the one used for tuning was completed as fast and smoothly as possible: C – T – C – L – C – B – C – R – C.

A total of five repetitions were carried out before switching to automated orientation control and the process repeated. The forward facing camera images were recorded, as well as both the user input target (joystick coordinates) and tracked image target coordinates. These tests were used to assess the efficacy of the automated orientation control in terms of its ability to track a target and use the coordinates to adjust the orientation of RollerBall.

⁶⁶ This was chosen to just give enough traction to traverse the tube and was determined during the practice run

Stage two: RollerBall was placed into the straight, narrowing diameter tube (Figure 6.20) and a fixed target placed at one end. The user then attempted to traverse the length of the tube while maintaining the target in the centre of the camera view (automated expansion control was activated). This was done for five repetitions before being repeated with automated orientation control activated. In this case, the user just had control of the *Global speed*. Again, the forward facing camera images were recorded, as well as both the user input target (joystick coordinates) and tracked image target coordinates. These tests were used to gain a better understanding of the feasibility of full autonomous control and allow final conclusions to be made on the overall RollerBall concept.

6.4.3. Results and discussion

6.4.3.1. Force sensing and camera feedback

A sequence of images from one repetition in both tubes and a screenshot showing the GUI (user feedback) are shown in Figure 6.21 and Figure 6.22 respectively.

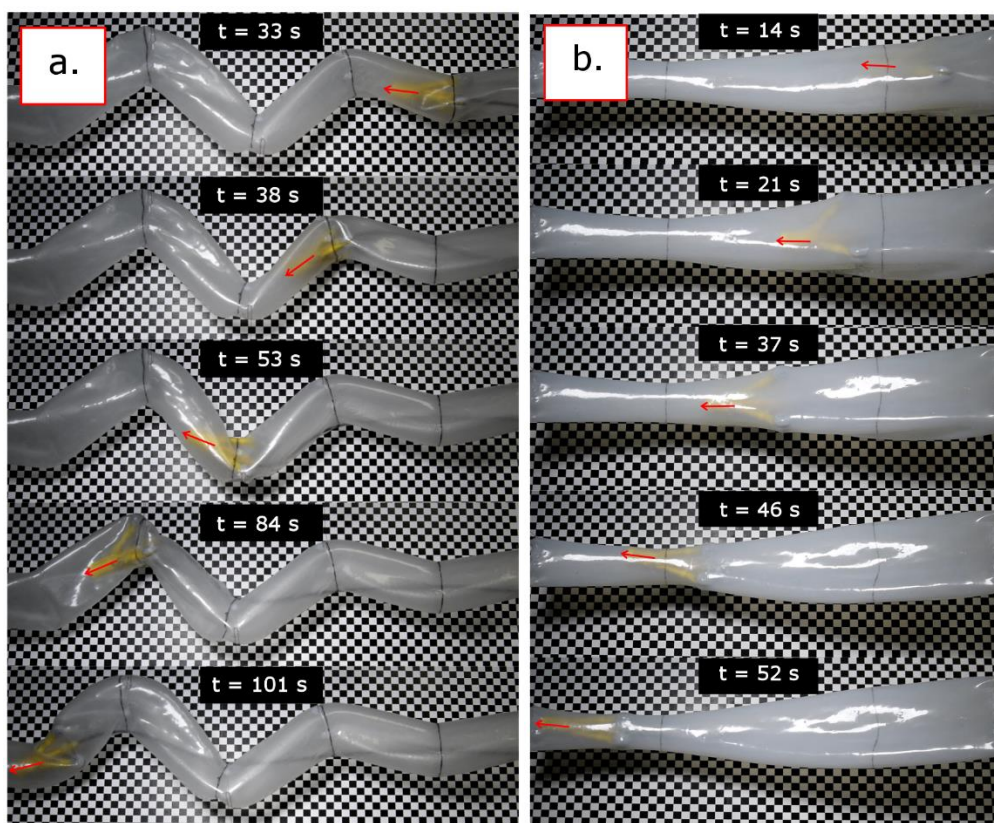


Figure 6.21 – A sequence of images from the manual tests which included camera feedback.

a. Shows one repetition from the tube with multiple corners and b. shows one repetition from the tube with changing diameter.



Figure 6.22 – A screenshot of the GUI during one test.

The coordinates of the joystick are displayed to the user (T_{joystick}). a. Shows how the force is displayed to the user. “Manual override” (b.) is selected, indicating to the user that they must control arm force and orientation.

The GUI slightly improved the usability by providing a fixed reference for the orientation control. However, a view of the entire robot was still necessary to navigate around acute bends. The camera was positioned ca. 80 mm from the wheels and so judging when to start turning into the corner was difficult; this further highlighted the disadvantage of having a long device.

RollerBall successfully traversed the length of both tubes in all repetitions. The results are shown in Table 6.5:

Table 6.5 – The main results from the Manual tests with camera feedback.

Tube	Success rate (n = 5)	Average forward speed (n=5)	Average backward speed (n = 5)
<i>Multiple corner</i>	100%	7.2 ± 0.9 mm/s	15.4 ± 2.3 mm/s
<i>Changing diameter</i>	100%	7.7 ± 0.6 mm/s	13.4 ± 2.5 mm/s

The inclusion of the forward facing camera and slight reduction in lumen friction appeared to improve the locomotion efficacy and controllability, with average speeds and success rates higher than in the first manual control tests. Interestingly, the backward locomotion

speed was significantly higher than the forward (particularly in the tube with multiple bends). This was noted for two reasons:

1. Less emphasis was placed on maintaining a central orientation during backward locomotion.
2. But more significantly, while reversing, the wheels approach the corners first and pull the rest of the robot body around the corner – this means that the long body does not have to be carefully navigated/lined-up before traversing a bend.

The maximum force and user speed input (*Global speed*) from a single repetition in the tube with changing diameter are shown in Figure 6.23.

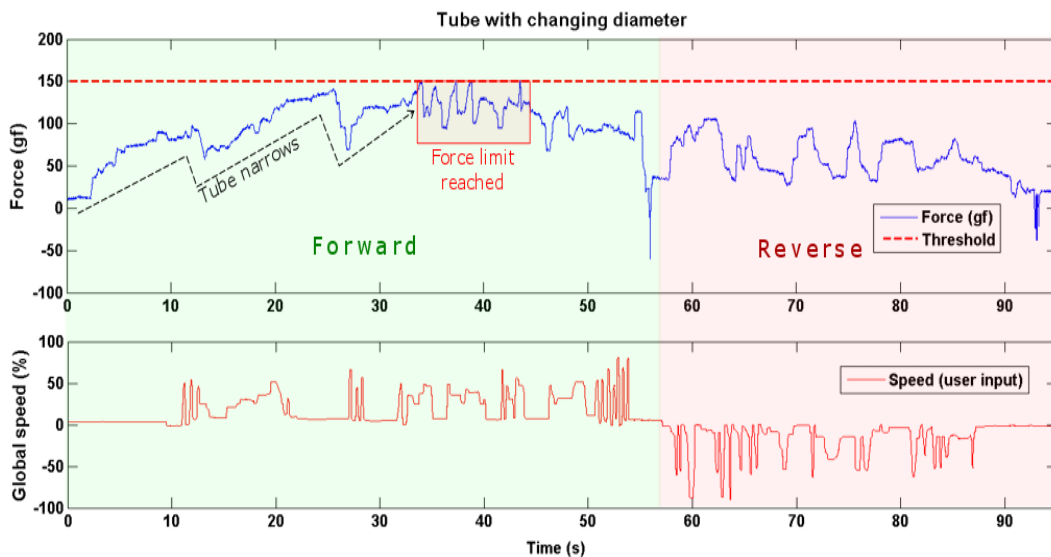


Figure 6.23 – Plots showing the maximum arm force and Global speed (user input) from one repetition in the tube with changing diameter.

The green region is when the robot is moving forwards and the red, when the robot is in reverse. The software force limit of 150 gf is shown by the red dotted line.

As expansion force was not closely monitored, during the first 35 seconds of the forward movement of RollerBall, the maximum force is shown to increase steadily, with occasional reductions where the user noted excessive deformation and contracted the arms. The force limit was reached and the automated safety mechanism engaged; the force plot shows successive increasing and decreasing force showing the switching between the user demand to expand and the software overriding due to the force limit. This was in the continually narrowing section of the tube, where the user could not effectively adjust the *Global speed*, orientation and arm angle simultaneously. The *Global speed* trace highlights the significant user input required and the characteristic pulsating movement as the user switches from

adjusting the orientation (or arm angle) to advancing forwards (increasing the *Global speed*). There were some occasions where the user was able to advance with a consistent positive *Global speed*, showing that smooth locomotion was feasible on some occasions.

The force and *Global speed* plots in the tube with multiple corners (Figure 6.24) further highlight the significant user input required to control RollerBall.

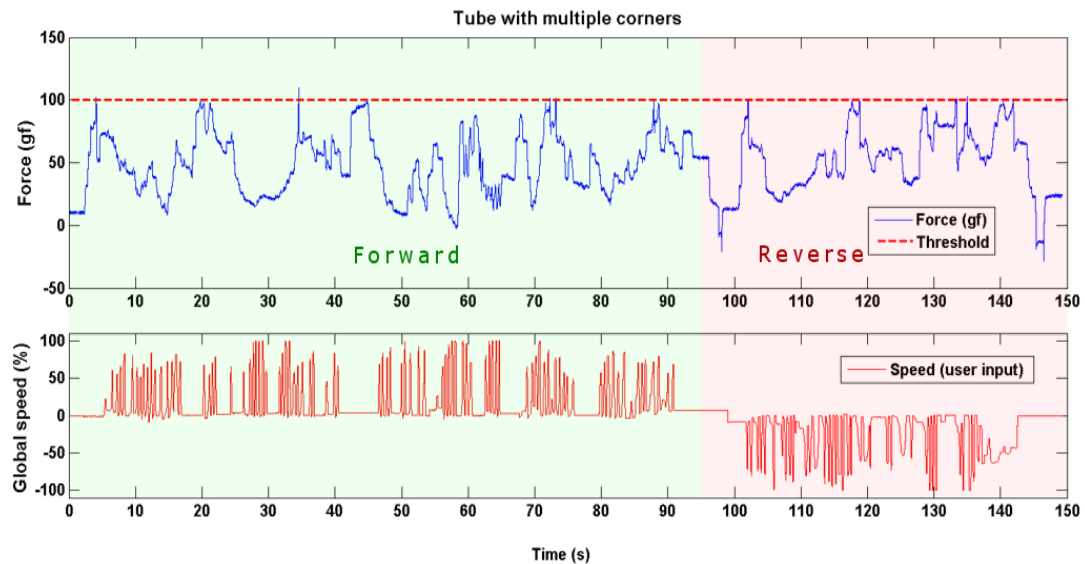


Figure 6.24 – Plots showing the maximum arm force and Global speed (user input) from one repetition in the tube with multiple corners.

The green region is when the robot is moving forwards and the red, when the robot is in reverse. The software force limit of 100 gf is shown by the red dotted line.

The force reached the maximum safe limit on multiple occasions. The force was also seen to reduce to approximately zero as the user contracted the arms to assist with traversing a bend, thus the force trace has a very “jagged” appearance. This alternating between the force limit and zero force is largely due to the lack of individual arm control, which has been mentioned and will be further described in the next section. The *Global speed* trace emphasised the characteristic pulsating locomotion and this time, there were even fewer occasions when consistent (smooth) locomotion was achieved.

6.4.3.2. Automated force control

Despite the limitations seen when developing the automated force control (such as not being able to fully utilise Integral and Derivative components of the PID controller), automating the arm angle (force control) was shown to be achievable with the current prototype and control strategy used. A desired force range was maintained for the majority of the test durations, while traversing three different geometry tubes. Figure 6.25 shows the

maximum force and *Global speed* under both manual and automated expansion control from one repetition in the changing diameter tube.

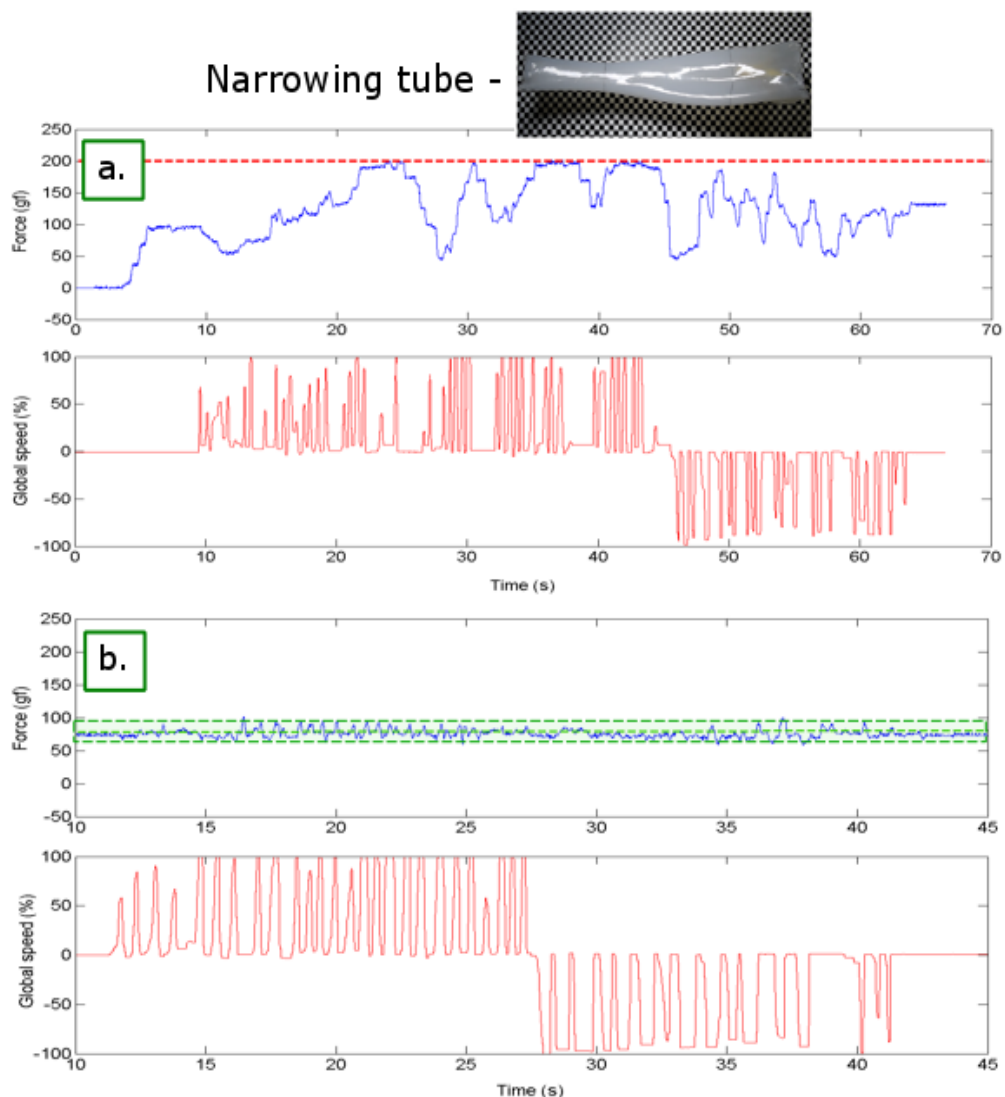


Figure 6.25 – Plots showing the maximum arm force and Global speed (user input) from one repetition in the tube with changing diameter – under both manual and auto force control.

a. Shows the results from the manual test. The software force limit of 200 gf is shown by the red dotted line. b. shows the results from the automated force control test. The green region is a 20 % desired range.

As with previous tests, these results show the significant user input required and the resulting poor control over arm force during manual control. The *Global speed* is made up of many narrow (short duration) peaks, highlighting the necessity to make short, pulsating movements (Figure 6.25, a.). In comparison, the automated expansion control has a much more consistent force output and is kept within the 20% desired range (Figure 6.25, b.). The lack of user input required to control the arms meant that more attention could be given to

position and orientation control. This is seen by the slightly wider (longer duration) *Global speed* peaks, indicating that prolonged (smooth) forward movement was achieved.

The maximum force exceeded the safety margin in the tests in the narrowing tube with multiple, localised ridges (star-shaped annotations in Figure 6.26, b.). This shows the challenge of continuously adjusting arm force with both global and local changes in diameter, as the force can rapidly increase with a small net movement of the robot.

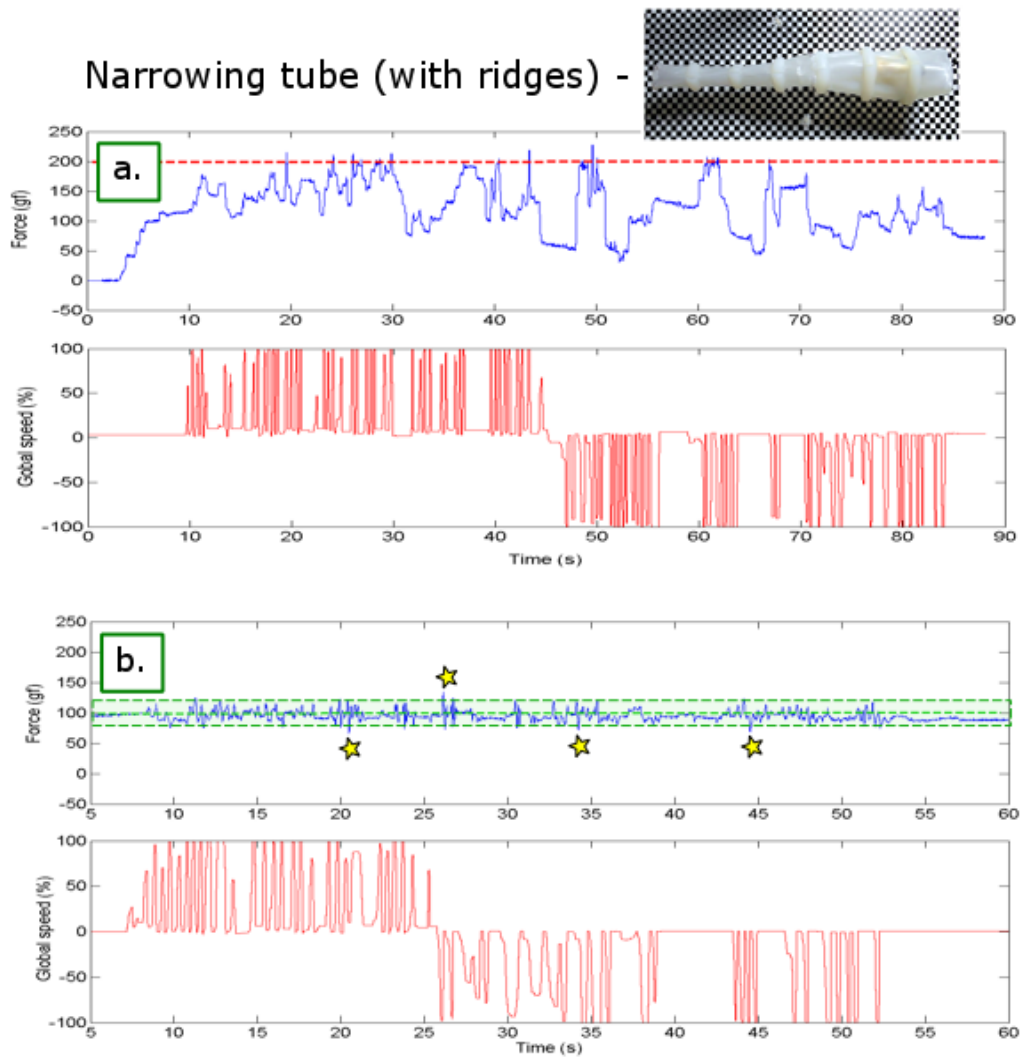


Figure 6.26 – Plots showing the maximum arm force and Global speed (user input) from one repetition in the tube with changing (global and local) diameter – under both manual and auto force control.

- a. Shows the results from the manual test. The software force limit of 200 gf is shown by the red dotted line. b. shows the results from the automated force control test. The green region shows the 20 % desired range and star-shaped annotations indicate when the maximum force exceeded this range.

Figure 6.27 shows the results from one repetition in the tube with multiple corners.

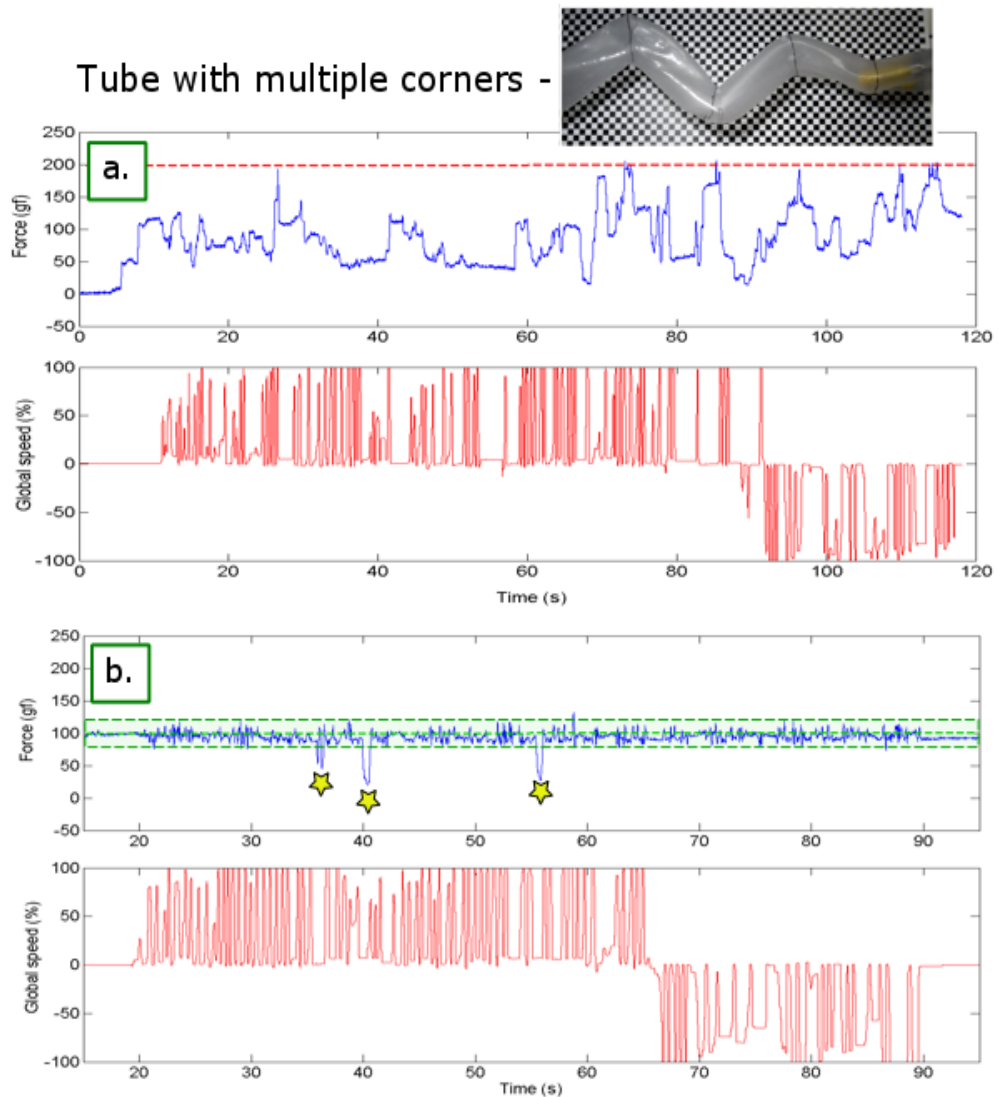


Figure 6.27 – Plots showing the maximum arm force and Global speed (user input) from one repetition in the tube with multiple corners – under both manual and auto force control.

a. Shows the results from the manual test. The software force limit of 200 gf is shown by the red dotted line. b. shows the results from the automated force control test. The green region shows the 20 % desired range and star-shaped annotations indicate when the maximum force exceeded this range (this time from the user manually contracting the arms).

The force was kept within 20 % of the desired value for the majority of the tests. Again, the noisy appearance of the force traces, and the fact that the force exceeds the desired range in some cases, shows that the expansion controller cannot respond fast enough to maintain a desired force while moving. The arms had to be manually contracted on several occasions in this tube (marked with star-shaped annotations in Figure 6.27, b.); this was done to free the device when it got stuck at a corner and is shown by the sudden drop in force.

Although not immediately noticeable on the previous Figures 6.25 – 6.27, generally, usability was markedly enhanced by automating the expansion control as the user had one less task to control and traction was more consistently maintained. However, the pulsating locomotion characteristic remains with or without automated expansion control showing that the simultaneous control of orientation and position is the most demanding aspect of control.

The reduced demand on the user meant that the average speed was increased in both movement directions; Table 6.6 summarises these results.

Table 6.6 – The results from the Manual and Auto force control tests.

	Tube	Success rate (n = 5)	Average forward speed (n=5)	Average backward speed (n = 5)
Manual expansion control	Changing diameter	100%	11.9 ± 1.4 mm/s	16.8 ± 2.1 mm/s
	Changing diameter + ridges	100%	11.1 ± 0.7 mm/s	11.1 ± 2.0 mm/s
	Multiple corners	100%	11.4 ± 3.3 mm/s	25.9 ± 0.5 mm/s
Automated expansion control	Changing diameter	100%	24.6 ± 1.6 mm/s	29.6 ± 4.5 mm/s
	Changing diameter + ridges	100%	20.0 ± 2.4 mm/s	15.9 ± 3.6 mm/s
	Multiple corners	100%	15.9 ± 0.6 mm/s	30.5 ± 0.6 mm/s

Again, locomotion in reverse was seen to result in a higher average movement speed. Less emphasis on orientation control by the user cannot alone explain it; the concept efficacy appears to be improved because of the arm arrangement. However, this was not the case in the tube with ridges, where movement in reverse was slower and was attributed to the ridges more easily obstructing the wheels – and having a greater impact on control - in this direction.

The fundamental limitation of not being able to individually adjust each arm of this current RollerBall concept was clear in these tests and is shown in Figure 6.28.

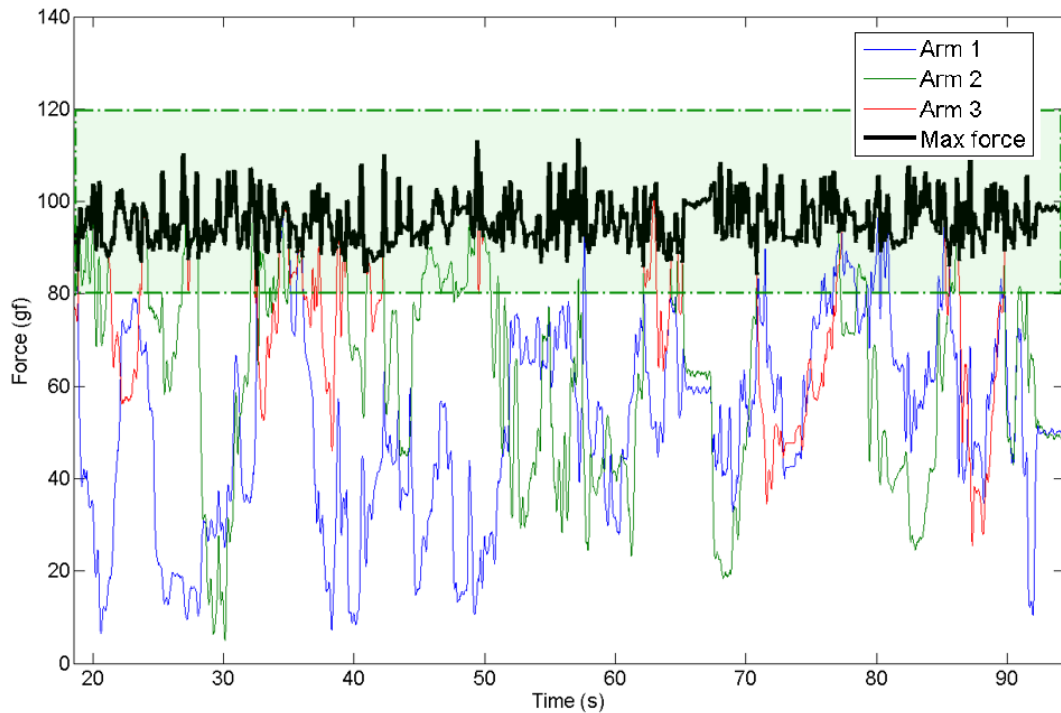


Figure 6.28 – A plot showing the high variability between force outputs from all three arms during one test.

The green region indicates the desired force range. A force of less than 20 gf on any arm would likely have resulted in a loss of traction at that wheel.

While the maximum force is maintained at approximately the desired amount (100 gf), the force on one or more of the arms can be very low and may result in a complete loss of traction. Little can be done about this except increase the desired force and risk damaging the lumen or robot. There is also the question of arm angle and the resulting change in applied normal load. This was mentioned in the design of RollerBall and presents an issue with the current expansion control. Ideally, the arms require position feedback, which can then be used to calculate the arm angle and hence estimate a more realistic magnitude of force applied normal to the lumen. Currently, in a large diameter lumen, the arms may only detect a small force (since only a small component of the applied force is normal to the arm); when in reality the arms are applying a significantly larger force as the majority of it is applied parallel to the arm axis.

6.4.3.3. Automated orientation control

Stage 1 – Adjusting orientation while robot is stationary

The robot was able to navigate through the entire sequence successfully in all ten (including both manual and auto) repetitions. Automated orientation control significantly improved the performance in a number of ways:

The most obvious was the lack of user input required. The successful completion of the sequence under automated control shows the feasibility of future image tracking and autonomy developments. The trajectory and locomotion efficiency was greatly improved. This can be seen qualitatively in Figure 6.29, which contrasts the coordinates of the tracked Target in all five repetitions under both manual and auto control.

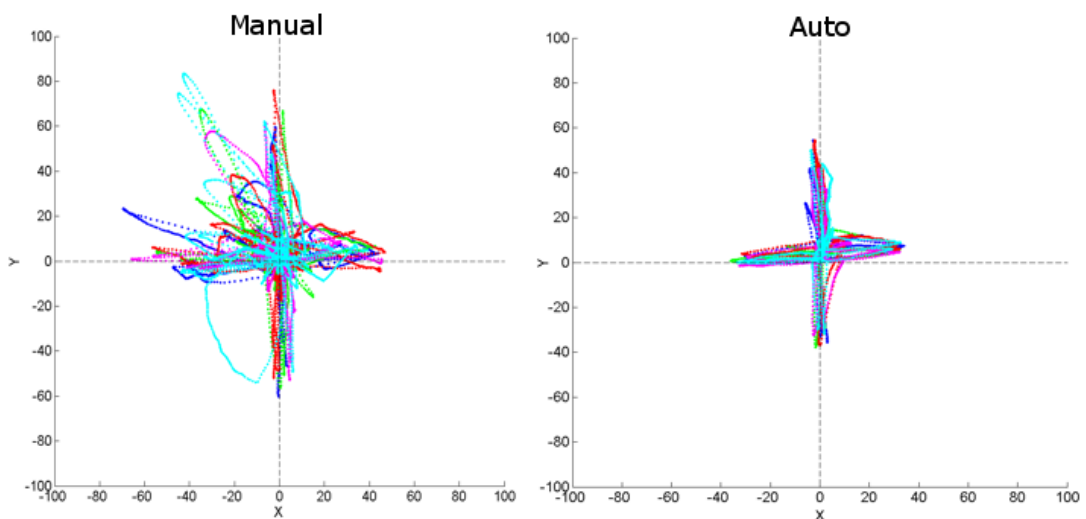


Figure 6.29 – A comparison of the x-y plots of the tracked Target, from all repetitions, under Manual and Auto orientation control.

The profiles for each repetition in the Auto plot are similar, showing repeatability. The shape is also what you would expect from the sequence used: a distinct cross. The Manual plot is in stark contrast to this; the profiles show high variability between repetitions and the overall shape only loosely represents a cross. The success of the automated control in this sequence (compared to that used to tune the system) validates the efficacy of both the method used to calculate wheel speeds and the closed-loop orientation control strategy.

Figure 6.30 provides further insight into the performance enhancement.

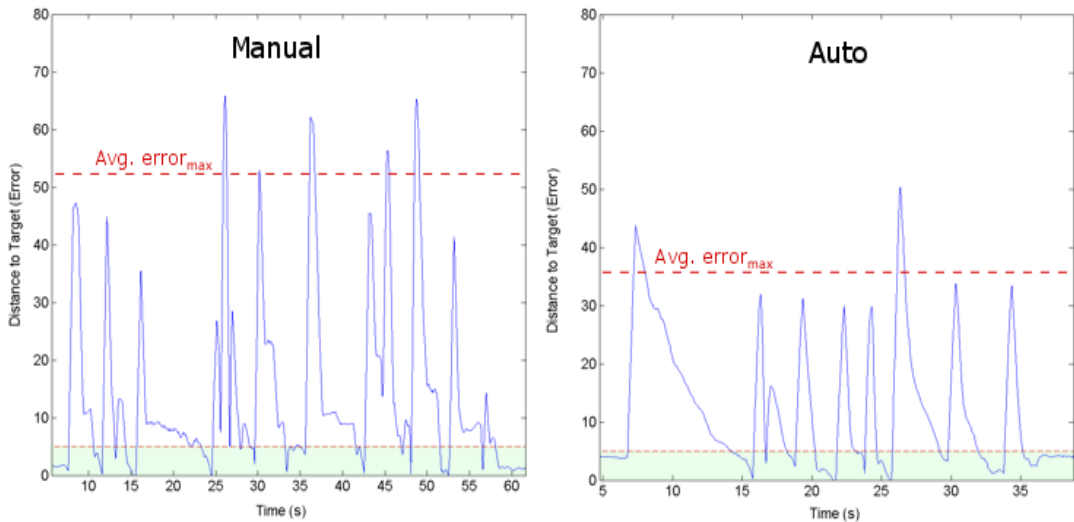


Figure 6.30 – A comparison of the error plots of the tracked Target, from one repetition, under Manual and Auto orientation control.

The average error was calculated and annotated with a red dotted line. The green region indicates the accepted error.

An immediate difference between Manual and Auto in Figure 6.30 is the average maximum error. This indicates that, during Manual control, the user frequently and significantly overshoot the Target. This is also shown by the greater number of peaks, each representing one movement orientation adjustment. Manual control also took longer to complete the sequence; this is shown by the time axis and summarised in Table 6.7: 49.8 seconds versus 25.5 seconds.

Table 6.7 – The results from the manual and automated orientation control tests.

	Average number of peaks (movements) (n=5)	Average time to complete sequence (n = 5)
<i>Manual control</i>	27.4 ± 10.5	49.8 ± 6.7 s
<i>Auto control</i>	9.6 ± 1.5	25.5 ± 5.2 s

Fine orientation adjustments were particularly difficult under Manual control. This is shown by the greater average number of features (27.4 versus 9.6), particularly at low errors – representing multiple small robot movements (user inputs) taken to accurately align with the Target. Some of the variance in both the x-y plots and the error plots may be from an unwanted offset (such as friction) on the individual wheel speeds.

Stage 2 – Adjusting orientation while robot is moving

The final stage of testing attempted to show the feasibility of combining automated expansion and orientation control to provide semi-autonomous movement through the colon, where the user only has to control *Global speed*. Semi-autonomous control was achieved, however, the performance was suboptimal. The x-y plots from the best repetition during manual and semi-autonomous (Auto) control are shown in Figure 6.31.

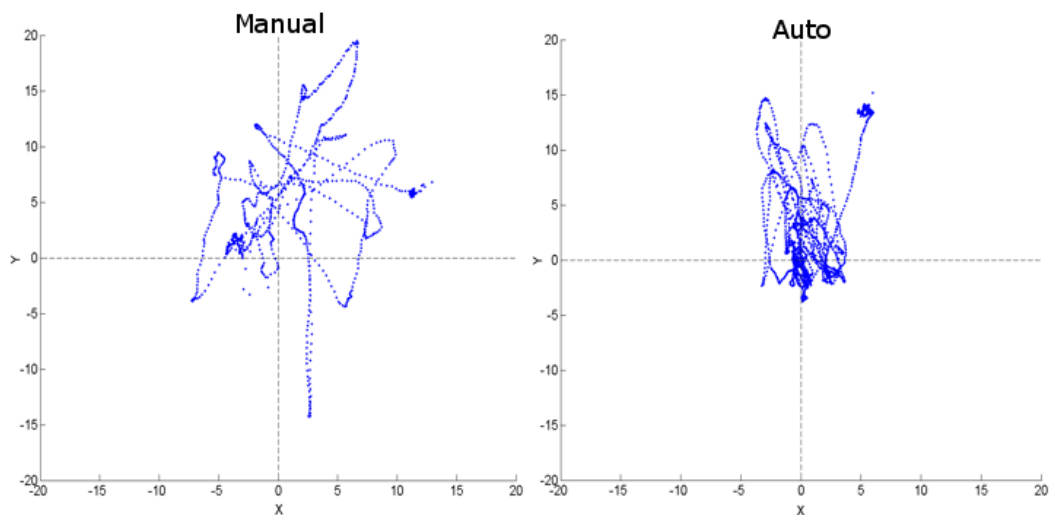


Figure 6.31 – A comparison of the x-y plots of the tracked Target, from one repetition, under Manual and Auto orientation control – during forward movement.

Ideally, the Target would be kept consistently in the centre of the camera view and therefore, both x-y plots would have a close grouping of coordinates about the origin (0, 0). The erratic movements displayed on the plots, particularly under Manual control, emphasise the challenge of maintaining a central orientation while moving the robot forwards. Automated control appears to improve the movement efficiency (with a closer grouping of the Target coordinates) however, the closed-loop control is not responsive enough to achieve smooth locomotion (which would have appeared as a very tight grouping of Target coordinates). Interestingly, the majority of movements in both x-y plots are located above the origin. This is due to the instability of the prototype from the offset CoM and the requirement to frequently lift the robot tip (counteracting gravity).

Figure 6.32 and Table 6.8 provide greater insight into the differences between Manual and semi-autonomous robot control.

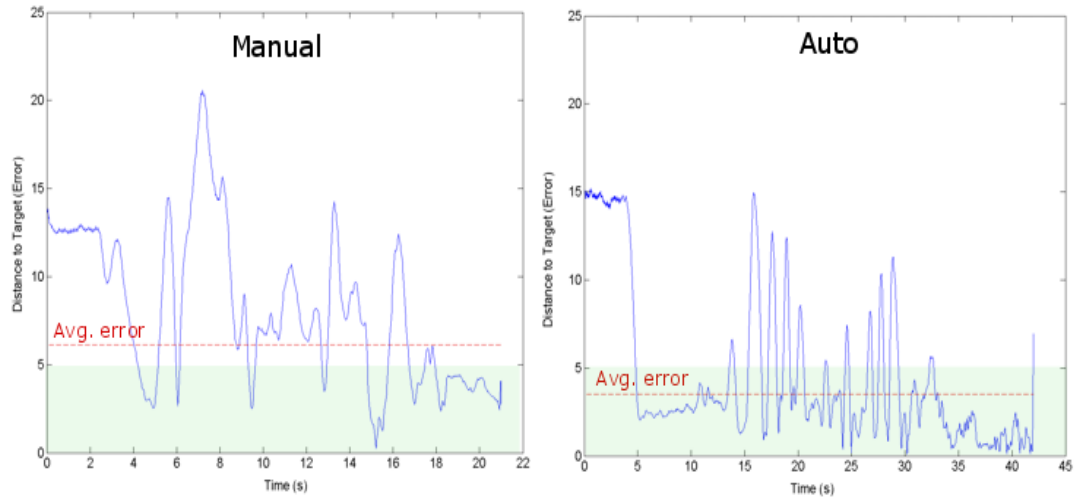


Figure 6.32 – A comparison of the error plots of the tracked Target, from one repetition, under Manual and Auto orientation control – during forward movement.

The average error was calculated and annotated with a red dotted line. The green region indicates the accepted error.

Table 6.8 – The results from the manual and automated orientation control tests.

	Avg. no. of peaks (movements) above Dead-band (n=5)	Avg. error (n = 5)	Avg. time outside of Dead-band (n = 5)	Avg. time to traverse tube (n = 5)
Manual control	10.0 ± 1.4	7.7 ± 1.5	15.0 ± 4.0 s	24.2 ± 3.3 s
Semi-auto control	13.0 ± 2.6	3.9 ± 0.5	6.9 ± 1.6 s	41.2 ± 4.9 s

The semi-autonomous control carries out more frequent adjustments, shown by the higher average number of peaks above the dead-band (13 versus 10). However, the time outside of the dead-band is less - as is the average error - indicating that the automated orientation control does improve orientation adjustment accuracy. This accuracy appears to come at a cost as the average time to traverse the tube is significantly longer with the semi-autonomous control. This longer duration was because slower *Global speeds* had to be used to give the automated orientation controller sufficient time to correct for the change in orientation – ie. greater speed could have been achieved if maintaining the central orientation was not important or, if a more responsive and advanced controller was used.

6.5. Summary – Closed-loop control

In Chapter 5, the integrated RollerBall platform was developed and full control over the device’s position, orientation and arm angle was achieved in purpose built, synthetic silicone tubes. Intuitive Xbox controller inputs were then used to manually control the device.

Despite the success of the tests, it was clear that autonomy was needed as the simultaneous manual control of position (*Global speed* and direction), orientation (differential *Turning speeds*) and arm angle was challenging. However, the overall efficacy of the locomotion technique and method used to adjust the motor speeds was shown.

In this Chapter, the subsequent inclusion of a forward facing camera and a lower friction lumen slightly improved usability and locomotion efficacy. During these tests, monitoring the *Global speed* (user input) and maximum arm force highlighted the necessity of having more advanced (closed-loop) control with a faster response time. Strain gauges were used to provide the arm force feedback and they could repeatedly acquire accurate force measurements. However, this required post processing to account for the non-linear material properties of the 3D printed resin. The feasibility of compensating for this non-linearity was demonstrated but not incorporated in real-time, hence the force sensing system had a degree of inaccuracy. The force feedback was used to automate the arm expansion with satisfactory performance – mechanical features of the current prototype (such as friction and back-lash) were limiting factors on performance. Despite these issues, the arm angle could be controlled in closed loop and this was shown to greatly improve usability, locomotion efficacy and avoid excessive (unsafe) force application.

The final control development was automating the orientation control using the camera feedback. A control strategy that used the coordinates of a tracked image as the Target for the *Position and Orientation control* program was successfully implemented. The device could autonomously adjust its orientation and track a user defined movement pattern while stationary. It did this with much greater performance than when done manually. Slight variance between movements in different directions showed that control efficiency and usability (both auto and manual) could be improved by including wheel position feedback. This could be used to reduce the unwanted offsets applied to the speeds by friction in the individual wheel mechanisms. This is achievable but requires added hardware and software complexity. To complete the evaluation of RollerBall, tests were done to assess whether full semi-autonomous control was feasible (ie. the user defines *Global speed* and the robot advances while controlling arm angle and orientation autonomously). Results indicated that this level of autonomy is plausible, but the mechanical design of the current prototype (such as the high inertial load on the expansion motor and the low camera frame rate) severely complicates this.

Chapter 7

Discussion and conclusions

There is no doubt that the successful development of a mobile colonoscopy robot could have a major global impact on the diagnosing and treating of colonic diseases. The work presented in this thesis not only provides insight into the development of a robotic platform for hydro-colonoscopy, but also into the wider challenge of designing, fabricating, controlling and testing small *in vivo* robots.

The work in this thesis has made a number of significant contributions to the field, notably:

1. A robust method of evaluating robots for use in a complex biological lumen environments.
2. An optimum solution proposed for gaining traction on the intestinal lumen based on a review of literature and an in-depth experimental evaluation of 3D printed tread patterns.
3. An effective control strategy for a mobile, wheeled, intra-luminal robot.

7.1. Discussion

The RollerBall concept is a novel solution to locomotion in the colon and one that provides improved performance and functionality when compared to the current state-of-the-art summarised in Chapter 2. The actuation of spherical wheels by high power DC motors not only gives precise control of robot movement, but has the advantage over other locomotion techniques of providing continuous shear of the wheel contact – thrust can be produced even in the presence of significant slip. Because of this, net thrust, and in most cases movement speeds, are likely to be greater than other devices (particularly impact-driven [77], inchworm [87, 88], legged [91, 92] and all swimming devices reviewed [64, 67, 73, 74]). Literature on related robots puts little emphasis on the inclusion and effective use of on-board diagnostic and therapeutic tools. This is a major requirement if such a device is to improve on the conventional colonoscope and one that other mobile colonoscopy robots (particularly inchworm [87, 88], magnetic [62] and swimming devices [64, 67, 73, 74]) may be limited by because of their lack of a central and stable, yet mobile, platform. RollerBall includes a compact expansion mechanism to actively adapt the wheels to the local diameter of the colon lumen. The complexity of this mechanism is reduced significantly by actuating all three arms using a single DC motor; the result is an elegant solution to maintaining

contact with the lumen while maintaining high mobility. The stable platform that RollerBall can provide at any given location within the colon is a key strength compared to other designs and could greatly increase the ability for it to house and effectively use on-board tools. The subsequent development of this concept to a full working prototype revealed a number of challenges and proposed solutions.

Fabrication will always be a challenge with small, complex electro-mechanical, *in vivo* devices, as there is both the essential requirement to operate in constrained environments and the desired requirement for further miniaturisation to improve mobility and safety of the device. The size of RollerBall was governed largely by the size of the DC motors used, but also by the desire to reduce fabrication complexity and improve durability. 3D printing using DLP (Digital Light Projection) technology was a logical choice for the manufacturing technique. It has the ability to accurately recreate small, complex parts from CAD models at an acceptable cost. It also supports the iterative design process used to develop the prototype, with replacement parts rapidly fabricated on demand. A limitation in the 3D printer material was discovered and is one that many will encounter with current resin-based printers: the photo-cured material first requires post curing and then is subject to degradation over subsequent prolonged exposure to light and extreme temperatures. The resin also exhibits a non-linear response to loading, and plastic deformation (material creep) was evident during prolonged loading of the arms. Despite these, the advantages of 3D printing still make this an attractive solution and future advancements in the technology will likely address the current limitations. 3D printing was an essential part of this work and it is easy to speculate that without it, the prototype development would not have been possible. The overall size of RollerBall could be considerably reduced by using smaller (4 mm) commercially available DC motors and with minor design refinements to more efficiently package the components. However, it will likely require a different method of fabrication as the smaller, plastic parts may not have the required structural durability. One example may be the technique of selective laser sintering or melting (SLS or SLM) metal powders to create parts with significantly higher strength, but with some dimensional inaccuracy and significant post-processing required [140]. Assembly would also be more challenging because all components will likely be scaled-down and so require more care and precision to handle.

Biological environments are complex and accessing them to carry out frequently tests on a robot at various stages of development is not always possible or practical. This was particularly true for RollerBall and the colon. However, because of the inherent complexity

and variability in biological environments the efficacy of *in vivo* robots can only be shown empirically, no matter how promising the concept seems at conception and how refined the design. To evaluate the RollerBall concept and direct the development of the control and other refinements, a testing process was created that could be utilised and built upon by others developing *in vivo* robots. The first stage was to test the individual mechanical components; characterising and validating their performance. The next step was to identify key components that cannot be assessed effectively without using biological tissue (for example, the work on gaining traction necessitated a biological substrate, as an investigation of the completely unique, complex frictional characteristics was essential). In cases such as this, biological tissues must be used and incorporated into a test rig. A compromise may have to be made on the number of biological variables that are controlled - but it should repeatedly recreate the *key* biological conditions. The other components of the robot can be assessed using a synthetic environment. This segregation reduces the complexity of the testing protocol and enables numerous iterative stages of testing and refining. The colon was abstracted into key geometries (features) and properties. Because the traction had been explored separately, recreating the frictional characteristics in these tests was not as essential and so they could be fabricated using a durable silicone. Complexity (in both the testing and fabrication) was further reduced by splitting the features across a number of environments (for example, one tube with no corners but a varying diameter and another with a constant diameter but multiple corners). In addition to the reduced complexity, this also allowed the individual aspects of the prototype to be evaluated in a much more controllable, repeatable and targeted approach. Although RollerBall did not reach this stage, after sufficient iterations of testing and design refinement are made, the device could then be evaluated more realistically in a biological environment, with the previous steps giving confidence that the device will function. It is imagined that these biological tests would themselves be divided into three stages: tests in biological samples carried out in a laboratory setting (*ex vivo*); tests in either a cadaveric human or animal model and lastly; *in vivo* tests in a living human or animal.

A major requirement for RollerBall to be successful was the attaining of sufficient traction to provide locomotion, while avoiding trauma to the sensitive tissue. A thorough exploration of relevant literature and the evaluation of several 3D printed wheel treads showed that traction can be gained on this mucus covered surface, with friction coefficients ranging from 0.34 during continuous shear and as high as 0.76 when static. The large difference between static and dynamic traction suggests that ideally, the wheels should have torque feedback and hence be able to control slip. Modifications to the tread geometry and scale were shown

to significantly reduce the trauma caused, but it appears that a trade-off has to be made on the amount traction achieved. An array of elongated hexagonal pillars (1000 μm in length, 500 μm in width, 330 μm in depth and spaced 250 μm apart) caused negligible trauma while providing functional levels of traction (in static and dynamic cases). It was evident in this work that there is still room for further improvement and so an optimum, bioinspired patterned surface that considered what was learnt from literature and the experimental work was proposed. The approach is to use a hierarchy of hexagonal shaped pillars. The larger underlying pillars should be made from a soft, visco-elastic material to conform to the substrate while also providing environmental resistance and low trauma. The superficial, micro-scale pillars should have a hydrophobic coating and be made from a comparatively stiffer material for improved de-wetting, micro tissue deformation and high wear resistance. The combination of both scales should provide maximum traction by increasing contact de-wetting and exploiting both micro and macro sources of resistance. These insights, and the proposed solution, may have applications outside of the colon. A number of medical and surgical instruments require high traction and low trauma, such as mobile robots in the small intestine [135], abdominal cavity [79, 141] and soft tissue surgical graspers [142] to name a few.

The size and shape of the colon can be highly variable along its length - controlling any device in this will likely be a challenge. The rigid design of RollerBall provides a number of advantages, such as the ability to use high power DC motors and the stable platform the arm arrangement provides. However, there is an obvious compliance mismatch: the environment is extremely soft and mobile, and the robot is rigid, with fixed linkages. The result of this is the necessity for advanced, closed-loop control to not only provide effective locomotion but also improve safety and reduce the demand on the user; the simultaneous control of the many actuators proved to be an onerous task when carried out under full manual control. Tests also highlighted that the lack of feedback and autonomy could damage both the robot and the environment. The solution was to automate the two main components of the robot control, the arm force (angle) and the orientation adjustment. Closed-loop control of the arm force was effective at creating compliance and despite features of the current prototype limiting the performance, a desired force range was approximately maintained and showed the efficacy of this approach. It may be logical to include a compliant section in the arm that would ease the control complexity by providing some passive deformation. This could be done however, it presents some challenges that are not immediately obvious. The first is the added length that this section would add, given that the DC motors are also packaged in the arms. The other is the potential loss of traction

in narrow apertures: as the arms approach the chassis of the robot (a small angle) the tissue could contact the arms, deform them and reduce the degree of contact of the aft wheels.

The accurate and precise control of robot orientation is crucial to this device's efficacy; with the resulting high mobility improving both locomotion and the effective use of tools. The method used to map the user inputs to motor outputs showed that the device could be controlled intuitively but with significant effort. This was particularly so given the offset CoM present in the current prototype and the environment used, which lacked fluid support (ie. buoyancy in the robot to counteract the CoM). The question was posed whether semi-autonomous control of the device was possible, as this would result in the procedure having very high usability and could improve overall functionality. Feasibility of the expansion control was demonstrated, so the only remaining aspect to automate was the orientation control. This was done using an elegant approach of using the images from the camera and the unique features of the colon as feedback. The control requires a reference and since the trajectory of the robot in the colon can be anywhere in three dimensional space, this limits the use of gravity as a reference. The feasibility of this control strategy was shown by successfully automating the orientation adjustment while stationary. Semi-autonomous control of arm force and device orientation, while moving at a user defined speed, was shown to be plausible but is limited by current technology.

At this point, it is natural to ask whether the device is suitable for clinical (commercial) use and what it might take to reach that stage. The successful fabrication of the prototype, the demonstrated locomotion efficacy and the possibility of improving the autonomous control suggest that it is plausible that RollerBall could be used in a clinical setting. However, it would require the refinement of a number of aspects, including: more advanced orientation control using a high framerate camera and effective processing of the images; the wheels should be fitted with position (and ideally, torque) feedback to reduce the variability between wheel speeds and hence reduce movement error; ideally, there should be individual control of the arms and they should also include position feedback to calculate the normal force at different arm angles (Compliant sections could be included in the arm design to reduce the demand on the controller); biocompatible materials should be used for obvious safety reasons. The material should also be sufficiently durable and combined with a fabrication technique with the required precision; the overall size of the device will have to be reduced significantly. This will require more efficient packaging of the components and the use of smaller DC motors; there is also the question of the required encapsulation and sterilisation. The device could be designed to have some degree of modularity, allowing

certain components (eg. the arms) to be disposable. The other components need to be sealed and made from a material that can be sterilised effectively; and lastly, the cost of this robot would undoubtedly be high and could limit its wide-spread adoption. The aforementioned modularity (disposable components) and further refinements made to reduce complexity could bring the cost down to an acceptable level.

It is clear that many challenges need to be addressed before RollerBall could be used clinically; some technical (such as additional feedback, miniaturisation and more advanced control), some commercial (such as a reduction in the complexity and associated fabrication cost) and some clinical (for example, the change in practice, the associated training required and the need for sterilisation). Many of these are associated with the complexity of RollerBall (both in terms of the physical design and the control). A promising alternative locomotion technique for a mobile colonoscopy robot is proposed in Appendix D and considers the area of soft robotics. RollerBall may be best suited to another application that does not require as many modifications to the design – industrial, pipe-inspection robots for example. The design and control aspects of RollerBall meet a large number of the main requirements set out by Mirats-Tur et al. [143], including: adaptability to different tube diameters; ability to function in water⁶⁷; high mobility; ability to house a number of sensors; high movement speed; and autonomous navigation (to which RollerBall is well on its way).

7.2. Conclusions

The work presented in this thesis on the design, fabrication, control and testing of RollerBall provides insight into this specific research area and the wider challenge of developing *in vivo* robots for healthcare.

The aim of this PhD was to develop a mobile robot to traverse the length of a fluid-filled colon, while providing a stable platform for the use of surgical tools. RollerBall was developed and although it didn't completely meet the requirements, was shown to be a viable solution. The original objectives were successfully achieved:

- Current literature was reviewed to gain a better understanding of the technical challenge and appropriate locomotion techniques. This showed the major need for alternatives to the conventional colonoscopy, suggested requirements for a mobile robot and wheeled locomotion was seen to be one of the more promising locomotion techniques.

⁶⁷ RollerBall has not been made water-tight, however, a fluid environment does suit the design because of the intended inclusion of a buoyant electronics module.

- An existing concept, RollerBall, was evaluated and a number of design modifications made to it. A final, detailed design of the robot was included and the fabrication of a durable prototype described. The performance of individual mechanisms of this prototype were then characterised in a series of benchtop tests, revealing that they function as intended.
- A thorough review of literature on the essential requirement of gaining traction on the colon was carried out and the insights used to design, test and propose a suitable tread pattern for RollerBall. The hexagonal array of pillars showed that high traction and low trauma is possible on the colon.
- The complete, integrated robotic system was then developed and both manual and semi-autonomous methods of control were explored in a number of iterative tests in synthetic lumens. These showed the efficacy of the locomotion technique, control strategy and possibility of making the device autonomous.

In addressing the objectives, many of the desired robot specifications were also achieved.

Table 7.1 summarises these:

Table 7.1 – A summary of how the RollerBall prototype met the desired specifications

Original specification	Actual performance/value	Comments
Diameter less than 26 mm and length not more than 40 mm.	Diameter of 35 mm and length of 95 mm.	Specification not met, but could be with further miniaturization and the use of 4 mm DC motors (See Section 8.1).
A linear speed of 3.85 mm/s.	Average speeds ranging from 11 – 30.5 mm/s were achieved.	The DC motors provided high rotational speed and so, provided slip is controlled, speeds significantly above 3.85 mm/s can be achieved.
Move in forward and reverse directions through a flexible lumen. Traverse a range of corners from 30 ° to 120 °	RollerBall was able to stop, start, move forwards, reverse and traverse corners ranging between 30 ° and 100 °.	The length of the prototype hindered progress around acute flexures and should be addressed to improve mobility.
Greater than 1 N gross thrust.	Assuming a normal load of 100 gf, the expected gross thrust is 1.62 N.	Results in Chapter 4 only considered a maximum normal load of 50 gf however, 100 gf could be safely used. This gives the stated gross thrust assuming a linear relationship

		between normal load and traction.
Maximum pressure at wheel interface less than 3 Bar. No mechanical induced trauma beyond mucosal layer after 10 s of continuous slip.	Force was successfully limited in the control software. No trauma was inflicted beyond the mucosa when using the small scale hexagonal tread pattern.	This could be greatly improved using a compliant material for the tread pattern.
Working diameter of 26 mm (required diameter) to ca. 62 mm.	The expansion mechanism used allowed the prototype to operate successfully in lumen diameters ranging from 40 – 90 mm.	This could be reduced by miniaturising the prototype but highlights the efficacy of the expansion mechanism in adapting the robot to a large change in diameter.
Able to fix the robot position and orientation (fixed platform).	RollerBall provides a fixed, stable platform.	This provides a distinct advantage over devices such as inchworm and passive capsules.
Last at least 10 hours of continuous, manual handling and normal operation (locomotion) without failure.	No part failures were recorded after more than 10 hours of normal use.	Robustness could be greatly improved by using a stronger, more durable material such as titanium.

It was concluded that RollerBall has the potential to be used in a clinical setting, but this would require further research and consideration of commercialisation aspects (such as mass manufacture) to achieve.

Chapter 8

Future work

This chapter briefly summarises some of the main aspects to this PhD which would benefit from further investigation – particularly if RollerBall is to be used in a biological environment.

8.1. Miniaturisation and fabrication

One of the most significant factors limiting the use of the current RollerBall prototype in a biological environment is its size. A larger scale was used to ease fabrication and to improve durability with the 3D printing material used. It was envisaged that a 30 % reduction in the overall size would be feasible using commercially available 4 mm DC motors. With no other changes to the design, this would reduce the dimensions to approximately 25 mm in diameter (arms collapsed) and 70 mm in length (Figure 8.1). This new diameter meets the required value of 26 mm however, the length does not and would require further reduction. One method to reduce the length could be to use smaller gear reductions in the wheel motors (which currently exceed torque requirements). The layout of the motors and gear assemblies could also be refined to make more efficient use of the space. And finally, significantly smaller cameras are available commercially and would greatly reduce the length of the electronics module.

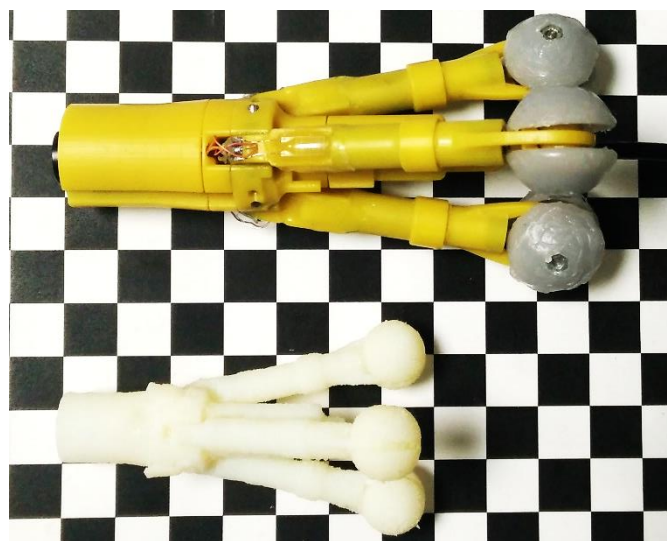


Figure 8.1 – An image showing an approximately 30 % smaller model of RollerBall, next to the existing prototype. The grid is comprised of 1 cm squares.

Fabricating the smaller scale device shown in Figure 8.1 would be a challenge and would require careful selection of the material and a suitable fabrication technique. It may also require a simplification of the design to avoid excessively small features. A proposed solution is to use a metal 3D printing technique – this technology has a comparable resolution to conventional, plastic 3D printing methods, with greatly improved strength. The metal used should be biocompatible to allow its safe use *in vivo*, such as titanium.

8.2. Encapsulation and design refinements

Encapsulation is another crucial body of work required. Seals should be included to protect the electronics contained within the robot. As mentioned previously, containing the majority of the electronics in the front module reduces the complexity of encapsulation by requiring fewer seals. A reduction in the complexity of the rest of the concept design would also assist in this area and should be investigated further.

RollerBall would benefit from a number of additional design modifications:

- A failsafe mechanism to manually collapse the arms and allow device removal. This was envisaged as a mechanical release mechanism in the robot, actuated by the user pulling a cable running through a working channel in the tether. Keeping the mechanism simple and purely mechanical would be an advantage as it could increase robustness and reduce cost. This or a more suitable, alternative approach, should be explored.
- The electronics module was located at the front of the device partly due to the future potential of including buoyancy to counteract the offset CoM. This should be investigated further and could greatly improve robot control and stability in a flooded environment.
- A method of individually actuating the arm angles would be of great benefit. This was not explored in this thesis but, if achieved, could greatly improve stability and locomotion efficacy by ensuring all wheels are in contact with the lumen and under an optimum load for traction.

8.3. Optimising functional surfaces for high traction and low trauma against soft tissues

The work on gaining traction in the colon had some promising results that would benefit from further investigation:

- The effect of surface area, velocity and surface hydrophobicity should be explored in a similar, repeatable method. These were not explored in this thesis and have shown varying, sometimes contradictory, results in literature.
- No studies have thoroughly assessed what effect tread compliance has on traction and trauma. This, and the previous point, should ideally be carried out in an even more biologically accurate environment and validated *in situ*.
- Despite the robust protocol used, the experimental work on trauma did not provide as clear results as hoped. The work in this thesis could be built on to give a more quantitative trauma assessment. More specifically, multiple repetitions could be used to increase confidence in the results. A more effective method of storing and slicing the samples could also be used to improve histology results.
- Although it would likely require significant work, the bio-inspired solution that was proposed for high traction and low trauma against tissue should be explored as it shows great promise. It may provide an effective interface for a number of medical applications.
- Lastly, the more advanced tread pattern must be incorporated onto the spherical wheels and its functional performance assessed *in vivo*.

8.4. Electronics and control

The majority of the electronics hardware for the current RollerBall prototype was kept separate from the device to simplify the development process. As a result, the motor PWM signals were transmitted down the length of the tether alongside the camera signal and all three strain signals from the arms. Although this method was implemented successfully and reduced the complexity of the on-board electronics, it required a total of 20 individual wires to achieve and was seen to increase noise in the strain output. Developing on-board strain conditioning circuits and motor driver boards would significantly reduce the number of wires required in the tether and could reduce unwanted noise in the strain signal by transmitting data digitally (eg. via I2C). Fewer wires could reduce tether induced drag in the colon because of the resulting reduction in stiffness and mass of the tether.

Provided individual arm actuation is achieved, a more robust method of sensing force should be developed and used for closed-loop control of each arm. Crucial to the efficacy of this control is a reduction in the inertial load seen by the actuator. This would depend on the actuation mechanism used, but could be achieved by reducing the mass of the arms and using an actuator that does not require a multiple stage gearbox. A more advanced method

of compensating for the different forces on the arm during expansion and contraction should be explored as switching PID constants introduces instability.

A method of closed-loop orientation control, that used the haustral ridges as references, was proposed in this thesis. Orientation control was shown to be feasible by successfully tracking a user defined target however, further work is required to develop the *in vivo* image tracking. Specifically, a method of robustly detecting the haustral ridges (and hence lumen centre) should be investigated. The main challenge is expected to be in filtering the camera images to extract the required features and also in reducing the associated processing time.

RollerBall would also benefit from two additional sources of feedback. The first is a method to detect (and hence control) slip – be it wheel position/speed, wheel torque or a combination of the two. This could improve traction by exploiting the static friction coefficient and improve locomotion efficiency by reducing movement error. The second source of feedback is the arm angle. This could not only be used to improve arm control but also be used to calculate the force applied normal to the tissue at different arm angles.

8.5. Test environment

A noteworthy limitation in the work carried out in this thesis is the colon environment used to assess the robot. This was chosen to allow repeatable testing and was deemed suitable for the preliminary stage of the concept development. The traction work on porcine tissue increased confidence in the robot's ability to gain traction *in vivo*, however, a more biologically accurate environment should be used in future developments. It is proposed that an *ex vivo* section of porcine colon could be suspended from a rigid frame as an intermediate stage between silicone tubes and *in vivo* animal (or human cadaver) trials. The performance of the robot in a flooded environment should also be investigated. This could begin in silicone tubes, similar to those used in this thesis, and would show the efficacy of the proposed buoyancy method used to improve stability.

REFERENCES

1. Kaplan, G.G., *The global burden of IBD: from 2015 to 2025*. Nat Rev Gastroenterol Hepatol, 2015. **12**(12): p. 720-727.
2. Luengo-Fernandez, R., et al., *Economic burden of cancer across the European Union: a population-based cost analysis*. The lancet oncology, 2013. **14**(12): p. 1165-1174.
3. Liu, X., et al., *Automated measurement of quality of mucosa inspection for colonoscopy*. Procedia Computer Science, 2010. **1**(1): p. 951-960.
4. Siegel, R., C. Desantis, and A. Jemal, *Colorectal cancer statistics, 2014*. CA Cancer J Clin, 2014. **64**(2): p. 104-17.
5. CRUK. *Bowel Cancer Statistics*. 2016 December 2016]; Available from: <http://www.cancerresearchuk.org/health-professional/cancer-statistics/statistics-by-cancer-type/bowel-cancer>.
6. Gavin, D.R., et al., *The national colonoscopy audit: a nationwide assessment of the quality and safety of colonoscopy in the UK*. Gut, 2013. **62**(2): p. 242-9.
7. Olympus. *Colonoscope*. [cited 2017; Available from: http://www.olympusamerica.com/presspass/press_pass_cut/images/msg/GIF-H180lg.jpg].
8. Alazmani, A., et al., *Quantitative assessment of colorectal morphology: Implications for robotic colonoscopy*. Medical Engineering & Physics, 2016. **38**(2): p. 148-154.
9. Mitchell, R.M., et al., *Successful colonoscopy; completion rates and reasons for incompleteness*. Ulster Med J, 2002. **71**(1): p. 34-7.
10. Taylor, D.P., et al., *Comparison of compliance for colorectal cancer screening and surveillance by colonoscopy based on risk*. Genet Med, 2011. **13**(8): p. 737-43.
11. Eickhoff, A., et al., *Colon anatomy based on CT colonography and fluoroscopy: Impact on looping, straightening and ancillary manoeuvres in colonoscopy*. Digestive and Liver Disease, 2010. **42**(4): p. 291-296.
12. Sadahiro, S., et al., *Analysis of Length and Surface-Area of Each Segment of the Large-Intestine According to Age, Sex and Physique*. Surgical and Radiologic Anatomy, 1992. **14**(3): p. 251-257.
13. Tytgat, G., *Gastroenterological Endoscopy*. 2010: Georg Thieme Verlag.
14. Paparo, F., et al., *Computed tomography of the bowel: A prospective comparison study between four techniques*. European Journal of Radiology, 2013. **82**(1): p. E1-E10.
15. Strodel, W.E., et al., *Therapeutic and Diagnostic Colonoscopy in Nonobstructive Colonic Dilatation*. Annals of Surgery, 1983. **197**(4): p. 416-421.
16. Marchesini, R., et al., *Ex-Vivo Optical-Properties of Human Colon Tissue*. Lasers in Surgery and Medicine, 1994. **15**(4): p. 351-357.
17. Wang, K.D. and G.Z. Yan, *Research on measurement and modeling of the gastro intestine's frictional characteristics*. Measurement Science and Technology, 2009. **20**(1): p. 015803.
18. Online, E.B., *Large intestine: mucosa and musculature in humans*. 2013: Encyclopædia Britannica.
19. Cunningham, D., et al., *Colorectal cancer*. The Lancet. **375**(9719): p. 1030-1047.
20. Logan, R.F.A., et al., *Outcomes of the Bowel Cancer Screening Programme (BCSP) in England after the first 1 million tests*. Gut, 2012. **61**(10): p. 1439-1446.
21. Martín-López, J.E., et al., *Efficacy of CT colonography versus colonoscopy in screening for colorectal cancer*. Radiología (English Edition), 2011. **53**(4): p. 355-363.
22. Howard, K., et al., *Preferences for CT colonography and colonoscopy as diagnostic tests for colorectal cancer: a discrete choice experiment*. Value Health, 2011. **14**(8): p. 1146-52.

23. van Gils, P., et al., *A literature review of assumptions on test characteristics and adherence in economic evaluations of colonoscopy and CT-colonography screening*. Eur J Cancer, 2009. **45**(9): p. 1554-9.
24. Osama, A., H.H. Solieman, and H.A. Zaytoun, *Role of CT virtual colonoscopy versus conventional colonoscopy in the evaluation of colonic polyps*. The Egyptian Journal of Radiology and Nuclear Medicine, 2013. **44**(3): p. 425-432.
25. Tapia-Siles, S.C., S. Coleman, and A. Cuschieri, *Current state of micro-robots/devices as substitutes for screening colonoscopy: assessment based on technology readiness levels*. Surgical Endoscopy, 2016. **30**(2): p. 404-413.
26. Hafner, M., *Conventional colonoscopy: Technique, indications, limits*. European Journal of Radiology, 2007. **61**(3): p. 409-414.
27. Seeff, L.C., et al., *How many endoscopies are performed for colorectal cancer screening? Results from CDC's survey of endoscopic capacity*. Gastroenterology, 2004. **127**(6): p. 1670-1677.
28. Hopkins, J. *Colonoscope in colon*. [cited 2017; Available from: http://www.hopkinsmedicine.org/gastroenterology_hepatology/clinical_services/basic_endoscopy/colonoscopy.html].
29. Sedlack, R.E., *Training to competency in colonoscopy: assessing and defining competency standards*. Gastrointestinal Endoscopy, 2011. **74**(2): p. 355-U259.
30. Britannica. *Colonoscopy examination*. [cited 2017; Available from: <https://www.britannica.com/science/colonoscopy>].
31. Sages. *Colonoscope looping*. [cited 2017; Available from: <https://www.sages.org/image-category/fundamentals-diagnostic-colonoscopy/>].
32. Barclay, R.L., et al., *Colonoscopic withdrawal times and adenoma detection during screening colonoscopy*. New England Journal of Medicine, 2006. **355**(24): p. 2533-2541.
33. Harris, J.K., et al., *Factors associated with the technical performance of colonoscopy: An EPAGE Study*. Dig Liver Dis, 2007. **39**(7): p. 678-89.
34. van Rijn, J.C., et al., *Polyp miss rate determined by tandem colonoscopy: a systematic review*. Am J Gastroenterol, 2006. **101**(2): p. 343-50.
35. Gurudu, S.R. and F.C. Ramirez, *Quality measurement and improvement in colonoscopy*. Techniques in Gastrointestinal Endoscopy, 2012. **14**(1): p. 21-28.
36. Singh, H., et al., *Colonoscopy and its complications across a Canadian regional health authority*. Gastrointest Endosc, 2009. **69**(3 Pt 2): p. 665-71.
37. Rex, D.K., et al., *Quality indicators for colonoscopy*. Gastrointest Endosc, 2006. **63**(4 Suppl): p. S16-28.
38. Bowles, C.J.A., et al., *A prospective study of colonoscopy practice in the UK today: are we adequately prepared for national colorectal cancer screening tomorrow?* Gut, 2004. **53**(2): p. 277-283.
39. Liberman, A.S., I. Shrier, and P.H. Gordon, *Injuries sustained by colorectal surgeons performing colonoscopy*. Surg Endosc, 2005. **19**(12): p. 1606-9.
40. Chung, Y.W., et al., *Patient factors predictive of pain and difficulty during sedation-free colonoscopy: a prospective study in Korea*. Dig Liver Dis, 2007. **39**(9): p. 872-6.
41. Committee, A.S.o.P., et al., *Complications of colonoscopy*. Gastrointest Endosc, 2011. **74**(4): p. 745-52.
42. Denis, B., et al., *Harms of colonoscopy in a colorectal cancer screening programme with faecal occult blood test: a population-based cohort study*. Dig Liver Dis, 2013. **45**(6): p. 474-80.
43. Navaneethan, U., et al., *Prevalence and risk factors for colonic perforation during colonoscopy in hospitalized inflammatory bowel disease patients*. J Crohns Colitis, 2011. **5**(3): p. 189-95.

44. Korman, L.Y., et al., *Characterization of forces applied by endoscopists during colonoscopy by using a wireless colonoscopy force monitor*. *Gastrointest Endosc*, 2010. **71**(2): p. 327-34.
45. Leung, F.W., et al., *A proof-of-principle, prospective, randomized, controlled trial demonstrating improved outcomes in scheduled unsedated colonoscopy by the water method*. *Gastrointest Endosc*, 2010. **72**(4): p. 693-700.
46. Pohl, J., et al., *Water infusion for cecal intubation increases patient tolerance, but does not improve intubation of unsedated colonoscopies*. *Clin Gastroenterol Hepatol*, 2011. **9**(12): p. 1039-43 e1.
47. Leung, F.W., et al., *Water-aided colonoscopy: a systematic review*. *Gastrointest Endosc*, 2012. **76**(3): p. 657-66.
48. Ransibrahmanakul, K., et al., *Comparative Effectiveness of Water vs. Air Methods in Minimal Sedation Colonoscopy Performed by Supervised Trainees in the US - Randomized Controlled Trial*. *American Journal of Clinical Medicine*, 2010. **7**(3): p. 113-118.
49. Leung, J., et al., *A randomized, controlled trial to confirm the beneficial effects of the water method on U.S. veterans undergoing colonoscopy with the option of on-demand sedation*. *Gastrointest Endosc*, 2011. **73**(1): p. 103-10.
50. Friedland, S., T. Kaltenbach, and R. Soetikno, *Use of The Double Balloon Enteroscope System to Complete Incomplete Colonoscopy*. *Techniques in Gastrointestinal Endoscopy*, 2008. **10**(3): p. 124-127.
51. Lee, D.W., et al., *Use of a variable-stiffness colonoscope decreases the dose of patient-controlled sedation during colonoscopy: a randomized comparison of 3 colonoscopes*. *Gastrointest Endosc*, 2007. **65**(3): p. 424-9.
52. Hewett, D.G. and D.K. Rex, *Cap-fitted colonoscopy: a randomized, tandem colonoscopy study of adenoma miss rates*. *Gastrointest Endosc*, 2010. **72**(4): p. 775-81.
53. DeMarco, D.C., et al., *Impact of experience with a retrograde-viewing device on adenoma detection rates and withdrawal times during colonoscopy: the Third Eye Retroscope study group*. *Gastrointest Endosc*, 2010. **71**(3): p. 542-50.
54. Ng, W.S., et al., *Development of a Robotic Colonoscope*. *Digestive Endoscopy*, 2000. **12**: p. 131 - 135.
55. Kim, B., et al., *Inchworm-like colonoscopic robot with hollow body and steering device*. *Jsm International Journal Series C-Mechanical Systems Machine Elements and Manufacturing*, 2006. **49**(1): p. 205-212.
56. Vucelic, B., et al., *The aer-o-scope: proof of concept of a pneumatic, skill-independent, self-propelling, self-navigating colonoscope*. *Gastroenterology*, 2006. **130**(3): p. 672-7.
57. Groth, S., et al., *High cecal intubation rates with a new computer-assisted colonoscope: a feasibility study*. *Am J Gastroenterol*, 2011. **106**(6): p. 1075-80.
58. Hawes, R.H., *Endoscopic innovations*. *Gastrointest Endosc*, 2013. **78**(3): p. 410-3.
59. Menciassi, A., M. Quirini, and P. Dario, *Microrobotics for future gastrointestinal endoscopy*. *Minim Invasive Ther Allied Technol*, 2007. **16**(2): p. 91-100.
60. Van Gossum, A., et al., *Capsule Endoscopy versus Colonoscopy for the Detection of Polyps and Cancer*. *New England Journal of Medicine*, 2009. **361**(3): p. 264-270.
61. Ciuti, G., A. Menciassi, and P. Dario, *Capsule Endoscopy: From Current Achievements to Open Challenges*. *Biomedical Engineering, IEEE Reviews in*, 2011. **4**: p. 59-72.
62. Arezzo, A., et al., *Experimental assessment of a novel robotically-driven endoscopic capsule compared to traditional colonoscopy*. *Dig Liver Dis*, 2013. **45**(8): p. 657-62.
63. Kassim, I., et al., *Locomotion techniques for robotic colonoscopy*. *Ieee Engineering in Medicine and Biology Magazine*, 2006. **25**(3): p. 49-56.

64. Carta, R., et al., *Wireless powering for a self-propelled and steerable endoscopic capsule for stomach inspection*. Biosens Bioelectron, 2009. **25**(4): p. 845-51.
65. Kennedy, G.C. and J.K. Holt. *Developing a high efficiency means of propulsion for underwater vehicles*. in *Southcon/95. Conference Record*. 1995.
66. Holt, J.K. and D.G. White. *High efficiency, counter-rotating ring thruster for underwater vehicles*. in *Autonomous Underwater Vehicle Technology, 1994. AUV '94., Proceedings of the 1994 Symposium on*. 1994.
67. Chen, B., et al., *Research on the Kinematic Properties of a Sperm-Like Swimming Micro Robot*. Journal of Bionic Engineering, 2010. **7**: p. S123-S129.
68. Ha, N.S. and N.S. Goo, *Propulsion Modeling and Analysis of a Biomimetic Swimmer*. Journal of Bionic Engineering, 2010. **7**(3): p. 259-266.
69. Mazumdar, A., et al. *A compact, maneuverable, underwater robot for direct inspection of nuclear power piping systems*. in *Robotics and Automation (ICRA), 2012 IEEE International Conference on*. 2012.
70. Korde, U.A., *Study of a jet-propulsion method for an underwater vehicle*. Ocean Engineering, 2004. **31**(10): p. 1205-1218.
71. Mohseni, K., *Pulsatile vortex generators for low-speed maneuvering of small underwater vehicles*. Ocean Engineering, 2006. **33**(16): p. 2209-2223.
72. Polsenberg-Thomas, A.M., J. Burdick, and K. Mohseni. *An experimental study of voice-coil driven synthetic jet propulsion for underwater vehicles*. in *OCEANS, 2005. Proceedings of MTS/IEEE*. 2005.
73. Shuxiang, G., et al. *Underwater Swimming Micro Robot Using IPMC Actuator*. in *Mechatronics and Automation, Proceedings of the 2006 IEEE International Conference on*. 2006.
74. Wang, Z., et al., *A micro-robot fish with embedded SMA wire actuated flexible biomimetic fin*. Sensors and Actuators A: Physical, 2008. **144**(2): p. 354-360.
75. Takagi, K., et al. *Development of a Rajiform Swimming Robot using Ionic Polymer Artificial Muscles*. in *Intelligent Robots and Systems, 2006 IEEE/RSJ International Conference on*. 2006.
76. Kosa, G., M. Shoham, and M. Zaaroor. *Analysis of a Swimming Micro Robot*. in *Biomedical Robotics and Biomechatronics, 2006. BioRob 2006. The First IEEE/RAS-EMBS International Conference on*. 2006.
77. Carta, R., et al., *A multi-coil inductive powering system for an endoscopic capsule with vibratory actuation*. Sensors and Actuators A: Physical, 2011. **172**(1): p. 253-258.
78. Hong, D.W., M. Ingram, and D. Lahr, *Whole Skin Locomotion Inspired by Amoeboid Motility Mechanisms*. Journal of Mechanisms and Robotics, 2009. **1**(1): p. 011015.
79. Sliker, L.J., et al., *Surgical evaluation of a novel tethered robotic capsule endoscope using micro-patterned treads*. Surg Endosc, 2012. **26**(10): p. 2862-9.
80. Young-Sik, K., et al. *Design and motion planning of a two-moduled indoor pipeline inspection robot*. in *Robotics and Automation, 2008. ICRA 2008. IEEE International Conference on*. 2008.
81. Jungwan, P., K. Taehyun, and Y. Hyunseok. *Development of an actively adaptable in-pipe robot*. in *Mechatronics, 2009. ICM 2009. IEEE International Conference on*. 2009.
82. Liu, Q., T. Ren, and Y. Chen, *Characteristic analysis of a novel in-pipe driving robot*. Mechatronics, 2013. **23**(4): p. 419-428.
83. Lambrecht, B.G.A., A.D. Horchler, and R.D. Quinn. *A Small, Insect-Inspired Robot that Runs and Jumps*. in *Robotics and Automation, 2005. ICRA 2005. Proceedings of the 2005 IEEE International Conference on*. 2005.
84. Kim, Y.T. and D.E. Kim, *Novel Propelling Mechanisms Based on Frictional Interaction for Endoscope Robot*. Tribology Transactions, 2010. **53**(2): p. 203-211.

85. Crespi, A. and A.J. Ijspeert, *Online Optimization of Swimming and Crawling in an Amphibious Snake Robot*. Robotics, IEEE Transactions on, 2008. **24**(1): p. 75-87.
86. Dario, P., et al., *Modeling and Experimental Validation of the Locomotion of Endoscopic Robots in the Colon*. The International Journal of Robotics Research, 2004. **23**(4): p. 549-556.
87. Phee, L., et al., *Analysis and development of locomotion devices for the gastrointestinal tract*. Biomedical Engineering, IEEE Transactions on, 2002. **49**(6): p. 613-616.
88. Kundong, W., et al. *Squirm robot with full bellow skin for colonoscopy*. in *Robotics and Biomimetics (ROBIO), 2010 IEEE International Conference on*. 2010.
89. Karagozler, M.E., et al. *Miniature Endoscopic Capsule Robot using Biomimetic Micro-Patterned Adhesives*. in *Biomedical Robotics and Biomechanics, 2006. BioRob 2006. The First IEEE/RAS-EMBS International Conference on*. 2006.
90. Stefanini, C., *Modeling and Experiments on a Legged Microrobot Locomoting in a Tubular, Compliant and Slippery Environment*. The International Journal of Robotics Research, 2006. **25**(5-6): p. 551-560.
91. Weida, L., et al. *A Novel Locomotion Principle for Endoscopic Robot*. in *Mechatronics and Automation, Proceedings of the 2006 IEEE International Conference on*. 2006.
92. Quirini, M., et al. *Design of a Pill-Sized 12-legged Endoscopic Capsule Robot*. in *Robotics and Automation, 2007 IEEE International Conference on*. 2007.
93. Kim, H.M., et al., *Active locomotion of a paddling-based capsule endoscope in an in vitro and in vivo experiment (with videos)*. Gastrointest Endosc, 2010. **72**(2): p. 381-7.
94. Heijnsdijk, E.A., et al., *Inter- and intraindividual variabilities of perforation forces of human and pig bowel tissue*. Surg Endosc, 2003. **17**(12): p. 1923-6.
95. Moshkowitz, M., et al., *A novel device for rapid cleaning of poorly prepared colons*. Endoscopy, 2010. **42**(10): p. 834-6.
96. Lee, S.H., et al., *An optimal micropatterned end-effector for enhancing frictional force on large intestinal surface*. ACS Appl Mater Interfaces, 2010. **2**(5): p. 1308-16.
97. Paparo, F., et al., *Computed tomography of the bowel: a prospective comparison study between four techniques*. Eur J Radiol, 2013. **82**(1): p. e1-e10.
98. Gao, P., et al., *Microgroove cushion of robotic endoscope for active locomotion in the gastrointestinal tract*. Int J Med Robot, 2012. **8**(4): p. 398-406.
99. Buselli, E., et al., *Evaluation of friction enhancement through soft polymer micro-patterns in active capsule endoscopy*. Measurement Science and Technology, 2010. **21**(10): p. 105802.
100. Dodou, D., P. Breedveld, and P.A. Wieringa, *Mucoadhesives in the gastrointestinal tract: revisiting the literature for novel applications*. Eur J Pharm Biopharm, 2005. **60**(1): p. 1-16.
101. Smart, J.D., *The basics and underlying mechanisms of mucoadhesion*. Adv Drug Deliv Rev, 2005. **57**(11): p. 1556-68.
102. Dodou, D., et al., *Mucoadhesive films inside the colonic tube: performance in a three-dimensional world*. J R Soc Interface, 2008. **5**(28): p. 1353-62.
103. Dodou, D., P. Breedveld, and P.A. Wieringa, *Stick, unstick, restick sticky films in the colon*. Minim Invasive Ther Allied Technol, 2006. **15**(5): p. 286-95.
104. Dodou, D., P. Breedveld, and P.A. Wieringa, *Friction manipulation for intestinal locomotion*. Minim Invasive Ther Allied Technol, 2005. **14**(3): p. 188-97.
105. Tramacere, F., et al., *The morphology and adhesion mechanism of Octopus vulgaris suckers*. PLoS One, 2013. **8**(6): p. e65074.
106. Ge, D., et al., *Quantitative study on the attachment and detachment of a passive suction cup*. Vacuum, 2015. **116**: p. 13-20.

107. Patronik, N.A., et al. *Improved Traction for a Mobile Robot Traveling on the Heart*. in *2006 International Conference of the IEEE Engineering in Medicine and Biology Society*. 2006.
108. Lyle, A.B., J.T. Luftig, and M.E. Rentschler, *A tribological investigation of the small bowel lumen surface*. *Tribology International*, 2013. **62**: p. 171-176.
109. Egorov, V.I., et al., *Mechanical properties of the human gastrointestinal tract*. *Journal of Biomechanics*, 2002. **35**(10): p. 1417-1425.
110. Christensen, M.B., K. Oberg, and J.C. Wolchok, *Tensile properties of the rectal and sigmoid colon: a comparative analysis of human and porcine tissue*. Springerplus, 2015. **4**: p. 142.
111. Higa, M., et al., *Passive mechanical properties of large intestine under in vivo and in vitro compression*. *Med Eng Phys*, 2007. **29**(8): p. 840-4.
112. Shamsuddin, A.M., P.C. Phelps, and B.F. Trump, *Human Large Intestinal Epithelium - Light-Microscopy, Histochemistry, and Ultrastructure*. *Human Pathology*, 1982. **13**(9): p. 790-803.
113. Cone, R.A., *Barrier properties of mucus*. *Adv Drug Deliv Rev*, 2009. **61**(2): p. 75-85.
114. Gustafsson, J.K., et al., *An ex vivo method for studying mucus formation, properties, and thickness in human colonic biopsies and mouse small and large intestinal explants*. *Am J Physiol Gastrointest Liver Physiol*, 2012. **302**(4): p. G430-8.
115. Lai, S.K., et al., *Micro- and macrorheology of mucus*. *Adv Drug Deliv Rev*, 2009. **61**(2): p. 86-100.
116. Finkelstone, L., E. Wolf, and M.W. Stein, *Etiology of small bowel thickening on computed tomography*. *Canadian Journal of Gastroenterology*, 2012. **26**(12): p. 897-901.
117. Kim, D.E. and Y.T. Kim, *Biotribological investigation of a multi-tube foot for traction generation in a medical microrobot*. *Proceedings of the Institution of Mechanical Engineers, Part H: Journal of Engineering in Medicine*, 2009. **223**(6): p. 677-686.
118. Atuma, C., et al., *The adherent gastrointestinal mucus gel layer: thickness and physical state in vivo*. *American Journal of Physiology-Gastrointestinal and Liver Physiology*, 2001. **280**(5): p. G922-G929.
119. Kim, J.S., et al., *Experimental investigation of frictional and viscoelastic properties of intestine for microendoscope application*. *Tribology Letters*, 2006. **22**(2): p. 143-149.
120. Lyle, A.B., et al., *Preliminary Friction Force Measurements on Small Bowel Lumen When Eliminating Sled Edge Effects*. *Tribology Letters*, 2013. **51**(3): p. 377-383.
121. Zhang, C., et al., *Modeling of Velocity-dependent Frictional Resistance of a Capsule Robot Inside an Intestine*. *Tribology Letters*, 2012. **47**(2): p. 295-301.
122. Accoto, D., et al. *Measurements of the frictional properties of the gastrointestinal tract*. in *World Tribology Congress*. 2001.
123. Chen, H., et al., *Bioinspired Surface for Surgical Graspers Based on the Strong Wet Friction of Tree Frog Toe Pads*. *ACS Appl Mater Interfaces*, 2015. **7**(25): p. 13987-95.
124. Barnes, W.J., et al., *Elastic modulus of tree frog adhesive toe pads*. *J Comp Physiol A Neuroethol Sens Neural Behav Physiol*, 2011. **197**(10): p. 969-78.
125. Varenberg, M. and S.N. Gorb, *Hexagonal Surface Micropattern for Dry and Wet Friction*. *Advanced Materials*, 2009. **21**(4): p. 483-486.
126. Drotlef, D.M., et al., *Morphological studies of the toe pads of the rock frog, *Staurois parvus* (family: Ranidae) and their relevance to the development of new biomimetically inspired reversible adhesives*. *Interface Focus*, 2015. **5**(1): p. 20140036.
127. Drotlef, D.-M., et al., *Insights into the Adhesive Mechanisms of Tree Frogs using Artificial Mimics*. *Advanced Functional Materials*, 2013. **23**(9): p. 1137-1146.
128. Iturri, J., et al., *Torrent Frog-Inspired Adhesives: Attachment to Flooded Surfaces*. *Advanced Functional Materials*, 2015. **25**(10): p. 1499-1505.

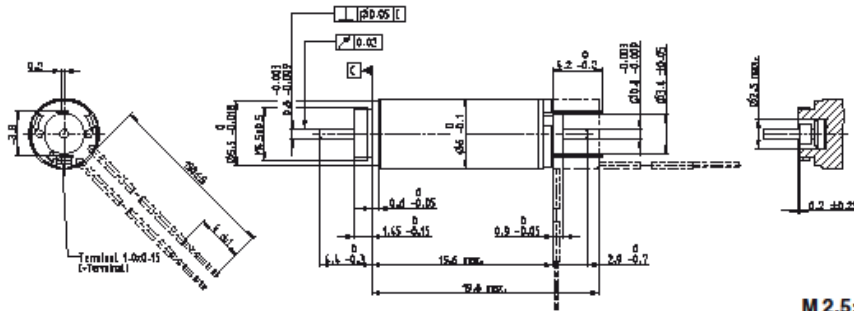
129. Murarash, B., Y. Itovich, and M. Varenberg, *Tuning elastomer friction by hexagonal surface patterning*. *Soft Matter*, 2011. **7**(12): p. 5553.
130. Persson, B.N.J., *Wet adhesion with application to tree frog adhesive toe pads and tires*. *Journal of Physics: Condensed Matter*, 2007. **19**(37): p. 376110.
131. Cho, J.R., et al., *Numerical investigation of hydroplaning characteristics of three-dimensional patterned tire*. *European Journal of Mechanics - A/Solids*, 2006. **25**(6): p. 914-926.
132. Fwa, T., et al., *Effectiveness of Tire-Tread Patterns in Reducing the Risk of Hydroplaning*. *Transportation Research Record: Journal of the Transportation Research Board*, 2009. **2094**: p. 91-102.
133. Persson, B.N.J., et al., *Rubber friction on wet and dry road surfaces: The sealing effect*. *Physical Review B*, 2005. **71**(3).
134. Gupta, R. and J. Frechette, *Measurement and scaling of hydrodynamic interactions in the presence of draining channels*. *Langmuir*, 2012. **28**(41): p. 14703-12.
135. Glass, P., E. Cheung, and M. Sitti, *A legged anchoring mechanism for capsule endoscopes using micropatterned adhesives*. *IEEE Trans Biomed Eng*, 2008. **55**(12): p. 2759-67.
136. Majidi, C., *Soft robotics: a perspective—current trends and prospects for the future*. *Soft Robotics*, 2014. **1**(1): p. 5-11.
137. Yoshida, H., Y. Morita, and K. Ikeuchi, *Biological lubrication of hydrated surface layer in small intestine*. *Tribol. Interface Eng. Ser.: Tribol. Res. Des. Eng. Syst*, 2003. **41**: p. 425-428.
138. Gong, J.P., *Friction and lubrication of hydrogels—its richness and complexity*. *Soft Matter*, 2006. **2**(7): p. 544-552.
139. Kararli, T.T., *Comparison of the gastrointestinal anatomy, physiology, and biochemistry of humans and commonly used laboratory animals*. *Biopharmaceutics & Drug Disposition*, 1995. **16**(5): p. 351-380.
140. Olakanmi, E.O., R.F. Cochrane, and K.W. Dalgarno, *A review on selective laser sintering/melting (SLS/SLM) of aluminium alloy powders: Processing, microstructure, and properties*. *Progress in Materials Science*, 2015. **74**: p. 401-477.
141. Rentschler, M.E., S.M. Farritor, and K.D. Iagnemma, *Mechanical Design of Robotic In Vivo Wheeled Mobility*. *Journal of Mechanical Design*, 2007. **129**(10): p. 1037.
142. Heijnsdijk, E.A.M., et al., *Slip and damage properties of jaws of laparoscopic graspers*. *Surgical Endoscopy and Other Interventional Techniques*, 2004. **18**(6): p. 974-979.
143. Tur, J.M.M. and W. Garthwaite, *Robotic devices for water main in-pipe inspection: A survey*. *Journal of Field Robotics*, 2010. **27**(4): p. 491-508.
144. Majidi, C., *Soft Robotics: A Perspective—Current Trends and Prospects for the Future*. *Soft Robotics*, 2013. **1**(P): p. 5-11.
145. Kim, S., C. Laschi, and B. Trimmer, *Soft robotics: a bioinspired evolution in robotics*. *Trends Biotechnol*, 2013. **31**(5): p. 287-94.
146. Pfeifer, R., M. Lungarella, and F. Iida, *The challenges ahead for bio-inspired 'soft' robotics*. *Communications of the ACM*, 2012. **55**(11): p. 76.
147. Lin, H.T., G.G. Leisk, and B. Trimmer, *GoQBot: a caterpillar-inspired soft-bodied rolling robot*. *Bioinspir Biomim*, 2011. **6**(2): p. 026007.
148. Shepherd, R.F., et al., *Multigait soft robot*. *Proceedings of the National Academy of Sciences*, 2011. **108**(51): p. 20400-20403.
149. Ying, S., et al., *Variable Stiffness Structures Utilizing Fluidic Flexible Matrix Composites*. *Journal of Intelligent Material Systems and Structures*, 2008. **20**(4): p. 443-456.

150. Jiang, A., et al. *Design of a variable stiffness flexible manipulator with composite granular jamming and membrane coupling*. in *Intelligent Robots and Systems (IROS), 2012 IEEE/RSJ International Conference on*. 2012.
151. Yong-Jae, K., et al., *A Novel Layer Jamming Mechanism With Tunable Stiffness Capability for Minimally Invasive Surgery*. *Robotics, IEEE Transactions on*, 2013. **29**(4): p. 1031-1042.
152. Wagner, N.J. and J.F. Brady, *Shear thickening in colloidal dispersions*. *Physics Today*, 2009. **62**(10): p. 27-32.
153. Kuder, I.K., et al., *Variable stiffness material and structural concepts for morphing applications*. *Progress in Aerospace Sciences*, 2013. **63**: p. 33-55.
154. Stokes, A.A., et al., *A Hybrid Combining Hard and Soft Robots*. *Soft Robotics*, 2014. **1**(1): p. 70-74.
155. Laschi, C., et al., *Soft Robot Arm Inspired by the Octopus*. *Advanced Robotics*, 2012. **26**(7): p. 709-727.

APPENDIX A: DC motor and gearbox data sheets

maxon DC motor

RE 6 Ø6 mm, Precious Metal Brushes, 0.3 Watt



M 2.5:1

- Stock program
- Standard program
- Special program (on request)

Part Numbers

B with cables
A with terminals

386790	386781	386782	386783
349180	349190	349191	349192

Motor Data

Values at nominal voltage		1.5	3	4.5	6	
1	Nominal voltage	V	1.5	3	4.5	6
2	No load speed	rpm	18500	18600	18600	18600
3	No load current	mA	42.6	21.3	14.2	10.7
4	Nominal speed	rpm	4680	5670	5400	5340
5	Nominal torque (max. continuous torque)	mNm	0.302	0.324	0.318	0.316
6	Nominal current (max. continuous current)	A	0.453	0.342	0.158	0.118
7	Stall torque	mNm	0.419	0.485	0.469	0.465
8	Starting current	A	0.581	0.336	0.217	0.161
9	Max. efficiency	%	54	57	56	56
Characteristics						
10	Terminal resistance	Ω	2.58	8.92	20.8	37.2
11	Terminal inductance	mH	0.0227	0.0907	0.204	0.363
12	Torque constant	mNm/A	0.72	1.44	2.16	2.88
13	Speed constant	rpm/V	13300	6630	4420	3310
14	Speed / torque gradient	rpm/mNm	47500	41000	42400	42700
15	Mechanical time constant	ms	7.45	7.19	7.24	7.24
16	Rotor inertia	gcm ²	0.015	0.0167	0.0163	0.0162

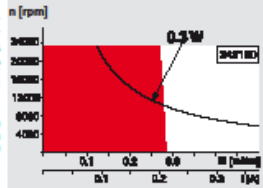
Specifications

- Thermal data**
- 17 Thermal resistance housing-ambient 77 K/W
 - 18 Thermal resistance winding-housing 16.2 K/W
 - 19 Thermal time constant winding 1.39 s
 - 20 Thermal time constant motor 16.3 s
 - 21 Ambient temperature -20...+65°C
 - 22 Max. permissible winding temperature +85°C
- Mechanical data (sleeve bearings)**
- 23 Max. permissible speed 23000 rpm
 - 24 Axial play 0.02 - 0.1 mm
 - 25 Radial play 0.012 mm
 - 26 Max. axial load (dynamic) 0.15 N
 - 27 Max. force for press fits (static) 10 N
 - 28 Max. radial load, 4 mm from flange 0.6 N

- Other specifications**
- 29 Number of pole pairs 5
 - 30 Number of commutator segments 5
 - 31 Weight of motor 2.3 g

Values listed in the table are nominal.
Explanation of the figures on page 70.

Operating Range



Comments

- Continuous operation
In observation of above listed thermal resistance (lines 17 and 18) the maximum permissible winding temperature will be reached during continuous operation at 25°C ambient.
- Thermal limit.
- Short term operation
The motor may be briefly overloaded (recurring).
- Assigned power rating

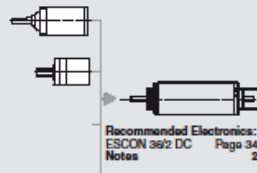
maxon Modular System

Overview on page 20-25

- 1 Planetary Gearhead
- 2.3 g

Ø6 mm
0.002 - 0.03 Nm
Page 242

Spindle Drive
Ø6 mm
Page 293



Recommended Electronics:
ESCON 36/2 DC Page 342
Notes 22

APPENDIX B: 3D printer resin (LS600) data sheet



Perfactory® Material



LS600

EnvisionTEC's LS600 is for use in producing very accurate parts with high feature detail on EnvisionTEC's 3D printers. With added stability and surface quality, this material produces parts with high impact resistance similar to thermoplastics. Tough, complex parts can be built with a superb surface quality compared with competing technologies. LS600 provides superb detail without sacrificing speed or durability and has the best overall mechanical stability over time. It provides considerable processing latitude and is ideal for markets that demand accurate RTV patterns, durable concept models, highly accurate parts, and humidity and temperature resistant parts.

Mechanical Properties*		
ASTM Method	Description	LS600
D638M	Tensile Modulus	1,800 MPa
	Tensile Strength at Break	60 MPa
	Elongation at Break	4.39%
D2240	Hardness (Shore D)	85
D256A	Izod Impact (Notched)	0.63 J/cm ³
Thermal and Electrical Properties		
ASTM Method	Description	LS600
E1545-00	Glass Transition Temperature	61°C
D648	HDT @ 0.46 MPa	57°C
	HDT @ 1.81 MPa	48°C
Physical Properties		
Description	LS600	
Appearance	Opaque yellow-beige	
Viscosity	140 cP at 30°	
Density	1.10 g/cm ³	

*All data provided is preliminary data and must be verified by the individual user.

Recommended Machines
Desktop XL, Perfactory® 4 Standard, Perfactory® 4 Standard XL, Perfactory® 4 Mini XL, Perfactory® 4 Mini, Perfactory® 3 Mini Multi Lens

Applications
MCAD

EnvisionTEC GmbH
 Brüsseler Straße 51 • D-45968
 Gladbeck • Germany
 Phone +49 2043 9875-0
 Fax +49 2043 9875-99

EnvisionTEC, Inc.
 15162 S. Commerce Dr.
 Dearborn, MI 48120 • USA
 Phone +1-313-436-4300
 Fax +1-313-436-4303

envisiontec.com
 info@envisiontec.com



APPENDIX C: Calculations for the tissue tension during traction tests

Longitudinal stress (thin walled)

Tissue dimensions: mean thickness of 1 mm; mean diameter of 28.7 mm (width once cut of ca. 90 mm).

Colonoscopy intraluminal pressure: 22 mmHg = 0.00293 MPa

$$\sigma_L = \frac{P \cdot D}{4 \cdot t} \quad (1)$$

$$F_L = \sigma_L \cdot A \quad (2)$$

σ_L is the longitudinal stress, P is the intraluminal pressure, D is the diameter, t is the tissue thickness, F_L is the longitudinal force and A is the cross-sectional area of the tissue sample.

The cross-sectional area (A) is ca. 90 mm², therefore the longitudinal force is calculated as 1.89 N or ca. 193 gf.

APPENDIX D: An alternative, soft robotic locomotion concept

Many of the challenges involved in developing a mobile colonoscopy robot such as RollerBall could be alleviated by reducing the overall complexity. One method of doing this is using soft materials that passively conform to the surroundings, reducing excessive localised regions of stress (trauma) and reducing the required control complexity. This “soft robotic” approach is explored in the subsequent pages.

D.1. Soft robotics

The area of bio-inspired soft robotics has achieved considerable research interest over the last few years. To date, the majority of robots have been designed to have strong, stiff bodies in order to achieve precise movements and to transmit high loads efficiently. With an ever increasing number of robotic devices coming into contact with humans, both *ex vivo* and *in vivo*, biocompatibility has become increasingly important. As a result, the conventional stiff-

bodied robots are being considered less and less suitable for the interaction with the relatively soft tissues of the human body as they tend to have rigidity 3 to 10 orders of magnitude higher than the biological tissue (Figure A.D.1). This understandably introduces issues with safety as the high rigidity materials apply high contact pressures on the soft tissue [144, 145].

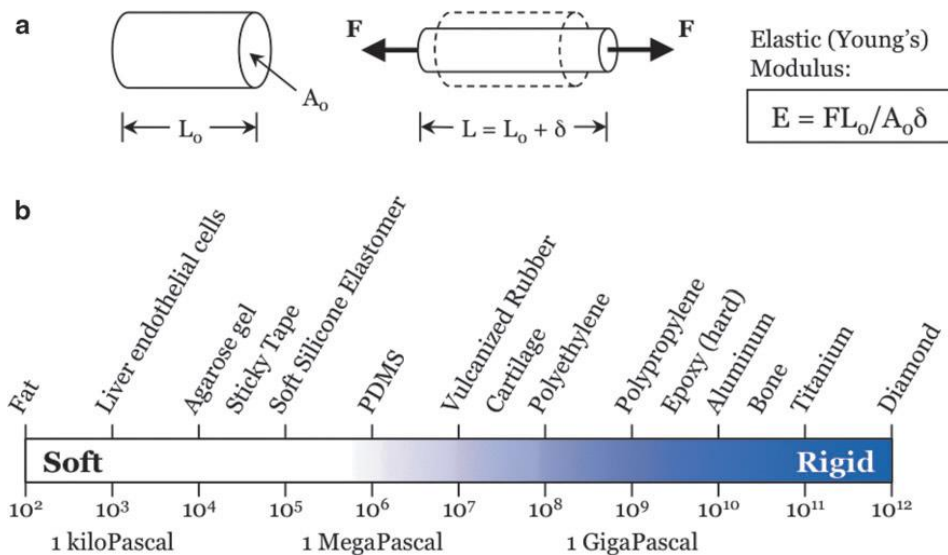


Figure A.D.1 – A range of elastic moduli of several common materials. [144]

Usually through an investigation of the animal world, soft robotics not only aims to provide devices with the means of safely interacting with sensitive tissue but also the means of traversing the unpredictable and unstructured environment of the human body. It does this by “exploiting the ‘mechanical intelligence’ of soft materials” [145]. Soft robots can be built with a minimum number of actuators, relying on the morphology and “intelligence” of the smart materials. This reduction in actuators and relying on passive elements has a positive effect on the simplicity and robustness of such a device [146]. More specifically, a robot with soft components has the following primary advantages [145]:

- Having a body that can deform and re-shape itself to access varying apertures.
- The ability to conform to surfaces, thus distributing load over a larger area and increasing contact time. This ultimately lowers the force exerted on the surrounding surfaces and the consequent probability of tissue damage.
- The soft components often result in a more robust mechanism that can absorb and adapt to unexpected loads.

Two examples of soft robots are shown in Figures A.D.2 & A.D.3.

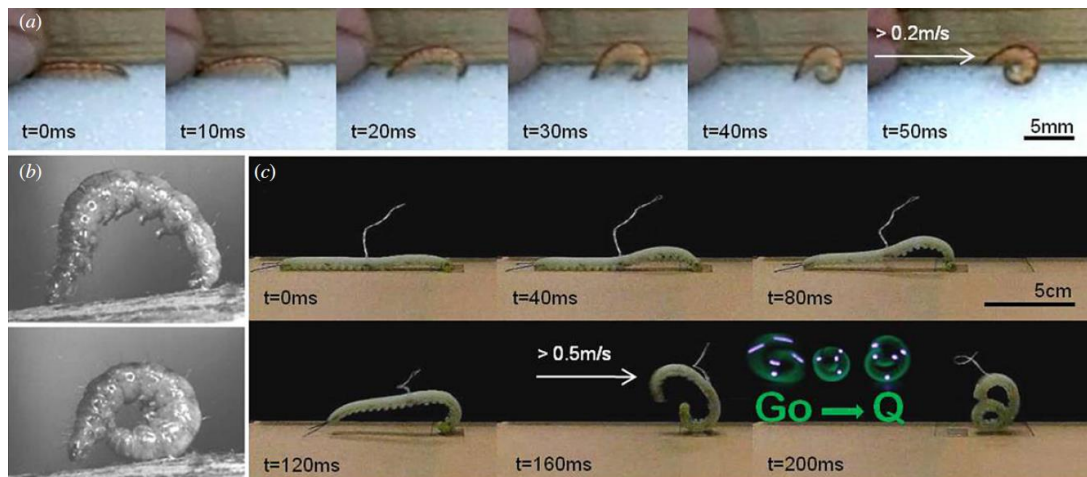


Figure A.D.2 – Example #1 of a soft robot (GoQBot). [147]

GoQBot is a soft, caterpillar like robot that uses shape memory alloy actuators to alter its shape.

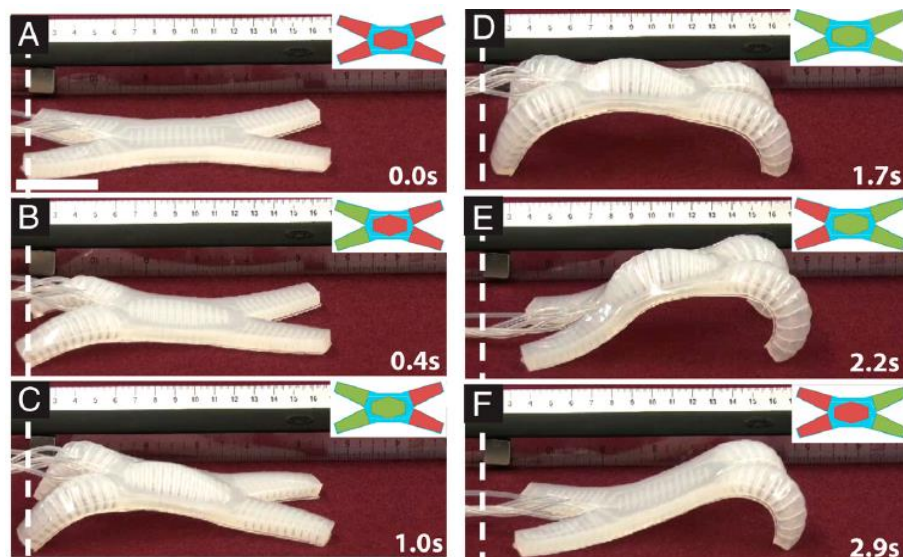


Figure A.D.3 – Example 2 of a soft, multi-gait robot. [148]

The “Multi-gait” device shown above is made out of soft, silicone-like materials. It uses a pneumatic channel design based on the “pneu-net” architecture. Pressurized air is forced into different segments of the device to actuate its limbs.

A device designed using soft robotic principles would clearly have an advantage in the sensitive, complex and overall challenging environment of a fluid distended colon. However, in nature, soft bodied animals are predominantly small, highlighting two limitations with soft robotics, namely: body weight is not easily supported without a rigid skeleton and the

flexibility of the soft components prevents the exerting of large forces. The first limitation may not be of concern to a hydro-colonoscopy device as it will be both small and supported by the fluid medium⁶⁸. The second limitation suggests the need for the use of composite materials, both flexible and rigid. A promising solution is the use of *variable compliant* materials. This involves the use of smart materials that can vary their stiffness, changing from a rigid state when transmitting load, to a flexible state when interacting with sensitive surfaces (or other conditions where deformation is required).

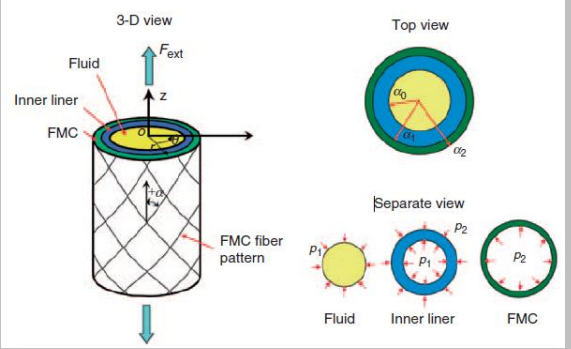
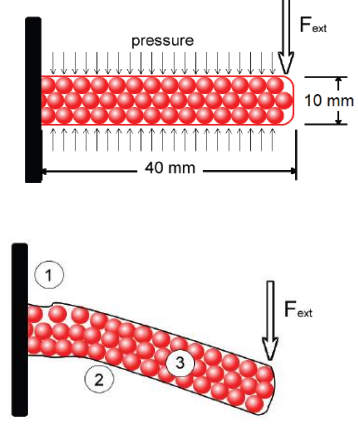

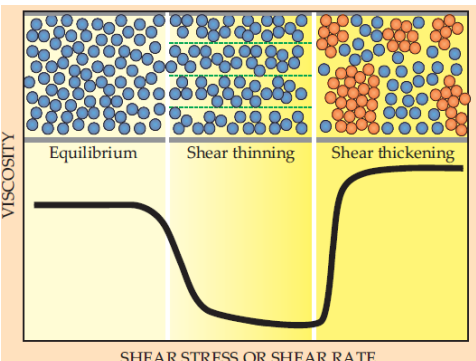
D.1.2. Variable compliance

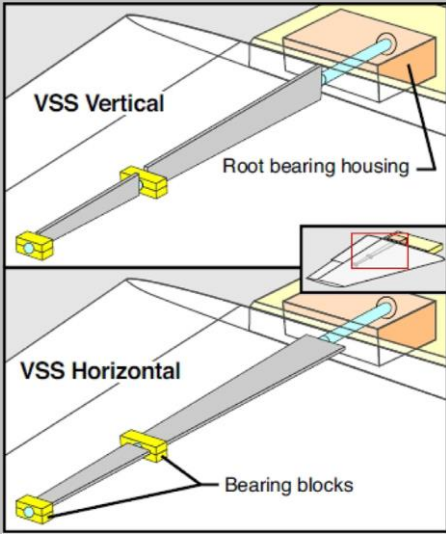

The material selection for soft robotics is crucial. During forward propulsion, when a force is being applied to the tissue by the device, the propulsion mechanism of the robot needs to be in a sufficiently rigid state so that the force can be transmitted efficiently. Too flexible and excessive deformation will ensue. However, as previously mentioned, any device that comes into contact with tissue should ideally be soft and deformable to ensure biocompatibility. To attain sufficient biocompatibility, the principle of '*Compliance matching*' should therefore be used.

This principle states that materials contacting each other should have a similar compliance/rigidity so that forces are evenly distributed and interfacial stress concentrations are kept to a minimum [144]. The additional requirement of increased stiffness for the transmitting of force suggests the need for a material that can significantly and dynamically alter its modulus/stiffness. Table A.D.1 shows some of the methods and materials used to achieve this:

⁶⁸ In the natural world, soft-bodied squid have been able to increase their size due to the support of the surrounding water.

Table A.D.1 – Some methods of achieving variable compliance.

Method	Description
<p>Pressurized air/liquid (Fluidic flexible matrix composites)</p> 	<p>This consists of a flexible inner tube surrounded by a matrix of high performance fibres (such as carbon). Controlling the flow of a fluid within the tube, using valves, allows control of the tube's stiffness. A closed valve results in a stiff structure as the incompressible fluid supports the tube [149].</p>
<p>Granular jamming</p> 	<p>A flexible tube is filled with granules. While at atmospheric pressure, the tube is loosely surrounding the granules. The granules are therefore free to move and a low stiffness results. Creating a vacuum within the flexible tube reduces the volume within it. This compresses the granules, forcing them together into a solid, stiff structure [150].</p>
<p>Scale jamming</p> 	<p>This is a similar mechanism to granular jamming. In this case, however, a series of interlocking scales are pressed together using an external force. This increases friction between the scales, reducing their ability to freely slide past each other thus increasing the overall stiffness [151]</p>
<p>Shear-thickening/thinning</p> 	<p>Shear thickening/thinning fluids consist of a fluid medium with a suspension of non-aggregating solid particles. The viscosity of the fluid is altered when exposed to a shear stress as the interaction of the particles changes [152].</p>

<p>Orientation dependent (Variable stiffness spar)</p> 	<p>This involves the exploiting of the mechanical properties of a beam. The cross-sectional shape results in direction dependent stiffness (dual stiffness: rigid state and flexible state). The beam can be easily rotated to switch between the two states [153].</p>
<p>Shape memory alloy (SMA)</p>	<p>Shape memory alloys have the ability to transition between two atomic configurations when heated above a certain transition temperature. This is often used to provide actuation but as the stiffness varies between the two states, it could be used for variable compliance applications [153].</p>
<p>Shape memory polymer (SMP)</p>  <p>www.crgp.com</p>	<p>As with SMAs, SMPs can be used in variable stiffness applications. They are more effective than SMAs for this application as they are said to have larger reversible strains. Furthermore, they can be customized to have a user defined glass transition temperature [153].</p>
<p>Low melting point metal</p>	<p>A metal with a low melting point could be used. A bismuth-based alloy, which contains indium, has a “sharp melting point.” The state of the metal (solid or liquid) could be changed depending on the stiffness requirement.</p>

It is clear that achieving variable compliance is possible and that there are a number of ways to do so. However, it is important to note that most methods require an external input, such as heat or pressure, which would add complexity to the device. If variable compliance is used it should be carefully chosen with biocompatibility in mind.

D.1.3. Soft actuators

A soft robot would require soft actuators. Biological muscles show some of the ideal attributes of a soft actuator: They have a high contraction ratio; they are efficient; they are intrinsically compliant and yet can smoothly adjust their stiffness to, for example, a high stiffness load-carrying/impact state [146]. A few soft actuators currently being used or researched are listed below:

- Dielectric elastomers.
- Ionic polymer metal composites (IPMC).
- Shape memory alloy (SMA).
- Shape memory polymer (SMP).
- Liquid crystal elastomers.
- Pressurized air/liquid (McKibben's muscles or bellows).

There are a large number of different soft actuators available suggesting that it may be possible to design a completely soft robot.

D.1.4. Summary

Soft robotics is an exciting area of research that focuses on the interaction of robotic devices with sensitive environments (such as the human body). A soft bodied device has a clear advantage for use in the colon, reducing the chance of tissue damage, increasing robustness and increasing adaptability without the need for advanced control. Material selection is crucial and is dependent on the function of each component. Some components can be permanently soft while others benefit from variable compliance. In the latter, there are a number of technologies available for this. There are also a number of soft actuators available which could increase the percentage of soft materials used in the device. While a completely "soft" device may have a biocompatibility advantage, a hybrid device could be more effective. Each component of the robot could be tailored to its specific use, with structural components made out of more rigid materials and components that contact the sensitive tissue out of soft materials. An example of this is shown in Figure A.D.4, where a rigid device is used to house the circuitry and the robotic gripper is made out of soft materials:

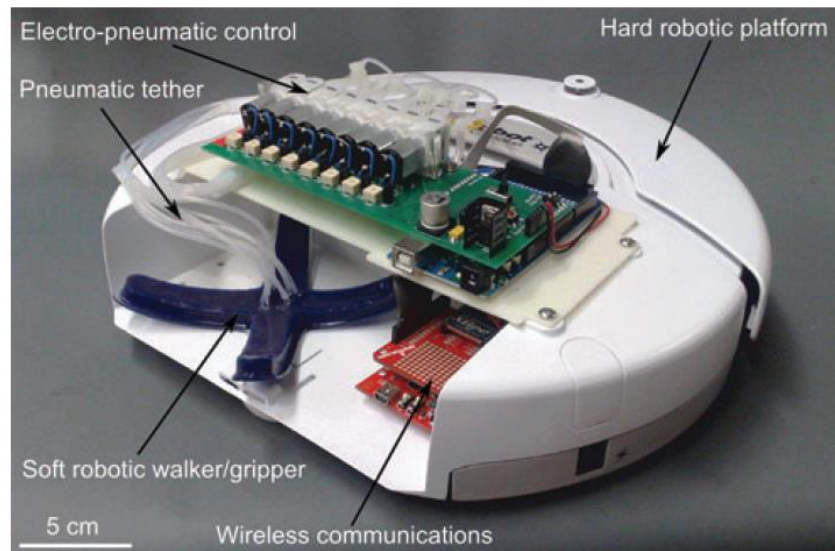


Figure A.D.4 – An example of a hybrid robotic device that uses both soft and rigid materials. [154]

D.2. Soft colonoscopy robot - Conceptual design

Octopuses have the remarkable ability to adapt to their surroundings. They highlight one of the many advantages of having a soft body that can adapt to the environment. An octopus-like device was therefore the starting point of the design. Octopus tentacles have a complex array of muscles, laid out in varying orientations, as shown in Figure A.D.5.

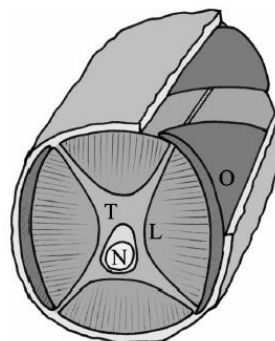


Figure A.D.5 – The basic muscle layout of an octopus tentacle. N – central nervous fibres, T – transverse muscles, L – longitudinal muscles and O – Oblique muscles. [155]

Work has been carried out by [155] to develop a robotic tentacle. The biological design was simplified to include fewer muscles (SMA actuators) and yet it remains a complex mechanism (Figure A.D.6).

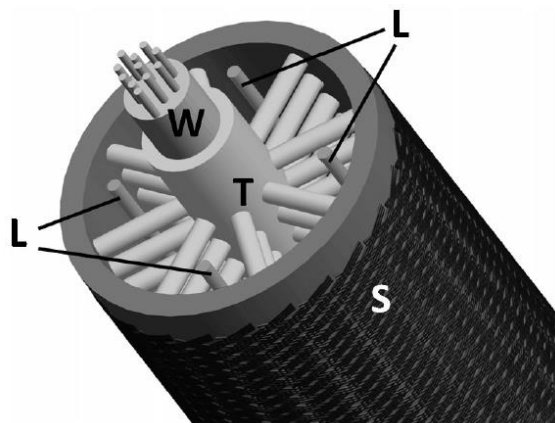
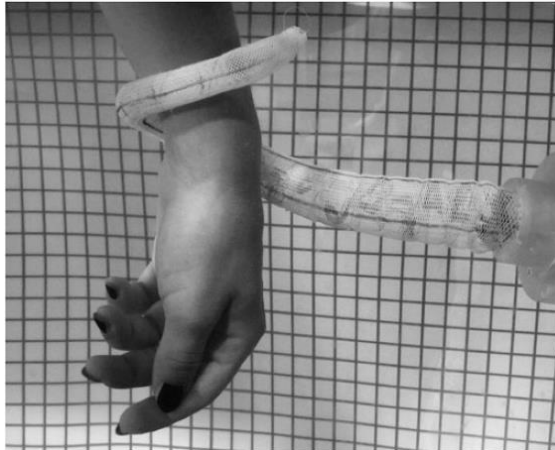


Figure A.D.6 – A robotic octopus tentacle. L – longitudinal actuators, T – transverse actuators, W – central wires and S – support structure. [155]

The use of a similar design for a miniaturized, *in vivo* colonoscopy robot seems unrealistic due to the complexity of both the mechanism and the required control.

D.2.1. Sweeping action

The many degrees of freedom of an octopus limb could be reduced to a simple sweeping action. This constrains the limb to one plane, rather than the complex alternative. This sweeping action, with the soft and flexible limbs sweeping back and forth, mimics the movement of cilia found in nature.

How this could be implemented with a colonic based device is shown in Figure A.D.7.

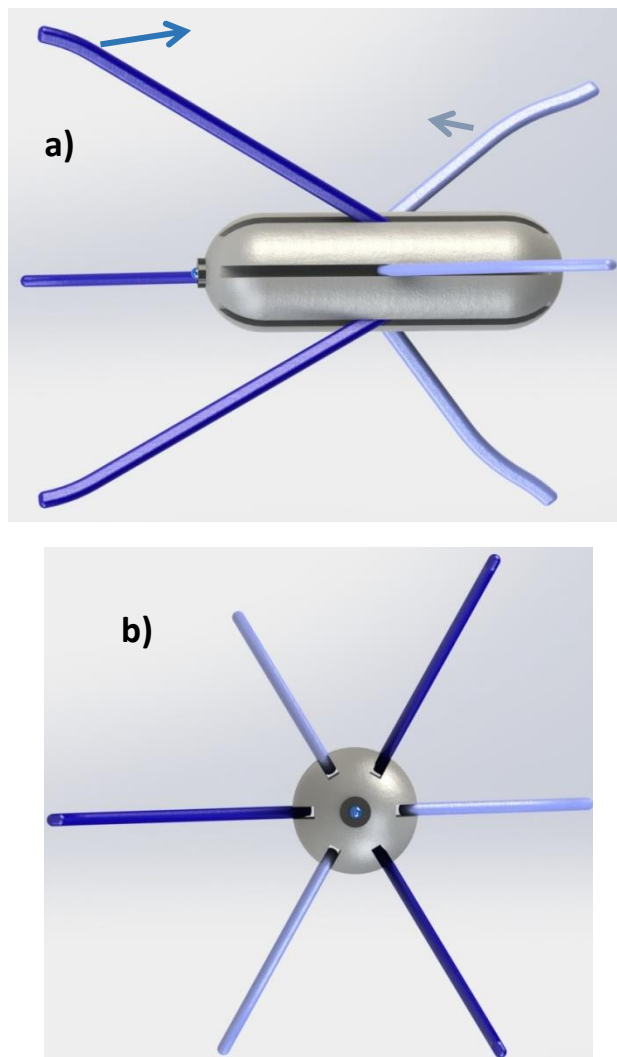


Figure A.D.7 – Concept using sweeping locomotion. a) Side view. b) Front view.

During the propulsion sweep, some limbs make contact with the surrounding environment. They then conform to it before gaining traction and imparting a propulsive force. The limbs then sweep back to the original position. This is repeated by equally spaced radial limbs to achieve a net forward displacement. The use of six limbs that work in two groups of three could result in efficient locomotion. One group sweeps backward to propel the device (propulsion phase), while the other group sweeps forward to prepare for the next propulsive sweep (return phase).

There are a number of potential issues with this design, however. Firstly, the limbs that are sweeping forward (return phase) should not make contact with the surrounding tissue. Any contact would result in a force that opposes the propulsive force, thus lowering the

locomotion efficiency. This would be particularly evident in small diameter environments where the space is restricted (Figure A.D.8).

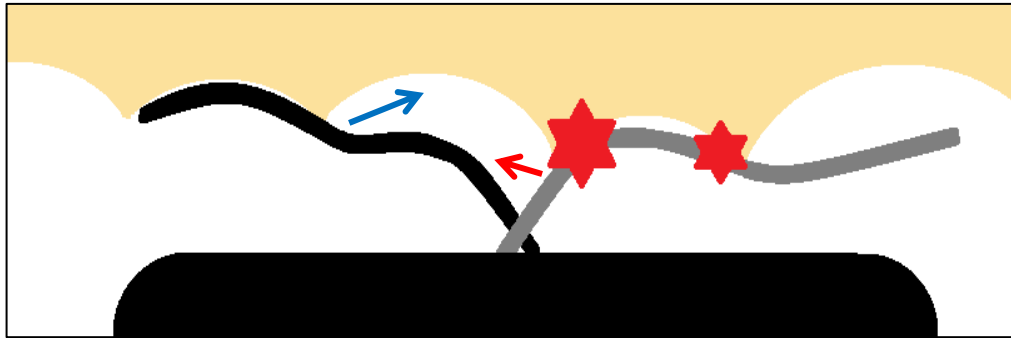


Figure A.D.8 – Diagram showing locomotion inefficiency in small diameter colon.

The blue arrow indicates the propulsive phase and the red arrow shows the non-propulsive, return phase. The red stars indicate unwanted collision with the lumen.

This could be overcome by having some control over the shape and/or compliance of the limbs. Furthermore, the limbs in the propulsive phase could be used to distend the colon, removing it from the path of the return phase limbs. During the return phase, the limbs could either be actively bent to avoid contact with the surrounding tissue or their stiffness could be reduced. With the latter, if the limbs did make contact during the return phase, their low stiffness would result in minimal force transmission. This is a possible solution but introduces additional complexity into the system.

D.2.2. Paddling action

The issues of high complexity and inefficient locomotion found in the sweeping form of locomotion could be solved by removing the return phase, and thus simplifying it further. This can be achieved by using a paddling action: a continuous rotation rather than a two phase system. A simple diagram of this is shown in Figure A.D.9:

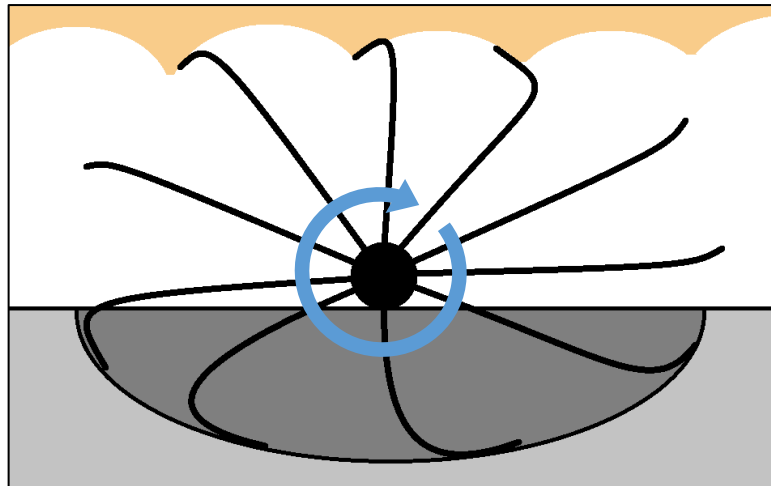


Figure A.D.9 – Schematic showing basic paddle action.

The return phase occurs inside the robot body thus ensuring a negative propulsive force is not applied to the lumen.

The paddle is rotated as shown in Figure A.D.9. As an individual vane comes into contact with the tissue it deforms and then imparts a propulsive force (as with a sweeping action). The paddle continues to rotate, pulling the vane past the tissue, through a trough in the device and ready for a second propulsive sweep. This mechanism could significantly reduce the overall complexity as only a simple rotation is required. The device could also operate more effectively in small diameter environments as there will be no opposing force from a return phase. Additionally, having a number of paddles, each with multiple vanes, could result in a smooth form of locomotion. The challenge with this paddle design is to minimize losses as the vanes are pulled through the body of the robot. Whilst in the trough, a vane will have to be deformed excessively which would require a force. Moreover, there would be a friction force generated between the vane and the trough. The summation of this deformation force, friction force and propulsive force must be less than the stall torque of the motor.

A design that incorporates variable compliant paddles, arranged evenly around the robot chassis has the potential to:

- Provide a stable platform, as some arms/vanes will always be anchoring it to the surrounding tissue.
- Provide an adaptable, non-traumatic locomotion mechanism due to the use of soft, flexible limbs.
- Be simple to control due to the use of soft materials which reduce the need for sensing as they passively conform to the tissue surface.